

TH-1047

**Laboratoire de Géophysique Interne et Tectonophysique
(Observatoire de Grenoble)**

et

Laboratoire d'études des Transferts en Hydrologie et Environnement

THESE

présentée par

Uta GABRIEL

pour obtenir le titre de

Docteur de l'Université Joseph Fourier - Grenoble I

Spécialité: Géophysique - Géochimie - Géomécanique

**TRANSPORT REACTIF DE L'URANYLE:
MODE DE FIXATION SUR LA SILICE ET LA GOETHITE;
EXPERIENCES EN COLONNE ET REACTEUR FERME; SIMULATIONS**

Date de soutenance: 6 Février 1998

Composition du jury

C.W. Schläpfer	Président	Professeur, Université, Fribourg
W. Kinzelbach	Rapporteur	Professeur, ETH, Zürich
M. Sardin	Rapporteur	Directeur de Recherches CNRS, LSGC, Nancy
L. Charlet	Examineur	Professeur Université J. Fourier, LGIT, Grenoble
J.P. Gaudet	Examineur	Ingenieur de Recherches UJF, LTHE, Grenoble
E. Giffaut	Examineur	Radiochimiste, ANDRA
J.C. Vial	Examineur	Directeur de Recherches CNRS, Spectrometrie Physique, Grenoble

REMERCIEMENTS

Avant d'exposer les résultats et les conclusions, je tiens à remercier toutes celles et tous ceux qui m'ont accompagnée et aidée à avancer sur ce chemin.

Je remercie les membres du jury d'avoir bien voulu juger mon travail: Messieurs Wilhelm Schlaepfer (président), Wolfgang Kinzelbach et Michel Sardin (rapporteurs), Laurent Charlet, Jean-Paul Gaudet, Eric Giffaut et Jean-Claude Vial (examineurs).

Mes remerciements vont à Laurent Charlet et Alain Manceau pour m'avoir accueillie dans leur équipe de Géochimie de l'Environnement au Laboratoire de Géophysique Interne et Tectonophysique et à Michel Vauclin pour m'avoir accueillie au sein du Laboratoire d'études des Transferts en Hydrologie et Environnement.

Je souhaite exprimer ici ma profonde gratitude à mes deux directeurs de thèse Laurent Charlet et Jean-Paul Gaudet : c'était votre coopération scientifique - coopération entre un géochimiste et un expert du transfert - qui était à la base de cette recherche. Vous avez suivi mes travaux avec un intérêt constant et une confiance imperturbable en leurs réussites.

Merci, Laurent Charlet, pour la proposition du sujet, pour les discussions scientifiques enrichissantes et pour le support personnel.

Merci, Jean-Paul Gaudet, pour l'encadrement patient, dans la théorie et la pratique des expériences en colonnes et de même pour les discussions fructueuses pendant la phase de rédaction du mémoire.

Je remercie Lorenzo Spadini, grand connaisseur de la chimie en solution aqueuse et spécialiste de l'analyse d'équilibres chimiques, pour avoir partagé ses connaissances avec moi, pour sa disponibilité et ses nombreux conseils.

Merci aux autres membres du groupe de la géochimie de l'environnement du LGIT, Martine Musso, Bruno Lanson, Laurent Eybert pour m'avoir aidée dans la résolution des nombreux problèmes pratiques.

Un merci tout particulier à l'équipe de la Silice Poreuse au Laboratoire de Spectrométrie Physique. C'est vous qui avez rendu possible l'ensemble de ces travaux en me fournissant le matériel pour doser mon uranyle en solution. Merci Jean-Claude Vial, Fernand Madeore, Irina Mihalcescu, Sonja Letant, ... pour l'aide pratique et pour les nombreuses discussions sur le phénomène de la luminescence. J'ai adoré l'ambiance dans votre équipe.

Je ne veux pas oublier de mentionner dans mes remerciements Axel Brachmann, un bon ami de Freiberg, qui m'a familiarisée avec la luminescence de l'uranyle et qui, ensuite, m'a invitée dans le Centre de Recherche de Rossendorf en Allemagne, pour effectuer des mesures.

La rédaction de ce mémoire n'aurait pas été possible sans des discussions nombreuses avec des spécialistes. Mes remerciements pour leur intérêt vont à

Gerhardt Geipel, responsable de l'équipement et spécialiste de la luminescence au centre de Recherche de Rossendorf, Allemagne;

Wladimir Degoda, spécialiste de la luminescence de l'uranyle en contact avec la silice, chercheur à l'Université de Kiev;

Scott Tyler, spécialiste de la modélisation du transfert réactif, en année sabbatique au LTHE;

Wilhelm Schlaepfer, Professeur de la Chimie Inorganique à l'Université de Fribourg en Suisse, avec lequel j'ai également pu discuter de la luminescence et du transfert réactif de l'uranyle.

Je veux remercier aussi les équipes de secrétaires du LGIT et du LTHE pour leur gentillesse et leur aide.

Ce travail m'a permis de faire la connaissance et de rencontrer l'amitié des étudiants de trois laboratoires. Un grand merci à Alix, Céline, André, Manue, Arnaud, Christophe, Désirée, Françoise, Stéphanie, Christian, Soumia, Enriqué, Anne, Fabrice, Géraldine, Jean-Claude, Mirko, Gille, Tarik, Sandrine, Sophie, Robert, Rachel, Florence, Luiz, Michel, Pierre, Roméo, Florentina, Suzanna, ... pour avoir partagé avec moi la vie de tous les jours, les soucis d'un travail scientifique, mais aussi tous les bons moments. Veuillez me pardonner si j'ai oublié quelques uns d'entre-vous.

Susanne, Céline et Béatrice, merci pour votre amitié et votre aide dans des situations difficiles.

Enfin, les mots me manquent pour exprimer tout ce que je dois à Frank et à mes parents: c'est votre amour qui m'a porté et qui m'a permis d'aller jusqu'au bout.

TABLE DES MATIERES

	SYNOPSIS	1
	Organisation du mémoire	
	Introduction	
	Objectifs	
	Méthodologies expérimentales	
	Modèles appliqués	
	Résultats principaux	
I	MECANISMES DE LA FIXATION DE L'URANYLE SUR UNE SURFACE REACTIVE (caractérisation spectroscopique de la spéciation sur la silice amorphe)	27
II	TRANSPORT REACTIF DE L'URANYLE DANS UN SOL ARTIFICIEL (en condition de fond géochimique invariant)	63
III	SIMULATION EXPERIMENTALE D'UNE DESORPTION ACCIDENTELLE (après variation soudaine des conditions géochimiques)	101
	CONCLUSION	147
	PERSPECTIVES	151
	BIBLIOGRAPHIE	153
	ANNEXE	163

SYNOPSIS

ORGANISATION DU MEMOIRE

Ce mémoire est composé d'un synopsis reprenant les principaux résultats acquis, suivi de publications détaillant les trois grandes étapes des travaux:

- I Spéciation de l'uranyle sur la surface des particules de silice étudiée par spectroscopie induite par laser pulsé (Uranyl surface speciation on silica particles by TRLIL spectroscopy)**
à soumettre à « *Journal of Colloid and Interface Science* »

- II Transport réactif de l'uranyle dans une colonne de goethite: Expériences et simulations (Reactive uranyl transport in a goethite column: An experimental and modelling study)**
accepté par « *Chemical Geology* »

- III Désorption accidentelle de l'uranyle à partir d'un matériel poreux faiblement contaminé: Simulations expérimentales et numériques (Accidental desorption of uranyl from a low contaminated porous material: Experimental and numerical simulations)**
à soumettre à « *Environmental Science and Technology* »

Les publications sont indexées au cours du mémoire par ces chiffres romains. La présentation des travaux et résultats a permis de dégager des conclusions générales et de développer quelques perspectives pour de futurs travaux.

INTRODUCTION

L'exploitation minière de l'uranium a laissé dans plusieurs parties du monde des déchets miniers et des mines ouvertes (pour les Etats Unis par exemple un résumé est donné par Landa et Gray, 1995), qui représentent de grands risques pour l'environnement. Deux régions particulièrement concernées en Europe sont les deux états de « Thuringe » et de « Saxe » dans le sud-est de l'Allemagne (Deissmann et al., 1995; Geipel et al., 1994; Gellermann et al., 1995). Là l'uranium a été exploité et extrait pendant plusieurs décennies. Au début, dans les années cinquante, l'extraction était faite sur place par de petites entreprises. Puis dans les années soixante-dix et quatre-vingt l'extraction a été centralisée dans de très grandes entreprises; or la région est densément peuplée. Ces sources de contamination en uranium ont donc ici été étudiées dans le but d'estimer les risques associés à ces déchets et encourus par l'homme, et de définir les projets de réhabilitation nécessaires.

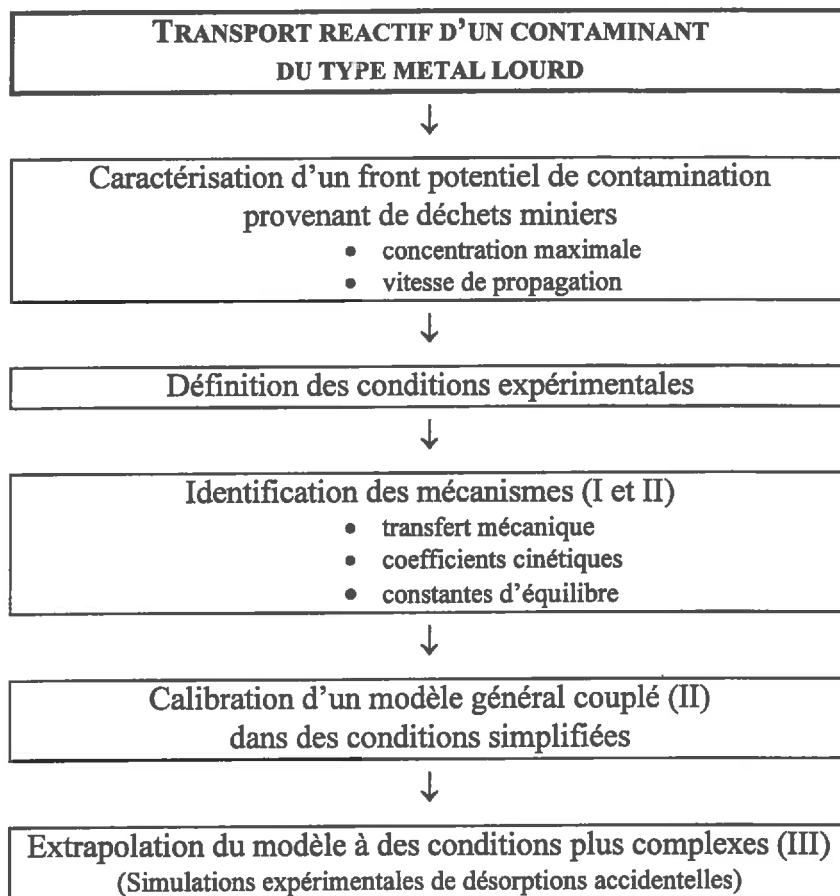


Figure 1 Méthodologie d'évaluation du risque associé à un contaminant
(Les chiffres romains indiquent les chapitres de ce mémoire.)

Pour évaluer les risques associés aux fuites d'uranium vers les aquifères avoisinantes il est indispensable de connaître précisément la façon dont l'uranium peut être transporté dans la nature tout en interagissant avec elle, ce que l'on appelle son transport réactif. Parmi les interactions on trouve des processus d'immobilisation par fixation sur la phase solide et des réactions dans la phase liquide et mobile. La méthode générale d'étude du transport réactif d'un contaminant est résumée sur la figure 1.

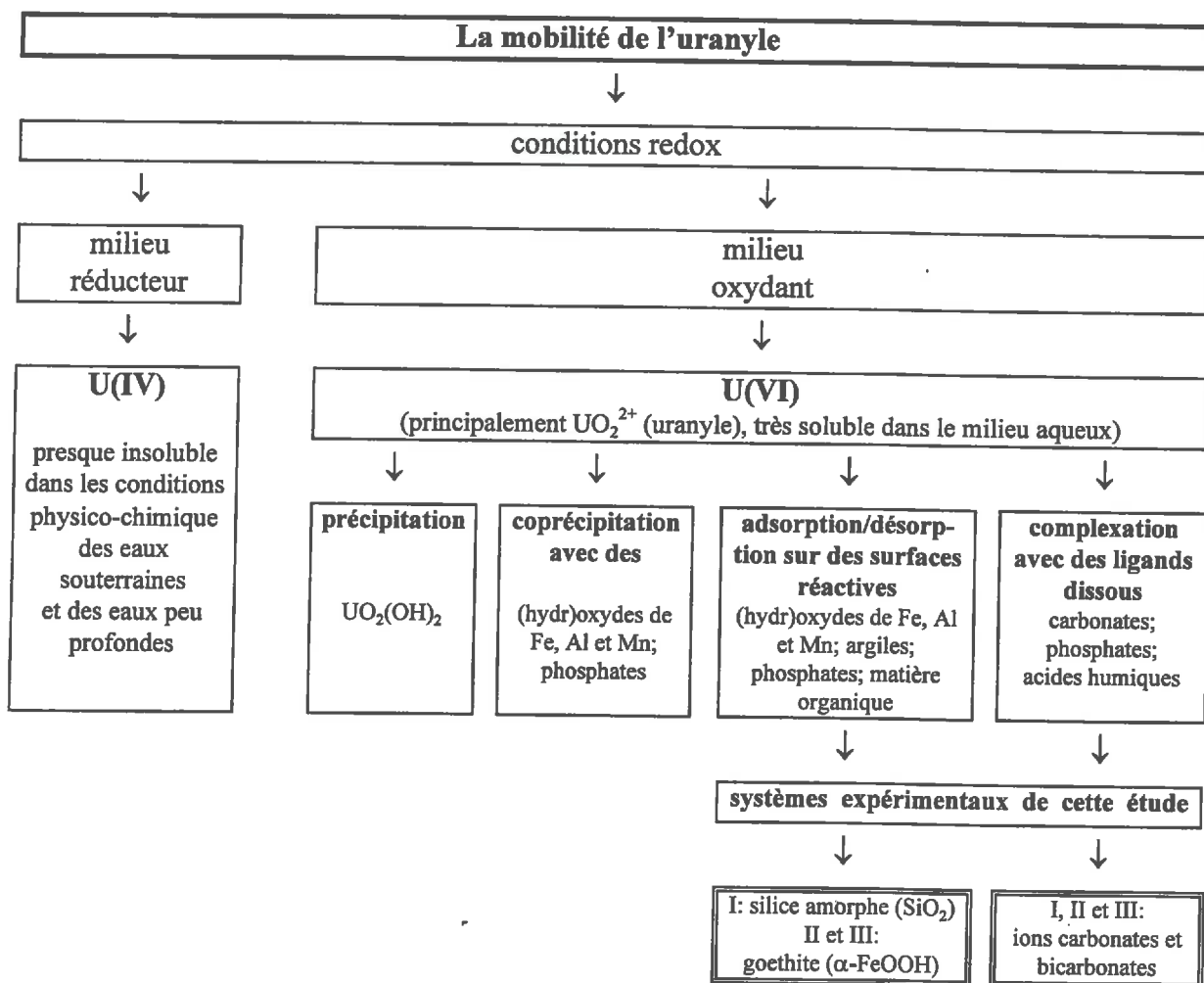


Figure 2 Facteurs contrôlant la mobilité de l'uranyle dans la nature et définition du système expérimental

La géochimie de l'uranium est résumée sur la figure 2. Sous forme réduite U(IV), l'uranium est peu soluble dans l'eau superficielle et souterraine. Sous forme oxydée (l'ion uranyle), il est au contraire très soluble, sa mobilité étant contrôlée par la compétition entre des réactions avec les phases solides (comme l'adsorption, la désorption, la coprécipitation) et des réactions en solution (comme l'hydrolyse et la complexation avec des ligands).

Pour étudier les mécanismes prépondérants dans le transport réactif de l'uranyle nous avons choisi de travailler à l'échelle de réacteurs fermés ou de colonnes de laboratoire (ordre de grandeur: 15 cm). Nous nous sommes limités aux conditions de flux d'eau simple : régime d'écoulement permanent, milieu poreux saturé en eau et homogène.

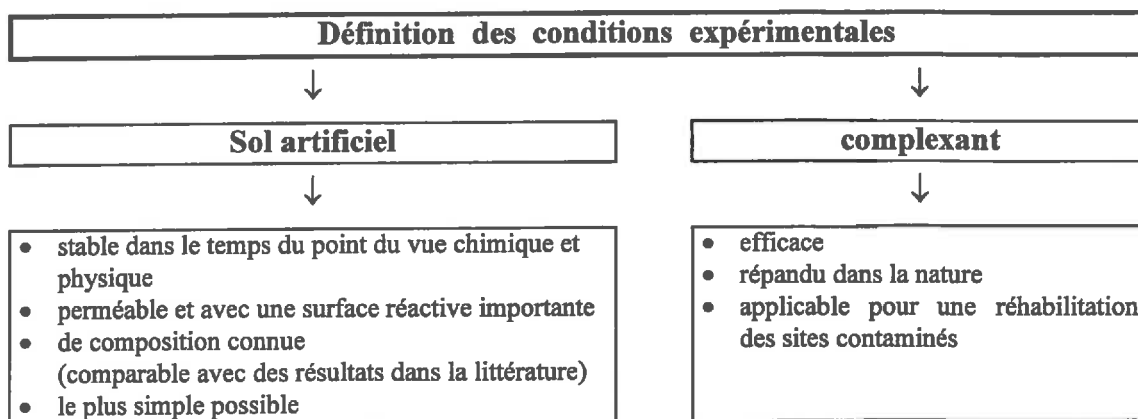


Figure 3 Critères de la définition du système pour une étude sur la mobilité d'un contaminant du type métal lourd

Il a été, dans une première étape, nécessaire de définir un système; les critères retenus pour le choix des composants sont résumés sur la figure 3. Nous avons choisi deux systèmes différents comme systèmes modèles, pour les raisons suivantes.

SILICE AMORPHE-CARBONATE-URANYLE (I)

La *silice amorphe* permet la caractérisation de la spéciation de l'uranyle par la spectroscopie de luminescence. Cette luminescence est provoquée par laser pulsé et observée en temps résolu (« time-resolved laser-induced luminescence », TRILIL). La méthode est très sensible à l'environnement de l'uranyle, mais elle limite le choix de la surface réactive.

Le *carbonate* a été choisi comme complexant en solution dans les deux systèmes (I, II et III) pour les raisons suivantes. (i) Il est très souvent présent à des concentrations élevées dans les déchets miniers à cause d'anciens processus d'extraction. (ii) L'équilibre entre les ions carbonates et bicarbonates, le CO_2 de l'air et le calcaire en phase solide représente le tampon de pH le plus important des eaux naturelles. Les concentrations des ions carbonates sont importantes pour des valeurs de pH élevées. (iii) Les ions carbonates paraissent être des complexants favorables pour le nettoyage des sites contaminés à l'uranium, car leur impact dans les autres compartiments de la nature est relativement faible.

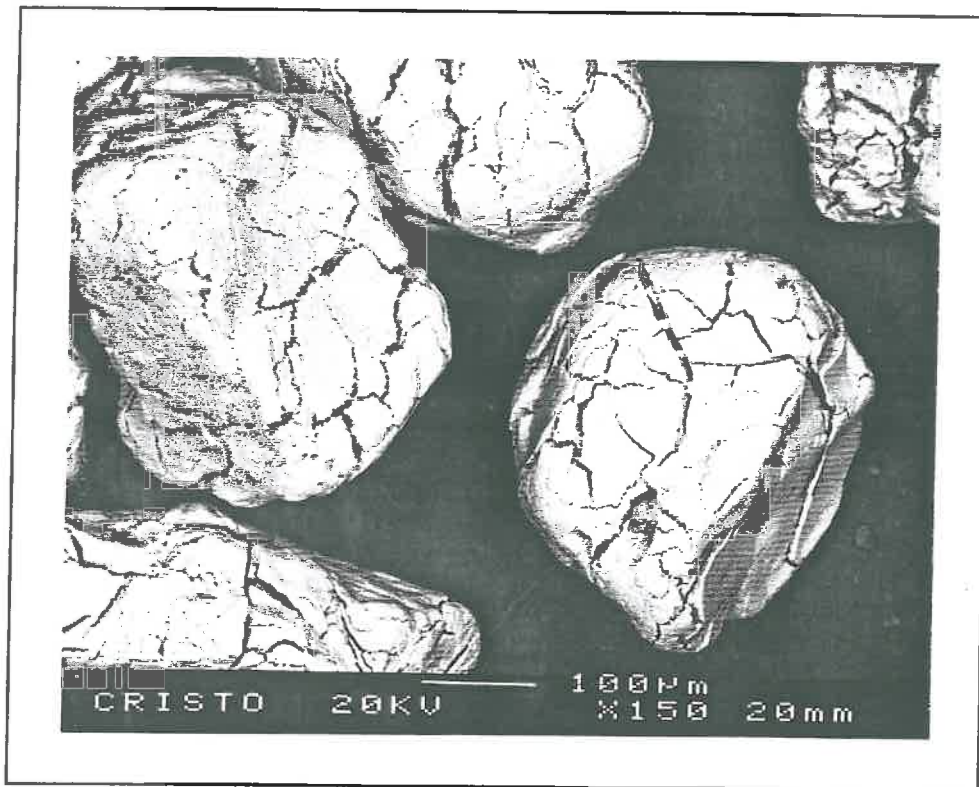


Figure 4 Sable de cristobalite (taille de particules: 125 - 315 μm)

CRISTOBALITE-GOETHITE-CARBONATE-URANYLE (II et III)

La *cristobalite*, matériau sableux, permet une percolation aisée. Il s'agit d'une forme minéralogique de la silice formée à haute température à partir d'un quartz. Ce traitement thermique crée des fissures et des fractures, dans lesquelles il est possible de fixer la goethite comme « phase réactive » le quartz n'adsorbant pas, dans une eau carbonatée, l'uranium(VI) (figure 4).

La *goethite* est un oxyhydroxyde de fer fréquemment rencontré dans des sols. Elle a une grande surface spécifique et une forte réactivité vis à vis d'ions tels que l'uranyle, le bicarbonate ou le silicate. Par rapport aux oxydes de fer hydratés, elle a l'avantage d'être stable dans le temps.

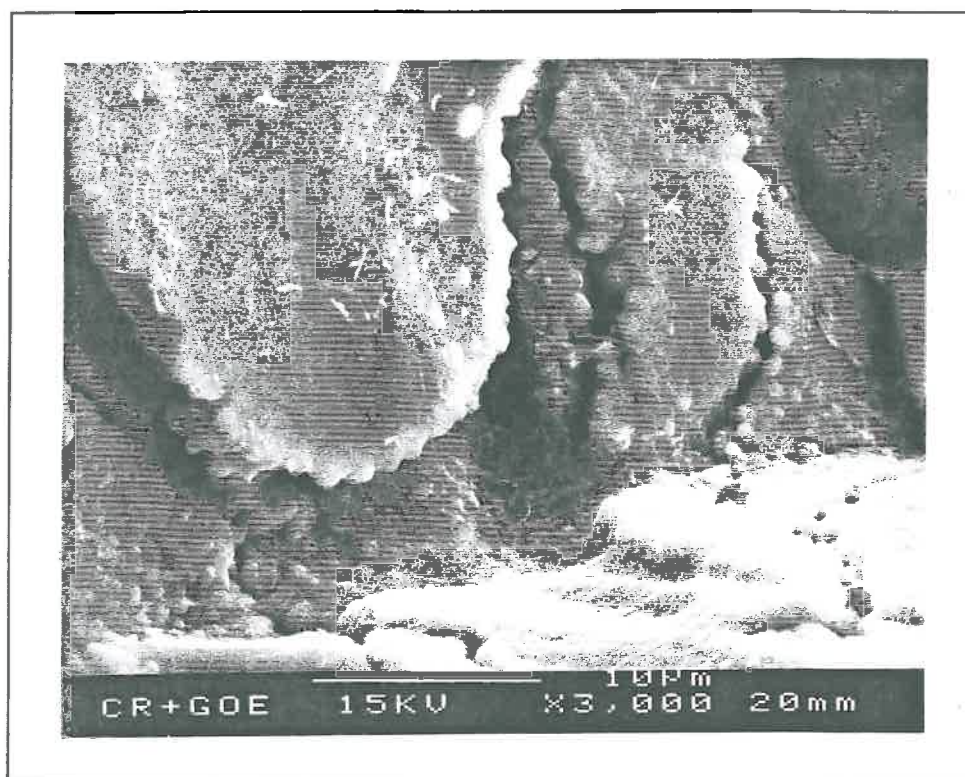


Figure 5 Sol artificiel (il a été possible de coller la goethite dans les fissures c'est-à-dire d'attacher les aiguilles de goethite dans les fissures.)

Nous avons considéré ce « sol artificiel » (figure 5), comme modèle physique de déchets miniers réels. Sa mise au point a été délicate (décrite spécifiquement dans II), tant pour le support sableux (cristobalite) car il a fallu tamiser et laver le sable avec de l'acide, que pour les surfaces réactives (goethite) et leur association avec le sable (Scheidegger, 1993).

Nous avons utilisé (après mise au point) la spectroscopie « TRLIL » comme méthode analytique pour mesurer les concentrations en uranyle dans les échantillons d'eau prélevés lors des expériences. Cette méthode a permis de doser tous les échantillons (I, II et III) avec ces concentrations variant sur quatre ordres de grandeur et aussi d'étudier les complexes formés par l'uranyle et la surface de la silice amorphe (I). La base théorique de la luminescence est détaillée dans I et la méthodologie de la mesure avec le système expérimental ainsi que le traitement des données sont décrits en détail dans II.

OBJECTIFS

- I. **Etudier le mécanisme de la fixation de l'uranyle sur la silice amorphe avec la spectroscopie de TRLIL.** A la suite de travaux de plusieurs auteurs qui ont invoqué différents complexes pour expliquer le plateau d'adsorption de l'uranyle sur plusieurs minéraux en fonction du pH, nous avons voulu différencier ces complexes de surface à des concentration des traces. Le but était de tester si les différents paramètres de la luminescence (temps de vie, longueur d'onde d'émission, intensité) de la silice une fois mise en contact avec une solution contenant de l'uranyle, pouvaient être utilisés pour *la quantification et la caractérisation structurale des complexes de surface formés par l'uranium.*

- II. **Etudier le transport réactif de l'uranyle dans un sol artificiel sous des conditions de fond géochimiques constantes** (pH, teneur en bicarbonate du sodium). A l'aide d'expériences sous conditions tant statiques que dynamiques, nous avons identifié les paramètres contrôlant ce transport. *En couplant des modèles de la chimie et du transfert de l'eau nous avons obtenu une évaluation et un calibrage des modèles généraux.*

- III. **Simuler expérimentalement une désorption accidentelle dans le sol artificiel.** Nous avons voulu simuler la situation d'un changement brutal de conditions de fond géochimiques dans un milieu poreux contaminé, comme on le trouve autour des mines et des déchets d'extraction de l'uranium. Il a été envisagé d'*identifier les paramètres contrôlant la vitesse de propagation et la concentration maximale du front de contamination provenant des déchets.* On a voulu tester si ce type d'expériences *confirme les résultats obtenus sous des conditions de fond géochimiques constantes c'est-à-dire tester la possibilité d'extrapolation des modèles.*

METHODOLOGIES EXPERIMENTALES

Il existe principalement deux manières d'étudier les mécanismes de fixation d'un polluant (Schweich et Sardin, 1981): en conditions statiques (par exemple en réacteur fermé) ou en conditions dynamiques (par exemple en colonne du laboratoire, figure 6). Dans ce mémoire nous employons le terme « réacteur fermé » (correspondant au terme « batch ») pour spécifier des conditions stagnantes. Toutes les expériences sont réalisées à l'équilibre avec l'atmosphère (normalement on doit parler d'un système ouvert là aussi!).

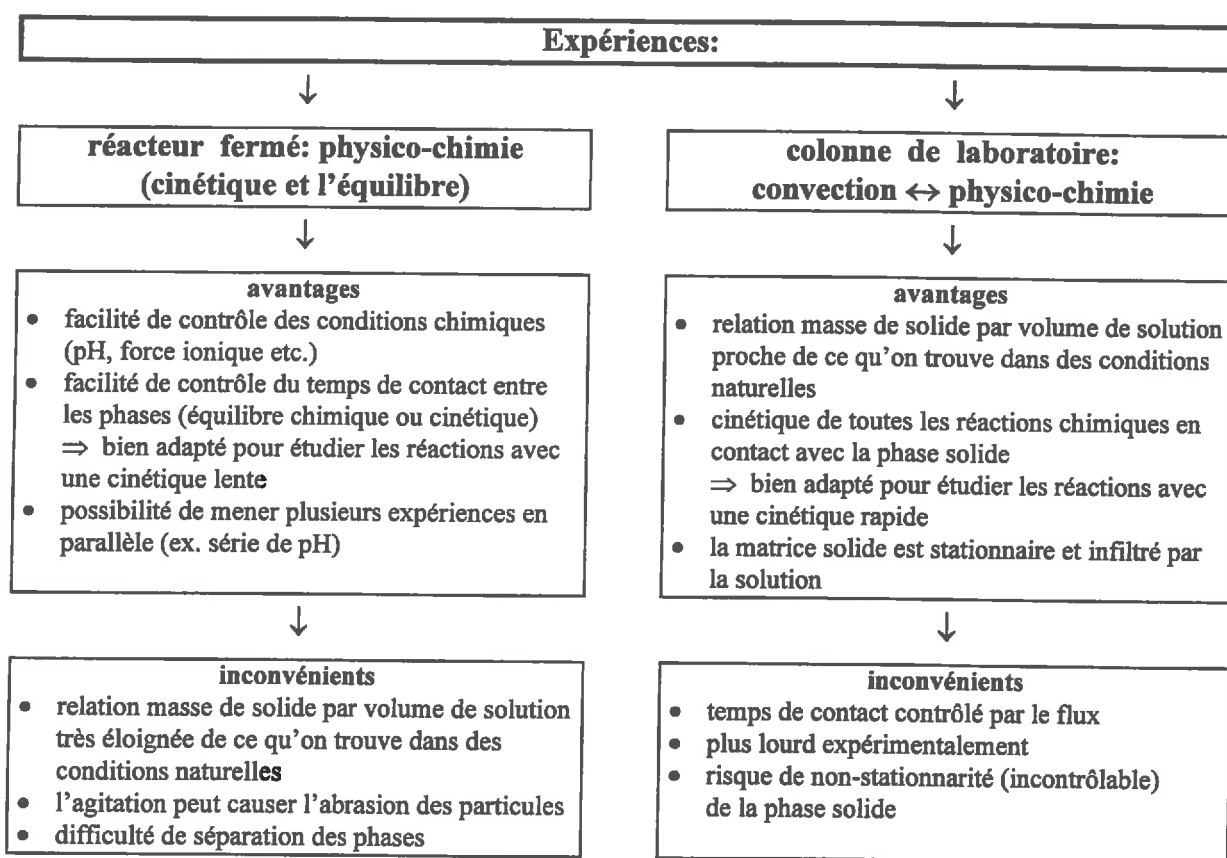


Figure 6 Avantages et inconvénients des expériences en réacteur fermé (« batch ») et en colonne du laboratoire

Les mécanismes d'adsorption de l'uranyle à la surface de la silice amorphe (I) et de la goethite (le sol artificiel, II) ont été étudiés dans des réacteurs fermés (mais ouverts à l'atmosphère). L'adsorption de l'uranyle sur la goethite (le sol artificiel) a également été étudiée sous conditions de flux dans des colonnes du laboratoire (réacteurs ouverts, II et III). La description et la comparaison des deux méthodologies expérimentales se trouvent principalement dans II.

MODELES

Les modèles appliqués dans les travaux présentés dans ce mémoire sont résumés sur la figure 7. Ces modèles peuvent être subdivisés entre modèles d'équilibres chimiques (GRFIT) et modèles qui permettent de coupler les réactions chimiques au transfert. Les modèles chimiques peuvent être subdivisés selon la définition des concentrations utilisée: (i) Des modèles phénoménologiques sont basés sur la concentration totale dissoute (et mesurable) du soluté (par exemple des isothermes d'adsorption, II et III). (ii) Les modèles déterministes sont basés sur la concentration libre du soluté (modélisation thermodynamique à l'équilibre incluant des effets électrostatiques de la charge de la surface, I et II). Le rapport entre les deux types de modélisation est discuté en détail dans II. Cette classification différencie des modèles à un composant (l'uranium soluble pris dans sa totalité : (i)) et à plusieurs composants (correspondant aux diverses espèces transportées : (ii)). Quelques modèles permettent d'inclure des lois cinétiques.

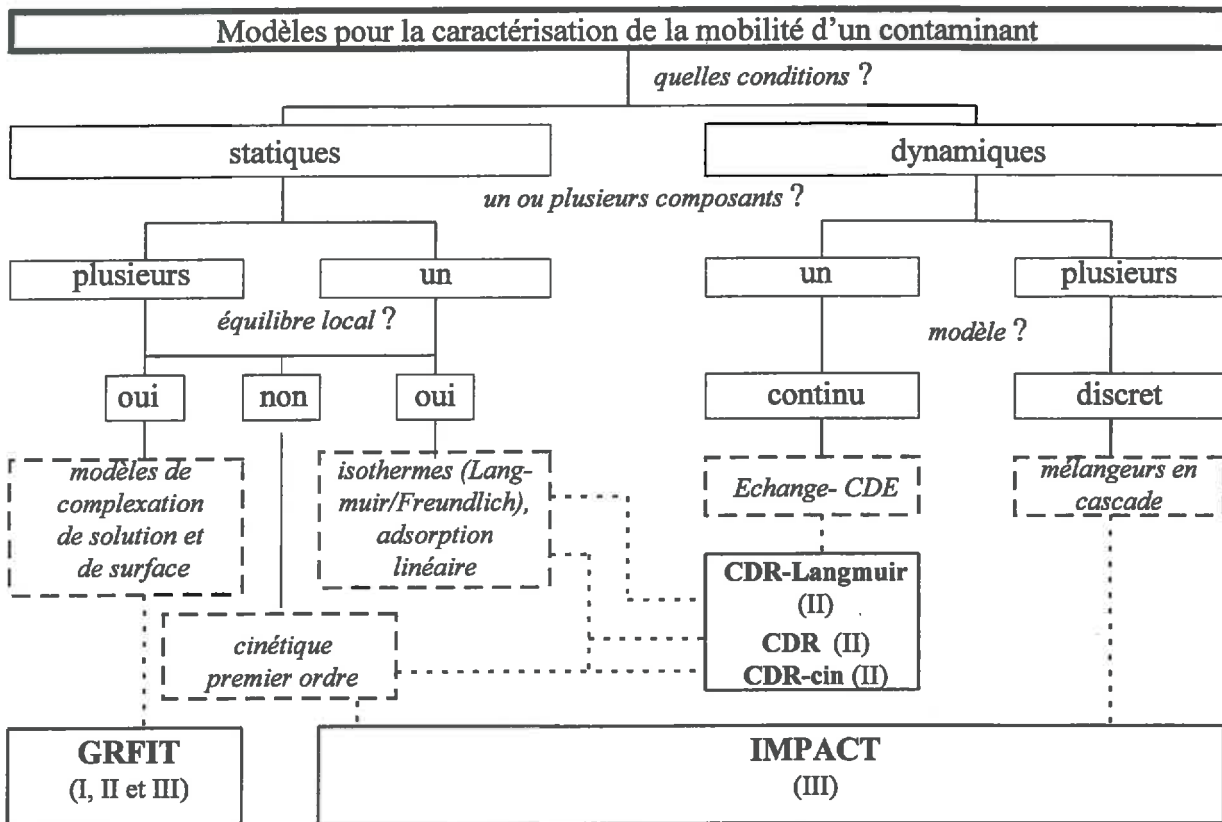


Figure 7 Les modèles utilisés dans ce mémoire.
Les chiffres romains indiquent les chapitres.

Le flux peut être modélisé par des équations différentielles d'espace et de temps (modèles continus, discutés dans II) ou par une série de mélangeurs en cascade (modèles discrets, appliqués dans III).

Deux codes de calculs, GRFIT et IMPACT, ont été utilisés. Ils diffèrent (i) par la possibilité ou non de décrire le transport de l'eau et (ii) par la méthode de calcul utilisée pour calculer les concentrations à l'équilibre.

GRFIT (Westall et Hohl, 1980; Ludwig, 1993) permet le calcul des équilibres chimiques en incluant des modèles de surface chargée. Nous avons utilisé le modèle de la couche compacte (« constant capacitance model »). Ce code est basé sur la minimisation de l'écart entre les concentrations totales calculées et observées, par des itérations (Newton-Raphson). Ce code a été utilisé principalement dans I et II.

IMPACT (Jauzein et al., 1989; Jauzein, 1988) est un code qui permet de calculer les équilibres chimiques et leur couplage au transfert. L'atteinte de l'équilibre chimique est calculée au moyen de vecteurs d'avancement des réactions. Le transfert de l'eau est modélisé par une série de mélangeurs, comme indiqué dans III.

ECDE, CDR, CDR-Langmuir et CDR-cin

Plusieurs modèles ont été développés dans le cadre de l'étude de la pollution des sols et des eaux souterraines, où les aspects chimiques ont été traités d'une manière phénoménologique. Le couplage entre les réactions chimiques et le transfert physique est établi par les bilans de masse pour l'eau et pour les différents solutés (développés en détail dans II).

RESULTATS PRINCIPAUX

Spéciation de l'uranyle sur la surface de la silice amorphe en fonction du pH (I)

Avec la méthode de spectroscopie de luminescence induite par laser pulsé (TRLIL), nous avons identifié par leur décalage (« shift ») des pics de luminescence, de 250 cm^{-1} vers le rouge, deux complexes formés par l'uranyle à la surface de la silice amorphe. Les deux complexes formés à pH 4-9 avec des traces d'uranyle ont des temps de vie de luminescence de 170 ± 25 et $360 \pm 50\ \mu\text{s}$ (figure 8).

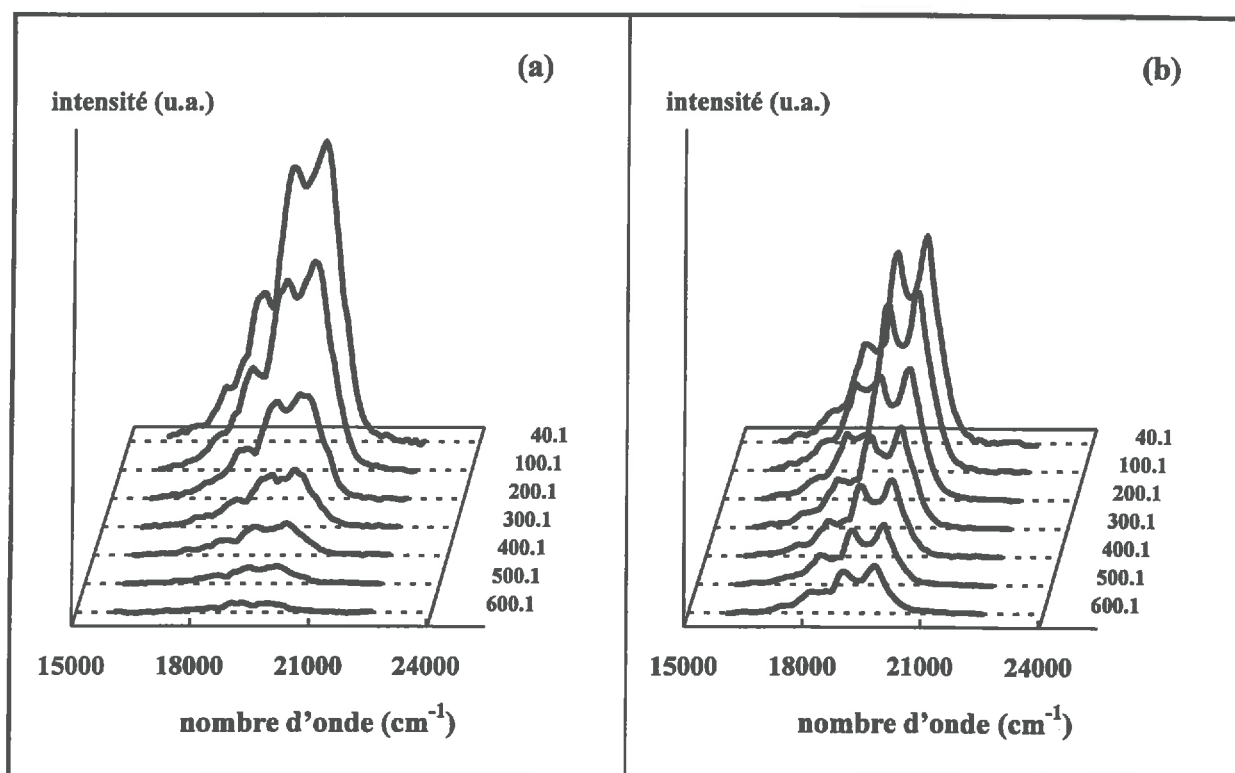


Figure 8 Spectres de fluorescence résolue dans le temps, après correction de la fluorescence de la silice amorphe à pH 4.41 (a) et 8.19 (b) (les chiffres représentent le temps en μs après le laser pulsé; l'intensité est tracée dans les mêmes unités arbitraires; concentration de particules $c_p = 1\text{ g dm}^{-3}$; $[\text{UO}_2^{2+}]_{\text{total}} = 1\ \mu\text{M}$)

Une petite partie de l'uranyle adsorbé aux valeurs de pH très élevées ne correspond à aucun composant de la fluorescence. Cette différence entre l'adsorption déterminée par analyse chimique et celle obtenue par exploitation de la luminescence a été interprétée comme la

preuve de l'existence d'un troisième complexe, non-luminescent et ternaire entre uranyle, carbonate et des sites de la surface (figure 9).

A partir des intensités extrapolées au temps égal zéro à l'aide des déclinis bi-exponentiels ainsi que les intensités obtenues par l'analyse des facteurs (figure 9), nous avons quantifié la spéciation de l'uranyle à la surface de la silice amorphe (tableau 1).

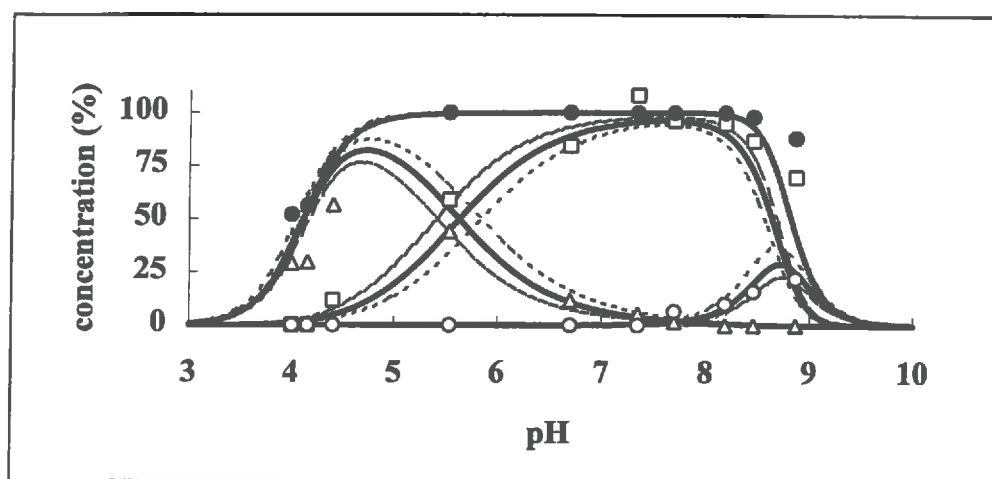


Figure 9 Spéciation de l'uranyle sur la surface de la silice amorphe à $[\text{UO}_2^{2+}]_{\text{total}} = 1 \mu\text{M}$. Les valeurs expérimentales sont basées sur les spectres à partir de $40 \mu\text{s}$ après le pulse du laser: □ et Δ représentent des complexes qui libèrent deux et trois protons; ○ représente le complexe ternaire silencieux; ● décrit la concentration totale adsorbée. La modélisation est basée sur les constantes d'équilibre reportées dans tableau 1.

Tableau 1 Constantes d'équilibre intrinsèques (logK) pour la spéciation sur la surface de la silice amorphe. (modèle de la couche compacte; $c_p = 1 \text{ g dm}^{-3}$; $\kappa = 7 \text{ F m}^{-2}$; $A_s = 169 \text{ m}^2 \text{ g}^{-1}$; $I = 0 \text{ M}$; $[\equiv\text{Si}(\text{OH})_2]_{\text{total}} = 0.51 \text{ mM}$; $[\text{H}_2\text{CO}_3^{\circ}]_{\text{libre}} = 16.4 \mu\text{M}$; $[\text{UO}_2^{2+}]_{\text{total}} = 1 \mu\text{M}$; $[\text{H}_4\text{SiO}_4^{\circ}]_{\text{total}} = 0.9 \text{ mM}$)

Réactions		logK	
$\equiv\text{Si}(\text{OH})_2 - \text{H}^+$	\leftrightarrow	$\equiv\text{SiO}_2\text{H}^-$	-6.98
$\equiv\text{Si}(\text{OH})_2 + \text{UO}_2^{2+} - 2 \text{H}^+$	\leftrightarrow	$\equiv\text{SiO}_2\text{UO}_2^{\circ}$	-4.8
$\equiv\text{Si}(\text{OH})_2 + \text{UO}_2^{2+} - 3 \text{H}^+ + \text{H}_2\text{O}$	\leftrightarrow	$\equiv\text{SiO}_2\text{UO}_2\text{OH}^-$	-10.46
$\equiv\text{Si}(\text{OH})_2 + \text{UO}_2^{2+} + \text{H}_2\text{CO}_3^{\circ} - 5 \text{H}^+ + \text{H}_2\text{O}$	\leftrightarrow	$\equiv\text{SiO}_2\text{UO}_2\text{OHCO}_3^{3-}$	-22.14

Nous avons observé le même décalage (« shift ») pour les séries obtenues à 1.0 et 0.1 μM d'uranyle. Nous en avons déduit l'absence de polymères d'uranyle formés à la surface de la silice, dans la gamme des concentrations « traces » utilisée.

La différence d'énergie entre les maxima du spectre de luminescence est liée à la distance entre l'uranium(VI) et les atomes d'oxygène en position axiale. Cette distance dépend du pourcentage de saturation de la charge positive de l'uranium dans le plan équatorial. On a donc conclu à une liaison chimique plus forte entre l'uranyle et la silice amorphe pour les complexes de la surface formés à haut pH. Un pourcentage plus élevé de la charge de l'uranium(VI) est compensé dans le plan équatorial, ce qui résulte en une distance plus longue entre l'uranium(VI) et les deux atomes d'oxygène en position axiale. Ces observations sont en accord avec des distances observées pour des complexes d'uranyle en solution (Aberg et al., 1983; Thompson et al., 1997) et d'autres formés à la surface des oxydes de fer hydratés (Waite et al., 1994), de la silice amorphe (Reich et al., 1996) ou pour l'uranyle présent dans un verre (Farges et al., 1992).

Le transport réactif de l'uranyle en fond géochimique constant (II et III)

Identification des paramètres hydrodynamiques (III)

Pour décrire les paramètres hydrodynamiques de la colonne nous avons observé la propagation d'un créneau d'uranyle dans des conditions où l'adsorption de l'uranyle est négligeable, c'est-à-dire à une concentration de bicarbonate de sodium de 50 mM.

En changeant le débit (figure 10) nous avons trouvé que la dispersivité (rapport entre le coefficient de dispersion et la vitesse de pore) était égale à 0.073 cm, ce qui correspond à un nombre de Peclet de 200 (modèle continu) ou à 100 mélangeurs en cascade (modèle discret).

Pour les deux courbes de percée, nous avons constaté que 7.5 % de la phase liquide contenue dans la colonne est immobile et liée à la microporosité. L'échange entre fractions mobiles et immobiles peut être décrit par une cinétique du premier ordre. La valeur de ce taux cinétique physique (le « coefficient d'échange ») est de 1.7 h^{-1} . La précision de ce paramètre ajusté décroît avec la teneur en eau immobile, et est donc faible dans le cas présent.

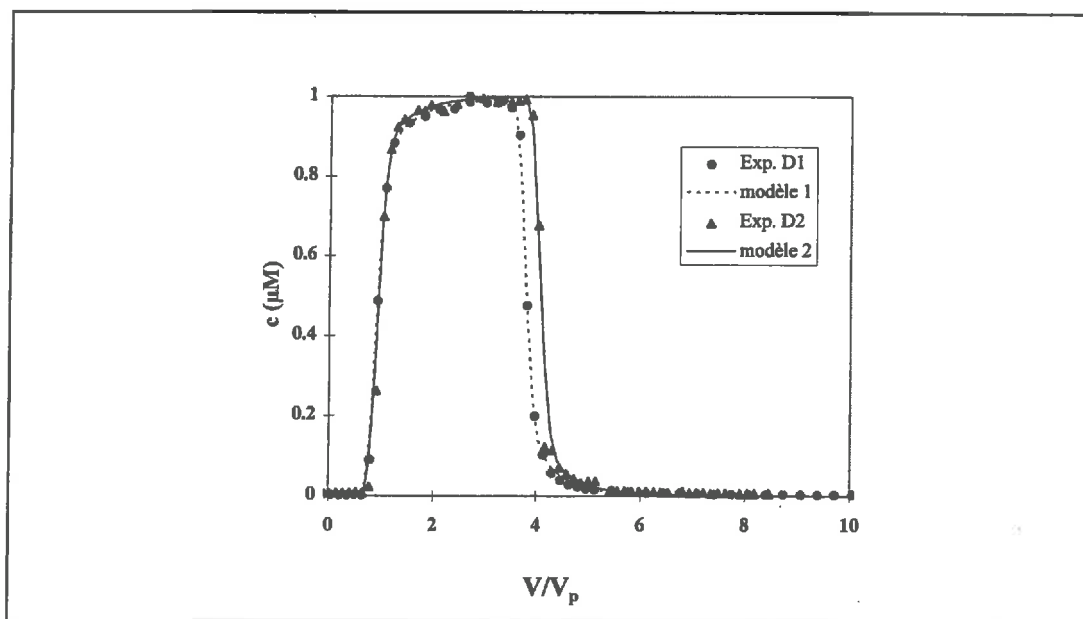


Figure 10 Courbes de percée en fond géochimique constant de 50 mM bicarbonate de sodium à deux débits différents (Exp. D1: débit égal à $0.83 V_p \text{ h}^{-1}$; Exp. D2: débit égal à $0.083 V_p \text{ h}^{-1}$; concentration de l'uranyle à l'entrée de la colonne $c_0 = 1 \text{ µM}$; modèle: MIM).

Identification des paramètres chimiques en conditions dynamiques (II)

Nous avons observé la propagation d'un créneau d'uranyle dans la colonne, pour des conditions de fond géochimiques constantes, c'est-à-dire en présence de 10 mM bicarbonate de sodium en équilibre avec l'atmosphère, soit à $\text{pH } 9 \pm 0.2$. Pour distinguer l'adsorption de l'uranyle sur le support sableux de la colonne (cristobalite) de celle sur la surface réactive (goethite), nous avons mené une expérience dans les conditions chimiques décrites, mais avec une colonne contenant que de la cristobalite (figure 11). Aucun retard n'est alors observé, ce qui indique que toutes les réactions d'adsorption sont contrôlées par la goethite, et elle seule.

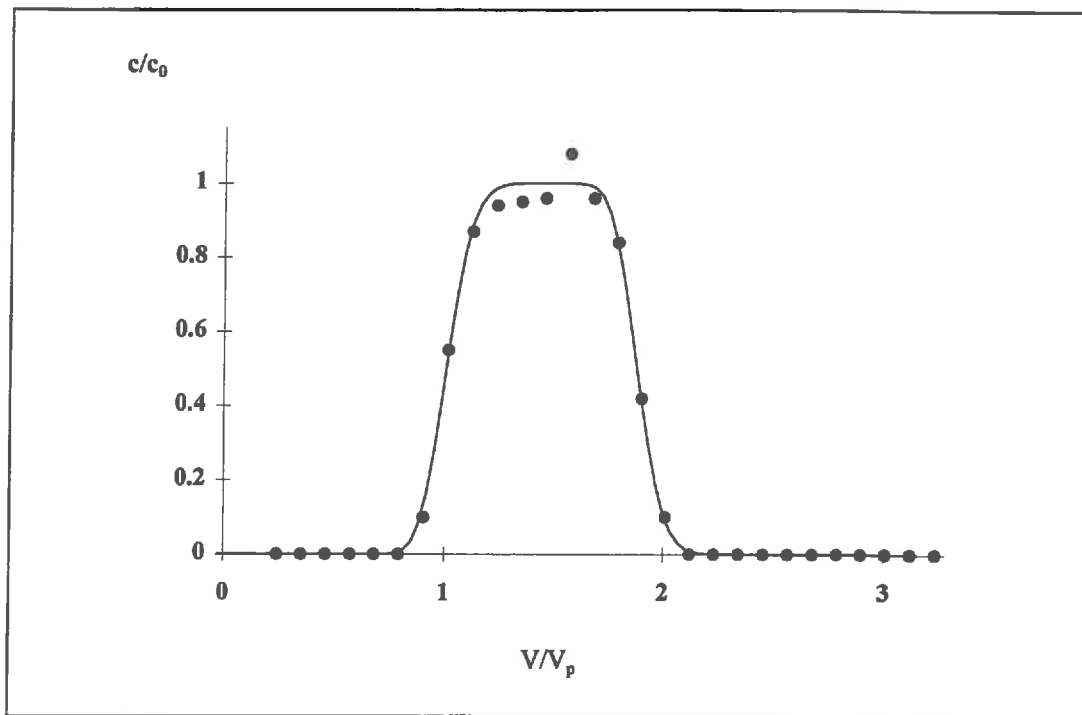


Figure 11 Courbe de percée dans une colonne de cristobalite pure ($[\text{NaHCO}_3]_{\text{total}} = 10 \text{ mM}$; $c_0 = 1 \text{ } \mu\text{M}$; débit égal à $0.83 V_p \text{ h}^{-1}$; modèle: CDR avec un facteur de retard $R = 1$)

Nous avons constaté une conservation de la masse de l'uranyle dans la colonne en présence de goethite, ce qui indique une adsorption réversible sur la goethite. Selon Hsi et Langmuir (1985), cette adsorption est réversible pendant 4 heures.

Les paramètres sur lesquels nous avons joué dans les expériences, et les caractéristiques de l'adsorption ainsi mises en évidence étaient :

a. *la concentration initiale en solution (isotherme d'adsorption).*

Le système d'adsorption de l'uranyle sur la goéthite dans 0.01 M NaHCO₃ en équilibre avec l'atmosphère (pH 9 ± 0.15) est contrôlé par un isotherme d'adsorption non-linéaire. Dans l'intervalle de concentration de 0.05 à 0.1 µM l'isotherme paraît être presque linéaire (quantités adsorbées proportionnelles aux concentrations en solution) avec un coefficient de distribution voisin de 1 ℓ g⁻¹ (similitude de courbes de percée des expériences 2 et 3 sur la figure 10). Cette linéarité n'est plus vérifiée au delà: à une concentration initiale de 10 µM on trouve un coefficient de distribution de 0.6 ℓ g⁻¹ (expérience I1 sur la figure 12).

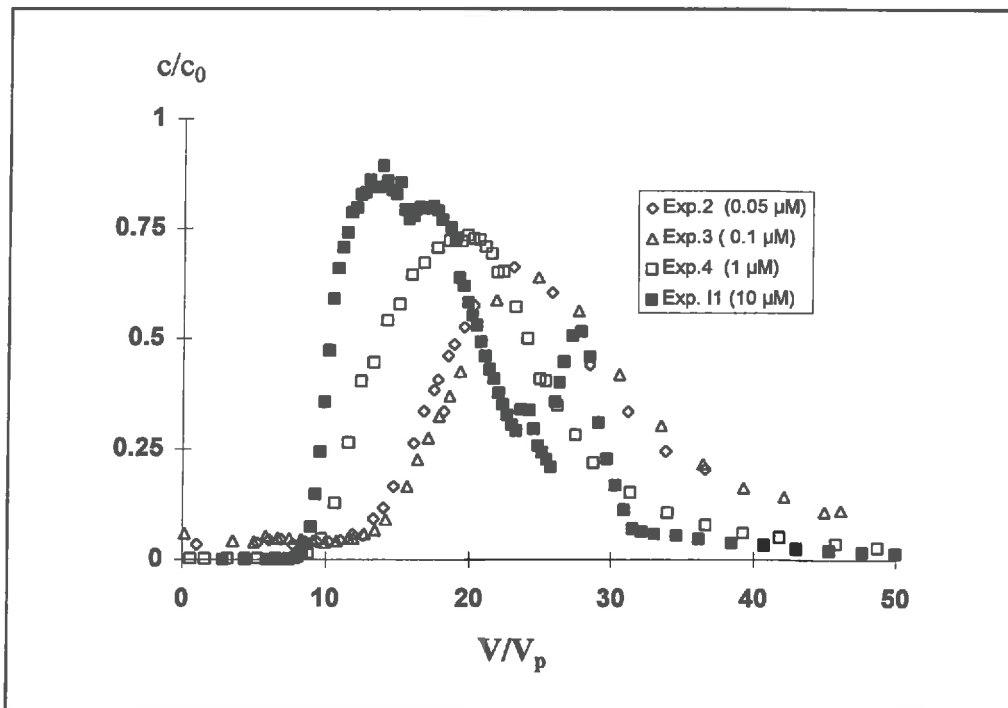


Figure 12 Courbes de percée en fond géochimique constant de 10 mM bicarbonate de sodium à plusieurs concentrations de l'uranyle à l'entrée de la colonne (Les concentrations indiquées entre parenthèses représentent c₀; débit égal à 0.83 V_p h⁻¹.)

b. le débit (la cinétique réactionnelle de l'adsorption).

Pour une concentration initiale en solution de $1 \mu\text{M}$, nous avons montré l'influence de la cinétique de l'adsorption et de la désorption. Dans les conditions de débit de 0.083 volume de pore par heure (Exp. 5 sur figure 13), le système est proche de l'équilibre. Par contre pour un débit 10 fois plus fort (Exp. 4 sur figure 13), la concentration maximale observée est inférieure à la concentration initiale de $1 \mu\text{M}$. Cet effet est dû à la cinétique et paraît être moins important pour des concentrations plus élevées. Ceci montre que la courbe de percée est influencée tant par la cinétique que par la non-linéarité de l'isotherme d'adsorption.

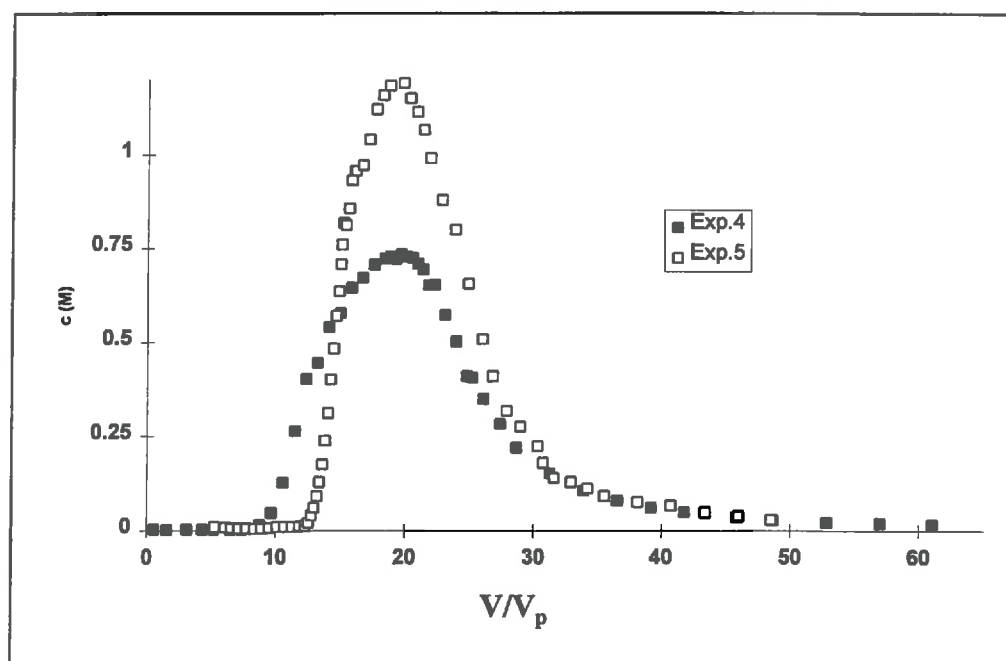


Figure 13 Courbes de percée en fond géochimique constant de 10 mM bicarbonate de sodium à deux débits différents ($c_0 = 1 \mu\text{M}$; Exp. 4: débit égal à $0.83 V_p \text{ h}^{-1}$; Exp. 5: débit égal à $0.083 V_p \text{ h}^{-1}$)

Comparaison entre résultats obtenus en réacteur fermé et en colonne (II)

Nous avons également étudié le système en réacteur fermé, en gardant la concentration de l'uranyle ou du carbonate constante.

Le coefficient de distribution obtenu en réacteur fermé et en colonne (lié au facteur de retard) permet de comparer les phénomènes d'adsorption/désorption observés dans des conditions statiques et dans des conditions dynamiques. Les deux types d'expérience ne conduisent pas aux mêmes résultats (figure 14).

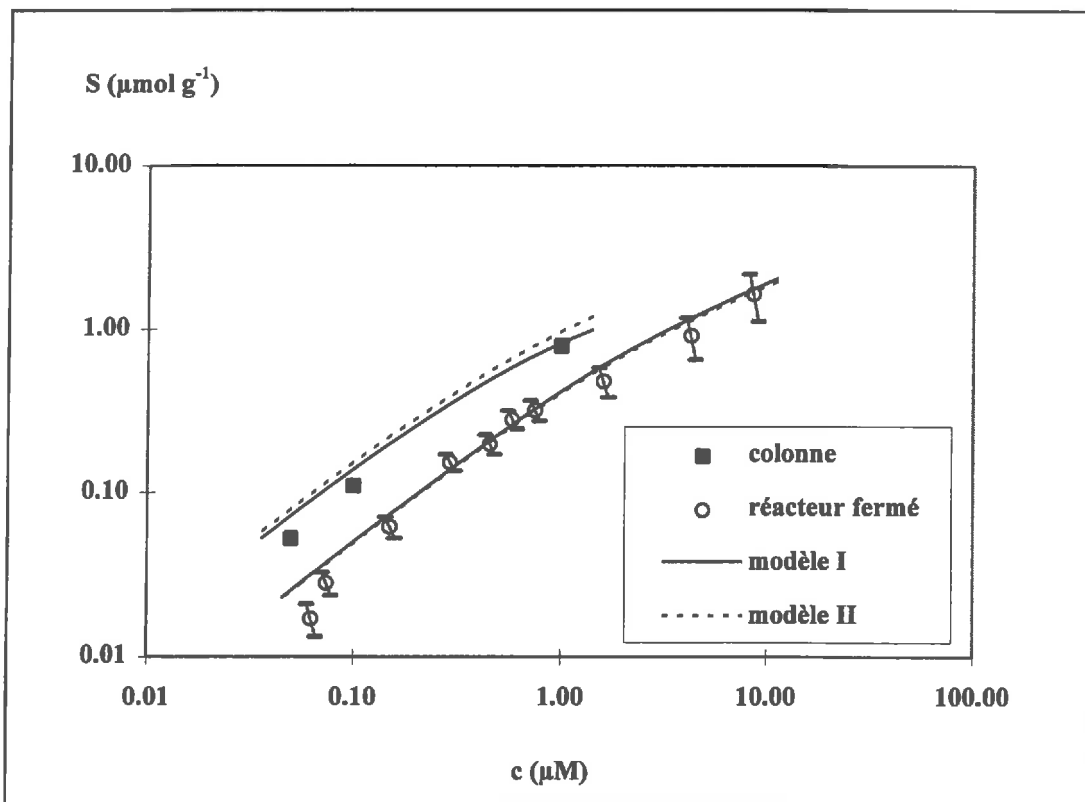


Figure 14 Comparaison des résultats expérimentaux obtenus en réacteur fermé et en colonne avec une modélisation thermodynamique (modèle I: $\text{Fe}^{\text{w}} 1\text{p}$, $\text{Fe}^{\text{s}} 2\text{p}$; modèle II: $\text{Fe}^{\text{w}} 2\text{p}$, $\text{Fe}^{\text{s}} 2\text{p}$)

Le temps de résidence de l'eau était plus long dans les expériences en réacteur fermé (12 jours) que dans les expériences en colonne (1.2 et 12 heures). Ceci a provoqué une dissolution beaucoup plus importante de silice dans le premier cas car la silice dissoute s'adsorbe également sur la goethite au pH considéré. Pour décrire l'adsorption de l'uranyle sur la goethite, il apparaît alors indispensable de prendre en compte la compétition sur les sites réactifs entre uranyle, carbonate, silice dissoute et protons.

La comparaison des résultats obtenus dans des conditions statiques et dynamiques doit donc être faite idéalement dans des conditions chimiques identiques, ce qui n'est pas évident.

Dans notre système (CRISTOBALITE-GOETHITE-CARBONATE-URANYLE) l'adsorption/désorption de l'uranyle est en compétition avec les réactions de complexation suivantes (figure 14) :

- *complexation de surface (compétition pour des sites d'adsorption)* : des protons, des ions silicates et carbonates. Toutes ces réactions ont modifié l'adsorption de l'uranyle, par des effets électrostatiques dus à la charge de la surface.
- *complexation en solution (compétition pour des ions uranyles)* : avec les hydroxydes (réaction d'hydrolyse) et les ions carbonates/bicarbonates.

Des expériences menées dans des conditions dynamiques paraissent plus appropriées et fiables pour découvrir et caractériser une non-linéarité dans l'isotherme d'adsorption car la précision sur les concentrations des espèces adsorbées est plus grande.

Modélisation des interactions chimiques dans des conditions statiques (II)

Un modèle thermodynamique a été élaboré, en considérant :

- *pour l'uranyle* : l'hydrolyse et sa complexation avec le carbonate.
La complexation avec la silice dissoute est négligée, car la complexation - uranyle - silice dissoute est inexistante à pH élevé.
- *pour les sites d'adsorption* : nous avons considéré pour des sites de surface la compétition entre protons, silice dissoute, ions uranyles et ions carbonates/bicarbonates.

Tableau 2 Constantes d'équilibre intrinsèques (logK) pour la spéciation sur la goethite
(modèle de la couche compacte; $c_p = 0.82 \text{ g dm}^{-3}$; $A_s = 80.5 \text{ m}^2 \text{ g}^{-1}$; $\kappa = 1.75 \text{ F m}^{-2}$;
 $[\equiv\text{Fe}^{\text{w}}\text{O}_2\text{H}]_{\text{total}} = 0.253 \text{ mM}$; $[\equiv\text{Fe}^{\text{s}}\text{O}_2\text{H}]_{\text{total}} = 1.25 \text{ }\mu\text{M}$;
 $[\text{UO}_2^{2+}]_{\text{total}} = 1 \text{ }\mu\text{M}$; $[\text{H}_2\text{CO}_3^\circ]_{\text{libre}} = 16.4 \text{ }\mu\text{M}$; $I = 0 \text{ M}$;
réacteur fermé: $[\text{H}_4\text{SiO}_4^\circ]_{\text{total}} = 0.76 \text{ mM}$; *colonne*: $[\text{H}_4\text{SiO}_4^\circ]_{\text{total}} = 21.4 \text{ }\mu\text{M}$)

Réactions	logK
$\equiv\text{Fe}^{\text{s/w}}\text{O}_2\text{H} + \text{H}^+ \leftrightarrow \equiv\text{Fe}^{\text{s/w}}\text{O}_2\text{H}_2^+$	7.33
$\equiv\text{Fe}^{\text{s/w}}\text{O}_2\text{H} - \text{H}^+ \leftrightarrow \equiv\text{Fe}^{\text{s/w}}\text{O}_2^-$	-9.88
$\equiv\text{Fe}^{\text{s/w}}\text{O}_2\text{H} + \text{H}_2\text{CO}_3^\circ - \text{H}_2\text{O} \leftrightarrow \equiv\text{Fe}^{\text{s/w}}\text{OHCO}_3^\circ$	3.62
$\equiv\text{Fe}^{\text{s/w}}\text{O}_2\text{H} + \text{H}_2\text{CO}_3^\circ - \text{H}^+ - \text{H}_2\text{O} \leftrightarrow \equiv\text{Fe}^{\text{s/w}}\text{OCO}_3^-$	-3.40
$\equiv\text{Fe}^{\text{s/w}}\text{O}_2\text{H} + \text{H}_4\text{SiO}_4^\circ - \text{H}_2\text{O} \leftrightarrow \equiv\text{Fe}^{\text{s/w}}\text{OH}_3\text{SiO}_4^\circ$	3.5
$\equiv\text{Fe}^{\text{s/w}}\text{O}_2\text{H} + \text{H}_4\text{SiO}_4^\circ - \text{H}^+ - \text{H}_2\text{O} \leftrightarrow \equiv\text{Fe}^{\text{s/w}}\text{OH}_2\text{SiO}_4^-$	-3.89
modèle I: (Fe^w 1p, Fe^s 2p)	
$\equiv\text{Fe}^{\text{w}}\text{O}_2\text{H} + \text{UO}_2^{2+} - \text{H}^+ \leftrightarrow \equiv\text{Fe}^{\text{w}}\text{O}_2\text{UO}_2^+$	4.307
$\equiv\text{Fe}^{\text{s}}\text{O}_2\text{H} + \text{UO}_2^{2+} - 2 \text{ H}^+ \leftrightarrow \equiv\text{Fe}^{\text{s}}\text{O}_2\text{UO}_2\text{OH}^\circ$	-0.044
modèle II: (Fe^w 2p, Fe^s 2p)	
$\equiv\text{Fe}^{\text{w}}\text{O}_2\text{H} + \text{UO}_2^{2+} - 2 \text{ H}^+ \leftrightarrow \equiv\text{Fe}^{\text{w}}\text{O}_2\text{UO}_2\text{OH}^\circ$	-3.13
$\equiv\text{Fe}^{\text{s}}\text{O}_2\text{H} + \text{UO}_2^{2+} - 2 \text{ H}^+ \leftrightarrow \equiv\text{Fe}^{\text{s}}\text{O}_2\text{UO}_2\text{OH}^\circ$	-0.044

Etant donné la complexité du mécanisme d'adsorption, traiter l'adsorption sous forme simplifiée (isotherme de type Langmuir ou Freundlich) ne semble pas être possible dans notre cas. Il est nécessaire d'inclure dans la description du mécanisme d'adsorption : les effets électrostatiques de la charge de surface, la compétition pour les sites d'adsorption entre les différents ions, et la complexation de l'uranyle en solution.

Cette description fine des phénomènes a été ramenée, dans la section suivante c'est-à-dire dans des conditions données, à une description de type Langmuir à deux sites. Dans ce cas, les paramètres ne sont plus ajustés mais calculés à partir du modèle thermodynamique le plus complet.

Simulation expérimentale d'une désorption accidentelle avec un sol artificiel (III)

En changeant les conditions chimiques dans la colonne, la désorption de l'uranyle a été découplée de la phase d'adsorption (réalisé en présence de $1 \mu\text{M}$ d'uranyle).

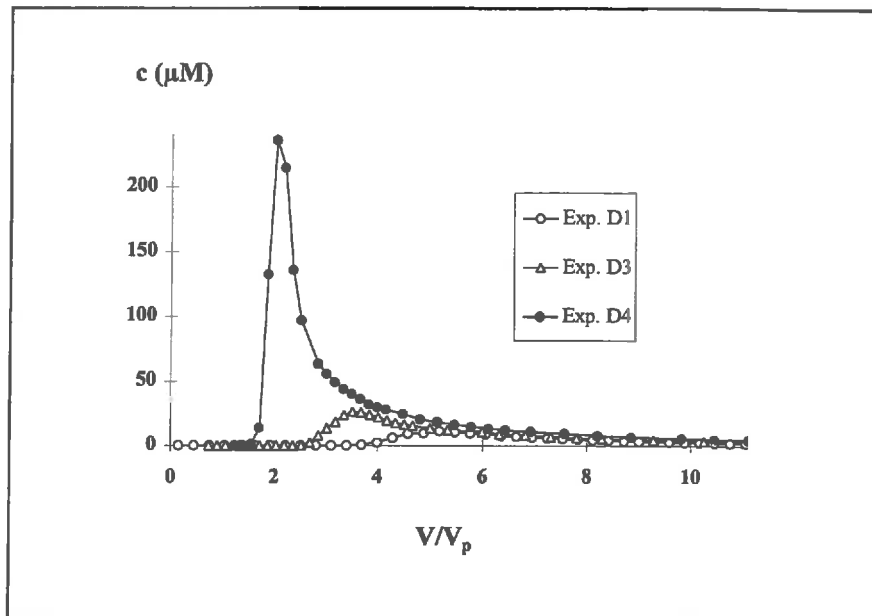


Figure 15 Courbes de percée après changement brutal des conditions géochimiques à une concentration de bicarbonate de sodium de 10 mM - variation de la durée de la période d'accumulation (débit égal à $0.83 V_p \text{ h}^{-1}$; volume écoulé pendant la période d'accumulation avec une solution de $[\text{UO}_2^{2+}]_{\text{total}} = 1 \mu\text{M}$ et de $[\text{NaHCO}_3] = 1 \text{ mM}$: Exp. D1: 1.65 dm^3 , Exp. D3: 4.2 dm^3 et Exp. D4: 11.8 dm^3)

Sur la figure 15, on note que l'augmentation de la quantité totale de l'uranyle dans le système change le temps de séjour de cet ion dans la colonne et cause une importante augmentation de sa concentration maximale à la sortie.

En changeant le débit de 0.83 volume de pores par heure à un dixième de cette valeur, nous avons testé l'influence de la cinétique sur le temps d'apparition et la concentration maximale de l'uranyle en sortie de colonne (figure 16). On observe que la concentration maximale de l'uranyle diminue et que son temps de séjour dans la colonne est plus long pour le débit le plus faible.

Dans ces expériences, la cinétique n'intervient donc pas comme dans les expériences précédentes où un débit plus élevé entraîne une diminution de la concentration maximale. Par contre, l'influence de la quantité totale de l'uranyle dans le système reste marquante.

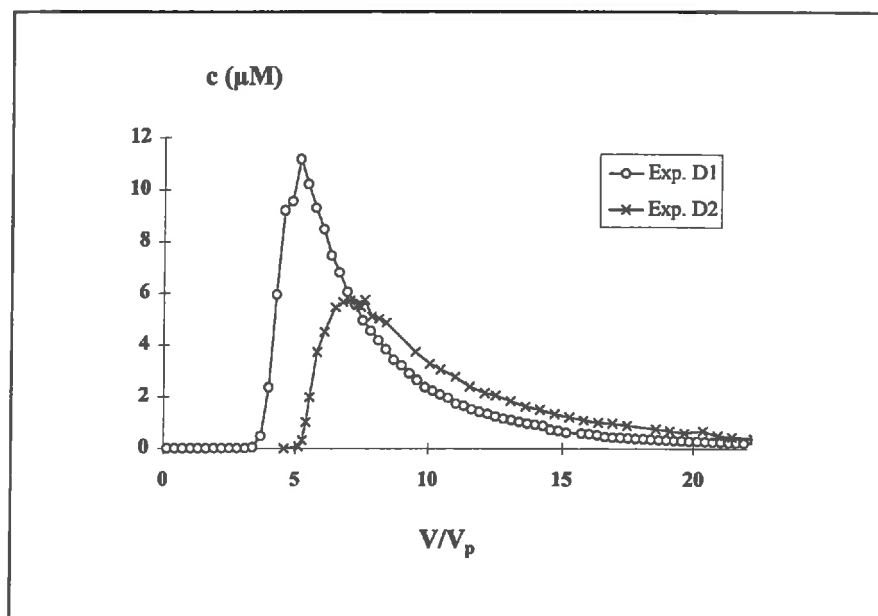


Figure 16 Courbes de percée après changement brutal des conditions géochimiques à une concentration de bicarbonate de sodium de 10 mM - variation du débit (Exp. D1: débit égal à $0.83 V_p h^{-1}$; Exp. D2: débit égal à $0.083 V_p h^{-1}$; volume écoulé pendant la période d'accumulation avec une solution de $[UO_2^{2+}]_{total} = 1 \mu M$ et de $[NaHCO_3] = 1 mM$: Exp. D1: $1.65 dm^3$ et Exp. D2: $1.58 dm^3$)

Durant la phase d'accumulation, la concentration de l'uranium(VI) à la sortie de la colonne est toujours d'au moins deux ordres de grandeur en dessous de celle introduite. Nous en concluons que la colonne n'est que partiellement contaminée à l'instant du changement des conditions géochimiques. Dans la phase de désorption, on distingue deux étapes qui sont l'étape d'enrichissement correspondant au passage du front de désorption par le milieu contaminé, et l'étape de propagation correspondant au passage du front dans le milieu non-contaminé. Dans ces deux étapes, la concentration maximale de l'uranyle est contrôlée par l'isotherme non-linéaire et la limitation cinétique de l'adsorption. Ces deux paramètres ne sont pas connus pour les expériences effectuées aux concentrations élevées de l'uranyle. Par ailleurs, on ne connaît ni le pourcentage de la colonne contaminée ni la concentration

maximale en solution dans la colonne qui apparaît lors du passage du front de désorption dans la partie non-contaminée. Une simulation exacte des « désorptions accidentelles » ne peut donc pas être proposée à partir de ces résultats expérimentaux.

On peut donner quelques exemples des relations entre une isotherme d'adsorption et la courbe de percée numérique correspondante en effectuant des simulations avec le code IMPACT (Jauzein et al., 1989). Sur la figure 17, on observe que la superposition d'une isotherme de Langmuir avec une adsorption limitée par une cinétique du premier ordre produit des courbes de percée numériques similaires aux résultats expérimentaux (figure 15) pour différentes concentrations du soluté appliquées à l'entrée de la colonne.

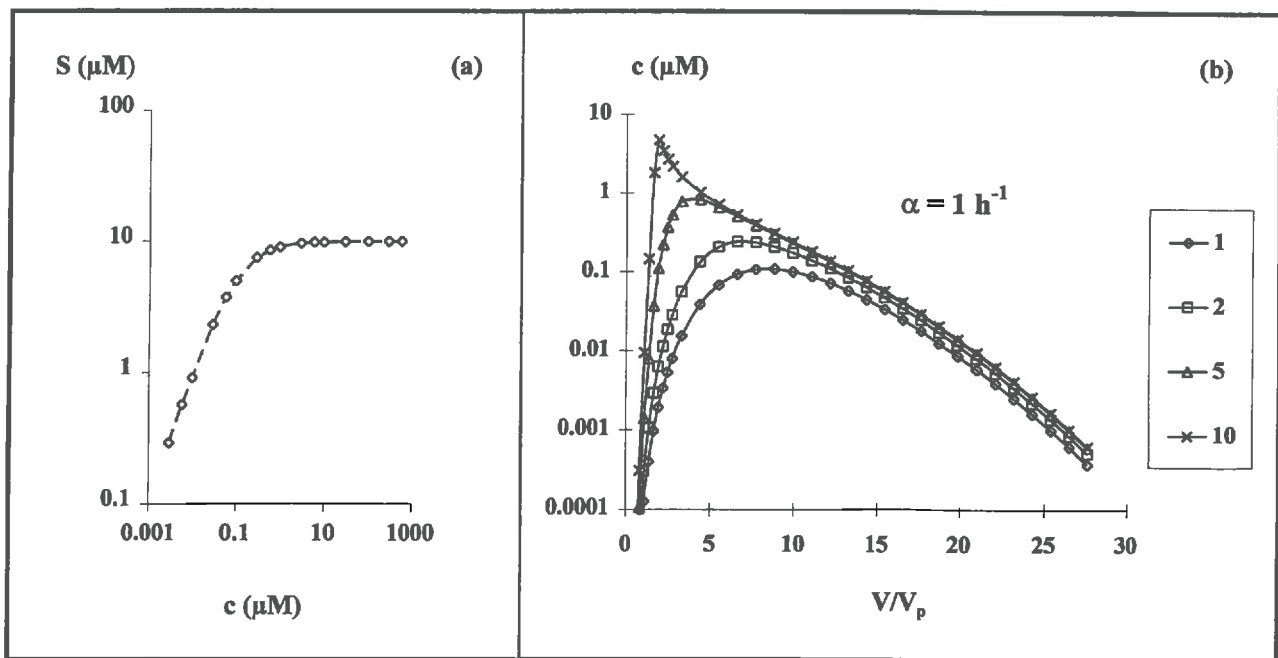


Figure 17 Courbes de percée numériques (b) pour une isotherme de type Langmuir (a), l'adsorption étant limitée par une cinétique de premier ordre (les chiffres représentent c_0 (μM); paramètres de la modélisation: débit égal à $0.83 V_p \text{ h}^{-1}$; $T_0 = 10 V_p$; $V_p = 36.2 \text{ cm}^3$; $J = 100$; échantillons = 5 cm^3 ; $K'_d = 10$; $S'_{\text{max}} = 10 \mu\text{M}$)

Sur la figure 18, une simulation numérique d'une désorption accidentelle de l'uranyle est comparée avec les résultats expérimentaux. Cette simulation est basée sur la supposition d'équilibre local car l'isotherme et la cinétique d'adsorption dans la gamme des concentrations élevées sont inconnues. Cet exemple met en évidence l'approche prometteuse de ce type de simulation lorsqu'on représente des conditions géochimiques variantes par un décalage (« shift ») de l'isotherme. Ce décalage symbolise la combinaison d'un coefficient de distribution (dépendant des conditions géochimiques de fond) avec une isotherme d'adsorption non-linéaire et se justifie partiellement par les résultats expérimentaux de Morrison et al. (1995). Cette approche bidimensionnelle reste néanmoins une représentation simplifiée de l'ensemble des réactions chimiques qui donnent la forme de l'isotherme non-linéaire de l'uranyle. Dans l'avenir, seule la détermination expérimentale des paramètres prépondérants permettra la simulation numérique réelle d'une désorption accidentelle.

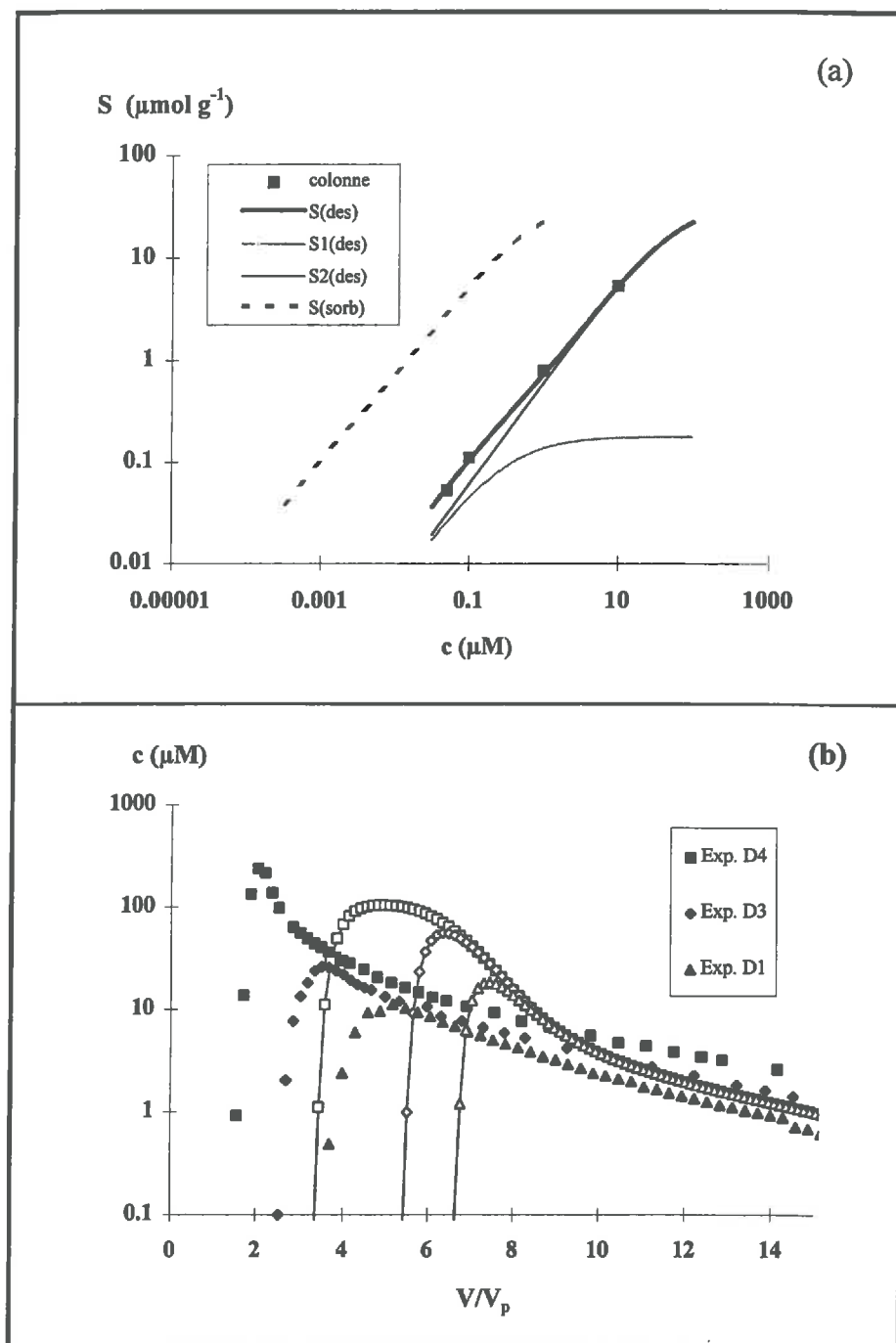


Figure 18 Isotherme de Langmuir (a) et simulations numériques correspondantes des résultats expérimentaux (équilibre local; $S_{\max 1} = 1.75 \mu\text{mol g}^{-1}$; $S_{\max 2} = 350 \mu\text{mol g}^{-1}$; $K_{L1} = 5.37 \times 10^5 \text{ M}^{-1}$; $K_{L2} = 1050 \text{ M}^{-1}$; décalage (« shift ») de l'isotherme = 100; $V_p = 36.2 \text{ cm}^3$, débit égal à $0.83 V_p \text{ h}^{-1}$)

ARTICLE I

URANYL SURFACE SPECIATION ON SILICA PARTICLES

STUDIED BY TRLIL SPECTROSCOPY

Gabriel, U.¹, Schlaepfer, C.W.², Vial, J.C.³, Brachmann, A.⁴, Geipel, G.⁴ and Charlet, L.^{1*}

¹Laboratoire de Géophysique Interne et Tectonophysique, UJF - CNRS (UMR 5559) Grenoble, France

²Institut de Chimie Inorganique, Université de Fribourg, Switzerland

³Laboratoire de Spectrométrie Physique, UJF, Grenoble, France

⁴Forschungszentrum Rossendorf, Germany

* to whom correspondence should be sent

ABSTRACT

The sorption of uranyl ions to amorphous silica has been studied in the presence of atmospheric CO₂ by laser-induced time-resolved luminescence spectroscopy at trace level concentrations (10⁻⁶ and 10⁻⁷ M). Two luminescent uranyl surface complexes have been identified in the pH range 4 to 9. Both complexes could be differentiated by lifetimes (170 ± 25 μs at low pH and 360 ± 50 μs at high pH) and luminescence emission spectra (250 cm⁻¹ red shift between the low pH and high pH spectra) and within the constant capacitance model framework they are described by mono-nuclear (1:1) complexes with release of 2 and 3 protons, respectively. When luminescence data were compared to wet chemistry sorption data, a third « silent » ternary uranyl-silica-carbonate surface complex had to be postulated to account partly for adsorption between pH 8.0 and 9.0. Three independent data sets led therefore to the identification of three different surface complexes, postulated as ≡SiO₂UO₂⁰, ≡SiO₂UO₂OH⁻ and ≡SiO₂UO₂OHCO₃³⁻. Aspects of the structure to luminescence parameter relationship are discussed.

INTRODUCTION

Uranium is a significant environmental contaminant. Because of its applicability as a source of energy and its military uses, it is extensively mined and extracted and has to be stored after use. At each step it can potentially get into contact with the environment, and thus accumulate in soils and sediments. Its mobility is then controlled by its chemical behaviour. In oxidised conditions, uranium is present as linear (O-U-O)²⁺ uranyl ion. This cation is easily adsorbed and thereby removed from solution in the near neutral pH range. In order to predict its migration behaviour this adsorption has been studied with several rock forming minerals and soil constituents. The measured adsorption/desorption edge is classically described with multi-complex surface complexation models (Waite et al., 1994; Turner, 1995) based on best fit criterion. In the present study, we identify surface complexes with spectroscopic « signatures ».

A classical technique to study surface complexes structure is EXAFS spectroscopy, and uranyl adsorption onto several minerals has been studied by this method (Waite et al., 1994, Dent et al., 1991, Reich et al., 1996). This detection technique requires however a surface coverage which is usually much larger than the ones found in natural or anthropogenically contaminated systems.

Therefore we have worked with another molecular near-structure identification tool namely time-resolved laser-induced luminescence (TRLIL) spectroscopy. In this method luminescence is induced by a pulsed laser. It is a particularly favourable technique to study chemical compounds having long luminescence lifetimes as for instance organic compounds characterised by double bonding, and actinides containing compounds, such as uranyl ions, where the covalent bonding is of delocalized π type. Thus the major advantages of TRLIL spectroscopy over other techniques such as NMR or EXAFS spectroscopy are (i) its enhanced sensitivity which allows to work at trace level concentrations, and its combined information on (ii) concentrations (intensities) and (iii) molecular structure (energies, lifetimes).

The TRLIL intensity is widely used in analytical chemistry to quantify uranyl concentration in solution. Uranyl concentration in water samples is linearly related with respect to the extrapolated initial luminescence intensity (at 515 ± 5 nm) when uranyl ions are complexed by a « 0.1 M phosphate based solution resulting in luminescence lifetimes between 250 and 300 μs » (Brina and Miller, 1992).

The structural information carried in a TRLIL spectrum has been recently deciphered in in-situ solution speciation studies (Moulin et al., 1995; Bernhard et al., 1996). The emitted luminescence light gives information on various solution complexes which differ by protonation and polymerisation, because they are characterised by specific luminescence life time and specific luminescence spectrum. Furthermore tetrahedral oxo-anions enhance the luminescence properties of uranyl in general (Brendler et al., 1996; Brina and Miller, 1992). Luminescence studies were also carried out to study the bonding character of uranyl on silica on the solid-water-interface. Wheeler and Thomas (1984) described an increase of the luminescence lifetime from 11 μs to 440 μs when aqueous silica was added to a 0.1 μM uranyl acetate solution which resulted in a pH shift from near neutral to about 10. The emission spectra shifted from 19455 cm^{-1} to 19724 cm^{-1} when the silica was added.

In the present study we used TRLIL spectroscopy to (i) describe quantitatively the overall adsorption reaction following the wet chemical approach of Brina and Miller (1992), (ii) identify and quantify the uranyl surface complexes at the silica-water-interface (by a *quantitative* interpretation of the luminescence data) and (iii) characterise the sorption complexes (*qualitative* interpretation of the luminescence data).

METHODS

Experimental

The silica sample used in this study (Aerosil 200) was provided by Degussa, Germany. It is a non-porous, X-ray amorphous material composed of spherical particles with a diameter of about 25 nm with a specific surface area of 169 m²/g (Osthols, 1995). All chemicals used in this study were of p.a. grade.

Silica suspensions (particle concentration $c_p = 1 \text{ g dm}^{-3}$) were prepared in 50 cm³ polypropylene bottles, at an ionic strength of 0.01 M NaNO₃/NaHCO₃. The total uranyl concentration was 0, 0.1 and 1 μM. For the three uranyl concentrations a series of 11 samples was prepared, with pH adjusted between 3 and 9 by addition of NaHCO₃. The surface area of the container walls was considered negligible compared to the one of the amorphous silica. Therefore no attempt was made to quantify adsorption onto the container walls. The samples were shaken for at least one week. Afterwards the pH was measured again and this final pH registered. The combined glass electrode (Metrohm) was calibrated using standard buffer solutions.

Several suspensions were sequentially filtered through 0.45, 0.2, 0.1 and 0.025 μm filter membranes. No significant difference was observed among the various filtered solutions with regard to uranyl concentrations. Therefore the whole series (containing 1 μM total uranyl concentration) was filtered through 0.45 μm membrane filters. Samples for the determination of the dissolved uranyl concentration were instantly acidified to pH 1 with nitric acid.

The dissolved uranyl concentration was measured (Brina and Miller, 1992), and the adsorbed uranyl concentration was determined by difference as the total uranyl concentration in the system was known. Measurements were performed with a pulsed nitrogen laser (VSL-337ND, Laser Science, inc.; 250 μJ/pulse, 15 Hz, wave length 337 nm), a luminescence measurement cell (quartz, 4 cm³, agitated), a photomultiplier (Hamamatsu 94302, tension of 500 V), a gelatine filter (Kodak 55, maximal transmission 67-69 % at 510-520 nm), a numerical oscilloscope (model: digitising oscilloscope 54501A 100MHz, Hewlett Packard) and a photodiode (PIN S1223-01, Hamamatsu) at the « Spectrometrie Physique » laboratory in

Grenoble, France. The uranyl ions were complexed with phosphoric acid and the decay between 50 and 200 μ s after the laser pulse was used to quantify the total uranyl solution concentration. Correction were made for the base line and instrumental drift. The method was calibrated using the addition method. The detection limit and precision were 3 nM and 5 %, respectively.

The luminescence measurements used to characterise the structure of surface complexes were done at the Radiochemistry Institute, Research Centre Rossendorf, Germany, using the following instruments and devices. The samples were introduced in a luminescence measurement cell (quartz, 4 cm³, agitated) and excited with a pulsed NdYAG laser at 266 nm (4 mJ/pulse, 8 ns pulse duration). The luminescence was captured with an optic fibre 0.5 m (spectrophysics). The spectra were registered using a diode array (700 diodes, 0.3 nm resolution). The diode array was controlled by a delay generator (600 V) which was triggered by the laser itself and delayed by a delay generator. The energy delivered by the laser was controlled by an optical meter. The experimental conditions are summarised in table 1.

Table 1 Measurement conditions for the characterisation of the surface complexes

delay	100 ns
gate	10000 ns
delay step	5000 and 20000 ns
points of one decay	31
laser shots per spectrum	200
spectra per measurement	3

Data treatment

The measured spectra contained about 600 data points. In order to reduce the number of points and decrease the noise/signal ratio we smoothed the data by a spline function and reduced the data set to 60 data points per spectrum. All data obtained in the system uranyl-silica-water were corrected for the background luminescence of the silica-water system.

The luminescence emitted by one complex i is a function of both time and wave number, and its decay follows an apparent first order law (Brina and Miller, 1992):

$$I_i(t, \nu) = I_i(0, \nu) \exp(-t / \tau_i) \quad (1)$$

where $I_i(t, \nu)$ and $I_i(0, \nu)$ are the luminescence intensities of complex i at the wave number ν and time t and t equal 0, respectively. τ_i is the luminescence lifetime of complex i .

The initial luminescence of an uranyl containing complex can not be measured directly. It is mixed with the fluorescence signal of water molecules and other contaminants such as organics produced by bacterial activity. Both have relatively high intensities but short life times of maximal 100 ns. Therefore we started to record the fluorescence signal after 40 μ s (table 1).

If all parameters of the experiment are kept constant, the initial luminescence intensity $I_i(0, \nu)$ is linked to the concentration S_i of the emitting complex i by:

$$I_i(0, \nu) = \omega_i^0(\nu) S_i \quad (2)$$

where $\omega_i^0(\nu)$ is a sum parameter incorporating the effects of absorption, the radiant and nonradiant transition probabilities (all characteristic for the emitting complex i) and several parameters characteristic of the measurement device and the pre-filter and post-filter effects. A detailed discussion is given by Berthoud et al. (1988) and Eliet (1996).

The luminescence intensity of n emitting complexes is justified to be additive. The overall luminescence intensity of a composite solution or suspension is then described by:

$$I(t, \nu) = \sum_{i=1}^n \omega_i^0(\nu) S_i \exp\left(-\frac{t}{\tau_i}\right) \quad (3)$$

The experimental conditions were chosen in order to observe the long-living luminescence components, i.e. the uranyl-silica complexes. Uranyl solution complexes UO_2^{2+} , UO_2OH^+ and $\text{UO}_2(\text{OH})_2^\circ$ present at this level of uranyl dilution have lifetimes of $1.7 \pm 0.2 \mu$ s, $32.8 \pm 2 \mu$ s and $3.2 \pm 0.2 \mu$ s (figure 1; Eliet et al., 1995). Only the first hydrolysed dissolved species emits a detectable proportion of its initial luminescence in the time gate under investigation (30, 5 and 0.2 % after 40.1, 100.1 and 200.1 μ s). Since adsorption is nearly complete at pH 5 (figure 2) this complex is not expected to occur at high concentrations and thus to have a significant impact of the overall luminescence spectra. In the high pH range uranyl solution speciation is

controlled by the formation of non luminescent carbonate containing complexes (Bernhard et al., 1996, Kato et al., 1994).

Concentration of all emitting complexes is related to the emitted luminescence light by equation (3). Therefore we extracted from both - the *spectra* ($t = \text{constant}$) and the *decays* ($\nu = \text{constant}$) - quantitative information on surface speciation.

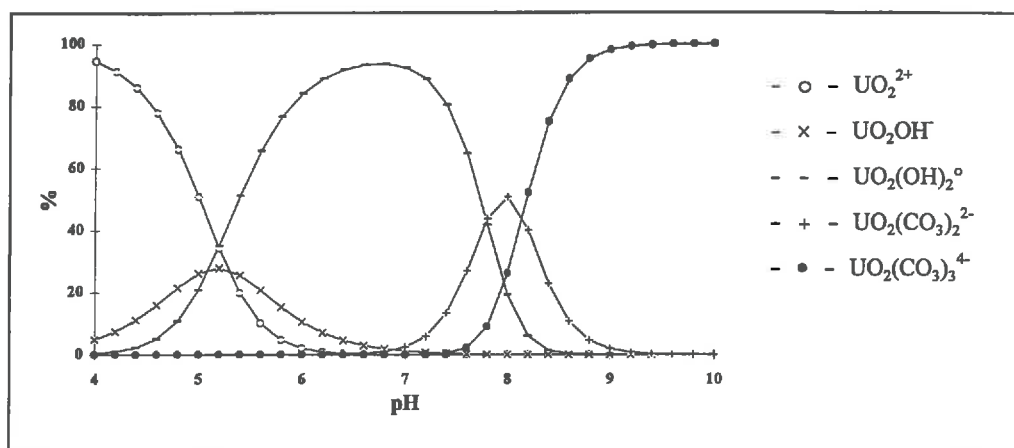


Figure 1 Solution speciation of uranyl using the constants listed in table 2 ($[\text{UO}_2^{2+}]_{\text{total}} = 1 \mu\text{M}$; $[\text{H}_2\text{CO}_3^{\circ}]_{\text{free}} = 16.4 \mu\text{M}$; $[\text{H}_4\text{SiO}_4^{\circ}]_{\text{total}} = 0.9 \text{ mM}$)

Table 2 Equilibrium constants ($\log K$) for the solution speciation ($I = 0 \text{ M}$; Grenthe et al., 1992; Stumm and Morgan, 1996)

Reaction	$\log K$
$\text{UO}_2^{2+} - \text{H}^+ + \text{H}_2\text{O} \leftrightarrow \text{UO}_2\text{OH}^+$	-5.2
$\text{UO}_2^{2+} - 2 \text{H}^+ + 2 \text{H}_2\text{O} \leftrightarrow \text{UO}_2(\text{OH})_2^{\circ}$	-10.3
$\text{UO}_2^{2+} + \text{H}_2\text{CO}_3^{\circ} - 2 \text{H}^+ \leftrightarrow \text{UO}_2\text{CO}_3^{\circ}(\text{aq.})$	-6.98
$\text{UO}_2^{2+} + 2 \text{H}_2\text{CO}_3^{\circ} - 4 \text{H}^+ \leftrightarrow \text{UO}_2(\text{CO}_3)_2^{2-}$	-16.42
$\text{UO}_2^{2+} + 3 \text{H}_2\text{CO}_3^{\circ} - 6 \text{H}^+ \leftrightarrow \text{UO}_2(\text{CO}_3)_3^{4-}$	-28.44
$\text{UO}_2^{2+} + \text{H}_4\text{SiO}_4^{\circ} - \text{H}^+ \leftrightarrow \text{UO}_2\text{H}_3\text{SiO}_4^+$	-2.4
$\text{H}_2\text{O} - \text{H}^+ \leftrightarrow \text{OH}^-$	-14
$\text{H}_4\text{SiO}_4^{\circ} - \text{H}^+ \leftrightarrow \text{H}_3\text{SiO}_4^-$	-9.74
$\text{H}_4\text{SiO}_4^{\circ} - 2 \text{H}^+ \leftrightarrow \text{H}_2\text{SiO}_4^{2-}$	-22.73
$\text{H}_2\text{CO}_3^{\circ} - \text{H}^+ \leftrightarrow \text{HCO}_3^-$	-6.35
$\text{H}_2\text{CO}_3^{\circ} - 2 \text{H}^+ \leftrightarrow \text{CO}_3^{2-}$	-16.68

The sum of concentrations of all emitting surface complexes is therefore equal to the total sorbed concentration S_{total} .

$$S_{\text{total}} = \sum_{i=1}^n S_i \quad (4)$$

Wave number resolved data (spectra)

At a given time t the measured luminescence intensity $I(\nu)$ (eq. 3) can be simplified to:

$$I(\nu) = \sum_{i=1}^n \omega_i^t(\nu) S_i, \quad (5)$$

where $\omega_i^t(\nu)$ is the characteristic spectrum of complex i at time t . Equation (5) is analogous to the Lambert-Beer law for absorption. The luminescence of an series of suspensions is given by the matrix equation (6).

$$\mathbf{I}(l,s) = \mathbf{w}(l,n) \mathbf{S}(n,s) \quad (6)$$

with

$\mathbf{I}(l,s)$ matrix of the measured luminescence spectra
 $\mathbf{w}(l,n)$ matrix of the luminescence spectra of the significantly different complexes
 $\mathbf{S}(n,s)$ matrix of the relative concentrations

and

l number of data points per spectrum
 s number of solutions (or measured spectra)
 n number of significantly different complexes

The mathematical task to be completed is to decompose the matrix of the luminescence data $\mathbf{I}(l,s)$ to a linear product of the matrices of the relative concentrations of the luminescent complexes $\mathbf{S}(n,s)$ and their specific luminescence spectra $\mathbf{w}(l,n)$.

Singular value decomposition of $\mathbf{I}(l,s)$ allows the determination of the number of emitting species n . Under the following conditions evolving factor analysis (EFA, Gampp et al., 1989) can be used for the model-free decomposition of the matrix $\mathbf{I}(l,s)$ after the number of species have been determined:

1. linear relationship between the measured luminescence intensity at the time t and the concentration of the luminescent complex S_i (eq. 5),
2. mass conservation (eq. 4),
3. the first and the last spectrum are due to only one species, respectively,
4. while passing from one pH to the next we observe the appearance of maximal one new emitting species and
5. the species disappear as pH increases in the same order as they have appeared (« first in - first out »).

Spectra are considered as « fingerprints ». The general composition of uranyl spectra is only partly known due to the rather complicated relation between the molecular near-order (distances and symmetries within the uranyl ion) and the characteristics of the emitted luminescence light (intensity, lifetime and wave number). Therefore at this stage no mathematical model of the experimental spectra shall be performed.

Time resolved integral values of the luminescence intensity (decays)

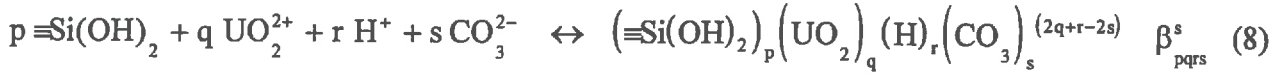
The EFA of the spectra indicated that mainly two complexes dominate the overall luminescence decay of the uranyl containing suspensions. Thus equation (3) can be reduced to a two term equation. At a given wave number ν (or within a given ν range) the decay is described by:

$$I(t) = I_{0,1} \exp\left(-\frac{t}{\tau_1}\right) \omega_1^0 S_1 + I_{0,2} \exp\left(-\frac{t}{\tau_2}\right) \omega_2^0 S_2 \quad (7)$$

The experimental intensity integral $I(t)$ between 19000 and 20000 cm^{-1} was adjusted. Mono-exponential decays were found at very low and very high pH values confirming the existence of mainly one luminescent surface complexes at extreme pH values, respectively. The luminescence decays of the intermediate pH values were adjusted assuming the lifetimes obtained at extreme pH and fitting the initial intensities. The experimental data could be described by the proposed model (bi-exponential decay) in the studied time gate (40.1 - 600.1 μs).

Surface complexation modelling

The adsorption of uranyl ions onto silica can be described at equilibrium by the following general complexation equation:



where β_{pqrs}^s is the conditional equilibrium constant, p, q, r and s are the (positive or negative) stoichiometry coefficients. The conditional equilibrium constant includes activity coefficients for solution species which were calculated with the Davies equation (Davies, 1962). Activity coefficients for all surface species are assumed to be equal to 1.0. $\equiv \text{Si}(\text{OH})_2$ is an hypothetical average surface adsorption site, susceptible to loose one proton according to:



The total concentrations of surface sites, uranyl and protons are given by eq. (10) to (12).

$$[\equiv \text{Si}(\text{OH})_2]_{\text{total}} = \sum_p \sum_q \sum_r \sum_s p \beta_{pqrs}^s [\equiv \text{Si}(\text{OH})_2]^p [\text{UO}_2^{2+}]^q [\text{H}^+]^r [\text{CO}_3^{2-}]^s \quad (10)$$

$$[\text{UO}_2^{2+}]_{\text{total}} = \sum_p \sum_q \sum_r \sum_s q \beta_{pqrs}^s [\equiv \text{Si}(\text{OH})_2]^p [\text{UO}_2^{2+}]^q [\text{H}^+]^r [\text{CO}_3^{2-}]^s \quad (11)$$

$$[\text{H}^+]_{\text{total}} = \sum_p \sum_q \sum_r \sum_s r \beta_{pqrs}^s [\equiv \text{Si}(\text{OH})_2]^p [\text{UO}_2^{2+}]^q [\text{H}^+]^r [\text{CO}_3^{2-}]^s \quad (12)$$

The concentrations of the carbonate ions is controlled by the equilibrium with the atmosphere resulting in a constant free concentrations of $\text{H}_2\text{CO}_3^\circ$.

The formation equilibrium constants of charged surface complexes (eq. 8 and 10) have to be corrected for the coulombic energy of the charged surface to obtain the corresponding intrinsic constants.

$$\beta_{pqrs(\text{int})}^s = \beta_{pqrs}^s \exp\left(\frac{(2q+r-2s)F\psi}{RT}\right) \quad (13)$$

where ψ is the acting surface potential. The total molar charge of the surface σ_t is given by

$$\sigma_t = \sum_p \sum_q \sum_r \sum_s (2q+r-2s) \beta_{pqrs}^s [\equiv \text{Si}(\text{OH})_2]^p [\text{UO}_2^{2+}]^q [\text{H}^+]^r [\text{CO}_3^{2-}]^s \quad (14)$$

To relate the total molar surface charge σ_t to the surface potential ψ the constant capacitance model (Schindler and Gamsjaeger, 1972) was used as the formation of outer sphere complexes could be excluded (Dent et al., 1992, Reich et al., 1996).

$$\psi = \frac{\sigma_t F}{A_s c_p \kappa} \quad (15)$$

A_s is the specific surface area ($\text{m}^2 \text{g}^{-1}$), c_p is the particle concentration (g dm^{-3}) and F is the Faraday constant, κ is the capacitance (F m^{-2}). The intrinsic stability constants, the total site concentration and the capacitance were deduced from the adjustment of the experimental luminescence data using the program GRFIT (Ludwig, 1993). The evaluation was based mainly on the goodness of fit (Westall, 1982).

RESULTS

Uranyl ions are nearly completely removed from solution between pH 5.5 and 8 by adsorption on filterable silica (figure 2).

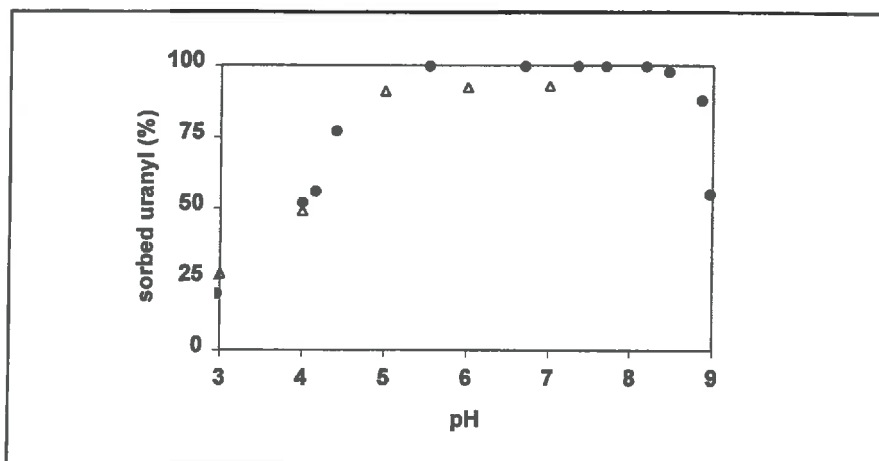


Figure 2 Experimental values of uranyl sorption as a function of pH (full circles: this study, open triangles: Dent et al., 1991)

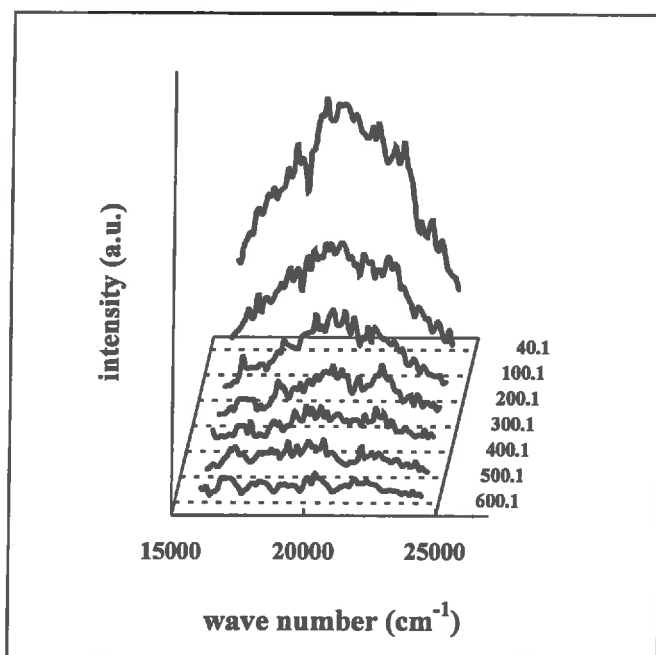


Figure 3 Time-resolved luminescence spectra of an aerosil suspension at pH 5.11 ($c_p = 1 \text{ g dm}^{-3}$; no uranyl ions, numbers are ns after the laser shot)

In order to characterise uranyl surface complexes by their emitted luminescence spectra, one must first eliminate all other luminescence components. The luminescence properties of aerosil suspensions recorded in absence of uranyl (figure 3) depict a broad, symmetrical, rather noisy maximum with a relatively short lifetime at about 20000 cm^{-1} . This maximum did not change its position on the wave number scale as function of pH (figure 4). Therefore the pure silica spectrum was subtracted from all spectra of the uranyl-silica-water system resulting in a zero baseline outside characteristic peaks of the uranyl luminescence.

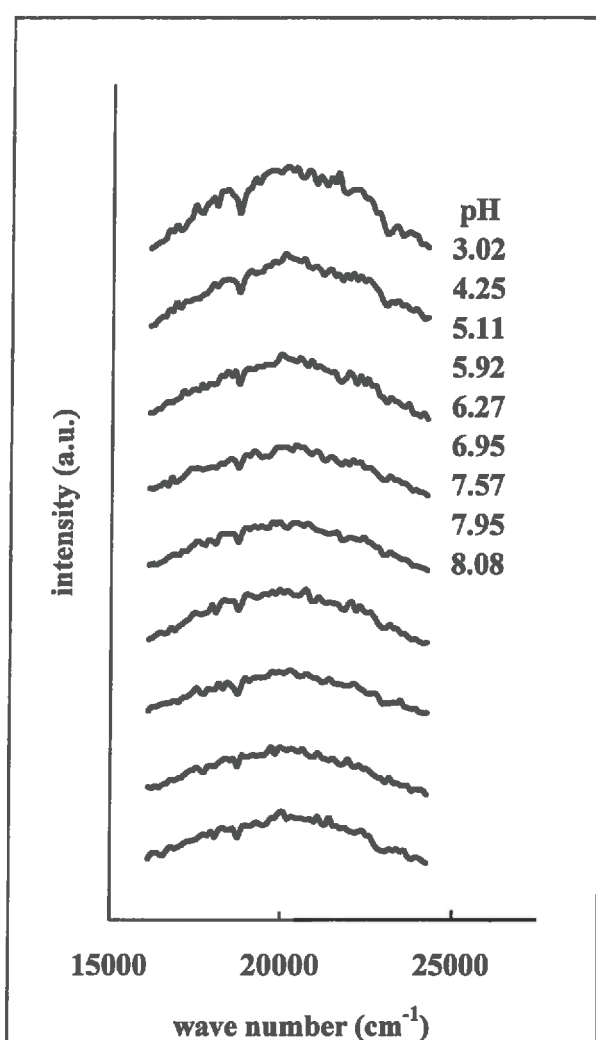


Figure 4 Luminescence spectra of aerosil suspensions at different pH (40.1 μs after the laser shot, $c_p = 1\text{ g dm}^{-3}$; no uranyl)

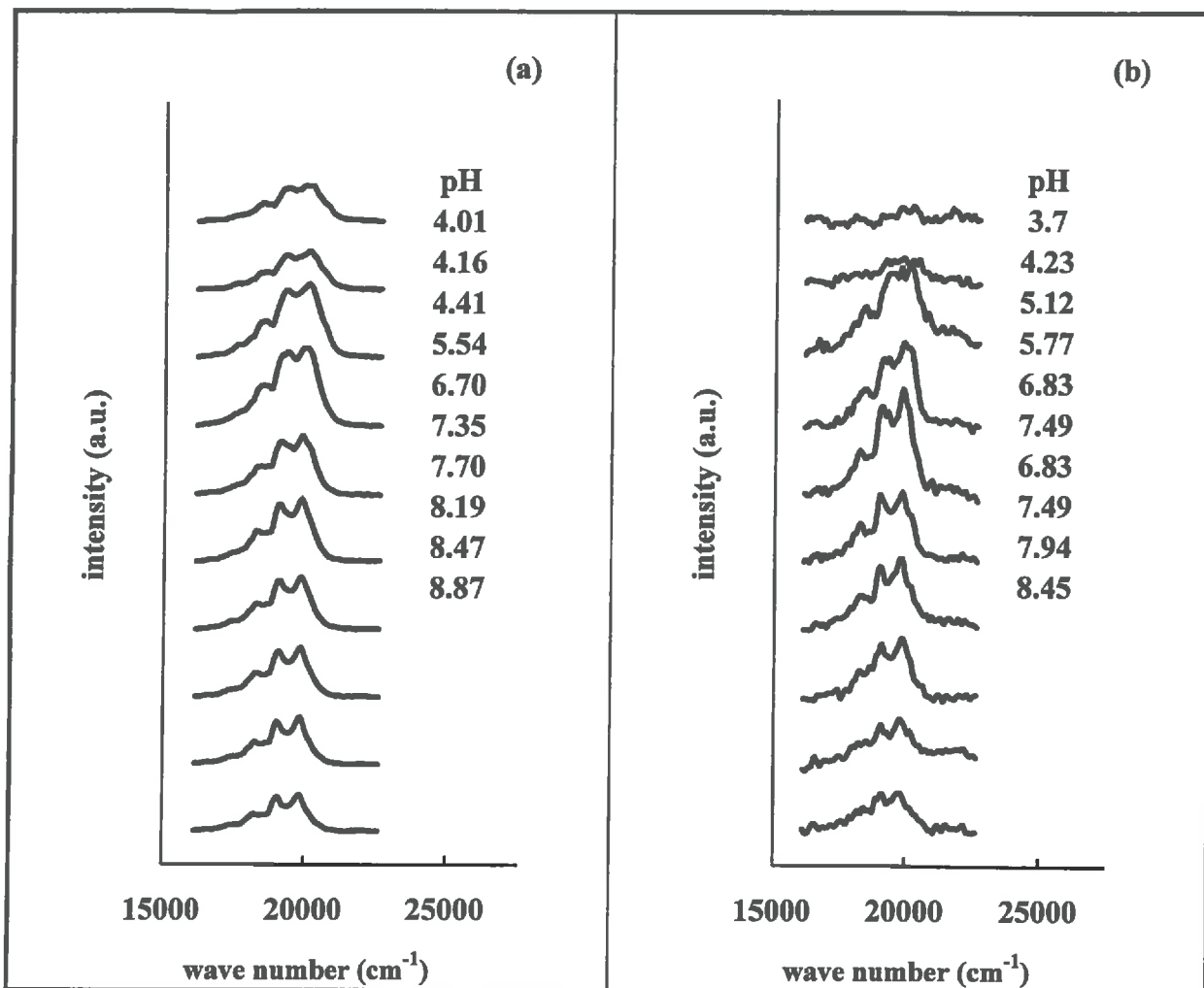


Figure 5 Background corrected spectra of the aerosil suspensions ($c_p = 1 \text{ g cm}^{-3}$) containing $1 \text{ }\mu\text{M}$ (a) and $0.1 \text{ }\mu\text{M}$ (b) uranyl; numbers represent the pH; intensity values are traced in the same arbitrary units as figure 4 for (b) and divided by 10 for (a).

Luminescence spectra at a total uranyl concentration of 1 and $0.1 \text{ }\mu\text{M}$ are compared in figure 5. The same trend was observed in both series. It appeared, that the luminescence signal was very weak at pH values below 4. Between pH 4 and 4.5 the intensity increased enormously as sorption shifts from 50 % to 80 %. The luminescence spectra in this pH range show the same maxima positions. Thus the same uranyl species is assumed to dominate the luminescence signal. In the 4.5 to 5.5 pH range the luminescence intensity remained at the same elevated level, but a second component appeared in the spectra, which is characterised by maxima at smaller wave numbers (about 250 cm^{-1} red-shift).

In the pH range 5.5 to 8 the spectra were dominated by this second component spectrum characterised by a better resolution, a larger life time and a smaller intensity at 40.1 μs (figure 6). In the 5.5 to 8 pH range we observed a decrease of the luminescence signal which is in contrast with total sorbed uranyl concentration which remains nearly equal to the total uranyl concentration (figure 1).

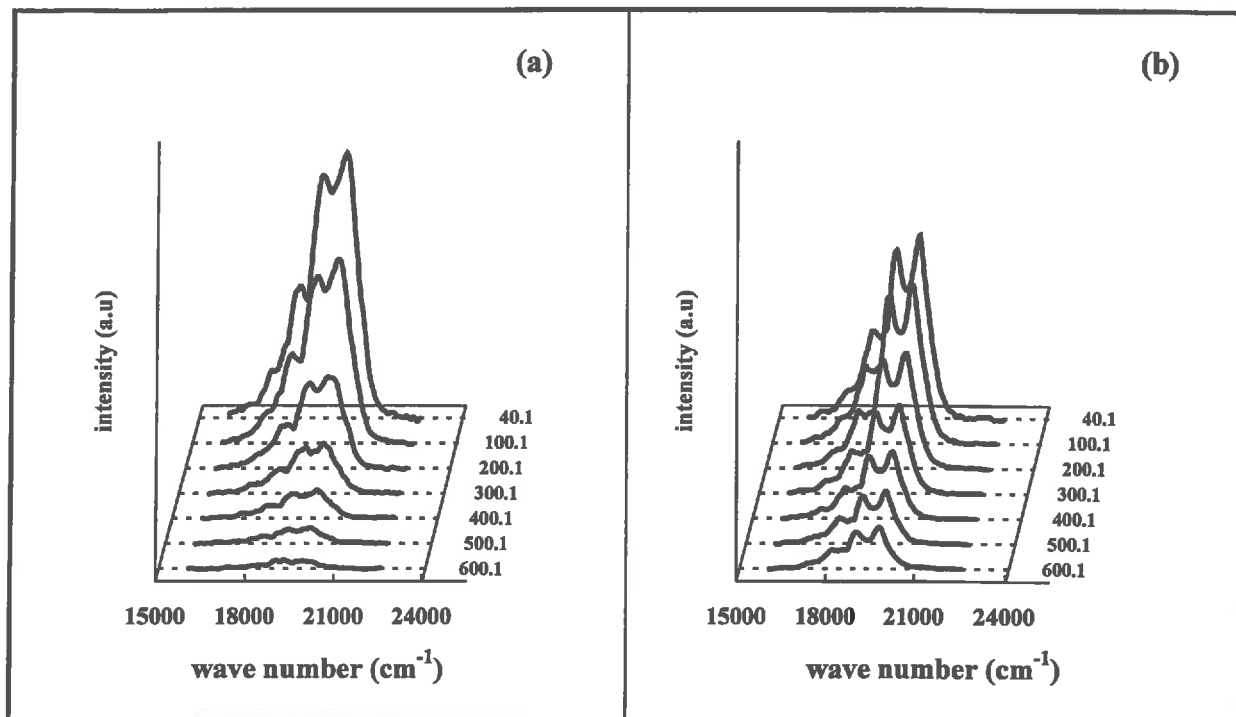


Figure 6 Background corrected time-resolved fluorescence spectra of aerosil suspensions at pH 4.41 (a) and 8.19 (b); numbers represent μs after the laser shot; intensity is traced in the same arbitrary units; $[\text{UO}_2^{2+}]_{\text{total}} = 1 \mu\text{M}$; $c_p = 1 \text{ g dm}^{-3}$

The spectra shown in figure 5a (total uranyl concentration of $1 \mu\text{M}$) were analysed by the evolving factor analysis (EFA) data procedure. The change of the dominance from one component to the other between pH 5.5 and 6.7 is confirmed (figure 7). The experimental data at a total uranyl concentration of $0.1 \mu\text{M}$ were adjusted with the same two composite spectra, which will be discussed later. The spectrum at pH 5.1 is still completely controlled by the first component spectrum, whereas at pH 5.8 both spectra have about the same importance. At pH 6.8 the second component dominates the spectrum (figure 8).

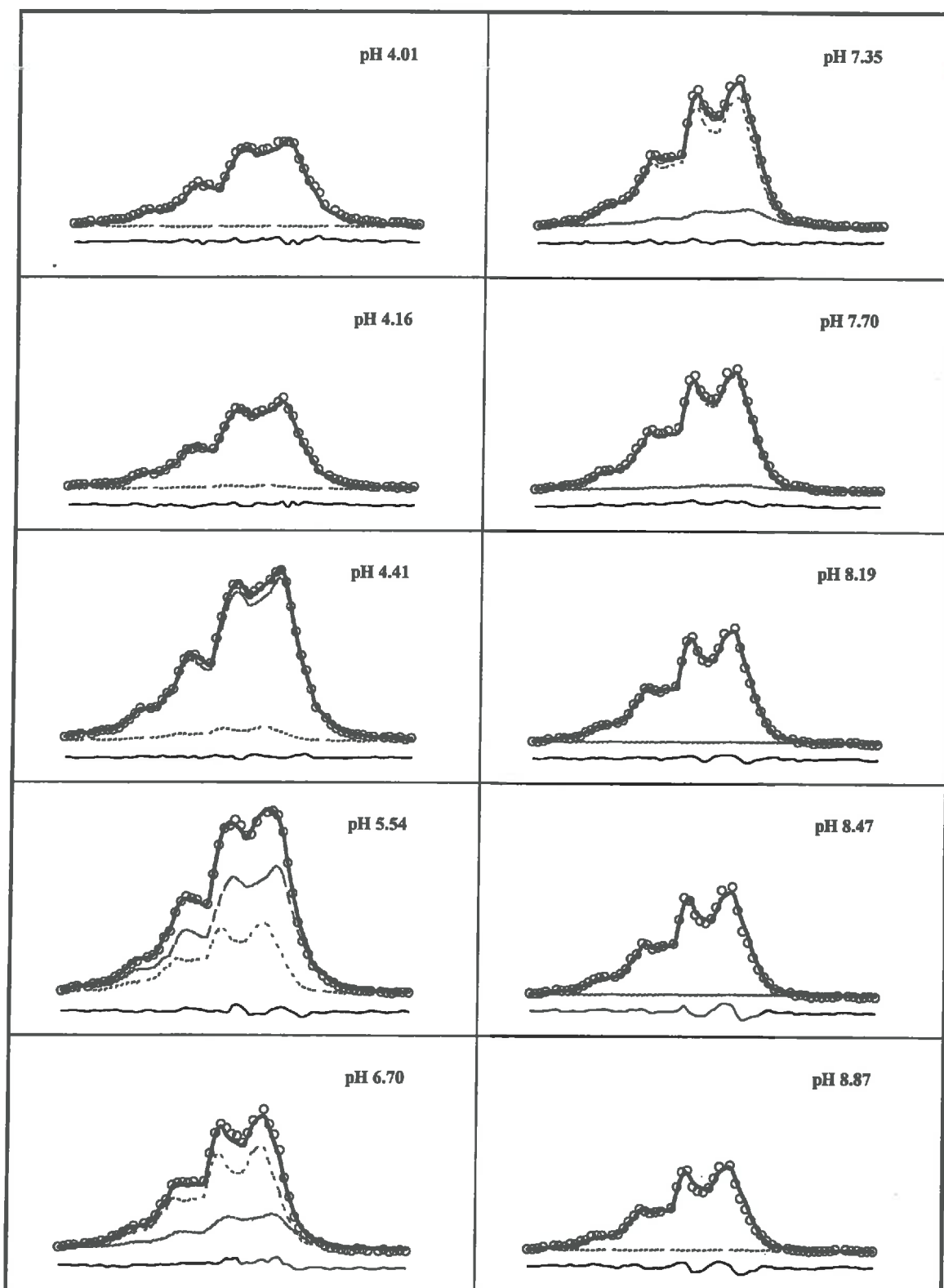


Figure 7 Background corrected experimental spectra (o) at total uranyl concentration of 1 μM adjusted using the composite spectra of figure 12 (dashed/dotted line: prevailing spectra at low/high pH, thick line: sum of both, thin line: remaining error; $c_p = 1 \text{ g dm}^{-3}$).

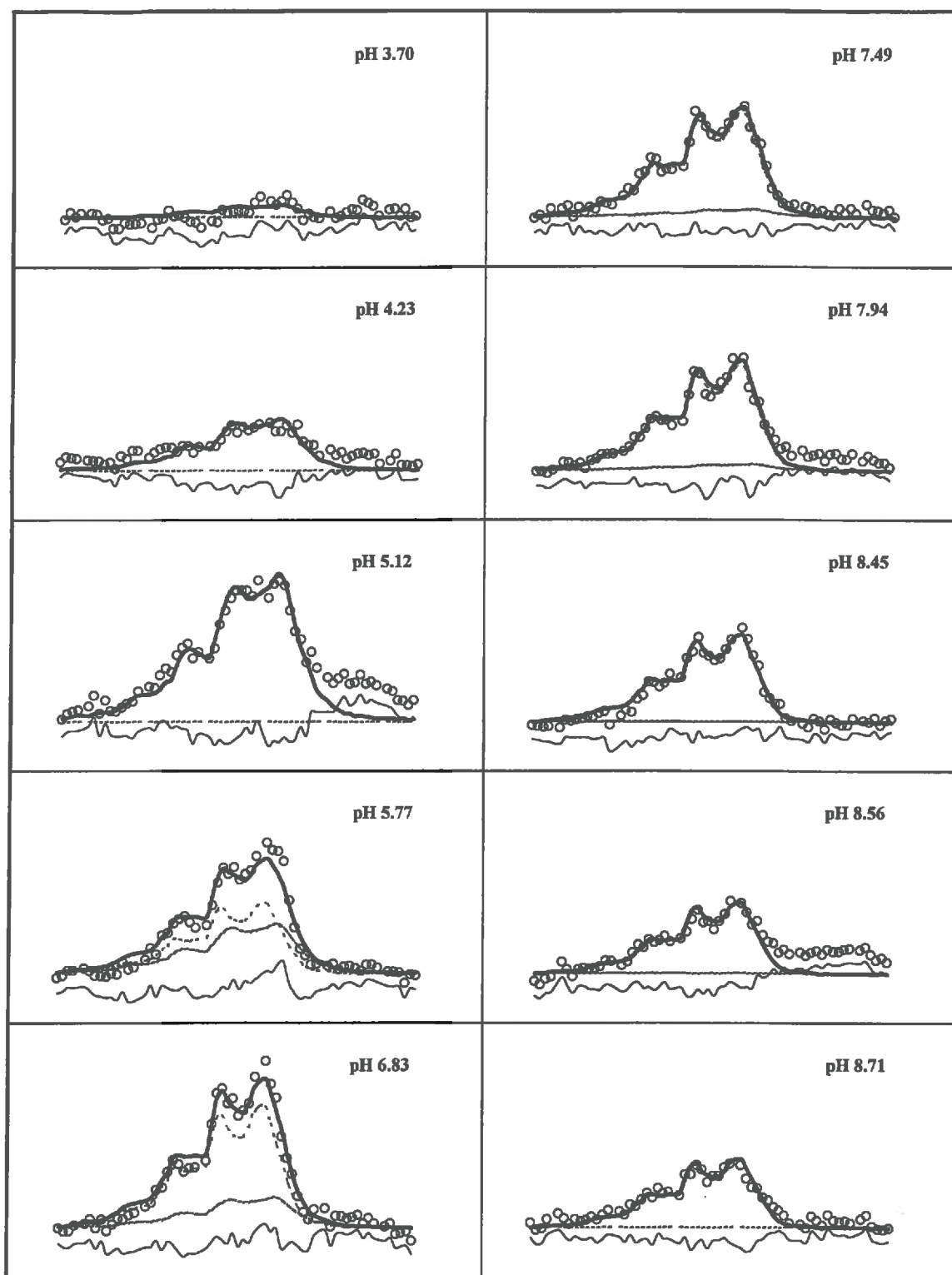


Figure 8 Same as figure 7, but for a total uranyl concentration of 0.1 μM .

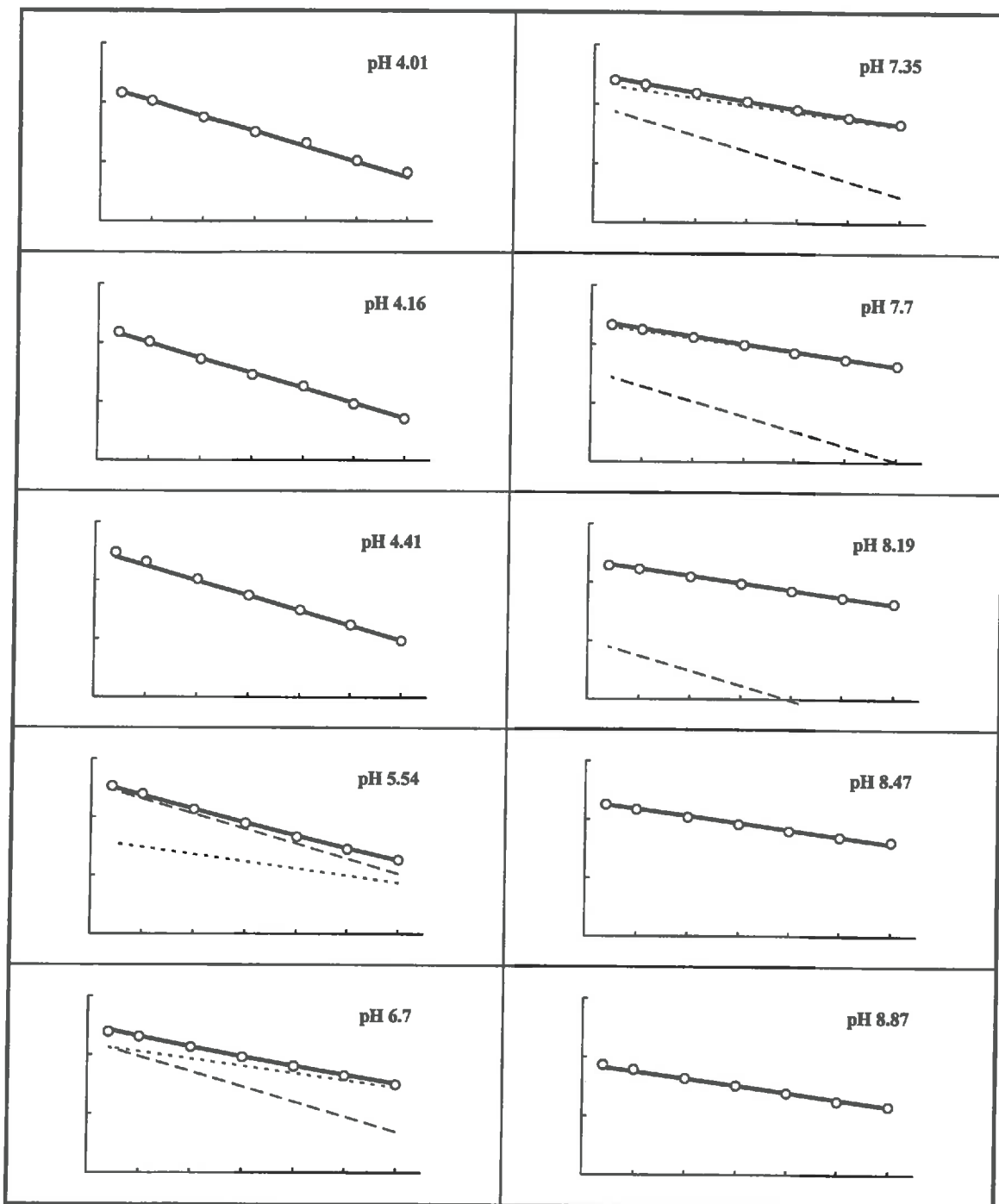


Figure 9 Background corrected experimental decays (o) for 1 μM total uranyl concentration in the suspension and bi-exponential adjustment (dashed/dotted line: mono-exponential decay with a life time of 170/360 μs ; x-axis: 0 $\mu\text{s} \leq t \leq 600 \mu\text{s}$; y-axis: -1 a.u. $\leq \log(I) \leq 2$ a.u.).

As complementary information, a two-exponential decay function was adjusted to the experimental decays of the 19000 to 20000 cm^{-1} intensity integral (eq. 7; figure 9). Again the shift from one surface complex to another occurs between pH 5.54 and 6.7. The mono-exponential decays at very low and very high pH values did not completely exclude the existence of minor components at these pH values, but confirmed the dominance of one species in each pH range. This confirmed the evolving factor analysis results. The determined lifetimes were 170 ± 25 and 360 ± 50 μs for samples prepared at low and high pH values, respectively.

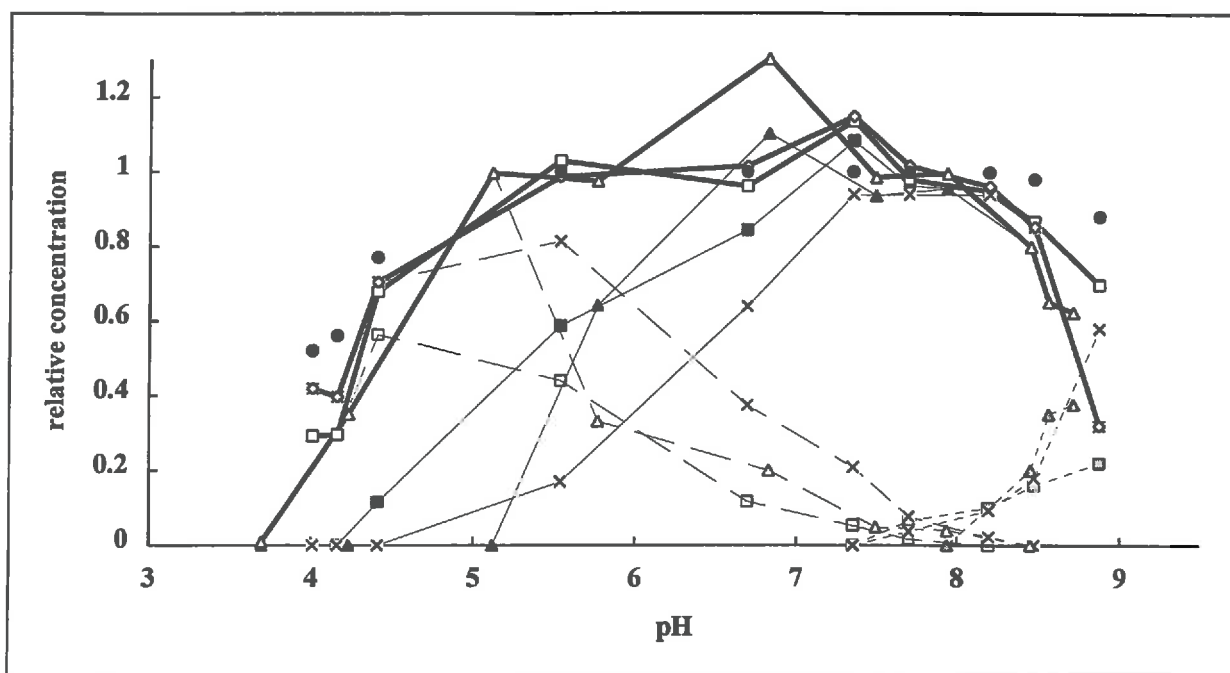


Figure 10 Comparison of the results of the data adjustments in figures 7 - 9

- spectra (1.67 & 0.48) at a total uranyl concentration 1 μM
- × decays (1.14 & 0.59) at a total uranyl concentration 1 μM ;
- △ spectra (1.05 & 0.54) at a total uranyl concentration 0.1 μM ;
- (numbers in parentheses represent ω_i^0 of eq. 2)
- experimental total sorbed concentration
- slashed, thin and dotted lines first, second and third complex;
- thick lines sum of the first and second complex;

As required for mass conservation (eq. 4) the weighed sum of the intensities of both luminescence components was adjusted to the experimentally determined total sorbed

concentration (weighing factors ω_i^0 of eq. 2 are given in figure 10 caption) in the 5.5 to 8.0 pH range. When the relative luminescence intensities of both complexes are compared, it appears that the low pH complex has about the double intensity (1.3 ± 0.4) when compared to the high pH one (0.54 ± 0.06).

A gap between the experimentally determined sorbed concentration and the sum of the intensities was observed between pH 8 and 9. This gap was interpreted as the presence of a carbonate-containing non-luminescent ternary surface complex (figure 10). Bernhard et al. (1996) reported the complexation with carbonate quenching the luminescence and therefore leading to no measurable signal at 1 μ s after the laser pulse. The same found Kato et al. (1994) who could not detect a luminescence signal of uranyl carbonate complexes in solution.

The similitude of sorption and spectral data obtained for total uranyl concentrations with one order of magnitude difference pointed out to the absence of surface uranium hydroxy-polymers. Therefore the results presented in figure 10, were described by a model in which the following three different surface complexes were assumed: two silica-uranyl-hydroxyl-complexes releasing 2 (I) and 3 (II) protons and one ternary silica-uranyl-hydroxyl-carbonato-complex releasing also 3 protons (III). All complexes are supposed to have bidentate structure.

Table 3 Intrinsic constants (logK) for the silica surface speciation

(Constant Capacitance Model; $c_p = 1 \text{ g dm}^{-3}$; $A_s = 169 \text{ m}^2 \text{ g}^{-1}$; $\kappa = 7 \text{ F m}^{-2}$; $I = 0 \text{ M}$;
 $[\equiv\text{Si}(\text{OH})_2]_{\text{total}} = 0.51 \text{ mM}$; $[\text{H}_2\text{CO}_3^\circ]_{\text{free}} = 16.4 \text{ }\mu\text{M}$; $[\text{H}_4\text{SiO}_4^\circ]_{\text{total}} = 0.9 \text{ mM}$; $[\text{UO}_2^{2+}]_{\text{total}} = 1 \text{ }\mu\text{M}$)

Reactions	logK
$\equiv\text{Si}(\text{OH})_2 - \text{H}^+ \leftrightarrow \equiv\text{SiO}_2\text{H}^-$	-6.98
$\equiv\text{Si}(\text{OH})_2 + \text{UO}_2^{2+} - 2 \text{H}^+ \leftrightarrow \equiv\text{SiO}_2\text{UO}_2^\circ$	-4.8
$\equiv\text{Si}(\text{OH})_2 + \text{UO}_2^{2+} - 3 \text{H}^+ + \text{H}_2\text{O} \leftrightarrow \equiv\text{SiO}_2\text{UO}_2\text{OH}^-$	-10.46
$\equiv\text{Si}(\text{OH})_2 + \text{UO}_2^{2+} + \text{H}_2\text{CO}_3^\circ - 5 \text{H}^+ + \text{H}_2\text{O} \leftrightarrow \equiv\text{SiO}_2\text{UO}_2\text{OHCO}_3^{3-}$	-22.14

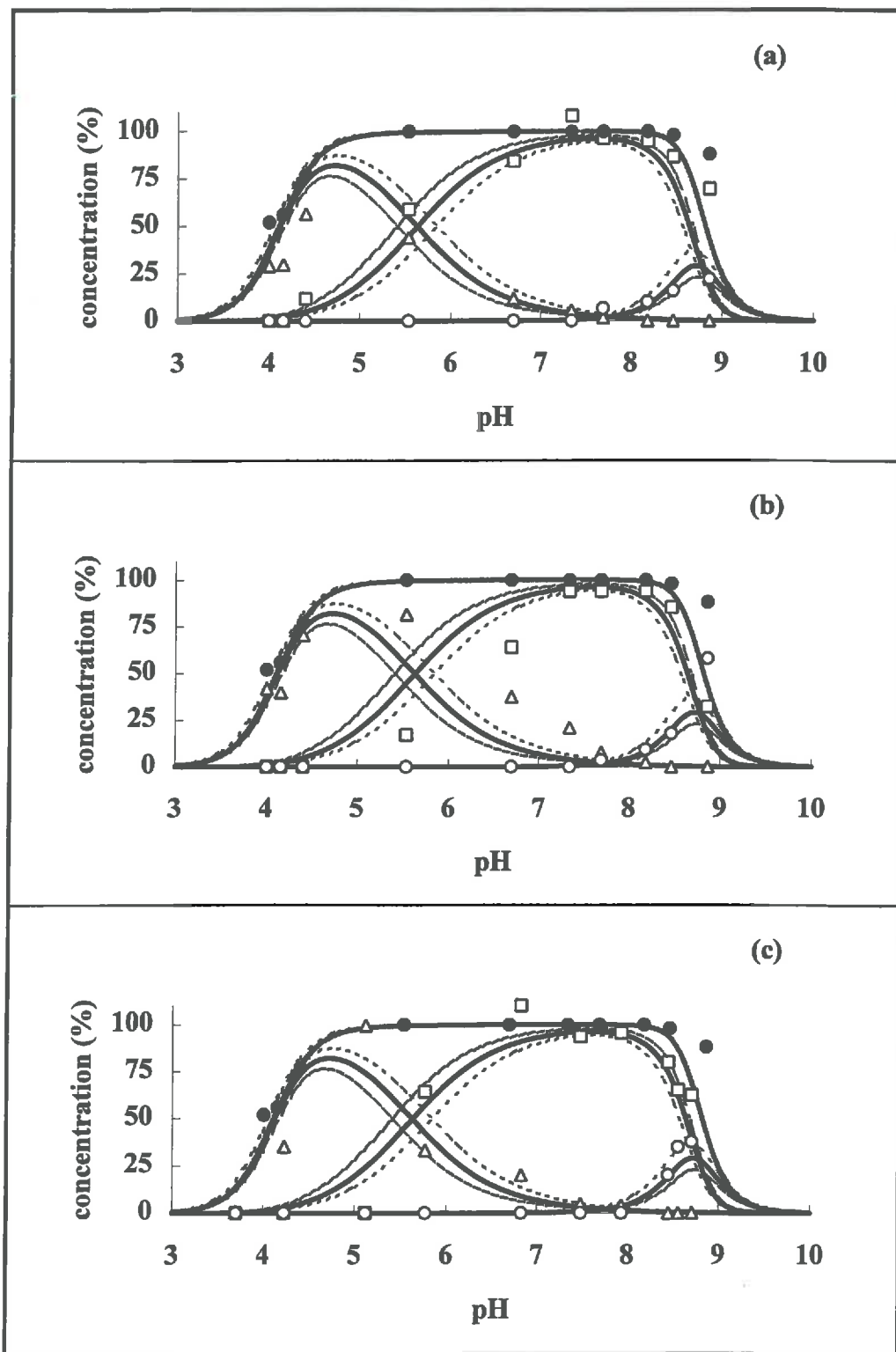


Figure 11 Uranyl surface speciation on the bases of the spectra (40 μ s after the laser shot) at a total uranyl concentration of 1 μ M (a) and 0.1 μ M (c), and of the exponential decays at the total uranyl concentration of 1 μ M (b) (constants in table 1, symbols \square , Δ , \circ and \bullet represent the lower and the higher protonated state; the carbonated surface species and experimental total sorbed concentration, respectively; dashed and dotted lines show the sensitivity analysis).

The best fit was obtained within the constant capacitance model when a capacitance of 7 F m^{-2} was assumed. The high capacitance value indicates a very thin capacitor layer. The corresponding logarithmic complexation constants are summarised in table 3. The logarithmic deprotonation constant was assumed to be 6.94 in accordance with the literature (Charlet et al., 1993; Osthols, 1995).

A sensitive analysis was performed on the complexation constant values. The most accurately defined points were the limits between the dominance fields. Therefore we evaluated the impact of a 0.1 log unit change for the complexation constants. As represented by the slashed and dotted lines in figure 11 constants of the first and the last complex were elevated when the one of the complex in the middle was diminished. It appeared that a 0.1 log unit change of the constants did not change the adsorption or the desorption edge, but shifted the limit between the dominance fields of the first and the second complex from 5.5 to 5.9 (figure 10). Modelled curves were closer to experimental data deduced from the spectra (with fixed time) than to those deduced from fixed energy (figure 11).

So far we have considered the luminescence spectra as « fingerprints » used only for the identification of the two surface complexes $\equiv\text{SiO}_2\text{UO}_2^\circ$ and $\equiv\text{SiO}_2\text{UO}_2\text{OH}$. However, they can be interpreted in terms of energy levels of excited state.

Six Gaussian peaks (figure 12) with the same peak width (600 cm^{-1}) are identified. The distance between the peaks was estimated at 800 cm^{-1} for the high pH spectrum and 830 cm^{-1} for the low pH spectrum. The 250 cm^{-1} red shift of the entire spectrum when passing from low to high pH values was already mentioned. The high pH spectrum is characterised by a much lower initial intensity for the same emitting concentration. These results shall now be compared to experimental data and theories from the literature.

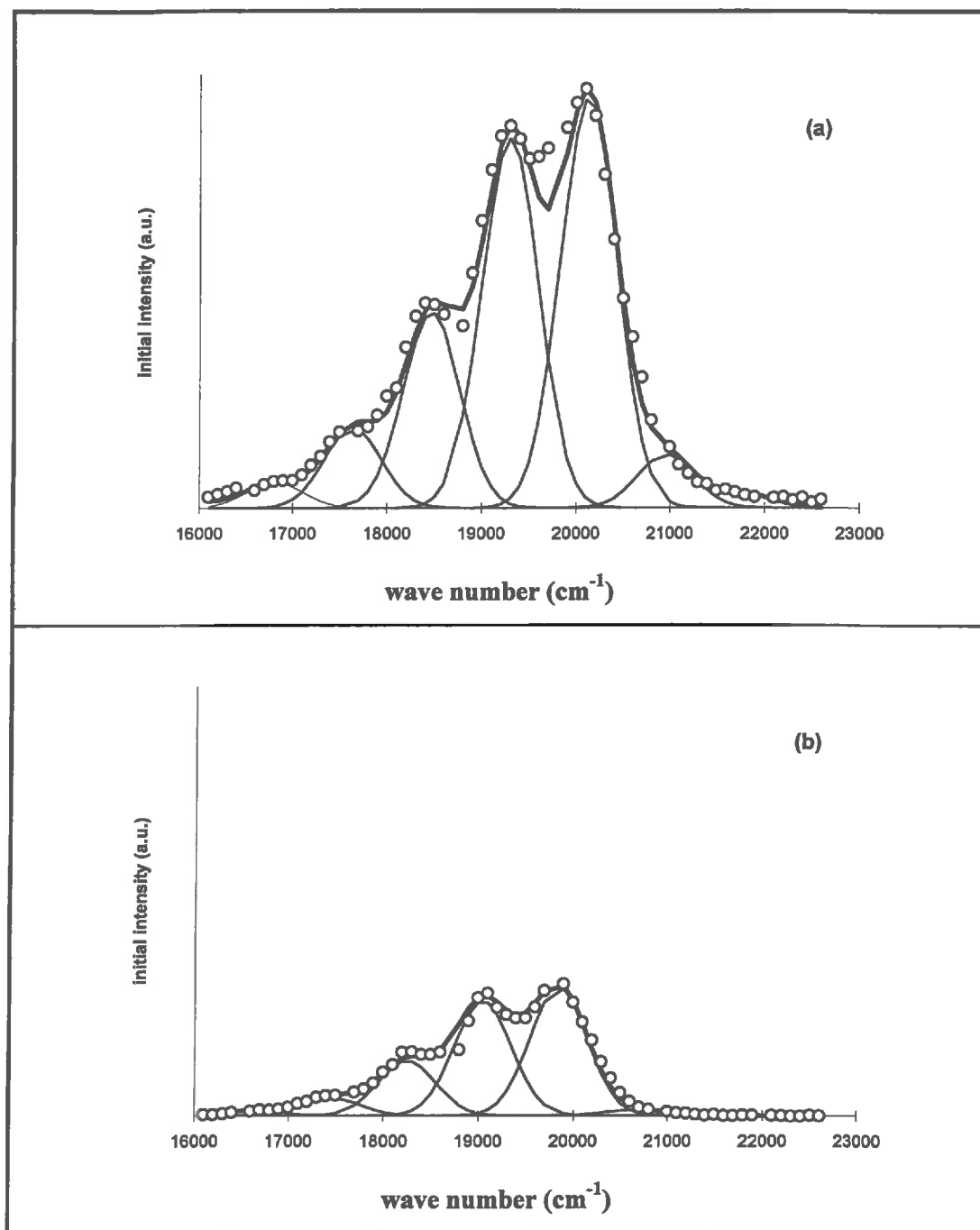


Figure 12 Composite spectra of the data adjustment using «evolving factor analysis» (Gampp et al., 1987) extrapolated to time equal zero and normalised to 1 μM sorbed uranyl.

DISCUSSION

The luminescence of the uranyl ion is a consequence of the excitation of one π bonding electron and an intersystem crossing into triplet state into an unoccupied 5f orbital of uranium (excited state; Moriyasu et al., 1977b). The emitted wave length should therefore be directly related to the bound length inside the uranyl ion.

The luminescence emission spectrum of the non-hydrolysed uranyl ion was extensively studied by Bell and Biggers (1968). They attributed the typical multi-peak pattern of the spectrum to two excited states with an energy difference to the ground state of 21270 and 20502 cm^{-1} . They showed the five lowest energy bands to have an average spacing of $855 \pm 20 \text{ cm}^{-1}$ and to result from the transition from the 20502 cm^{-1} energy level. They found the spacing to agree well with the Raman and IR frequencies of 850 cm^{-1} found for the symmetric vibration of the uranyl ion in its ground state. About the same distances between maxima were found by Moulin et al. (1995). The highest energy luminescence band (21270 cm^{-1}) was interpreted as the indication of a second excited energy level, with a resulting distance to the second highest energy luminescence band by only 768 cm^{-1} .

The life time seems to be mainly related to the symmetry; one factor which controls the life time of the excited state is the symmetry of the complexes. Transitions which are forbidden at high symmetry become feasible in lower symmetry. A second lifetime controlling factor is the quenching effect due to energy transfer (e.g. to molecular vibrators as O-H). If the uranyl ion is surrounded by 5 water molecules a rotational $D_{\infty h}$ symmetry (Glinka et al., 1995) is found. If several non-saturated oxygen atoms enter the equatorial plane the uranyl molecule is distorted resulting in elevated lifetimes.

These spectroscopic information have to be correlated to the molecular near-order of the uranyl ion. The distance of the U-O_{ax} bonding $R_{\text{U-O}_{\text{ax}}}^{\text{VI}}$ in nm is related to the wave-number of the symmetric stretching mode $\nu_1 (\Sigma_g^+, \text{Raman active, IR inactive, in } \text{cm}^{-1})$ for several solid uranyl compounds by Barlett and Cooney (1989):

$$R_{U-O_{ax}}^{VI} = 10.650(v_1)^{-2/3} + 0.0575 \quad (9)$$

In an acid aqueous solution without ligands the uranium atom is supposed to be surrounded by 5 equatorial H₂O molecules. The axial U-O_{ax} distance is 0.1702 nm and the equatorial one U-O_{eq} is 0.2421 nm. (Aberg et al., 1983). The inverse relationship between the average U-O_{eq} and U-O_{ax} distances in uranyl compounds is well defined (Veal et al., 1987). It is based on the bond valence model stating the bond strength ϵ (in valence units, v.u.) is related to the bond length:

$$\epsilon = \exp\left(\frac{R_{U-O}^{VI} - R_{exp}}{b}\right) \quad (10)$$

where R_{U-O}^{VI} is the bond valence parameter (0.2075 nm after Brese and O'Keefe, 1991) and b is equal to 0.037 nm (Brown and Altermatt, 1985). R_{exp} is the experimental U-O distance. Both distances are inversely related because the sum of bond valences for all bonds to the concerned atom should equal the atoms formal valence (Pauling, 1929) which is now rather called oxidation number. The oxidation number +6 of uranium is equal to the sum of 2 ϵ_{ax} and 4 to 6 ϵ_{eq} . For the aqueous uranyl ion one finds 5.5 v.u. for the two axial oxygen's and 2 v.u. for the five equatorial oxygen's. The proposed model slightly overestimates the sum of the bonding strength of the uranium(VI).

The charge of the axial oxygen atoms on the other hand is approximately balanced providing a rationale for the common observation of their lack of reactivity in aqueous systems and crystalline uranyl-compounds (Farge et al., 1992). This extreme stability of uranyl group geometry limits any bonding (solution complexation as well as adsorption reaction) to the equatorial plane, thereby indirectly also changing the U-O_{ax} distance.

For the adsorption of uranyl onto silica a bridging bidentate surface complex was already proposed by Stanton and Maatman (1963). This corresponds to the structure of the uranyl surface complex on ferrihydrite reported by Waite et al. (1994), who in fact observed a splitting of the equatorial shell (table 4). Uranyl surface complexes on silica were recently studied by Reich et al. (1996), who confirmed the splitting of the equatorial shell into two

shells separated by 0.021 nm (table 4), but did not deduce a structural model of the adsorption complex from their EXAFS results.

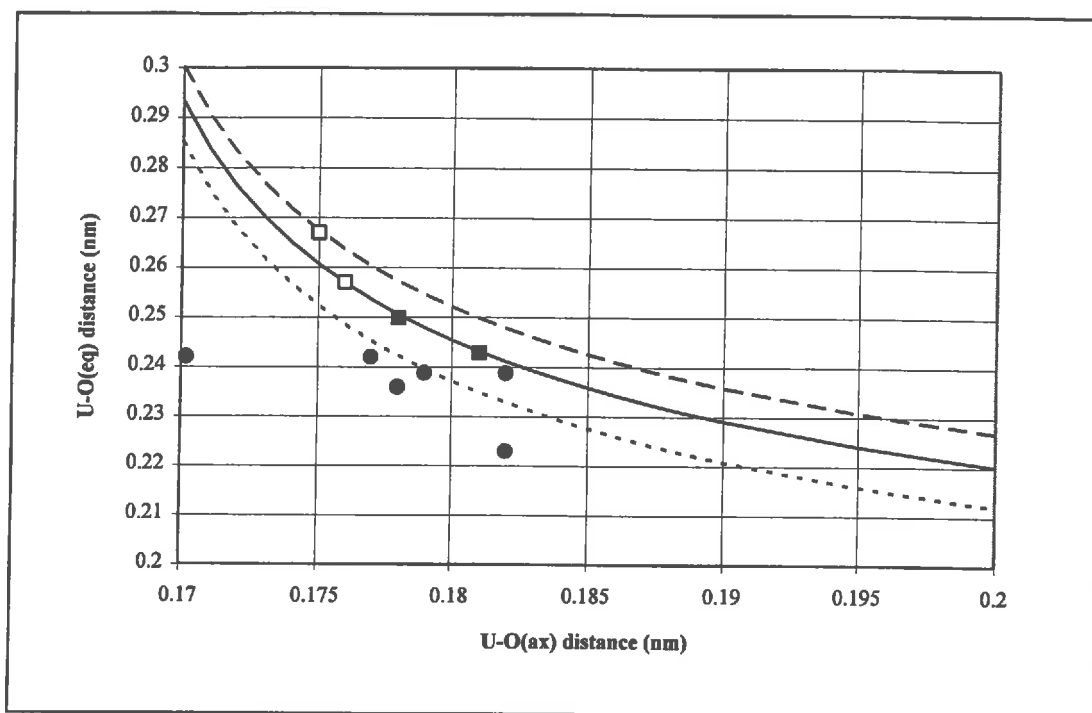


Figure 13 Relation between $U-O_{ax}$ and $U-O_{eq}$ distances for 4 (dotted line), 5 (full drawn line) and 6 (dashed line) oxygen atoms in the equatorial plane (after Veal et al., 1987; experimental values in table 4); filled circles: experimental values where both distances are known (EXAFS); open squares: $U-O_{ax}$ distances deduced from experimental Raman frequencies from literature; filled squares: $U-O_{ax}$ distances deduced from experimental luminescence frequencies from this study

The red shift of the spectrum and the much longer lifetime of uranyl, in the presence of silica particles as compared to homogeneous solution in an aqueous solution was first reported by (Wheeler and Thomas, 1984). A similar red shift was also observed by Glinka et al., 1995(a-c). But their samples were dried and heated and the luminescence behaviour of the solid was studied under continuous excitation. All luminescence measurements were done at low temperatures (70 and 4 K) making comparisons difficult.

However they reported also an important red-shift when passing from the solution sample to the solids and increasing the alteration temperature.

Table 4 Reported bond lengths of U-O_{ax} and U-O_{eq} in relation to vibration frequencies deduced ones from Raman and fluorescence spectroscopy measurements (bold written distances are obtained by EXAFS, italic written U-O_{eq} distances are estimated using eq. 9 and 10

description	U=O _{ax} nm	U-O _{eq} (coord.) nm	ν_1 Raman (cm ⁻¹) fluo distance	Reference
uranyl in HClO ₄	0.1702	0.2421 (5)	-	Aberg et al., 1983
uranyl in HClO ₄	<i>0.176</i>	<i>0.267 (5)</i>	855	Bell and Biggers, 1968
uranyl sulphate	<i>0.175</i>	<i>0.267 (6)</i>	860	Kuschnirenko et al., 1993
0.05 M uranyl nitrate	0.177	0.242 (6)	-	Thompson et al., 1997
0.05M uranyl nitrate (pH 2.75)	<i>0.174</i>	<i>0.267</i>	872	Morris et al., 1994
0.05M uranyl nitrate (pH 3.76)	<i>0.177</i>	<i>0.253</i>	840	Morris et al., 1994
uranyl sorbed on silica gel	0.178	0.229 (4) 0.250 (1.6)	-	Reich et al., 1996
uranyl sorbed onto silica low pH	<i>0.178</i>	<i>0.250</i>	830	p.w.
uranyl sorbed on ferrihydrite	0.179	0.234 (3) 0.246 (2, sorb.)	-	Waite et al., 1994
uranyl sorbed onto silica high pH	<i>0.181</i>	<i>0.243</i>	800	p.w.
UO ₂ ²⁺ in glass	0.182	0.24 (4)	-	Farges et al., 1992

When finally all known distances and luminescence properties within our studied system are compared (table 4) it appears that at this point no *quantitative* relation between luminescence properties and surface complex structures can be deduced. Several *qualitative* statements are possible.

1. Any adsorption or complexation reaction of the uranyl takes place in the equatorial plane, replacing the oxygen atoms of the water molecules by for example oxygen atoms of complexing anions or reactive surface sites.
2. As the water molecules are usually only partly replaced the symmetry of the uranyl molecule is decreased resulting in longer luminescence lifetimes. The decreasing symmetry should correspond to the splitting of the equatorial shell observed in EXAFS spectroscopy. The different reported coordination (four to six oxygen atoms) of the uranium atom in the equatorial shell (i) reflects the charge saturation of the coordinating oxygen atoms, (ii) but is also dependent from steric interactions.

3. Further on the bonding distances of uranium to the equatorial and the axial oxygen atoms are related via the Pauling Principle. Adsorption or complexation decreases the $U-O_{eq}$ distance, thereby increasing the $U-O_{ax}$ distance.
4. The $U-O_{ax}$ distance is closely related to the energy differences between the maxima within the luminescence emission spectra, and seems to control also the general spectral shift of the spectra.

When now these general conclusions are applied to our system we find:

1. The decreasing energy difference between the maxima as well as the general red-shift of the spectra reflects the intensity of the bonding in the equatorial plane. The low pH complex is assumed to be a neutral bidentate complex, two water molecules being replaced by reactive surface group oxygen atoms. The high pH surface complex is postulated to have essentially the same structure with a third water molecule being replaced by an $(OH)^-$ molecule.
2. No quantitative explication can be given at this point for the two observed lifetimes. Qualitatively it can be stated that less protons in the equatorial plane, water molecules being replaced by hydroxyl ions, causes longer luminescence lifetimes as less deactivation occurs via energy transfer into vibration modes.

We suppose that the surface complex at the water-solid-interface reported by Reich et al. (1996) for pH 3.6, the silica-uranyl-complex in the dried sample heated to 320 K (Glinka et al., 1995) and our low pH surface complex correspond to the same structure, a distorted, but still *fivefold co-ordination in the equatorial plane* resulting in shorter $U-O_{eq}$ and longer $U-O_{ax}$ bonding distances.

We assume further on that an identical molecular structure - *four-fold co-ordination in the equatorial plane* - is found in the uranyl silica glass samples of Farges et al. (1992) and the dried samples of uranyl sorbed on amorphous silica of Glinka et al. (1995) which were heated to 1200 K.

The dried samples treated at medium temperatures (Glinka et al., 1995) as well as our high pH ones are assumed to correspond to an intermediate state between the two.

CONCLUSION

TRLIL spectroscopy can be used to characterise surface species at trace level concentrations, not accessible to other techniques such as NMR or EXAFS. This is all the most important since sorption mechanisms may change with the ratio between the sorbate and the sorbing, i.e. with surface coverage the structure of the surface complexes changes as is reported by Morris et al. (1994) for the adsorption of uranyl on smectite and Chrisholm-Brause et al., (1994) on montmorillonite.

The concentration of the surface complexes were obtained from TRLIL spectroscopy data assuming the initial luminescence intensity to be proportional to the emitting complex concentration. Best adjustment of the data was obtained with a surface complexation model which includes two surface species: one complex at low pH predominant around pH 5 and characterised by the release of 2 protons ($\equiv\text{SiO}_2\text{UO}_2^\ominus$, i.e. 2 negative charges in the equatorial plane of the uranyl) and a second one at high pH predominant around 7.7 and characterised by the release of 3 protons ($\equiv\text{SiO}_2\text{UO}_2\text{OH}$, i.e. 3 negative charges in the equatorial plane). The complexation by solid silica is similar to the complexation by dissolved phosphate (Sandino, 1991). The difference between the adsorption reaction and the complexation in solution consists in the apparent location of the protons to be released upon complexation.

Uranyl carbonate ternary surface complexes have been widely postulated in the high pH range (Turner, 1995, Waite et al., 1994). In our experiments the existence of non-luminescent uranyl-silica-carbonate complexes ($\equiv\text{SiO}_2\text{UO}_2\text{OHCO}_3^{3-}$) is shown to account for the difference between the total initial luminescence intensity and the wet total sorbed concentration obtained from wet chemical studies.

When the luminescence data obtained in this study are compared to luminescence and structural data obtained in previous studies it appears that a bridging bidentate complex can be postulated for the entire pH range, which is hydrolysed at high pH. Formation of uranyl

polymers can be excluded since the same surface complexes were found at total uranyl concentration equal to 1 and 0.1 μM .

The spectral red shift from the fully hydrated uranyl to the first surface silica complex indicates a longer U-O_{ax} bonding distance. This results from a larger charge compensation of the uranyl (covalent bonding) within the equatorial plane. The same applies to the red shift observed between the two surface complexes.

The longer life times of the surface complexes (170 and 360 μs) compared to the low value (1 μs) of the solution complex $[\text{UO}_2(\text{H}_2\text{O})_5]^{2+}$ could be due to the decreasing symmetry of the U-O_{ax} bonding orbital (caused by the non-symmetrical charge distribution) and/or by an energy drainage to the OH bonding in the equatorial plane of the uranyl molecule.

PERSPECTIVES

The same surface complexes, i.e. emitted spectrum, were observed at 1 μM and 0.1 μM total uranyl concentration. This should be tested in the future on a larger range of total uranyl concentration at constant pH values, as it would give complementary information on potential non-linearity's of the adsorption isotherm of uranyl on silica. Another very promising type of experiments would be the determination of excitation spectra to characterise the quantum yield of the luminescence under variable chemical conditions.

Similar lifetimes (100-200 μs) and red shifts have been reported for uranyl solution complexes of other tetrahedral oxy-anions such as phosphates or sulphates. It would be interesting to study the luminescence parameters of uranyl in presence of various oxyanions as a function of pH. In the case of phosphate: are the water molecules in the equatorial plane of the uranyl ion deprotonated, as we assume for the silica surface complex, or does the phosphoric acid undergo stepwise deprotonisation resulting in constant luminescence properties?

The relation between the emitted wave number and the structure of the uranyl ions is now well established. However, several processes seem to control the lifetime. Symmetry is supposed to partly relieve the prohibition of certain transitions. O-H bonding acts as a molecular vibrator, maybe draining energy from the luminescence phenomenon. In order to discriminate among these factors some of the protons in the equatorial plane could be replaced by deuterium (Vial, 1997).

Our experiments were done with silica as sorbing solid as this solid is one of the few ones with which luminescence measurements are possible. In further experiments it should be tried to characterise surface complexes on other reactive surfaces such as iron oxides or hydroxides. This should be possible at low temperatures (Degoda, 1997). Since their structure is much

better understood than that of amorphous silica (Charlet and Manceau, 1993) this would allow to a structural interpretation of the observed non-linearities in the adsorption isotherms.

Finally, as TRLIL spectroscopy gives information at trace level concentrations it can be used to study in-situ adsorption reactions in batch experiments. This seems a promising method to study rapid kinetics as it avoids sampling and phase separation. It has to be kept in mind that this type of experiments can be carried out only in quartz vessels (neither glass nor plastic is possible as both materials absorb ultraviolet light and plastic is fluorescent itself). One could similarly follow in-situ the propagation of an uranyl front in a column.

REFERENCES

- Aberg, M., Ferri, D., Glaser, J. and Grenthe, I. (1983): Structure of the Hydrated Dioxouranium(VI) Ion in Aqueous solution. An X-ray Diffraction and ^1H NMR Study. *Inorg. Chem.*, 22, 3986-3989.
- Barlett, J. R. and Conney, R. P. (1989): On the determination of Uranium-Oxygen Bond Lengths in dioxouranium(VI) compounds by Raman spectroscopy. *Journal of Molecular Structure*, 193, 295-300.
- Bell, J. T. and Biggers, R. E. (1968): Absorption spectrum of the uranyl ion in Perchlorate Media. III. Resolution of the Ultraviolet Band Structure, Some Conclusions Concerning the Excited State of UO_2^{2+} . *J. Mol. Spectroscopy*, 25, 312-329.
- Berthoud, T., Decambox, P., Kirsch, B., Maichien, P. and Moulin, C. (1988): Direct Uranium Trace Analysis in Plutonium Solutions by Time-Resolved Laser-Induced Spectrofluorometry. *Anal. Chem.*, 60, 1296-1299.
- Bernhard, G., Geipel, G., Brendler, V. and Nitsche, H. (1996): Speciation of Uranium in Seepage Waters of a Mine tailing Pile Studied by Time-Resolved Laser-Induced Fluorescence Spectroscopy (TRLFS). *Radiochimica Acta*, 74, 87-91.
- Brendler, V., Geipel, G., Bernhard, G. and Nitsche, H. (1996): Complexation in the System $\text{UO}_2^{2+}/\text{PO}_4^{3-}/\text{OH}_{(\text{aq})}$: Potentiometric and Spectroscopic Investigations at very Low Ionic Strengths. *Radiochimica Acta*, 74, 75-80.
- Brese, N. E. and O'Keefe, M. (1991): Bond-valence parameters in solids. *Acta Cryst.*, B47, 192-197.
- Brown, I. D. and Altermatt, D. (1985): Bond valence parameters obtained from a systematic analysis of the inorganic crystal structure database. *Acta Cryst.*, B41, 244-247.
- Brina, R. and Miller, A. G. (1992): Direct Determination of Trace Levels of Uranium by Laser-Induced Kinetic Phosphorimetry. *Anal. Chem.*, 64, 1413-1418.
- Charlet, L. and Manceau, A. (1992): X-Ray Absorption Spectroscopic Study of the Sorption of Cr(III) at the Oxide-Water Interface. II. Adsorption, Coprecipitation and Surface Precipitation on Hydrated Ferric Oxide. *J. Coll. Interface Sci.*, 148(443-458).
- Charlet, L., Schindler, P. W., Spadini, L., Furrer, G. and Zysset, M. (1993): Cation adsorption on oxides and clays: The aluminium case. *Aquatic Science*, 55(4), 291-303.
- Chrisolm-Brause, C., Conradson, S. D., Buscher, C. T., Eller, P. G. and Morris, D. E. (1994): Speciation of uranyl sorbed at multiple binding sites on montmorillonite. *Geochim. Cosmochim. Acta*, 58(17), 3625-3631.
- Davies, C. W. (1962): *Ion Association*. Washington, D.C., Butterworth.
- Degoda, W. Ya. (1997): Personal communication.
- Dent, A. J., Ramsay, D. F. and Swanton, S. W. (1991): An EXAFS Study of Uranyl Ion in Solution and Sorbed onto Silica and Montmorillonite Clay Colloids. *J. Colloid Interface Science*, 150(1), 45-60.
- Eliet, V., Bidoglio, G., Omenetto, N., Parma, L. and Grenthe, I. (1995): Characterisation of Hydroxide Complexes of Uranium(VI) by Time-resolved Fluorescence Spectroscopy. *J. Chem. Soc. Faraday Trans.*, 91(15), 2275-2285.
- Eliet, V. (1996): Applications des techniques de fluorescence pour l'étude de l'Uranium dans des milieux homogènes et hétérogènes: réactions d'hydrolyse et photoréduction sur le bioxyde de Titane. Ph.D. Institut de l'Environnement du CCR d'Ispra. Paris, Université de Paris Sud, U.F.R Scientifique d'Orsay, 206 p.

- Farges, F., Ponader, C. W., Calas, G. and Brown, J., G. E. (1992):** Structural environments of incompatible elements in silicate glass/melt systems. *Geochim. Cosmochim. Acta*, 56, 4205-4220.
- Gampp, H., Maeder, M., Meyer, C. J. and Zuberbuehler, A. D. (1987):** Evolving factor analysis. *Comments Inorg. Chem.*, 6(1), 41-60.
- Glinka, Y. D. and Krak, T. B. (1995a):** Luminescence spectra of uranyl ions adsorbed on disperse SiO₂ surfaces. *Physical Review B*, 52(20), 14985-14995.
- Glinka, Y., Krak, T. B. and Beljak, Y., N. (1995b):** Investigations of adsorption properties of disperse SiO₂ surface by means of inorganic molecular probes using laser spectroscopy methods. *Journal of Molecular Structure*, 349, 215-218.
- Glinka, Y., Krak, T. B., Beljak, Y., N., Degoda, V. Y. and Ogenko, V. M. (1995c):** X-ray and photoluminophors based on SiO₂-UO₂²⁺ adsorption systems. *Colloids and surfaces. A: Physicochemical and Engineering Aspects*, 104, 17-27.
- Grenthe, I., Fuger, J., Lemire, R. J., Muller, A. B., Nguyen Trung, C. and Wanner, H. (1990):** Chemical Thermodynamics of Uranium, OECD Nuclear Energy Agency Data Bank.
- Kato, Y., Meinrath, G., Kimura, T. and Yoshida, Z. (1994):** A study of U(VI) Hydrolysis and Carbonate Complexation by Time-Resolved Laser-Induced Fluorescence Spectroscopy (TRLFS). *Radiochimica Acta*, 64, 107-111.
- Kushnirenko, I. Y., Glinka, Y. D., Degoda, V. Y., Krak, T. B. and Ogenko, V. M. (1993):** Luminescent properties of uranyl ions adsorbed on the surface of disperse silicon dioxide. *J. of Applied Spectroscopy*, 59(3-4), 687-692.
- Ludwig, C. (1993):** Koordinationschemie an der Grenzschicht Oxid/Wasser, I. Ternaere Oberflaechenkomplexe mit Cu(II) und organischen Liganden und TiO₂ (Anatas), II. Ein Modell zur Beschreibung der Deprotonierung von Al₁₃O₄(OH)₂₄(H₂O)₁₂⁷⁺. PhD thesis, Department of Inorganic Chemistry, University of Bern.
- Moriyasu, M., Yokoyama, Y. and Ikeda, S. (1977):** Quenching mechanisms of uranyl luminescence by metal ions. *J. Inorg. Nucl. Chem.*, 39, 2205-2209.
- Morris, D. E., Chrisholm-Brause, C. J., Barr, M. E., Conradson, S. D. and Eller, P. G. (1994):** Optical spectroscopic studies of the sorption of UO₂²⁺ species on a reference smectite. *Geochim. Cosmochim. Acta*, 58(17), 3613-3623.
- Moulin, C., Decambox, P., Moulin, V. and Decaillon, J. G. (1995):** Uranium Speciation in Solution by Time-Resolved Laser-Induced Fluorescence. *Analytical Chemistry*, 67(2), 348-353.
- Oesthols, E. (1995):** Thorium sorption on amorphous silica. *Geochim. Cosmochim. Acta*, 59(7), 1235-1249.
- Pauling, L. (1929):** The principles determining the structure of complex ionic crystals. *J. Amer. Chem. Soc.*, 51, 1010-1026.
- Reich, T., Moll, H., Denecke, M. A., Geipel, G., Bernhard, G., Nitsche, H., Allen, P. G., Bucher, J. J., Kaltsoyannis, N., Edelstein, N. M. and Shuh, D. K. (1996):** Characterization of Hydrous Uranyl Silicate by EXAFS. *Radiochimica Acta*, 74, 219-223.
- Schindler, P. W. and Gamsjaeger, H. (1972):** Acid-base reactions of the titanium dioxide (anatase)-water interface and the point of zero charge of titanium dioxide suspensions. *Kolloid Z. Z. Polym.*, 250, 759.
- Schindler, P. W., Fuerst, B., Dick, R. and Wolf, P. U. (1976):** Ligand properties of surface silanol groups. I. Surface complex formation with iron(3+), copper(2+), cadmium(2+) and lead(2+). *J. Colloid. Interface; Sci.*, 55(2), 469-475.

Stanton, J. and Maatman, R. W. (1963): The reaction between aqueous uranyl ion and the surface of silica gel. *J. Colloid Sci.*, 18, 132.

Swihart, G. H., Sen Gupta, P. K., Schlemper, E. O., Back, M. E. and Gaines, R. V. (1993): The crystal structure of moctezumite $[PbUO_2](TeO_3)_2$. *American Mineralogist*, 78, 835-839.

Turner, D. R. (1995): A uniform approach to surface complexation modeling of radionuclide sorption. Report CNWRA 95-001 of the Nuclear Regulatory Commission Contract NRC-02-93-005, Center for Nuclear Waste Regulatory Analyses, San Antonio, Texas.

Veal, B. W., Mundy, J. N. and Lam, D. J. (1987): Actinides in silicate glasses. *Handbook on Physics and Chemistry of the Actinides*. A. J. Freeman and G. H. Lander, Elsevier, 271-309.

Vial, J.-C. (1997): Personal communication.

Waite, T. D., Davis, J. A., Payne, T. E., Waychunas, G. A. and Xu, N. (1994): Uranium(VI) adsorption to ferrihydrite: Application of a surface complexation model. *Geochim. Cosmochim. Acta*, 58(24), 5465-5478.

Wheeler, J. and Thomas, J. K. (1984): Photochemistry of the Uranyl Ion in Colloidal Silica Solution. *J. Phys. Chem.*, 88, 750-754.

Westall, J. C. (1982): A computer program for the determination of chemical equilibrium constants from experimental data. Version 1.2. Corvallis, Oregon, Oregon State University.

ARTICLE II

REACTIVE TRANSPORT OF URANYL IN A GOETHITE COLUMN:

AN EXPERIMENTAL AND MODELLING STUDY

U. Gabriel¹, J.-P. Gaudet², L. Spadini¹, L. Charlet^{1*}

¹Laboratoire de Géophysique Interne et Tectonophysique, UJF - CNRS (UMR 5559) Grenoble, France

²Laboratoire d'Etude des Transferts en Hydrologie et Environnement, UJF, INPG, CNRS UMR 5564 Grenoble, France

* to whom the correspondence should be addressed

ABSTRACT

We investigated the adsorption of uranium(VI) at atmospheric CO₂ partial pressure in a bicarbonate background ionic medium (pH 9.0 ± 0.2). Goethite-coated sand was used as mine tailings model material. Both static, i.e. batch, and dynamic, i.e. column, experiments were performed. In the column experiments, uranyl adsorption was found to be far from local equilibrium at a pore velocity of 12.1 cm h⁻¹. However at a pore velocity of 1.21 cm h⁻¹, sorption was at or near equilibrium. The asymmetrical break-through curves indicated a non-linear adsorption isotherm and/or a kinetically controlled adsorption/desorption reaction. Both effects could be modelled by incorporating a retardation factor and either first-order adsorption kinetics or a Langmuir adsorption isotherm into the basic exchange and convection-dispersion equation. In batch experiments the silica dissolution induced a greater competition of aqueous silica species with carbonate and uranyl ions for adsorption on the goethite surface resulting in less uranyl adsorption than in the column experiments where the dissolved silica was negligible. The retardation factor from the dynamic experiments and the non-linear 'static' adsorption isotherm, as well as the effect of pH on surface and solution complexation by silica and carbonate ions, were taken into account within the framework of a general surface complexation model. This model included high and low affinity sites at a 1:200 ratio. The uranyl sorption was equally well reproduced under the assumption of the release of either one or two protons in the formation of the uranyl surface complex on the low affinity sites, and two protons on the high affinity sites. These different parameters have to be taken into account for the assessment of the long term interaction of uranium in mine waste tailings with the environment.

INTRODUCTION

The transport behaviour of contaminants in porous media such as soils, mine wastes or aquifers is controlled by the interaction between physical transfer and (im)mobilisation reactions, such as adsorption or precipitation. Uranium(VI) migration in anthropogenic porous media (mine waste) is in a large extent dependent on adsorption/desorption reactions with reactive surfaces present in soils and mine wastes (Yeh and Tripathi, 1991) and on uranyl complexation in solution with carbonate ions. Carbonate ions, whether produced by bacterial respiration or present in mine waste as extraction by-product, are known to be, together with phosphate ions and humic substances, one of the most important complexants of dissolved uranium(VI) (Bernhard, et al., 1996; Meinrath et al., 1996; Kato et al., 1994). A number of studies have been devoted to uranyl adsorption/desorption in closed systems, e.g. on goethite in the presence and/or absence of carbonate (Hsi and Langmuir, 1985, Kohler et al., 1992), on hydrous ferric oxide (Waite et al., 1994) or on mine waste material (Geipel et al., 1996). The adsorption mechanism has been studied by spectroscopic (e. g. Manceau et al., 1992) and thermodynamic (Dzombak and Morel, 1990) methods. Less attention has been paid to coupled hydro-geochemical transport models, in part due to the complicated solution chemistry of uranyl and to kinetically controlled adsorption reactions, although these models are used to evaluate the efficiency of liners or barriers to contain uranyl ions sorbed onto mine tailings and prevent uranium to reach into the underlying groundwater (Morrison et al., 1995a and 1995b) or to predict uranyl migration in a porous aquifer containing reactive surfaces (Tripathi and Yeh, 1991). The local equilibrium assumption (LEA) was justified in the studies of Morrison et al. (1995a) and (1995b) because they focused on the chemical controls of uranyl fixation. On the other hand, the LEA may not be applicable to the transport study of Tripathi and Yeh (1991), where kinetics of adsorption may be important.

Schweich and Sardin (1981) and Miller et al. (1989) showed that batch and column experiments are complementary for the understanding of the physico-chemical phenomena involved in transport of solutes in porous media. Based on the local equilibrium assumption (LEA), thermodynamic equilibrium coefficients should be the same for open and closed systems. This has been observed for cadmium adsorption on quartz sand (Buergisser et al., 1993), silicate adsorption on goethite and phosphate adsorption on Cecil clay (Miller et al.,

1989) and fluoride and proton adsorption on goethite (Scheidegger, 1993). Numerous other studies have shown, however, important differences in adsorption behaviour whether measured in static or dynamic systems (e.g. Persaud et al., 1983). Such discrepancies could be due to kinetically-controlled reactions or different chemical conditions in open versus closed systems. The reaction kinetics of systems far from equilibrium are usually described by global rates which are different for flow and batch systems (e.g. Sparks and Jardin, 1982, Akratanakul et al., 1983). Rates of many adsorption reactions are furthermore controlled by diffusion through the immobile thin film. The thickness of this film, which may then become a rate-controlling parameter, depends strongly on the macroscopic flow conditions. Column experiments are less affected by analytical errors (see below), and can better simulate field conditions than batch experiments because: (1) they achieve a high solid/solution ratio, (2) an immobile porous medium is percolated by a given solution, and (3) reaction products do not accumulate. On the other hand, flow experiments are often run at high flow velocity, and this leads to underestimate slow (e.g. dissolution) reactions of importance in field low-flow conditions.

To our knowledge no data have been published yet on the importance of adsorption/desorption kinetics for uranyl transport. The principal aim of this study is to quantify uranyl transport in a simplified, synthetic soil system. The thereby reduced number of parameters allows to observe more easily the determinant variabilities and surface stoichiometries used in the modelling of more complex natural systems. This study is based on column experiments that were carried out at high pH ($8.8 < \text{pH} < 9.1$). Thermodynamic constants were determined in static (batch) systems. The column support was goethite coated silica sand. While sand allows water percolation in the columns, the goethite serves as a model for the reactive surfaces present in mine waste, a model which is stable with time such that several experiments could be carried out using the same column under the assumption that ageing did not significantly change the surface properties.

MATERIALS AND METHODS

All solutions were prepared with analytical grade chemicals. Ortho-phosphoric acid 85 % was p.p.a. Ultrapure water ($18.2 \text{ M}\Omega \text{ cm}^{-1}$ quality) was prepared with a nanopure apparatus (MilliQPlus 185).

Goethite preparation

Goethite was produced according to Atkinson (1967). Solution A (0.65 dm^3 $0.5 \text{ M Fe(NO}_3)_3$ in 0.21 M HNO_3) was introduced drop by drop into solution B (1.35 dm^3 1.0 M NaOH). The precipitated ferrihydrite was aged for 4 days at 65°C to convert to goethite. The goethite was then washed with ultrapure water. The X-ray diffraction pattern was characteristic of crystalline goethite.

Goethite-coated sand preparation

Silica sand (supplied by Firma Haendel as 'Seesand, gegluht'; mineral: cristobalite) was sieved and the $125 - 315 \mu\text{m}$ fraction was kept for a chemical treatment consisting of 3 days immersion in an acid solution consisting of 1 HNO_3 conc. : 3 HCl conc. : 4 ultrapure H_2O (volume ratio). Goethite coating on SiO_2 was obtained by shaking a suspension containing goethite and the silica sand following the procedure of Scheidegger (1993). The quantity of fixed goethite is controlled by pH, the goethite content of the solution, and temperature. The following conditions were used: pH 4 (HNO_3), 0.3 g goethite and 1.8 g cristobalite per cm^3 solution at 20°C . The mixture was agitated for 24 h and then washed thoroughly with at least 10 litres of ultrapure water.

The goethite-coated sand used in the batch experiments contained 4.1 mg goethite per gram of cristobalite sand. The specific surface areas determined by BET were $0.03 \text{ m}^2 \text{ g}^{-1}$ for the cristobalite sand, $61 \text{ m}^2 \text{ g}^{-1}$ for the goethite and $0.36 \text{ m}^2 \text{ g}^{-1}$ for the goethite-coated sand. The latter value results in a specific surface area of $80.5 \text{ m}^2 \text{ g}^{-1}$ for the pure goethite. This discrepancy can best be explained by the preferential fixation of smaller goethite crystals. The coated and the pure cristobalite sand were examined by SEM, revealing fractured grains. This is probably due to the heating process to convert the quartz to cristobalite. The goethite needles were preferentially fixed in these fractures.

Column experiments

To ensure a statistically homogeneous matrix, columns (XK26 with 2 AK adapters, Pharmacia LKB Biotechnology) were filled using the following procedure: the column was fixed vertically and its lower end closed. Then a tube was inserted into the column with two grids, one at its end inside the column and the other 5 cm above this end. The sand was slowly introduced into the inserted tube while keeping the distance between the surface of the sedimented sand and the lower grid constant at 5 cm. Two columns were prepared, one filled with pure sand (100 g, length 14.8 cm, porosity 0.474), the other with goethite-coated sand (0.62 g goethite and 100 g sand, length 14.6 cm, porosity 0.467).

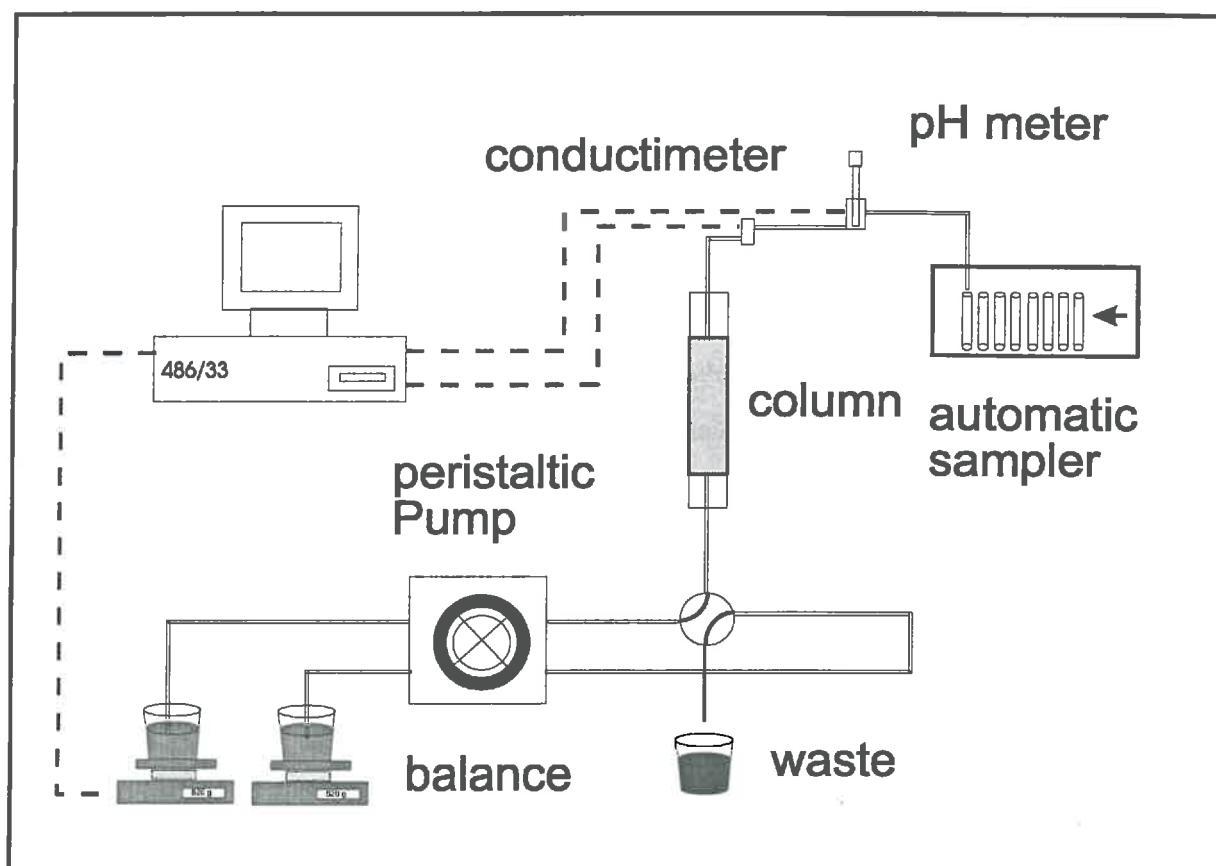


Figure 1 Experimental design for column experiments (see text for details).

The columns were saturated slowly with water to minimise air entrapment. In order to evacuate remaining air, 100 pore volumes of pure, well agitated water were percolated

through the columns. Afterwards the hydrodynamic parameters of the columns were determined by using chloride as a tracer.

The break-through curves (BTC's) of several uranyl pulses of different concentrations (0.05, 0.1 and 1 μM uranyl) were determined at a constant background carbonate concentration of 0.01 M (equilibrated with the atmospheric CO_2) and two flow rates (30 and 3 $\text{cm}^3 \text{h}^{-1}$). BTC's were registered continuously. The experimental set up is shown in figure 1. The following equipment was used and connected by capillary tubing (PTFE 19-0041-01, Pharmacia LKB Biotechnology): balance (PM48 Deltarange, Mettler), pump (Minipulse3, Gilson), valves (SRV-4, Pharmacia LKB Biotechnology), conductimeter (CORV62, Tacussel) with measurement cell (DEL-1, Tacussel) and pH-meter (model 701A/digital ionalyzer, Orion Research) with combined glass electrode (Metrohm). Samples were taken automatically with a fraction collector (FC205, Gilson) into tubes (polystyrene; 5 and 12 cm^3) containing 1 M HNO_3 (masses of tubes determined with and without the acid). Tubes were also weighed afterwards to correct for potential losses by evaporation. The balance, conductimeter and pH-meter were controlled by a personal computer. The volumes of the measurement cells of the conductivity ($V = 0.1 \text{ cm}^3$) and the pH ($V = 1.5 \text{ cm}^3$) were kept as small as possible to minimise mixing effects.

Batch experiments

For the batch experiments, 2 g of the goethite-coated sand were mixed with 10 cm^3 of solution in polyethylen centrifuge tubes in the presence of atmospheric CO_2 . Experiments were conducted by preparing the suspensions, adjusting the volumes, and as a last step, adding the uranyl aliquot to avoid desorption effects. Uranyl was added as uranyl nitrate. The ionic strength was a function of the carbonate concentration and was not adjusted. A first set of batch experiments (referred to as 'desorption edge batch experiments') was performed at $[\text{UO}_2^{2+}]_{\text{total}} = 1 \text{ }\mu\text{M}$ and $0.4 \text{ mM} \leq [\text{NaHCO}_3] \leq 20 \text{ mM}$ resulting in $7.5 \leq \text{pH} \leq 9.5$. The 'isotherm batch experiments' refer to different experimental conditions ($0.06 \text{ }\mu\text{M} \leq [\text{UO}_2^{2+}]_{\text{total}} \leq 10 \text{ }\mu\text{M}$ and $[\text{NaHCO}_3] = 10 \text{ mM}$). The samples were agitated for 10 days and then left open to the atmosphere for another two days. The pH was measured with a pH-meter (Metrohm 713) and a combined glass electrode (Metrohm). The solid and liquid phases were

separated by centrifugation and filtration (filter: <0.025 μm , VS WPO 1300, Millipore). The resulting natant solutions were immediately acidified to pH 1 with nitric acid. Silica concentrations were determined colorimetrically using the molybdate blue method (Strickland and Parsons, 1972). The analytical precision of the aqueous silica concentration is estimated to be in the range of 5 to 10 %.

Uranyl analysis

Uranyl was analysed using time-resolved laser-induced fluorescence (TRLIF) spectroscopy (Brina and Miller, 1992). The optical apparatus was placed in a black box and the quartz tube in a second black box to minimise the influence of scattered light (figure 2). One cm^3 of the sample was mixed with one cm^3 1.5 M phosphoric acid in a quartz tube (Suprasil, 4 cm^3 , layer thickness 1 cm) and agitated during the measurement. Aqueous uranyl was excited by a pulsed nitrogen laser (VSL-337ND, Laser Science, inc.; 250 μJ per pulse, 15 Hz, wave length 337 nm). The fluorescence decay was measured by a photomultiplier (Hamamatsu 94302, tension of 500 V) in a perpendicular direction to the laser after the light was passed through a gelatine filter (Kodak 55, maximal transmission 67-69 % at 510-520 nm). The amplified signal was measured and averaged by a numeric oscilloscope (digitising oscilloscope 54501A 100Mhz, Hewlett Packard) triggered by a photodiode (PIN S1223-01, Hamamatsu) which was also excited by the laser. An oscilloscope, which was set up to measure the decay between 50 μs before the laser pulse (to fix base line) and 450 μs after the laser pulse, was connected to a PC where the decay curves were registered. The same 0.5 μM uranyl standard solution was measured each time after 6 sample measurements in order to correct for changes in laser intensity (i.e. instrumental drift).

According to Brina and Miller (1992) the initial intensity I_0 is linearly correlated to the uranyl concentration, provided that all experimental factors and solution chemistry remain constant. The actual measured intensity $I(t)$ is influenced by quenching effects. The decay curve (Figure 2) can be fitted by applying a first order decay relationship of the following form:

$$I(t) = I_0 \exp\left(-\frac{t}{\tau_{\text{fluo}}}\right) \quad (1)$$

where τ_{flu} is the fluorescence life time and t is the time.

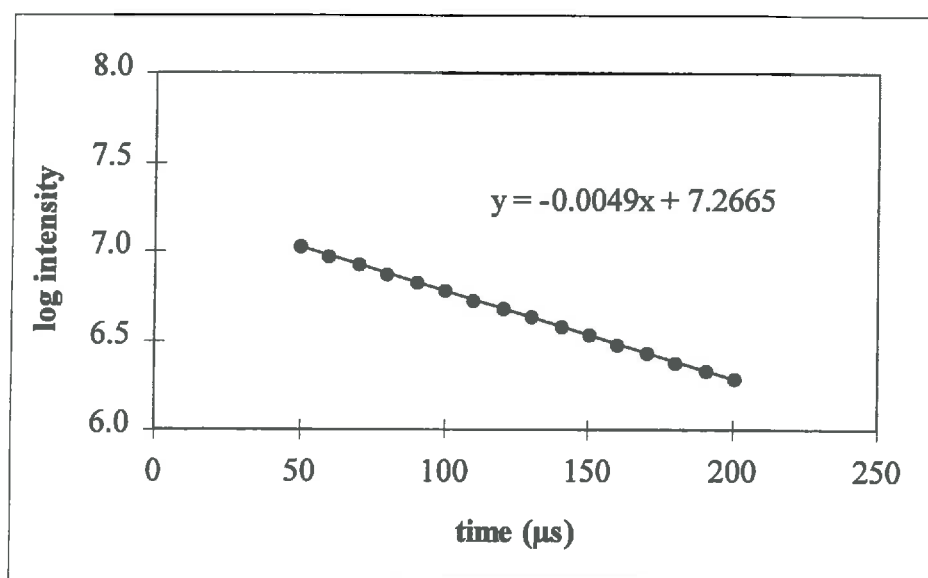
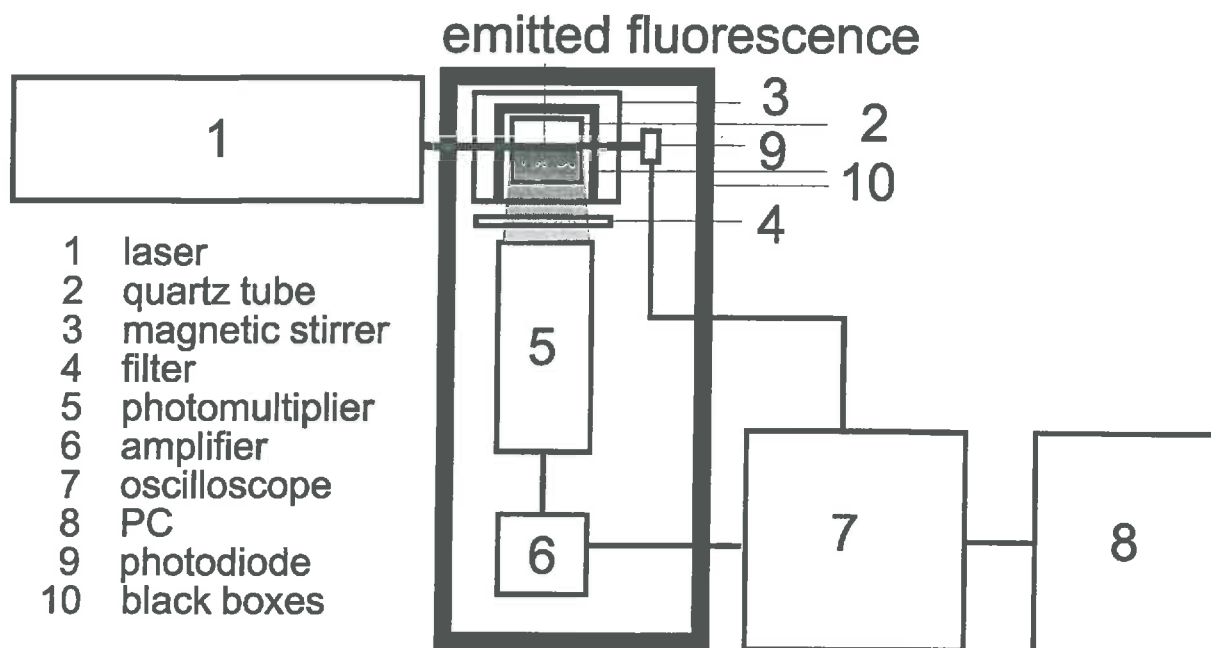


Figure 2 Experimental set-up for the uranium analysis and one example of the first order decay of the fluorescence of uranyl in the presence of 0.75 M H_3PO_4 ($0.5 \mu\text{M UO}_2^{2+}$).

The measured data were treated in the following manner

1. correction for the decay base line,
2. correction with a blank (absence of phosphate and uranyl) performed the same day and corrected for its own base line,
3. fitting of data with a first order exponential decay curve over a time interval of 50-200 μs , following the laser pulse and
4. correction for instrumental drift.

The analysing procedure was calibrated using internal standards, for all samples of the batch experiments, as well as for several samples of the column experiments. The formula used is expressed as:

$$I_0(n) = \beta_{\text{fluo}} \frac{V_0 c + nV_{\text{add}} c_{\text{add}}}{V_{\text{tot}}} \quad (2)$$

where n is the number of the addition step, β_{fluo} is the ratio between the initial fluorescence intensity and the corresponding uranyl concentration in the quartz cell ($3.9 \pm 0.4 \times 10^9$ arbitrary units (a.u.) M^{-1} uranyl); c is the original uranyl concentration in the sample (M) while V_{add} and c_{add} are the volume (cm^3) and the uranium concentration (M), respectively, of the added standard solution (preacidified to pH 1 with nitric acid, as for the samples). V_0 and V_{tot} are the added volume of the sample and the total volume (both in cm^3). The precision and detection limit are considered to be 5 % and 2×10^{-9} M.

DATA ANALYSIS AND MODELS

We shall first present the reactive transport models used in this study, and which incorporate adsorption reactions in a very simplified way (linear and Langmuir-like adsorption isotherms). Second, solution and surface complexation models are introduced, and the adsorption reactions under static conditions are discussed. Third, chemical adsorption models which include solution and surface complexation are related to the simplified, but useful Langmuir isotherm.

Reactive transport models

In a homogeneous porous medium, the one-dimensional transport of an adsorptive species is described by the following differential equation (Bear, 1979), which is usually referred to as the general exchange and convection-dispersion-equation (ECDE):

$$\frac{\partial c}{\partial t} + \frac{\rho}{\theta} \frac{\partial S}{\partial t} = D \frac{\partial^2 c}{\partial z^2} - v \frac{\partial c}{\partial z} \quad (3)$$

where S is the sorbed concentration in mol g^{-1} sorbent, ρ is the bulk density (defined in our case as mass of goethite per total volume of the column), θ is the volumetric water content, D is the dispersion factor, v is the interstitial velocity, and z and t are the local (distance) and temporal (time) differentiation variables. The concentration in the mobile phase c (M) can represent either the resident c_r or the flux c_f concentration. The first is obtained by phase separation of a column segment. The second is obtained from the BTC at the outlet of the column. Assuming pure convective-dispersive transfer, both concentrations are related by equation (4)

$$c_f = c_r - \frac{D}{v} \frac{\partial c_r}{\partial z} \quad (4)$$

and become equal when $D = 0$ (after Jury and Roth, 1990). The general ECDE is invariant, whatever concentration is used. In our experiments the mobile phase concentrations were measured at the outlet and corresponded therefore to the flux concentration c_f . In the following discussion c represents the flux concentration in the mobile phase. The initial and boundary conditions and the analytical solution were chosen accordingly and will be discussed below.

Different ECDE derived models (first order kinetics and linear adsorption)

The ECDE has analytical solutions for several simplified cases for adsorption reactions. When linear adsorption and local equilibrium can be assumed (model: **CDR**), a retardation factor R can be introduced into equation (3) (analytical solution in van Genuchten and Wierenga, 1976):

$$R \frac{\partial c}{\partial t} = D \frac{\partial^2 c}{\partial z^2} - v \frac{\partial c}{\partial z} \quad (5)$$

where R is defined as:

$$R = 1 + \frac{\rho K_d}{\theta} \quad (6)$$

and K_d is a distribution factor:

$$K_d = \frac{S}{c} \quad (7)$$

This distribution coefficient related retardation factor R can only be applied in the case of linear (eq. 7) and reversible adsorption. When local chemical equilibrium cannot be assumed, a rate law has to be introduced. For a first order rate law it follows that (model: **CDR-cin**):

$$\frac{\partial S}{\partial t} = \alpha [K_d c_r - S] = \alpha \left[\frac{(R-1)\theta}{\rho} c_r - S \right], \quad (8)$$

where α (h^{-1}) represents the global reaction rate. The linear adsorption can be described by K_d or R . The analytical solution of the model (eq. 3 and 8) is given in Toride et al. (1993) and Toride and Leij (1996) and is based on the following initial and boundary conditions:

$$c(z,0) = S(z,0) = 0 \quad (9a)$$

$$vc(0,t) - D \frac{\partial c(0,t)}{\partial z} = v\delta(t) \quad (9b)$$

$$\frac{\partial c(\infty,t)}{\partial z} = 0 \quad (9c)$$

where $\delta(t)$ is the Dirac input. The adsorption is assumed to be linear and reversible. The solution of equation (5) with the initial and boundary conditions given by (9a-c) is called $f_f(t)$. The final solution c_i consists of the convolution product with any input $g(t)$:

$$c_i(z,t) = \int_0^t g(t-\tau) f_f(z,\tau) d\tau \quad (10)$$

where f_f is given in the annex. We have used an excitation signal $g(t)$ of the form of a pulse with T_0 being the pulse length:

$g(t) = 0$ for $t < 0$ and $t > T_0$, and $g(t) = 1$ for $0 \leq t \leq T_0$.

Non-linear isotherm in the ECDE (Langmuir isotherm and local equilibrium assumption)

As analytical solutions do not exist for more complicated transport models, a numerical solution was also considered for modelling the experimental BTC's where no linear adsorption but instead Langmuir like adsorption is assumed.

$$S = S_{\max} \frac{K_L c}{1 + K_L c} \quad (11)$$

where S_{\max} is the maximum sorbing capacity in mol g⁻¹ sorbent and K_L is the sorption affinity in M⁻¹, an equilibrium describing coefficient. Equation (3) can then be rewritten (model: **CDR-Langmuir**) :

$$\frac{\partial c}{\partial t} \left(1 + \frac{\rho}{\theta} \frac{S_{\max} K_L}{(1 + K_L c)^2} \right) = D \frac{\partial^2 c}{\partial z^2} - v \frac{\partial c}{\partial z} \quad (12)$$

where $\frac{\partial S}{\partial t}$ has been expanded to $\frac{\partial S}{\partial c} \frac{\partial c}{\partial t}$.

The differentials in this equation are solved by finite differences methods. A limited Taylor series is used in the explicit discretisation procedure.

$$\frac{c_{k+1,i} - c_{k,i}}{\Delta t} \left(1 + \frac{\rho}{\theta} \frac{S_{\max} K_L}{(1 + K_L c_{k,i})^2} \right) = D \frac{c_{k,i-1} - 2c_{k,i} + c_{k,i+1}}{\Delta z^2} - v \frac{c_{k,i} - c_{k,i-1}}{\Delta z} \quad (13)$$

The indices k and i represent the temporal and local discretisation, respectively. Numerical diffusion, stability and convergence are controlled (Chaudari, 1971).

Moment analysis of the BTC

As a complementary tool, a moment analysis can be used to interpret the experimental BTC.

The nth moment is given by Jury and Roth (1990):

$$M(t^N) = \int_0^{\infty} t^N \frac{c(t)}{c_0} dt \quad (14)$$

where c_0 is the input concentration imposed for $0 \leq t \leq T_0$. The zero order moment is used for the mass balance and the first order moment is used in the calculation of the mean residence time, E (eq. 15), which is related to the retardation factor R_m by equation (16). This retardation factor is not the same as the retardation factor introduced in equations (5) and (8) as it is based on the gravity centre of the BTC and therefore represents an average of the adsorption and the desorption fronts. Expressions for E and R_m are given by:

$$E = \frac{M(t^1)}{M(t^0)} \quad (15)$$

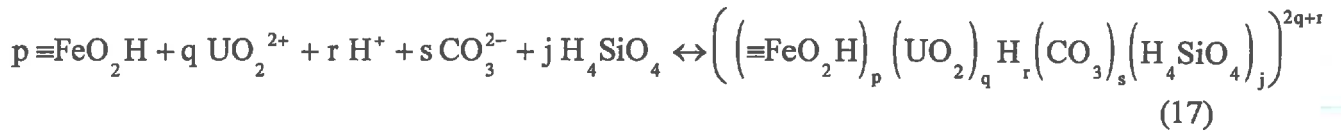
and

$$R_m = \frac{E - \frac{T_0}{2}}{T_{\text{tracer}}}, \quad (16)$$

where T_{tracer} is the mean residence time of a conventional inert tracer. Experimental data were interpolated with the software packet Mathcad6+ built-in spline function and this fitted curve was numerically integrated.

General surface complexation model

The surface complexation model is based on the chemical equilibrium approach and incorporates solution and surface speciation. The different surface and solution reactions can be expressed by the following general equilibrium:



where p , q , r , s and j are (positive or negative) stoichiometric coefficients. The bidentate binding mode for uranyl, silicate and carbonate ions suggests a $\equiv \text{FeO}_2\text{H}$ site, with two reactive surface oxygens, as the binding unit (Sigg, 1979; Spadini, 1993; Waite et al., 1994; van Geen et al., 1994).

The conditional equilibrium constants K_{pqrsj} for reaction (17) is given by :

$$K_{\text{pqrsj}} = \frac{\left[\left(\equiv \text{FeO}_2\text{H} \right)_p \left(\text{UO}_2 \right)_q \text{H}_r \left(\text{CO}_3 \right)_s \left(\text{H}_4\text{SiO}_4 \right)_j \right]^{2q+r-2s}}{\left[\equiv \text{FeO}_2\text{H} \right]^p \left[\text{UO}_2^{2+} \right]^q \left[\text{H}^+ \right]^r \left[\text{CO}_3^{2-} \right]^s \left[\text{H}_4\text{SiO}_4 \right]^j} \quad (18)$$

where $[\]$ refer to the molar concentrations of dissolved and surface species. The conditional equilibrium constants include activity coefficients for solution species which were calculated with the Davies equation (Davies, 1962). Activity coefficients for all surface species are assumed to be equal to 1.0. Solution equilibrium constants are given in table 1 and results of speciation computation can be found in figure 3.

Table 1 Equilibrium constants (logK) for the solution speciation (Grenthe et al., 1992; ionic strength $I = 0$; reaction products were written as to represent known structures contrary to the matrices derived definition in the text!).

Reaction		log K
$\text{UO}_2^{2+} - \text{H}^+ + \text{H}_2\text{O}$	$\leftrightarrow \text{UO}_2(\text{OH})^+$	-5.2
$\text{UO}_2^{2+} - 2 \text{H}^+ + 2 \text{H}_2\text{O}$	$\leftrightarrow \text{UO}_2(\text{OH})_2^0$	-10.3
$\text{UO}_2^{2+} - 3 \text{H}^+ + 3 \text{H}_2\text{O}$	$\leftrightarrow \text{UO}_2(\text{OH})_3^-$	-19.2
$\text{UO}_2^{2+} - 4 \text{H}^+ + 4 \text{H}_2\text{O}$	$\leftrightarrow \text{UO}_2(\text{OH})_4^{2-}$	-33.
$2 \text{UO}_2^{2+} - \text{H}^+ + \text{H}_2\text{O}$	$\leftrightarrow (\text{UO}_2)_2\text{OH}^{3+}$	-2.8
$2 \text{UO}_2^{2+} - 2 \text{H}^+ + 2 \text{H}_2\text{O}$	$\leftrightarrow (\text{UO}_2)_2(\text{OH})_2^{2+}$	-5.62
$3 \text{UO}_2^{2+} - 4 \text{H}^+ + 4 \text{H}_2\text{O}$	$\leftrightarrow (\text{UO}_2)_3(\text{OH})_4^{2+}$	-11.9
$3 \text{UO}_2^{2+} - 5 \text{H}^+ + 5 \text{H}_2\text{O}$	$\leftrightarrow (\text{UO}_2)_3(\text{OH})_5^+$	-15.55
$3 \text{UO}_2^{2+} - 7 \text{H}^+ + 7 \text{H}_2\text{O}$	$\leftrightarrow (\text{UO}_2)_3(\text{OH})_7^-$	-31.
$4 \text{UO}_2^{2+} - 7 \text{H}^+ + 7 \text{H}_2\text{O}$	$\leftrightarrow (\text{UO}_2)_4(\text{OH})_7^+$	-21.9
$\text{UO}_2^{2+} + \text{H}_2\text{CO}_3^0 - 2 \text{H}^+$	$\leftrightarrow \text{UO}_2\text{CO}_3^0$	-6.98
$\text{UO}_2^{2+} + 2 \text{H}_2\text{CO}_3^0 - 4 \text{H}^+$	$\leftrightarrow \text{UO}_2(\text{CO}_3)_2^{2-}$	-16.42
$\text{UO}_2^{2+} + 3 \text{H}_2\text{CO}_3^0 - 6 \text{H}^+$	$\leftrightarrow \text{UO}_2(\text{CO}_3)_3^{4-}$	-28.44
$\text{UO}_2^{2+} - \text{H}^+ + \text{H}_4\text{SiO}_4^0 + \text{H}_2\text{O}$	$\leftrightarrow \text{UO}_2\text{H}_3\text{SiO}_4^-$	-2.4

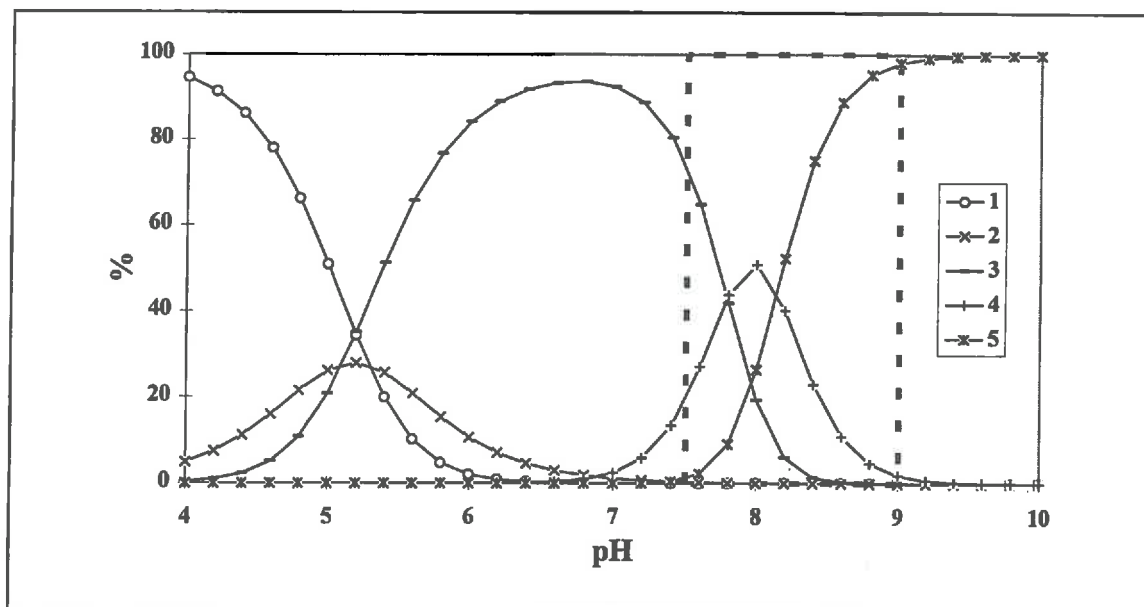


Figure 3 Solution speciation of uranyl using the equilibrium constants listed in table 1 ($[\text{UO}_2^{2+}]_{\text{total}} = 1 \mu\text{M}$; $[\text{H}_2\text{CO}_3^0]_{\text{free}} = 16.4 \mu\text{M}$; $[\text{H}_4\text{SiO}_4^0]_{\text{total}} = 0.9 \text{ mM}$; 1: UO_2^{2+} ; 2: $\text{UO}_2(\text{OH})^-$; 3: $\text{UO}_2(\text{OH})_2^0$; 4: $\text{UO}_2(\text{CO}_3)_2^{2-}$; 5: $\text{UO}_2(\text{CO}_3)_3^{4-}$; the dashed frame represents the studied pH range)

The total concentrations of surface sites, uranyl, protons and aqueous silica are given by equations (19) to (22).

$$\left[\equiv \text{FeO}_2 \text{H} \right]_{\text{total}} = \sum_p \sum_q \sum_r \sum_s \sum_j p K_{pqrsj} \left[\equiv \text{FeO}_2 \text{H} \right]^p \left[\text{UO}_2^{2+} \right]^q \left[\text{H}^+ \right]^r \left[\text{CO}_3^{2-} \right]^s \left[\text{H}_4 \text{SiO}_4 \right]^j \quad (19)$$

$$\left[\text{UO}_2^{2+} \right]_{\text{total}} = \sum_p \sum_q \sum_r \sum_s \sum_j q K_{pqrsj} \left[\equiv \text{FeO}_2 \text{H} \right]^p \left[\text{UO}_2^{2+} \right]^q \left[\text{H}^+ \right]^r \left[\text{CO}_3^{2-} \right]^s \left[\text{H}_4 \text{SiO}_4 \right]^j \quad (20)$$

$$\left[\text{H}^+ \right]_{\text{total}} = \sum_p \sum_q \sum_r \sum_s \sum_j r K_{pqrsj} \left[\equiv \text{FeO}_2 \text{H} \right]^p \left[\text{UO}_2^{2+} \right]^q \left[\text{H}^+ \right]^r \left[\text{CO}_3^{2-} \right]^s \left[\text{H}_4 \text{SiO}_4 \right]^j \quad (21)$$

$$\left[\text{H}_4 \text{SiO}_4 \right]_{\text{total}} = \sum_p \sum_q \sum_r \sum_s \sum_j j K_{pqrsj} \left[\equiv \text{FeO}_2 \text{H} \right]^p \left[\text{UO}_2^{2+} \right]^q \left[\text{H}^+ \right]^r \left[\text{CO}_3^{2-} \right]^s \left[\text{H}_4 \text{SiO}_4 \right]^j \quad (22)$$

The carbonate ion concentration is controlled in part by equilibria with atmospheric CO_2 , which results in a constant free concentration of $\text{H}_2\text{CO}_3^\circ$. The total silicate concentration $[\text{H}_4\text{SiO}_4]_{\text{total}}$ is controlled by the dissolution rate of cristobalite.

For charged surface complexes, the formation constant (given by eq. 18) is an apparent one and has to be corrected for the Coulombic energy of the charged surface to obtain the corresponding intrinsic constants (K_{pqrsj}^{int} , Schindler and Stumm, 1987).

$$K_{pqrsj}^{\text{int}} = K_{pqrsj} \exp \frac{(2q + r - 2s) F \Psi_0}{R_G T} \quad (23)$$

where F is Faraday's constant, R_G is the universal gas constant (the indices is given to distinguish it from the retardation factor R), and T is absolute temperature. The total charge of the surface σ_t is defined as:

$$\sigma_t = \sum_p \sum_q \sum_r \sum_s \sum_j (2q + r - 2s) K_{pqrsj} \left[\equiv \text{FeO}_2 \text{H} \right]^p \left[\text{UO}_2^{2+} \right]^q \left[\text{H}^+ \right]^r \left[\text{CO}_3^{2-} \right]^s \left[\text{H}_4 \text{SiO}_4 \right]^j \quad (24)$$

The constant capacitance model was used to relate the surface potential ψ_0 to the total charge of the surface σ_t . This surface model was found particularly applicable since EXAFS results indicate that uranyl ions form inner sphere surface complexes (Manceau et al., 1992; Waite, et al. 1994). The surface potential is given by Schindler and Kamber (1968):

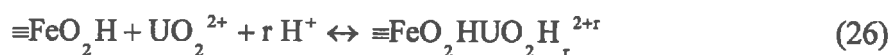
$$\Psi_0 = \frac{\sigma_t F}{\kappa A_s c_p} \quad (25)$$

A_s and c_p are the specific surface area ($\text{m}^2 \text{g}^{-1}$) and the particle concentration (g dm^{-3}), respectively. F is the Faraday constant. κ is the capacitance (F m^{-2}). Chemical equilibria computation was performed by the GRFIT code (Westall and Hohl, 1980; Ludwig, 1993).

Langmuir isotherm versus general surface complexation model

The above presented approach to model surface and solution speciation would demand the general exchange and convection-dispersion-equation (ECDE, eq. 3) to be simultaneously solved for all solution species within a (« multi-component ») transport model. Alternatively in mono-component transport models adsorption reactions are described only in a simplified way by adsorption isotherm equations where the sorbed concentration S (in mol g^{-1}) is expressed as a function of the dissolved (analytically measurable) concentration c (in M). The Langmuir equation (eq. 11) was found to be the most appropriate model for our experimental data. It is compared below to the general surface complexation model in order (i) to relate the measurable concentrations and adjusted parameters of the phenomenological Langmuir equation to the chemically based quantities of the general surface complexation model and (ii) to obtain information on the concentration range and conditions in which the Langmuir equation is valid.

For the uranyl ($0.05 \mu\text{M} \leq [\text{UO}_2^{2+}]_{\text{total}} \leq 1 \mu\text{M}$) - carbonate ($p_{\text{CO}_2} = 10^{-3.5}$, $[\text{NaHCO}_3]_{\text{total}} \leq 10 \text{ mM}$) - goethite - cristobalite system (i) no polynuclear uranyl surface complexes have been observed by EXAFS on hydrous ferric oxide by Waite et al. (1994) and by time-resolved laser-induced luminescence spectroscopy on amorphous silica in I, (ii) uranyl solution polymers can be excluded (table 1, figure 3), (iii) mononuclear surface complexes on goethite have been suggested by van Geen et al. (1994) for carbonate and Sigg (1979) for silicate ions (table 4, reactions 3-6) and (iv) since $[\text{NaHCO}_3]_{\text{t}} \gg [\text{UO}_2^{2+}]_{\text{t}}$ and (iv) equilibrium with the atmosphere leads to constant free carbonate concentration and $\text{pH}=9$. Therefore the stoichiometric coefficients p , q , r , s and j can be given the following values: $p=1$, $q=1$, $r=(-2,-1)$, $s=0$ and $j=0$. The general surface complexation equation (17) simplifies then to



and the intrinsic equilibrium constant is given by:

$$K_{11r00} = \frac{[\equiv\text{FeO}_2\text{H}\text{UO}_2\text{H}_r^{2+r}]}{[\equiv\text{FeO}_2\text{H}][\text{UO}_2^{2+}][\text{H}^+]^r} \exp\left(\frac{(2+r)F\Psi_0}{R_g T}\right) \quad (27)$$

The dissolved uranyl concentration c is equal to the sum of all uranyl complexes in solution ($p = 0$ in this case) and can therefore be related to the free uranyl concentration by the mass balance (eq. 20).

$$c = [\text{UO}_2^{2+}] \sum_r \sum_s K_{01rs0} [\text{H}^+]^r [\text{CO}_3^{2-}]^s \quad (28)$$

with $r = (0,-2)$ and $s = (0,1,3)$. As free carbonate concentration and pH were assumed to be constant, total and free concentrations of dissolved uranyl concentrations are related by:

$$c = [\text{UO}_2^{2+}] \beta_{\text{UO}_2} \quad (29)$$

where β_{UO_2} was found to be equal to 1.76×10^{-12} in the following experimental conditions:

pH = 9, ionic strength $I = 0.01$ M, equilibrium with the atmosphere at a partial pressure of CO_2 of $10^{-3.5}$ atm, and total uranyl concentration in the range of 10^{-9} to 10^{-5} M.

The maximal adsorption capacity S_{max} (mol g^{-1}) is related to the total site concentration $[\equiv\text{FeO}_2\text{H}]_{\text{total}}$ (M) by the particle concentration c_p (g goethite per dm^3 of solution)

$$[\equiv\text{FeO}_2\text{H}]_{\text{total}} = S_{\text{max}} c_p \quad (30)$$

Equally the concentration of the uranyl surface complex $\equiv\text{FeO}_2\text{H}\text{UO}_2\text{H}_r^{2+r}$ (M) is related to the sorbed concentration S (mol g^{-1})

$$[\equiv\text{FeO}_2\text{H}\text{UO}_2\text{H}_r] = S c_p \quad (31)$$

thus

$$[\equiv\text{FeO}_2\text{H}]_{\text{total}} - [\equiv\text{FeO}_2\text{H}\text{UO}_2\text{H}_r] = (S_{\text{max}} - S) c_p \quad (32)$$

The Langmuir equation is based on the concentration of the sites not occupied by uranyl ($S_{\text{max}} - S$), which equals the sum of all no uranyl containing surface complexes within the surface sites mass balance (eq. 19).

$$(S_{\text{max}} - S) c_p = [\equiv\text{FeO}_2\text{H}] \sum_r \sum_s \sum_j K_{10rsj} [\text{H}^+]^r [\text{CO}_3^{2-}]^s [\text{H}_4\text{SiO}_4]^j \quad (33)$$

with $p = 1$, $q = 0$, $r = (-1, 0, 1)$ $s = (0, 1)$ and $j = (0, 1)$. Under the additional assumption of a constant free silicate concentration and a constant surface potential (eq. 33) simplifies to

$$\left(S_{\max} - S \right) = \frac{\left[\equiv \text{FeO}_2 \text{H} \right] \beta_{\equiv \text{FeO}_2 \text{H}}}{c_p} \quad (34)$$

where $\beta_{\equiv \text{FeO}_2 \text{H}}$ is a constant ratio.

Substitution of equations (29) and (34) into equation (27) leads to:

$$\frac{K_{\text{eq}}}{\beta_{\text{UO}_2} \beta_{\equiv \text{FeO}_2 \text{H}} \left[\text{H}^+ \right]^r \exp \frac{(2+r)F\Psi_0}{RT}} = K_L = \frac{S}{c \left(S_{\max} - S \right)} \quad (35)$$

which is the Langmuir equation. K_L , the Langmuir coefficient, is independent of the number of protons released per sorbed uranyl, and any site competition effects change only the value of K_L . The fitted maximum sorption capacity of the Langmuir isotherm should therefore correspond to the total site concentration of the equilibrium model.

In summary, the basic assumptions required to reduce the surface complexation to a Langmuir equation are:

1. the total concentrations of all ligands exceed the total uranyl concentration,
2. the solution buffer capacity is high,
3. no polynuclear species in solution and on the surface do occur, and
4. low uranyl surface coverage and thus a constant exponential term is reached.

In most natural systems assumption (1), (3) and (4) are valid in soils and sediments with trace element contamination. Assumption (2) may be not straightforward in the geochemical conditions of surface and groundwater but if the solution is not buffered the specific chemical conditions change and the Langmuir approach is not applicable. In the case of the non-validity of any of the four assumptions we refer to Sposito, 1983, who stated that no information on the adsorption process can be deduced from a Langmuir isotherm.

RESULTS AND DISCUSSION

Column hydrodynamics

The hydrodynamic parameters of the pure silica and the goethite-coated silica columns were determined using chloride ion as a quasi-inert tracer. No chloride retardation occurred and the residence time of the tracer was about the time necessary to replace the gravimetrically-determined pore volume of 36.2 cm^3 ($R = 1 \pm 0.05$).

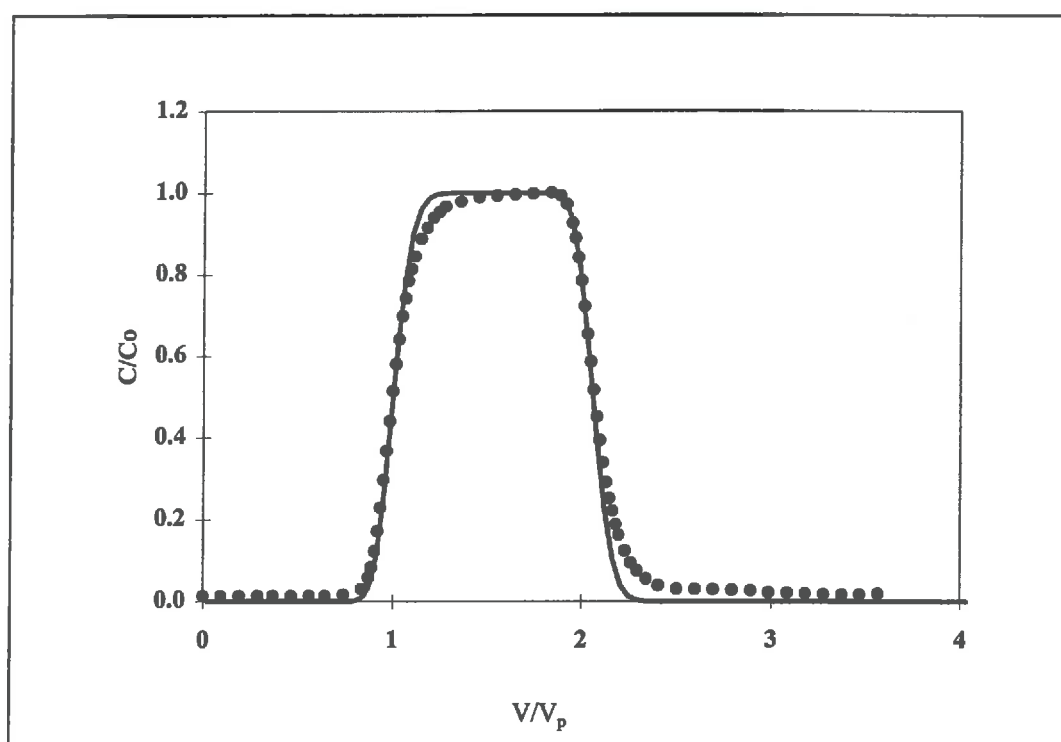


Figure 4 Break-through curve of a tracer experiment (column support: cristobalite + goethite; inlet concentration: 0.025 M NaCl; normalised values for outlet concentration and time (see text), filled circles represent experimental values, the line represents their fit (model: CDR, eq. 5).

The BTC was normalised on both axes by dividing the outlet concentration by the initial concentration of the pulse on the y-axis and the eluted water volume V by the pore volume V_p on the x-axis. The dispersion factor D for the $30 \text{ cm}^3 \text{ h}^{-1}$ flow rate experiment ($v=12.1 \text{ cm h}^{-1}$), determined by adjusting a simple convection-dispersion-model (CDR, eq. 5 with $R=1$), was

$0.6 \pm 0.3 \text{ cm}^2 \text{ h}^{-1}$ (figure 4). The expected D value, according to Pfannkuch (1963) is in the range of $0.14\text{-}0.32 \text{ cm}^2 \text{ h}^{-1}$ for particles with $\varnothing = 125 - 315 \text{ }\mu\text{m}$. The larger D value observed in our case can be explained by fractures and fissures within the cristobalite grains used in our experiments that may give rise to a small percentage of immobile water. For the $3 \text{ cm}^3 \text{ h}^{-1}$ flow rate experiment (figure 5, curve 5) the apparent dispersion are almost totally controlled by molecular diffusion, resulting in $D = 0.05 \text{ cm}^2 \text{ h}^{-1}$ (this represents $2/3$ of the molecular diffusion coefficient $D_{Cl} = 0.0731 \text{ cm}^2 \text{ h}^{-1}$ in free water). The BTC of uranyl through the pure silica column depicts practically no retardation (figure 5, Exp. 1). It can therefore be deduced in further calculations that uranyl ions do not adsorb on cristobalite at pH 9.

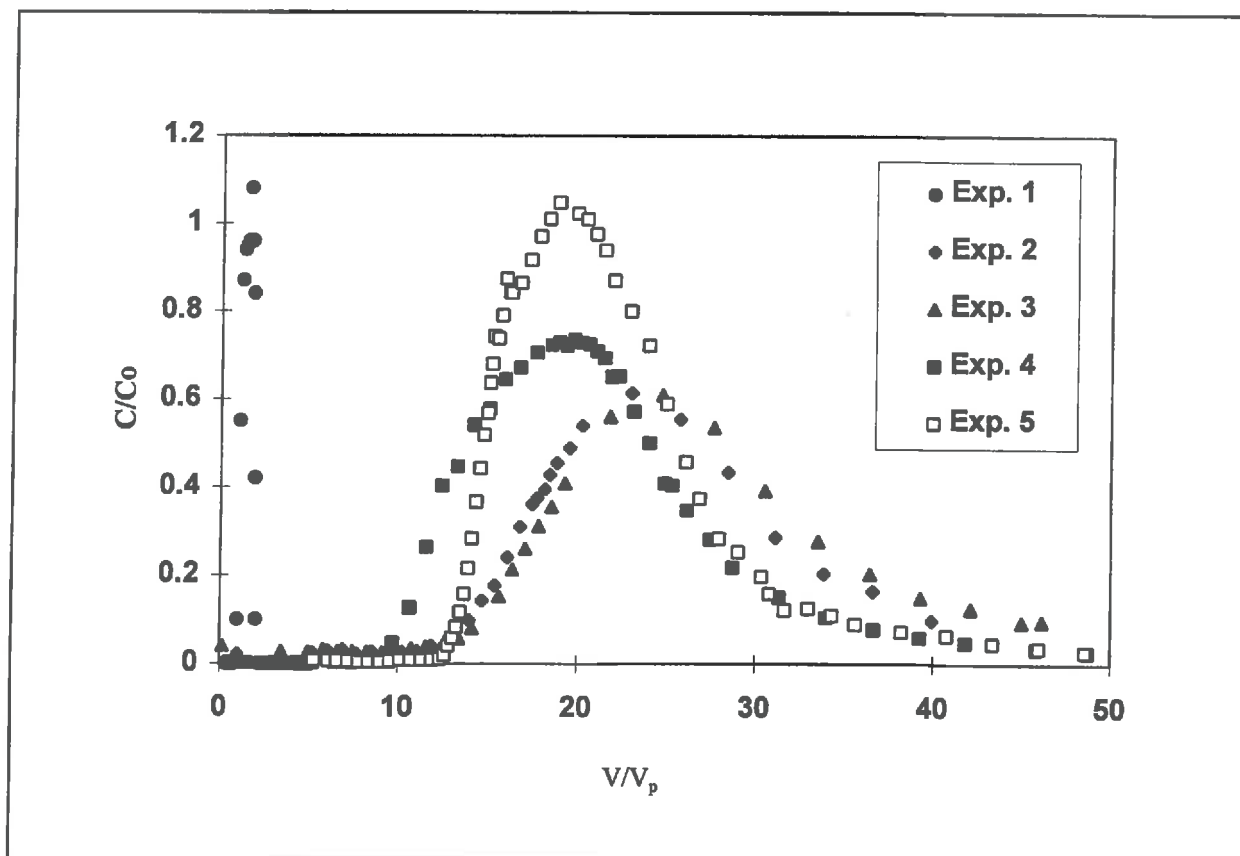


Figure 5 Break-through curves of the uranyl pulses in an otherwise pure bicarbonate solution (normalised values for concentration and time, see text for explication). Experimental conditions are listed in table 2.

Moment analysis of the BTC's

The four uranyl BTC's obtained with the goethite-coated sand column show a strong retardation and indicate a strong adsorption of uranyl onto the goethite surface (figure 5, Exp. 2 to 5). As described in the section Data analysis and models, the zero, first and second order moments (eq. 14, 15 and 16) were calculated for all five BTC's (table 2), obtaining the recovery rate, the mean uranyl residence time E , and the variance, respectively. The adsorption of uranyl onto goethite appears to be reversible, since the injected uranyl was always recovered in the interval $100 \pm 10\%$. The results from experiment 2 (91 % recovery) are less significant as the experiment was stopped too early and c_0 (the injected uranyl concentration, $0.05 \mu\text{M}$) was too close to the detection limit of 2 nM . The data from experiment 5 (108 % recovery) can be explained partly by desorption due to the slower flow velocity of uranium remaining adsorbed from precedent experiments (2-4). The retardation factors R_m calculated from the first order moment (eq. 16) are based on the gravity centre of the BTC's and represent therefore an average of the adsorption and desorption fronts (table 2).

Adsorption kinetics

The two BTC's obtained for equal uranyl concentrations but different flow velocities depict similar retardations, but different shapes of the adsorption front (figure 5, Exp. 4 and 5). The low flow velocity BTC ($3 \text{ cm}^3 \text{ h}^{-1}$, $1 \mu\text{M}$ uranyl; figure 5, Exp. 5) indicates that equilibrium has been established, as pointed out by the shape of the adsorption front and by the amplitude of the maximum concentration reached (more than 100 % of the input concentration for the low flow velocity BTC). On the other hand equilibrium is not reached in the high velocity experiment ($c/c_0 = 0.73$; figure 5, curve 4).

The observed non-symmetrical curves at both flow velocities (relative steep rising (adsorption) fronts and long flat tailings representing the desorption) indicate a non-linear (convex) adsorption isotherm. The effects convex adsorption isotherms have on the BTC if local equilibrium can be assumed was extensively described by Schweich and Sardin (1981). They described the generally flattening effects the dispersion has on a propagating concentration pulse to be superimposed by distortion of the originally symmetric pulse into a

self-sharpening adsorption and a *diffusive* desorption front. An excellent practical example of Cd^{2+} adsorption on cristobalite sand was given in Buergisser et al. (1993).

Table 2 Column experiments

	Experiment				
	1	2	3	4	5
column	crist.	crist. + goet.	crist. + goet.	crist. + goet.	crist. + goet.
flow rate ($\text{cm}^3 \text{h}^{-1}$)	30	30	30	30	3
pulse length (h)	0.90	14.16	13.98	13.94	138.93
uranyl (μM)	1	0.05	0.1	1	1
NaHCO_3 (mM)	10.42	10.02	10.04	10.42	10.42
pH	9.4..9.6	8.87..8.95	8.85..8.95	9.25..9.35	8.85..9.05
	Moment analysis (eq.14)				
First Moment B (h)	1.765	385	441	370	38203
mean Travel time E (h, eq. 15)	56.773	29.71	31.71	26.99	254.67
second Moment H	2913	962	1470	1527	799540
Variance	93.725	74.3	105.7	111.3	5330
recovery (%)	95.5	91.4	99.5	98.4	108.0
retardation factor R_m (eq.16)	1.08	18.69	20.41	16.32	15.29
	Transport model including first order kinetics (CDR-cin, eq. 3 & 8)				
rate constant (h^{-1})	30	1.7	1.7	1.7	1.2
dispersion ($\text{cm}^2 \text{h}^{-1}$)	0.6	0.6	0.6	0.6	0.04
retardation factor R	1.1	19	20	14.5	14
distribution coeff. ($\text{dm}^3 \text{g}^{-1}$)	-	1.05	1.1	0.79	0.76
	Nonlinearity of the isotherm				
ΔR (in %)	-	0.31 (1.65)	0.4 (2.0)	1.82 (12.6)	1.29 (9.2)

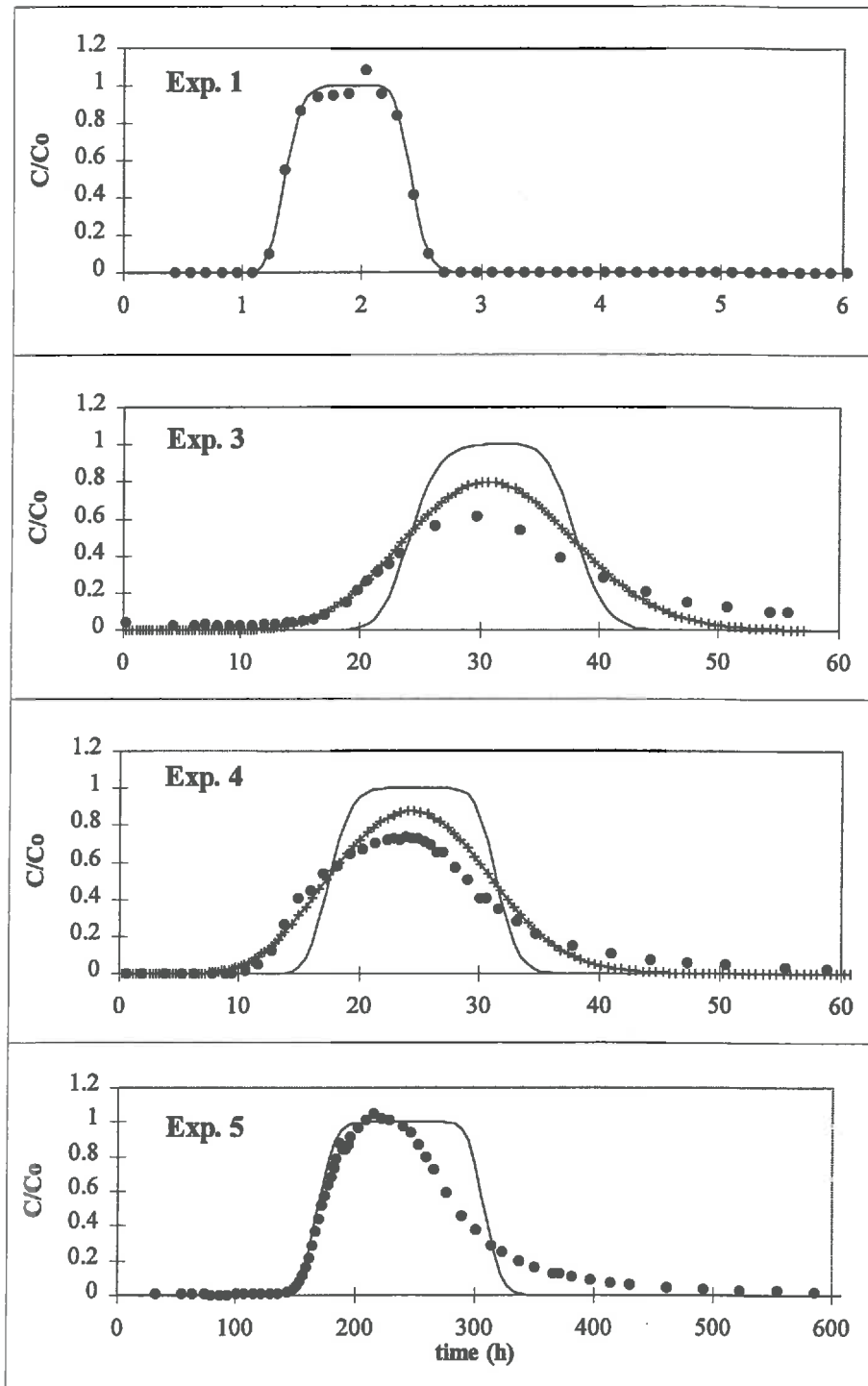


Figure 6 Comparison of observed break-through curves (•) and predicted transport simulations (- model: CDR, eq. 5) and (+ model CDR-cin, eq. 3 & 8). In both cases, linear adsorption behaviour is assumed. Normalised concentrations are plotted as a function of real time. Experimental conditions are listed in table 2.

As the shape of the adsorption front is only little influenced by a convex adsorption isotherm, we adjusted the rising parts of the BTC's with the model **CDR-cin** (eq. 3 and 8), assuming first order adsorption/desorption kinetics and linear adsorption (figure 6). The difference between the numerically calculated and the experimental desorption front is due to the nonlinear adsorption isotherm and/or different adsorption/desorption kinetics. The obtained retardation factors R differed from the ones calculated from the first moment which reflected both, adsorption and desorption. Experimental adsorption fronts could be adequately described, assuming a reaction rate of 1.7 h^{-1} for experiments 3 and 4 and local equilibrium (model: **CDR**, eq. 5) for experiment 5. The adsorption rate results in a half life of 25 min. This is rather long compared to the residence time of the eluting solutions (1.2 h at $30 \text{ cm}^3 \text{ h}^{-1}$ and 12 h at $3 \text{ cm}^3 \text{ h}^{-1}$). Thus only $\approx 87 \%$ of the reaction is accomplished at the rapid flow velocity. However, one must consider that the average residence time of the sorbent is different from the residence time of the eluting solution and it depends on the state of the sorbing material (i.e. on the saturation of the sites), the pulse duration, and the retardation factor. For the slow flow velocity (flow rate of $3 \text{ cm}^3 \text{ h}^{-1}$) the local equilibrium assumption can be applied (the residence time of uranyl is 127 h).

Non-symmetrical BTC and Langmuir-type adsorption

The relation between the non-symmetry of the BTC's and the non-linearity of the adsorption isotherm under the local equilibrium assumption was already discussed. Our experimental results indicate that the distorting effect of the nonlinear adsorption isotherm superposes not only the flattening effect of the dispersion (Schweich and Sardin, 1981) but also the similar one of the reaction kinetics. Therefore the increasing symmetry in the BTC's (figure 5) for the initial uranyl solutions concentrations from $1 \text{ }\mu\text{M}$ (exp. 4) to $0.05 \text{ }\mu\text{M}$ (exp. 2) characterises the decreasing non-linearity of the isotherm. Very similar, nearly symmetrical BTC's, are found in experiment 2 ($0.05 \text{ }\mu\text{M}$) and experiment 3 ($0.1 \text{ }\mu\text{M}$). The linear range of the adsorption isotherm is confirmed by the same retardation ($R=19.5 \pm 0.5$) within the experimental errors of 5 % of these BTC's, and also by the very similar values of the retardation factors obtained by moment analysis R_m and with the model **CDR-cin** R ($\Delta R=0.4$, i.e. about 2%). The higher initial uranyl solution concentration in Exp. 4 caused an earlier break-through (at 74 % of the passed volume) of the concentration pulse ($R=14.5$), indicating

less adsorption, thus confirming the convex isotherm (Buergisser et al., 1993). The less symmetrical BTC is also proven by the larger difference between the two retardation factors ($\Delta R=1.8$, i.e. about 13 %). The retardation factor R (model CDR-cin) obtained in the transport simulation can be used to calculate a distribution coefficient (eq. 6).

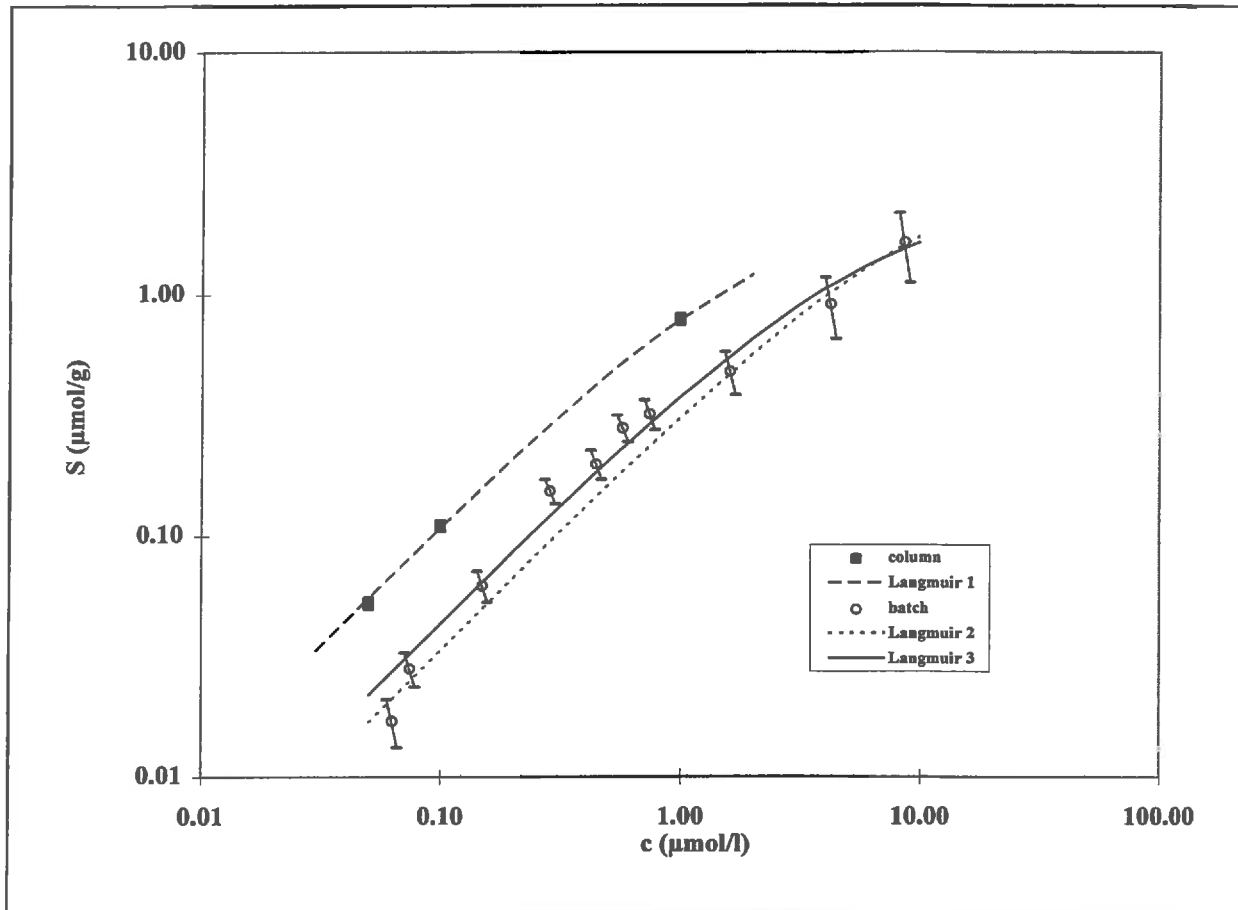


Figure 7 Langmuir isotherms (table 3) derived from batch adsorption data and transport experiments. Experimental points for the transport experiments were obtained from the retardation factors of model CDR-cin (table 2).

In figure 7 the experimental values describing uranyl adsorption in the column and isotherm batch experiments are compared. It appears that at equal uranyl solution concentration, uranyl adsorption was more important in the column than in the batch experiments. The experimental

data (figure 7) were fitted with the Langmuir equation (11) (Langmuir 1 and 2 in table 3; dashed and dotted line in figure 7).

The error bars in figure 7 indicate a much greater uncertainty in the batch data than for the data from the column experiments. In both cases the error in the solution concentrations was assumed to be 5 %. For any given batch experiment, the resulting error in the sorbed concentration would be 0.55 % for 90 % adsorption and 45 % for 10 % adsorption. On the contrary, the sorbed concentrations in the column experiments are much less affected by the errors of the uranyl analysis, since with 5 % error in the solution concentration the BTC is not shifted to a different retardation. Nonetheless, it should be noted that the sorbed concentration in the column experiments is susceptible to errors in flow measurement, which in our case is realised by measuring the diminishing mass of the solution in the reservoir (figure 1) and weighing the samples. Results from the batch experiments could be described by the Langmuir equation, assuming a similar adsorption capacity as in the more accurate column experiments (Langmuir 3 in table 3, full line in figure 7).

Table 3 Langmuir isotherms ($\equiv\text{FeO}_2\text{H} + \text{UO}_2^{2+} \leftrightarrow \equiv\text{FeO}_2\text{HUO}_2^{2+}$)

	S_{max} ($\mu\text{mol g}^{-1}$)	$\log K_L$	experiment
Langmuir 1	2.62	5.64	column
Langmuir 2	3.57	4.98	batch
Langmuir 3	2.62	5.22	batch

At a $3 \text{ cm}^3 \text{ h}^{-1}$ flow rate (experiment 5) adsorption is at equilibrium and the BTC could be modelled with a numerical solution for the non-linear adsorption (model: **CDR-Langmuir**, eq. 12, figure 8). In this solution we used the K_L value derived from the column experiments (observed retardation in experiments 2 - 4). Although the BTC could be adequately described by our numerical solution, such a model is of limited use as it is (as the Langmuir approach) limited to a given pH and ligand concentration. In order for the model to be valid for various solution conditions, a complexation model had to be developed.

Maximum care was taken to reproduce in batch and column experiments conditions that were as similar as possible. However, chemical conditions were not exactly the same in the column and batch experiments, due in part to fluid residence time differences. The greatest difference was the concentration of aqueous silica resulting from cristobalite dissolution. The contact time in the batch experiments was 12 days, which resulted in an aqueous silica concentration of about 1 mM, which is about one third of the solubility of quartz (figure 10c). In column experiments, dissolution of the cristobalite also occurred, but to a smaller extent (16 μM for the flow rate of $3 \text{ cm}^3 \text{ h}^{-1}$ and below the aqueous silica detection limit - i.e. below $2 \mu\text{M}$ - for the $30 \text{ cm}^3 \text{ h}^{-1}$ flow rate). At pH 9 no complexation of uranyl ions with aqueous silica occurs (figure 3), which is in accordance with the non-adsorption of uranyl onto silica at this pH. Therefore the aqueous silica had no influence on the solution speciation of uranyl and must affect the uranyl sorption isotherm via competitive sorption onto goethite. A 50 to 500 fold increase of the aqueous silica concentration reduces uranyl adsorption by 50 % (figure 7).

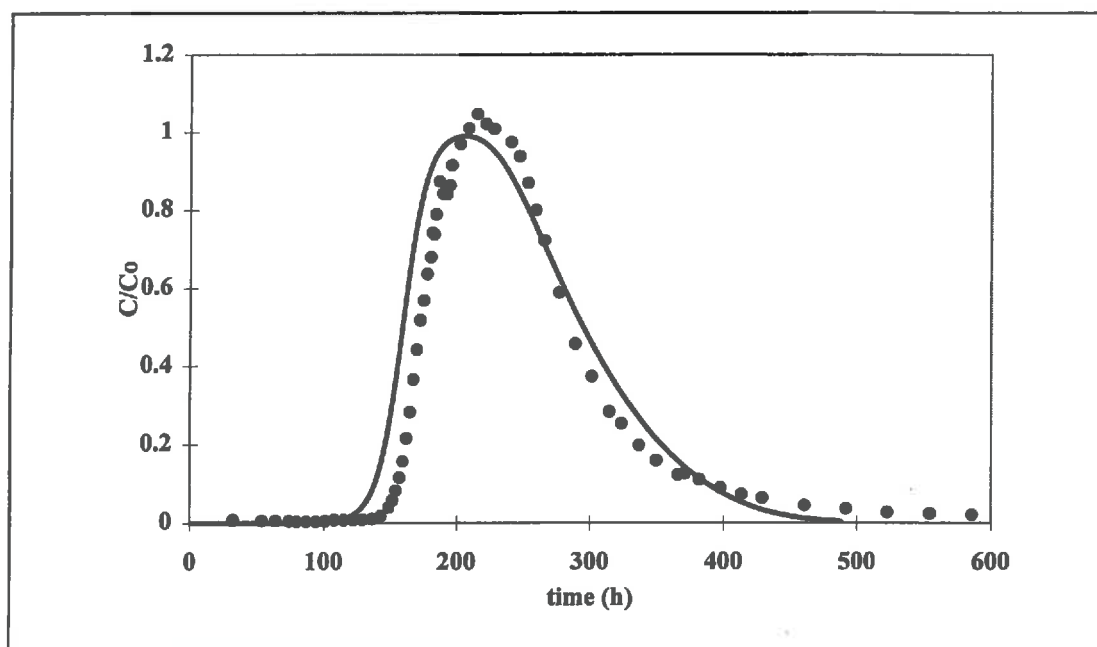


Figure 8 Transport simulation (model: CDR-Langmuir) of experiment 5 (•, initial uranyl concentration $1 \mu\text{M}$, flow rate $3 \text{ cm}^3 \text{ h}^{-1}$) assuming local equilibrium and the Langmuir isotherm derived from the adsorption fronts of column experiments 2-4 ($\log K_L = 5.64 \text{ M}^{-1}$, $S_{\text{max}} = 2.62 \mu\text{mol g}^{-1}$).

General surface complexation model

The intrinsic constants for the protonation/deprotonation equilibria (reactions 1 and 2 in table 4) and for the carbonate ion surface complexation (reactions 3 and 4 in table 4). They were obtained by adjusting data from van Geen et al. (1994) with a constant capacitance model (specific surface area $A_s = 45 \text{ m}^2 \text{ g}^{-1}$; specific capacitance $\kappa = 1.75 \text{ F m}^{-2}$; mass related total site concentration $[\equiv\text{FeO}_2\text{H}] = 0.173 \text{ mmol g}^{-1}$). The intrinsic silicate adsorption constants were obtained from experimental data reported by Sigg (1979), using a mass related total site concentration $[\equiv\text{FeO}_2\text{H}] = 0.35 \text{ mmol g}^{-1}$. We used our own set of protonation/deprotonation intrinsic constants, which are consistent with the currently accepted zero charge point (PZC) of $\text{pH} = 8.9$, rather than Sigg's (1979) constants (which lead to a PZC value of 7.3). Two silicate surface complexes were assumed (release of zero or one proton, reactions 5 and 6 in table 4). Sigg's titration data in the presence of aqueous silica were adequately described assuming an initial negative permanent charge of $55 \text{ } \mu\text{mol g}^{-1}$, which accounts for her low PZC value, and may have been due to either an initial contamination of the surface by carbonate ions (van Geen et al., 1994) or to Fe^{3+} substitution by Fe^{2+} : a substitution rate of 0.3 % for the goethite prepared after Atkinson et al. (1967) was observed which is comparable to the 0.5 % needed to explain the assumed permanent charge (Bidoglio et al., 1993). Our complete modelling set for the uranyl adsorption included the particle concentration $c_p = 0.82 \text{ g dm}^{-3}$; the specific surface area $A_s = 80.5 \text{ m}^2 \text{ g}^{-1}$; the specific capacitance $\kappa = 1.75 \text{ F m}^{-2}$ and the mass related total site concentration $[\equiv\text{FeO}_2\text{H}] = 0.309 \text{ mmol g}^{-1}$. The equilibrium constants are presented in table 4.

All experimental data (batch: isotherm and desorption edge; column: isotherm) were fitted by iteration using the Newton-Raphson procedure implemented in GRFIT (Ludwig, 1993). Different uranyl surface complexes were assumed, with a release of one to three protons. It appeared that the isotherm batch and column data ($\log K = -2.31$), as well as the desorption edge data ($\log K = -2.10$), could be adequately described, within the error bars, by using a single surface complex with a release of two protons (eq. 17, $r = -2$). The assumed mass related total surface site concentration ($0.309 \text{ mmol g}^{-1}$) and the maximum sorbed concentration of $1.65 \text{ } \mu\text{mol g}^{-1}$ indicate that only 0.5 % of the sites are occupied by uranyl. The resulting isotherm is linear since the influence of uranyl ions on the surface potential is negligible and the total site concentration is far from being the limiting parameter for uranyl

adsorption. The non-linearity of the adsorption isotherm is not obvious from the batch experimented data, due to the large experimental uncertainty (figure 7), but is clearly indicated by the dynamic results (figure 5).

Tab. 4 Intrinsic constants (log K) for the goethite surface speciation (Constant Capacitance Model; I = 0)

Reactions	logK	
$\equiv\text{Fe}^{s/w}\text{O}_2\text{H} + \text{H}^+ \leftrightarrow \equiv\text{Fe}^{s/w}\text{O}_2\text{H}_2^+$	7.33	(1)
$\equiv\text{Fe}^{s/w}\text{O}_2\text{H} - \text{H}^+ \leftrightarrow \equiv\text{Fe}^{s/w}\text{O}_2^-$	-9.88	(2)
$\equiv\text{Fe}^{s/w}\text{O}_2\text{H} + \text{H}_2\text{CO}_3^\circ - \text{H}_2\text{O} \leftrightarrow \equiv\text{Fe}^{s/w}\text{OHCO}_3^\circ$	3.616	(3)
$\equiv\text{Fe}^{s/w}\text{O}_2\text{H} + \text{H}_2\text{CO}_3^\circ - \text{H}^+ - \text{H}_2\text{O} \leftrightarrow \equiv\text{Fe}^{s/w}\text{OCO}_3^-$	-3.398	(4)
$\equiv\text{Fe}^{s/w}\text{O}_2\text{H} + \text{H}_4\text{SiO}_4^\circ - \text{H}_2\text{O} \leftrightarrow \equiv\text{Fe}^{s/w}\text{OH}_3\text{SiO}_4^\circ$	3.5	(5)
$\equiv\text{Fe}^{s/w}\text{O}_2\text{H} + \text{H}_4\text{SiO}_4^\circ - \text{H}^+ - \text{H}_2\text{O} \leftrightarrow \equiv\text{Fe}^{s/w}\text{OH}_2\text{SiO}_4^-$	-3.89	(6)
model I: (Fe^w 1p, Fe^s 2p)		
$\equiv\text{Fe}^w\text{O}_2\text{H} + \text{UO}_2^{2+} - \text{H}^+ \leftrightarrow \equiv\text{Fe}^w\text{O}_2\text{UO}_2^+$	4.307	(7)
$\equiv\text{Fe}^s\text{O}_2\text{H} + \text{UO}_2^{2+} - 2 \text{H}^+ + \text{H}_2\text{O} \leftrightarrow \equiv\text{Fe}^s\text{O}_2\text{UO}_2\text{OH}^\circ$	-0.044	(8)
model II: (Fe^w 2p, Fe^s 2p)		
$\equiv\text{Fe}^w\text{O}_2\text{H} + \text{UO}_2^{2+} - 2 \text{H}^+ + \text{H}_2\text{O} \leftrightarrow \equiv\text{Fe}^w\text{O}_2\text{UO}_2\text{OH}^\circ$	-3.13	(9)
$\equiv\text{Fe}^s\text{O}_2\text{H} + \text{UO}_2^{2+} - 2 \text{H}^+ + \text{H}_2\text{O} \leftrightarrow \equiv\text{Fe}^s\text{O}_2\text{UO}_2\text{OH}^\circ$	-0.044	(10)

Fe^w = less active sites on the dominant crystal faces; Fe^s = high reactive sites on the small crystal faces (e.g. end of the crystals or lattice defects). For proton, carbonate and silicate sorption Fe^{s/w} represents either site. Equation numbers are referred to in the text. Reaction products were written as to represent known or supposed structures (contrary to the matrices derived definition in the text!).

Site heterogeneity

The adjusted maximum sorption capacity of 2.62 μmol per g goethite of the Langmuir isotherm (table 3, figure 7) is in contradiction to the reported complete adsorption of 10 μmol g⁻¹ uranyl (Hsi and Langmuir, 1985, neutral pH, CO₂ excluded) and represents only about 1 % of the theoretical total surface site concentration (0.309 mmol sites g⁻¹ according to Dzombak and Morel, 1990, for 80.5 m² g⁻¹ and 2.31 sites nm⁻²). We concluded that this empirical maximum sorption capacity may in fact correspond to some high affinity sites located at the end of the goethite double chains of octahedral Fe. Although the (021) crystal faces are

reported to represent approximately 10 % of the total surface Benjamin and Leckie (1981) reported an even smaller proportion of the high affinity sites, and this proportion differed for the different cations (Cu, Zn and Pb). The high to low affinity site concentration ratio appears not be linearly related to the surface proportion of these sites. They appear to be also controlled by the type and the dimensions of the coordination polyhedra of the sorbed cation.

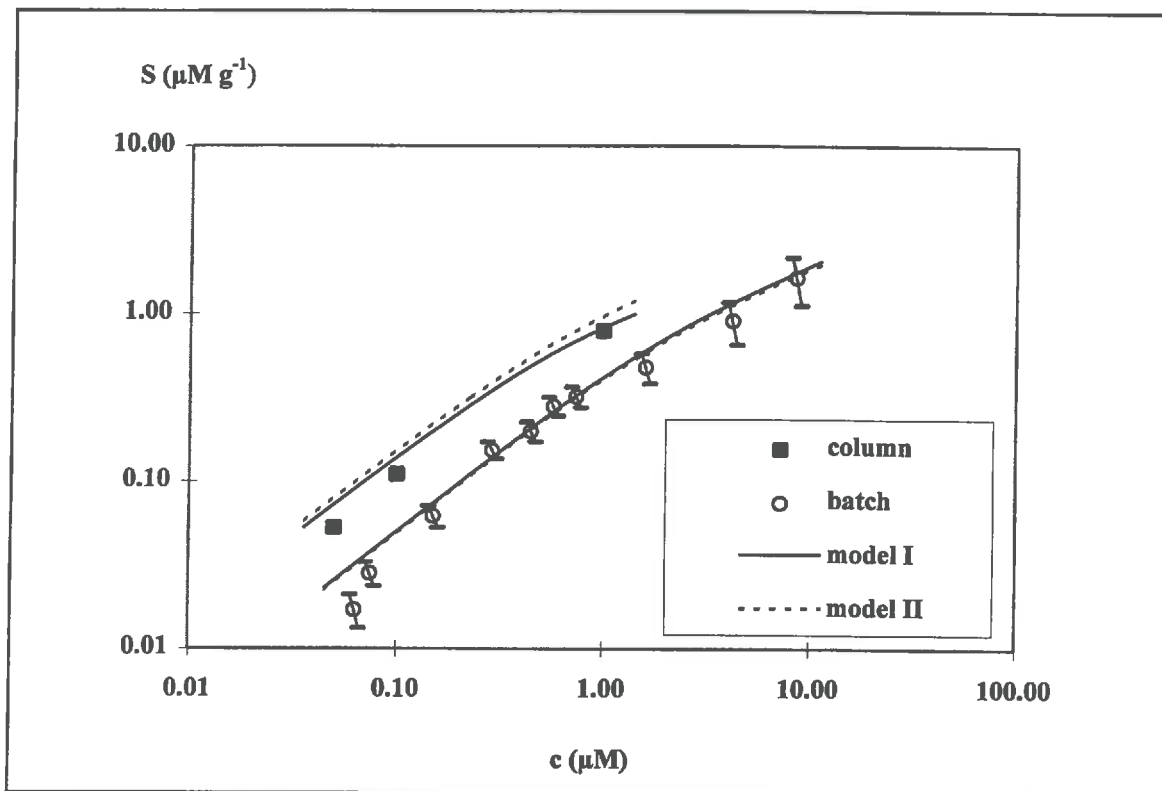


Figure 9 Surface complexation model (constant capacitance) to the batch adsorption data and transport experiments (experimental points from the kinetic transport model). model I: $\text{Fe}^{\text{W}} 1\text{p}$, $\text{Fe}^{\text{s}} 2\text{p}$; model II: $\text{Fe}^{\text{W}} 2\text{p}$, $\text{Fe}^{\text{s}} 2\text{p}$; Fe^{W} = less active sites on the dominant crystal faces; Fe^{s} = high reactive sites on the small crystal faces (e.g. end of the crystals or lattice defects); 1p and 2p denotes the release of one or two protons.

We assumed the presence of an additional stronger surface site, $\equiv\text{Fe}^{\text{s}}\text{O}_2\text{H}$, at a concentration ratio of $[\equiv\text{Fe}^{\text{s}}\text{O}_2\text{H}]:[\equiv\text{Fe}^{\text{W}}\text{O}_2\text{H}] = 1:200$, which is characterised by a higher affinity for uranyl. Indeed, equal adsorption affinities for various tetrahedral anions, such as selenate or arsenate, on both types of goethite surface sites had been reported (Manceau and Charlet, 1994), and we assume this to be true for aqueous silica as well. For large, sixfold-coordinated cations (e.g.

cadmium ions), adsorption is favoured on the reactive sites present on the crystal ends of goethite (021), and results in a non-linear adsorption isotherm (Venema et al., 1996). For the five-coordinated uranyl ions (Aberg et al., 1983; Thompson et al., 1997) similar edge-sharing surface complexes have been reported (Manceau et al., 1992; Waite et al., 1994). We therefore assumed that adsorption of uranyl occurs on high energy sites (with a release of two protons, reactions 8 and 10 in table 4) and on low energy sites (with a release of either one or two protons, reactions 7 and 9 table 4). Both models converged on the sorption isotherms (obtained from batch and from column experiments: figure 9) and on the pH desorption edge (figure 10) to approximately the same constants, so no precise stoichiometry of the reaction can be deduced from our data. Average intrinsic adsorption constants (table 4) lead to the computed curves reported in figures 9 and 10a.

The proposed surface complexation model adequately describes the adsorption data in terms of pH and uranyl concentration. However, for application purposes it might be beneficial to simplify the set of competing reactions. A way to simplify such computations is to calculate 'theoretical' Langmuir isotherms for both adsorption sites with the chemical equilibrium model. With our experimental data set this is however not possible as high energy sites dominate the sorption process in the explored concentration range. In order to obtain a convincing two-site Langmuir isotherm more column adsorption data, particularly in the higher concentration range, are necessary. Comparison of a two-site Langmuir fit to the parameters of the theoretically deduced Langmuir isotherm could give complementary information on the adsorption mechanism.

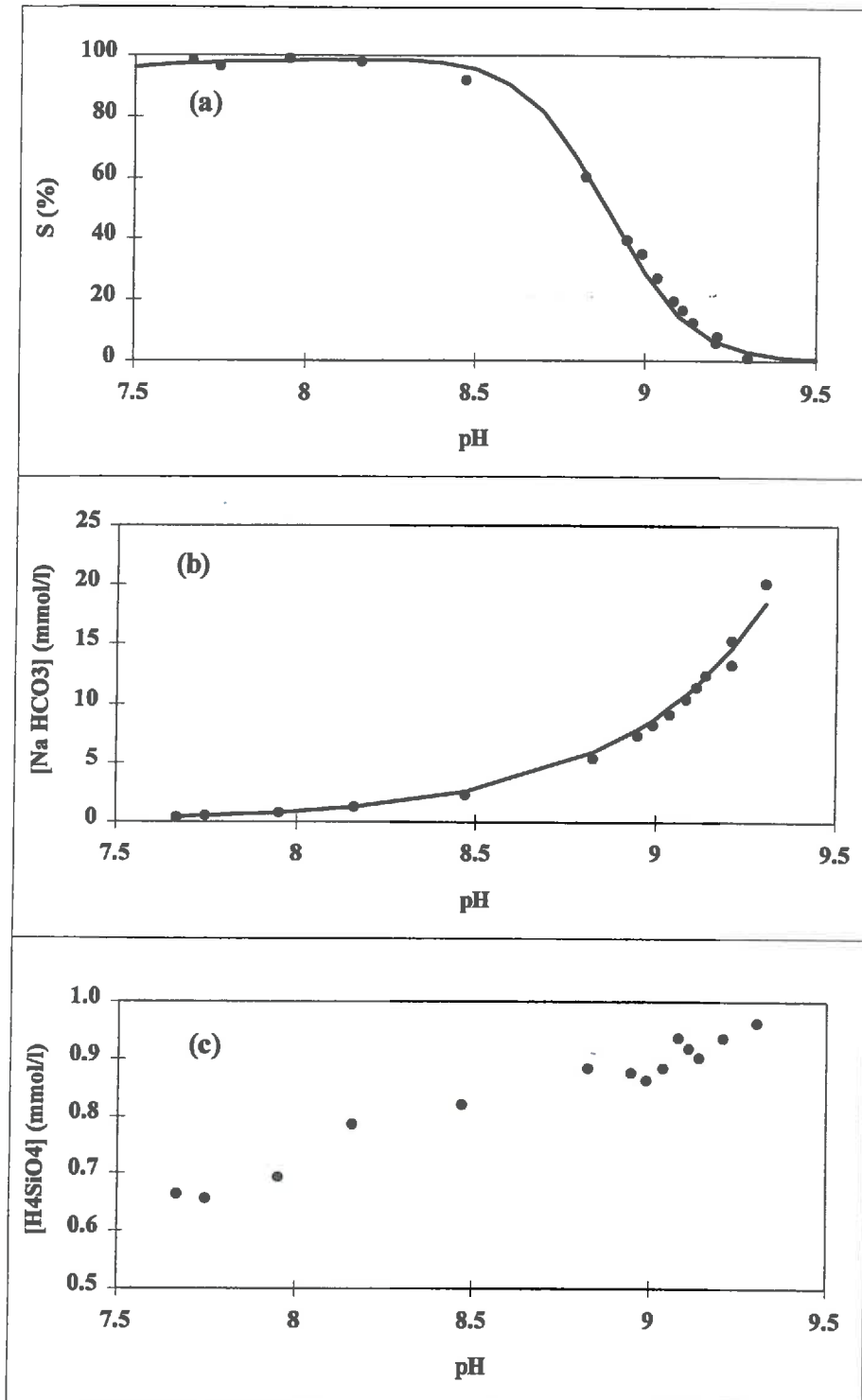


Figure 10 Experimental and calculated pH desorption edge for uranyl (1 μ M) on goethite in equilibrium with the atmosphere (a), experimental and calculated concentration of NaHCO₃ (b) and experimental concentration in silicic acid in the batch experiments (c). Constants for solution complexation are listed in table 1 and for the formation of surface complexes in table 3.

CONCLUSIONS

Movement of uranium out of mine waste material has to be taken into account in long term environmental risk assessments. It occurs in the aqueous phase and is controlled by interactions between dissolved uranium and mineral particles. Other aqueous species, such as silica and carbonate ions, may influence this movement since they may both form complexes with uranyl ions in solution and compete with uranyl ions for adsorption on the most reactive surface sites on mineral grains.

The transport of uranyl was studied in goethite-coated sand columns and the impact of competitive adsorption or solution complexation reactions with carbonate and aqueous silica was evaluated. Goethite (α -FeOOH), which shows a very high affinity towards uranyl ions, was chosen as a model mineral surface for this study, and was coated onto cristobalite sand, a non-reactive support. The observed Langmuir-like adsorption phenomena led to: (1) an earlier break-through of uranyl with increasing solution concentration, (2) a steep adsorption front and (3) a relatively flat desorption tail. Slow reaction kinetics caused smoother BTC's. The adsorption front was simulated applying the convection-dispersion-equation combined with the retardation concept and first order reaction kinetics (model: **CDR-cin**, eq. 3 and 8). The adsorption rate was found to be equal to 1.7 h^{-1} . The desorption front could only be modelled under the assumption of local equilibrium (model: **CDR-Langmuir**, eq. 12).

Both column and batch adsorption data, could be adequately described using either the Langmuir equation or a comprehensive surface complexation model. In both cases the maximum sorption capacity was fixed. The automatic adjustment of the Langmuir isotherm led to a surface site concentration of $2.62 \mu\text{mol g}^{-1}$. In the surface complexation model two sites were incorporated with a total site concentration of 0.31 mmol g^{-1} and a 1:200 ratio between the two sites.

A major conclusion of this study is the effect of aqueous silica which competes with uranyl ions for surface sites. Therefore, a simple addition of independent sorption phenomena for uranyl and aqueous silica/carbonate ions may highly oversimplify natural systems and lead to erroneous predictions.

ACKNOWLEDGEMENTS

We are grateful to the radiochemistry department of the Forschungszentrum Rossendorf, Germany, where one of the authors spent several weeks learning how to operate the equipment used to study time-resolved laser-induced fluorescence. U.G. also thanks the « Pole Européen » for a doctoral scholarship. The authors would like to express their gratitude to the team working on porous silica of the laboratory Spectrometrie Physique, Grenoble, for providing the material and assisting abundantly in the elaboration of the device to quantify the uranyl solution concentration. We thank Detlef Lazik, Umweltforschungszentrum Leipzig/Halle, Germany, for performing the BET surface area measurements. We also thank R. Hellmann for the assistance in the analysis of the aqueous silica and R. Hellmann and Scott Tyler for comments on the manuscript and improving the English.

ANNEX

Analytical solution of Toride et al. (1993) and Toride and Leij (1996)

(equations 3, 5, 8 and 9a, b, c)

$$f_f = c_0 * [\Gamma(z, t, R = 1) * e^{(-\alpha * (R-1) * t)} + \alpha * \sqrt{R-1} * \int_0^t \frac{\sqrt{\tau}}{\sqrt{t-\tau}} * \Gamma(z, \tau, R = 1) * H(\tau, t) d\tau] \quad (36)$$

with

$$\Gamma(z, \tau, R = 1) = \frac{z * \sqrt{R}}{2 * \sqrt{\pi} * D * \tau} * e^{[-\frac{R * z - \nu * \tau}{4 * D * R * \tau}]} \quad (37)$$

and

$$H(\tau, t) = e^{-\alpha * (R-1) * \tau - \alpha * (t-\tau)} * I_j * [2 * \alpha * \sqrt{(R-1) * (t-\tau) * \tau}] \quad (38)$$

where I_j is the modified Bessel function of the j^{th} order.

LITERATURE

- Aberg, M., Ferri, D., Glaser, J. and Grenthe, I., 1983. Structure of the Hydrated Dioxouranium(VI) Ion in Aqueous solution. An X-ray Diffraction and ^1H NMR Study. *Inorg. Chem.*, 22: 3986-3989.
- Atkinson, R. J., Posner, A. M. and Quirk, J. P., 1967. Adsorption of potential-determining ions at the ferric oxide-aqueous electrolyte interface. *J. Phys. Chem.*, 71: 550-558.
- Akratanakul, C.C., Boersma, L. and Klock, O. O., 1983. Sorption processes in soils as influenced by pore water velocity. II. Experimental results. *Soil Sci.*, 135: 331-341.
- Bear, J., 1972. *Dynamics of Fluids in Porous media*. American Elsevier, New York.
- Benjamin, M. M. and Leckie, J. O., 1981. Multiple-Site Adsorption of Cd, Cu, Zn, and Pb on Amorphous Iron Oxyhydroxide. *Journal of Colloid and Interface Sciences*, 79: 209-221.
- Bernhard, G., Geipel, G., Brendler, V. et Nitsche, H., 1996. Speciation of Uranium in Seepage Waters of a Mine tailing Pile Studied by Time-Resolved Laser-Induced Fluorescence Spectroscopy (TRLFS). *Radiochimica Acta*, 74, 87-91.
- Bidoglio, G., Gibson, P. N., O'Gorman, M. and Roberts, K. J., 1993. X-ray absorption spectroscopy investigation of surface redox transformations of thallium and chromium on colloidal mineral oxides. *Geochim. Cosmochim. Acta*, 57: 2389-2394.
- Brina, R. and Miller, A. G., 1992. Direct detection of trace levels of uranium by laser-induced kinetic phosphorimetry. *Anal. Chem.*, 64: 1413-1418.
- Buergisser, C. S., Cernik, M., Borkovec, M. and Sticher, H., 1993. Determination of Nonlinear Adsorption Isotherms from Column Experiments: An Alternative to Batch Studies. *Environ. Sci. Technol.*, 27: 943-948.
- Chaudhari, M., 1971. An improved Numerical Technique for Solving Multidimensional Miscible Displacement Equations. *Society of Petroleum Engineer Journal*, September: 277-284.
- Davies, C. W., 1962. *Ion Association*. Washington, D.C., Butterworth.
- Dzombak, D.A. and Morrel, F. M. M., 1990. *Surface Complexation Modeling: Hydrous Ferric Oxide*. New York, John Wiley and Sons.
- Geipel, G., Bernhard, G., Brendler, V. and Nitsche, H., 1996; Sorption of Uranium(VI) on Rock Material of a Mine Tailing Pile: Solution Speciation by Fluorescence Spectroscopy. *Radiochimica Acta*, 74: 235-238.
- Grenthe, I., Fuger, J., Konings, R. J. M., Lemire, R. J., Mueller, A. B., Nguyen-Trung, C. and Wanner, H., 1992. *Chemical Thermodynamics of Uranium: NEA-TDB, OECD, North-Holland, Amsterdam*.
- Hsi, C-K. D. and Langmuir, D., 1985. Adsorption of uranyl onto ferric oxyhydroxides: Application of the surface complexation site binding model. *Geochim. Cosmochim. Acta*, 52: 1931-1941.
- Jury, W. A. and Roth, K., 1990. *Transfer Functions and Solute Movement through Soil: Theory and application*. Basel, Boston, Berlin, Birkhaeuser, 1990.
- Kato, Y., Meinrath, G., Kimura, T. et Yoshida, Z., 1994. A study of U(VI) Hydrolysis and Carbonate Complexation by Time-Resolved Laser-Induced Fluorescence Spectroscopy (TRLFS). *Radiochimica Acta*, 64, 107-111.
- Kohler, M., Wieland, E. and Leckie, J. O., 1992. Metal-ligand-surface interactions during sorption of uranyl and neptunyl on oxides and silicates. *Water-Rock-Interaction, Khrarka and Maest* (eds.), Balkema, Rotterdam, 51-54.

- Ludwig, C., 1993. Koordinationschemie an der Grenzflaeche Oxid/Wasser, I. Ternaere Oberflaechenkomplexe mit Cu(II) und organischen Liganden und TiO₂ (Anatas), II. Ein Modell zur Beschreibung der Deprotonierung von Al₁₃O₄(OH)₂₄(H₂O)₁₂⁷⁺. PhD thesis, University of Bern.
- Lumsdon, D. G. and Evans, L. J., 1994. Surface complexation Model Parameters for Goethite (α -FeOOH). *Journal of Colloid and Interface Sciences*, 164: 119-125.
- Manceau, A. and Charlet, L., 1994. The mechanism of selenate Adsorption on Goethite and Hydrous Ferric Oxide. *Journal of Colloid and Interface Sciences*, 168: 87-93.
- Manceau, A., Charlet, L. Boisset, M. C., Didier, B. and Spadini, L., 1992. Sorption and speciation of heavy metals on hydrous Fe and Mn oxides. From microscopic to macroscopic. *Applied Clay Science*, 7: 201-223.
- Meinrath, G., Klenze, R. et Kim, J. I., 1996. Direct Spectroscopic Speciation of Uranium(VI) in Carbonate Solutions. *Radiochimica Acta*, 74, 81-86.
- Miller, D. M., Summer, M. E. and Miller, W. P., 1989. A comparison of Batch and Flow Generated Anion Adsorption Isotherms. *Soil Sci. Soc. Am. J.*, 53: 373-380.
- Morrison, S. J., Spangler, R. R. and Tripathi, V. S., 1995a. Adsorption of uranium(VI) on amorphous ferric oxyhydroxide at high concentrations of dissolved carbon(IV) and sulfur(VI). *Journal of Contaminant Hydrology*, 17: 333-346.
- Morrison, S. J., Tripathi, V. S. and Spangler, R. R., 1995b. Coupled reaction/transport modeling of a chemical barrier for controlling uranium(VI) contamination in groundwater. *Journal of Contaminant Hydrology*, 17: 347-367.
- Persaud, N., Davidson, J.M. and Rao, P.S.C., 1983. Miscible displacement of inorganic cations in a discrete homoionic exchange medium. *Soil Science*, 136(5): 269-278.
- Pfannkuch H. F., 1963. Contribution à l'étude des déplacements de fluides miscibles dans un milieu poreux; Thèse de troisième cycle présentée à l'Université de Paris; *Revue de l'IFP*, vol. XVIII, n°2.
- Scheidegger, A., 1993. Die Adsorption von Protonen, Fluorid und Cadmium in einer Goethit-Saeule. PhD Thesis ETH 10215 Zuerich.
- Schindler, P.W. and Kamber, H.R., 1968. Die Aciditaet von Silanolgruppen. *Helv. Chim. Acta*, 51: 1781-1786.
- Schindler, P. W. and Stumm, W., 1987. The surface chemistry of oxides, hydroxides and oxide minerals. *Aquatic Surface Chemistry*. Stumm. New York, John Wiley and Sons.
- Schweich, D. and Sardin, M., 1981. Adsorption, Partition, ion exchange and chemical reaction in batch reactors or in columns - A review. *Journal of Hydrology*, 50: 1-33.
- Sigg, L. M., 1979. Die Wechselwirkung von Anionen und schwachen Saeuren mit α -FeOOH (Goethite) in waessriger Loesung. PhD thesis ETH 6417, ETH Zuerich.
- Spadini, L., 1993. Struktur und Stabilitaet von Oberflaechenkomplexen im System Cd²⁺ - FeOOH, PhD thesis, Universitaet Bern.
- Sparks, D.L. and Jardine, P.M., 1982. Comparison of batch and miscible displacement techniques to describe potassium adsorption kinetics in Delaware soils. *Soil Sci. Soc. Am. J.*, 46: 875-877.
- Sposito, G., 1983. On the use of the Langmuir Equation in the Interpretation of Adsorption Phenomena: II. The « Two-site » Langmuir Equation. *Soil. Sci. Soc. Am. J.*, 46: 1147-1152.

Strickland, C. and Parsons, J. L., 1972. Determination of reactive silicate. In: Practical book of sea water analysis. Ed. Fisheries Research Board of Canada. 65-70.

Stumm, W. and Morgan, J. J., 1996. Aquatic chemistry: Chemical equilibria and rates in natural waters. John Wiley and Sons, Inc., New York, Chichester, Brisbane, Toronto, Singapore.

Thompson, H.A., Brown Jr., G.E. and Parks, G.A., 1997. EXAFS spectroscopic study of uranyl coordination in solids and aqueous solution. *American Mineralogist*, 82: 483-496.

Toride, N., Leij, F. J. and van Genuchten, M. T., 1993. A comprehensive Set of Analytical Solutions for Nonequilibrium Solute Transport With First-Order Decay and Zero-Order Production. *Water Resources Research*, 29(7), 2167-2182.

Toride N. and Leij F. J., 1996. Convective-Dispersive Stream Tube Model for Field-Scale Solute transport: Moment analysis. *Soil Sci. Soc. Am. J.*, 60: 342-352.

van Geen, A., Robertson, A. P. and Leckie, J. O., 1994. Complexation of carbonate species at the goethite surface: Implications for adsorption of metal ions in natural waters. *Geochim. Cosmochim. Acta*, 58(9): 2073-2080.

van Genuchten, M. T. and Wierenga, P. J., 1976. Mass Transfer Studies in Sorbing Porous Media I. Analytical solutions. *Soil Sci. Soc. Am. J.*, 40(4): 473-480.

Venema, P., Hiemstra, T. and van Riemsdijk, W.H., 1996. Multisite Adsorption of Cadmium on Goethite. *J. Colloid Interface Sci.*, 183: 515-527.

Waite T. D., Davis, J. A., Payne, T. E., Waychunas, G. A. and Xu, N., 1994. Uranium (VI) adsorption to ferrihydrite: Application of the surface complexation model. *Geochim. Cosmochim. Acta* 58: 5465-5478.

Westall, J. and Hohl, H., 1980. A comparison of Electrostatic Models for the Oxide/Solution Interface. *Advances Coll. Interface Sci.*, 12, 265-294.

Yeh, G.-T. and Tripathi, V. S., 1991. A Model for Simulating Transport of reactive Multispecies Components: Model Development and Demonstration. *Water Resources Research*, 27(12): 3075-3094.

Yeh, G.-T. and Tripathi, V. S., 1990. HYDROGEOCHEM: A coupled model of hydrological and geochemical equilibrium of multi-component systems. Oak Ridge Natl. Lab., Oak Ridge, TN, ORNL-6371, 312 p.

ARTICLE III

ACCIDENTAL DESORPTION OF URANYL FROM LOW CONTAMINATED POROUS MATERIAL: EXPERIMENTAL AND NUMERICAL SIMULATIONS

U. Gabriel¹, L. Charlet¹, J.-P. Gaudet^{2*}, S. Tyler^{2,3}

¹Laboratoire de Géophysique Interne et Tectonophysique, UJF, CNRS UMR 5559 Grenoble, France

²Laboratoire d'Etude des Transferts en Hydrologie et Environnement, UJF, INPG, CNRS UMR 5564 Grenoble,
France

³University and Community College System of Nevada, Reno, Nevada, USA

* to whom the correspondence should be addressed

ABSTRACT

We studied the impact, an accidental change in geochemical background conditions may have on the transport behaviour of uranyl through a porous material. This was experimentally observed in column leaching experiments in which adsorption and desorption were obtained under different chemical conditions, using an artificial soil (goethite coated cristobalite sand). During the adsorption step the column was charged with uranyl in conditions where adsorption is favoured so that the effluent was uranyl « free » even after the elution of 320 pore volumes. Following the pH positive shift (to desorption favouring conditions) we observed a dramatic uranyl break-through, followed by a very long tailing.

To understand the full transport mechanism, it has to be considered that the « homogeneous » column actually consists of a contaminated and a non-contaminated part at the time when chemical conditions are changed. The concentration at the contamination front within the column increases in the contaminated part and decreases in the non-contaminated part. The development of this front is a complex interaction of rate-limited non-linear adsorption and physical transport. By changing the flow rate and the total uranyl quantity in the system we could identify the influence of the different processes. But as the system included too many unknowns, at this stage no fully satisfactory transport model can explain all the observed phenomena.

INTRODUCTION

The sorption of uranyl has been studied on a variety of minerals (Waite et al. (1994), Bruno et al. (1995) and Morrison et al. (1995a) on *hydrous ferric oxide*; Liger (1996) and Ho and Miller (1985; 1986) on *hematite*; Hsi and Langmuir (1985) and Kohler et al. (1989) on *goethite*; Morris et al. (1994) on *smectite*; McKinley et al. (1995), Chrisholm-Brause et al. (1994) and Dent et al. (1991) on *montmorillonite*; Wersin et al. (1994) on *sulphide minerals*; Moll (1997), Reich et al. (1996) and Dent et al. (1991) on *silica*). Although most of this work is aimed at the characterisation of uranium mobility to evaluate sites or materials for used fuel storage or the risk of mine waste, little work has been published on this reactive transport per se and most studies were pure computational exercises (Yeh and Tripathi, 1991).

We focused the present study on rather « mildly » contaminated sites of mining and extraction residuals or to areas naturally enriched in uranium. The central two questions are: can these low contaminated sites present any risk for the environment or, formulated in another way, how dangerous are potential enriching mechanisms? Can these « enrichment mechanisms » be applied to clean up contaminated sites?

Experiments were done on an artificial soil in order to limit the number of parameters. Three criteria were applied to develop the experimental system. This system, which in addition to uranyl included a reactive sorbing surface and a complexing ligand in solution, was meant to be:

1. as simple as possible,
2. as near to nature as possible and
3. comparable to other results from the literature.

The first two points are somewhat contradictory, as processes in nature are usually a mixture of several effects and can not be represented in a simple way. The complexing ligand used in this study -carbonate ions - represents a compromise. Carbonate ions are known to be among the most important complexing agents of uranyl (Bernhard et al., 1996; Meinrath et al., 1996; Kato et al., 1994), together with phosphate ions (Sandino et Bruno, 1992; Brendler et al., 1996) or humic acids (Pompe, 1997; Brachmann, 1997).

Carbonate ions are very abundant in natural waters, due to (i) interactions with atmospheric CO₂, (ii) dissolution of carbonate containing rocks and (iii) bacterial activity leading to elevated CO₂ partial pressures in soils. Therefore no experimental simulations at near natural conditions and elevated pH values can be done in absence of CO₂. Carbonate ions are furthermore extensively used in in-situ leaching (Catchpole and Kirchner, 1995) and extraction processes (Torma et al., 1985). Therefore the extraction residuals have very often elevated pH values and carbonate concentrations.

The URANYL-CARBONATE-GOETHITE-CRISTOBALITE system has been extensively characterised in stable background geochemical conditions in a previous study (II). Column and batch experiments were used to characterise *linear vs. non-linear and rate-limited adsorption*.

In the present work we studied experimentally the influence of uranyl sorption characteristics - *linear vs. non-linear adsorption equilibria and reaction kinetics* - on the mobility of uranyl when background geochemical conditions are changed suddenly. Flow rate and the total uranyl quantity in the system are the critical experimental parameters

The theoretical point of interest of this study was the question of the application of existing one-component transport models to our multi-component problem. In figure 1 the main interacting processes as found out in II have been summarised. It seems obvious that only multi-component transport models should be able to describe the complex system. We will try to find out (i) how rate limited and/or non-linear adsorption reactions are shaping the breakthrough curve (BTC) of a sorbing solute and (ii) whether an estimation of the complex system is possible while using mono- or bi-component transport models. This is of practical interest as the hydrodynamic conditions found in the field are at present mainly reproduced by continuous spatial and temporal discretisation. The corresponding models include usually only one component.

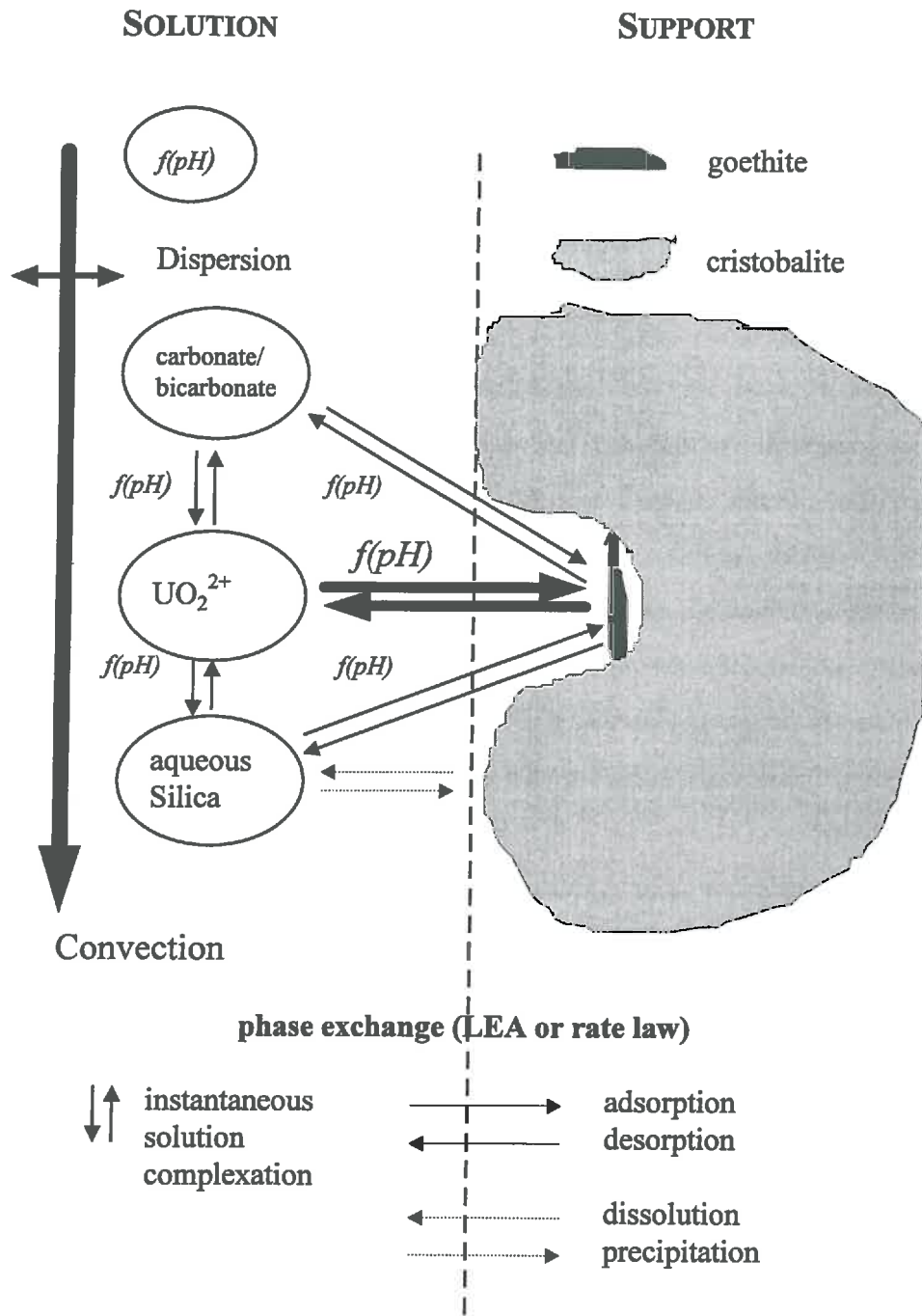


Figure 1 Uranyl fixation mechanism on goethite

METHODS

Experimental methods

The experimental set-up for the column experiments, the preparation of the column support and also the uranyl analysis has been described elsewhere (II). The water saturated column contained 100 g goethite-coated cristobalite sand (6.2 μg goethite per g cristobalite). Column length L and volumic water θ content were 14.6 cm and 0.467, respectively (pore volume $V_p = 36.2 \text{ cm}^3$).

Two experiments (table 1, experiment H1 and H2) were carried out to characterise the hydrodynamic conditions in the column. Uranyl could be used as inert tracer, for the background sodium bicarbonate concentration was 0.05 M, where adsorption of uranyl onto goethite is negligible.

Table 1 Experimental conditions of the column experiments

$[\text{NaHCO}_3]_{\text{sorp}}$	sodium bicarbonate concentration during adsorption
$[\text{NaHCO}_3]_{\text{stab}}$	sodium bicarbonate concentration during stabilisation
$[\text{NaHCO}_3]_{\text{des}}$	sodium bicarbonate concentration during desorption
I	ionic strength

	H1	H2	D1	D2	D3	D4	I1
c_0 (μM)	1	1	1	1	1	1	1
T_0 (pore volumes)	2.88	3.15	45.6	43.6	116	326	12.4
flow rate (ml h^{-1})	30	3	30	3	30	30	30
I (mM)	50	50	10	10	10	10	10
$[\text{NaHCO}_3]_{\text{sorp}}$ (mM)	50	50	1	1	1	1	10
$[\text{NaHCO}_3]_{\text{stab}}$ (mM)	-	-	0	-	-	-	-
$[\text{NaHCO}_3]_{\text{des}}$ (mM)	50	50	10	10	10	10	10
recovery (%)	100	99	109	95	87	102	97

The following four experiments (D1 to D4) were meant to simulate accidental uranyl mobilisation, as a consequence of a change in background geochemical conditions. The experiments included therefore two steps. (i) An accumulation period in which adsorption conditions were favoured (1 mM NaHCO_3 /9 mM NaNO_3 resulting in pH 8); and thus the column effluent solution is uranyl « free ». (2) A mobilisation step under conditions where desorption due to complexation of uranyl in solution (i. e. by dissolved carbonate ions) is highly favoured (10 mM NaHCO_3 resulting in pH 9).

In experiment D1 (table 1, figure 2) a uranyl-free stabilisation period (10 mM NaNO₃; pH 6, c₀ = 0) was added between the accumulation and the mobilisation period. As can be seen for the stabilisation period (figure 2), it was not possible to decrease the carbonate concentration and to desorb in acid conditions since the system is buffered by mineral surfaces with respect to OH⁻ and HCO₃⁻. Adsorption of carbonate onto goethite and/or the protonation of the goethite surface buffer the pH. The assumption of the desorption taking place at one pH, the « desorption » pH, would not be valid. On the contrary when the pH and the sodium bicarbonate concentration are increased we find nearly no pH retardation (1 to 2 V_p).

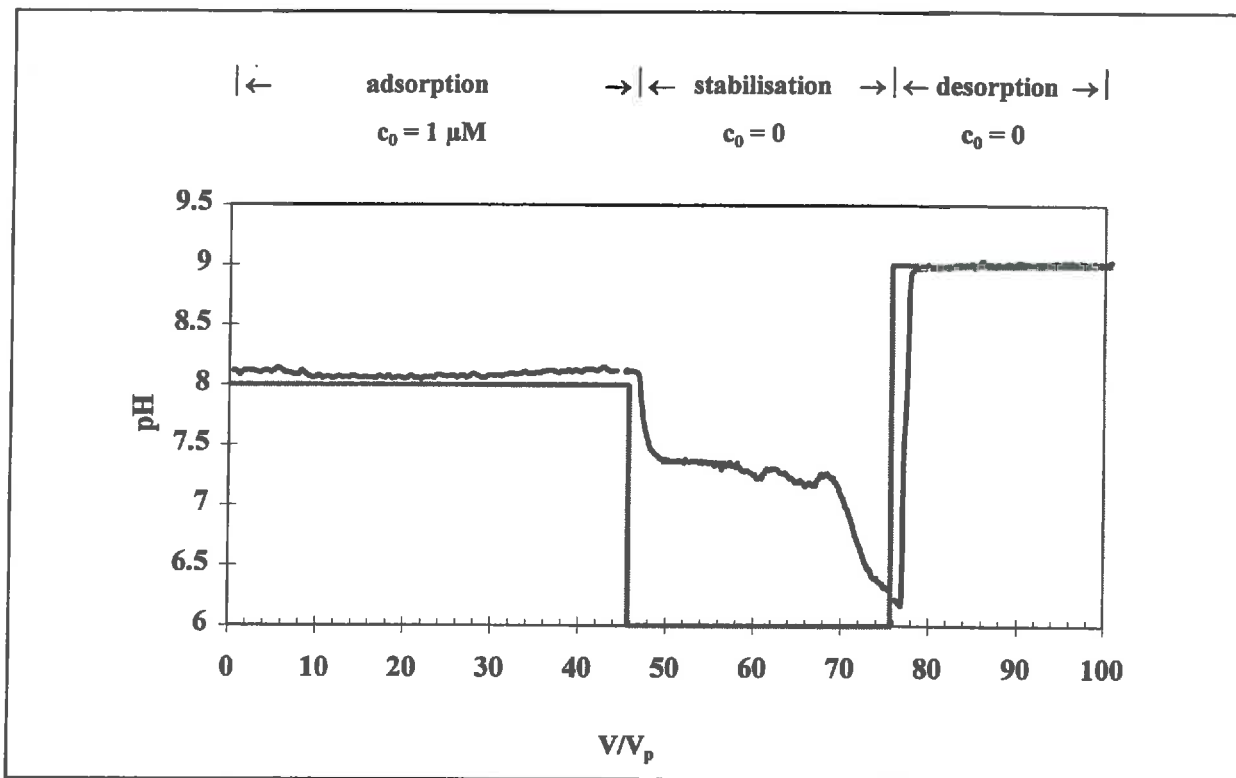


Figure 2 Experimental realisation of an accidental desorption (experiment D1, grey line: inlet pH, black line outlet pH, c₀ initial uranyl solution concentration)

In the following experiments no stabilisation period was added.

In experiment D2 chemical conditions and eluted volumes during the accumulation and the mobilisation periods were identical to experiment D1. Only the flow rate was reduced to 3 ml h⁻¹. In experiments D3 and D4 the total uranyl quantity in the system, i.e. the eluted volume during the accumulation period was varied preserving the input uranyl solution concentration.

One adsorption experiment (I1) was carried out under constant experimental conditions (10 mM NaHCO₃; pH 9) and an input uranyl concentration of 10 μM.

Data treatment

Adsorption isotherms from integration of the desorption front and the retardation factor

The adsorption isotherm (i. e. the S vs. c curve) can be deduced from the diffusive desorption front by a numerical integration under the condition that any other curve deforming process, such as dispersion or reaction kinetics, is negligible (Buergisser et al., 1993; Griffioen et al., 1992, Veldhuizen et al., 1995):

$$S = \frac{\theta}{\rho_d} \int_0^c \left(\frac{t(c')}{T_0} - 1 \right) dc \quad (1)$$

where S and c are the sorbed (mol g⁻¹) and dissolved (M) concentrations, θ and ρ_d the volumic water content and the bulk density (g goethite per ℓ total volume), t(c') the experimental retention time and T₀ the residence time of a conservative non-reactive tracer.

Other adsorption isotherm curves can be obtained from the adsorption front obtained under constant chemical conditions under the assumption that adsorption is linear (i.e. S proportional to c) and that reaction kinetics does not shift the BTC (suggested in II). Then distribution coefficients K_d can be deduced from the retardation factor R observed in the adsorption front:

$$K_d = \frac{S}{c} = \frac{(R-1)\theta}{\rho_d} \quad (2)$$

Approximation of the accidental desorption by an « isotherm shift »

An extensive presentation of mono-component transport models based on numerical and analytical solutions of the general exchange and convection-dispersion-equation (ECDE) can be found in II. Sorbed (S) and dissolved (c) concentrations can be related by linear adsorption (figure 3a) or non-linear adsorption isotherms (Langmuir (3b) and Freundlich (3c), as in all

figures in this section symbols were added to facilitate reading and do not represent experimental values). All three empirical adsorption laws can be easily included in mono-component transport models derived from the ECDE.

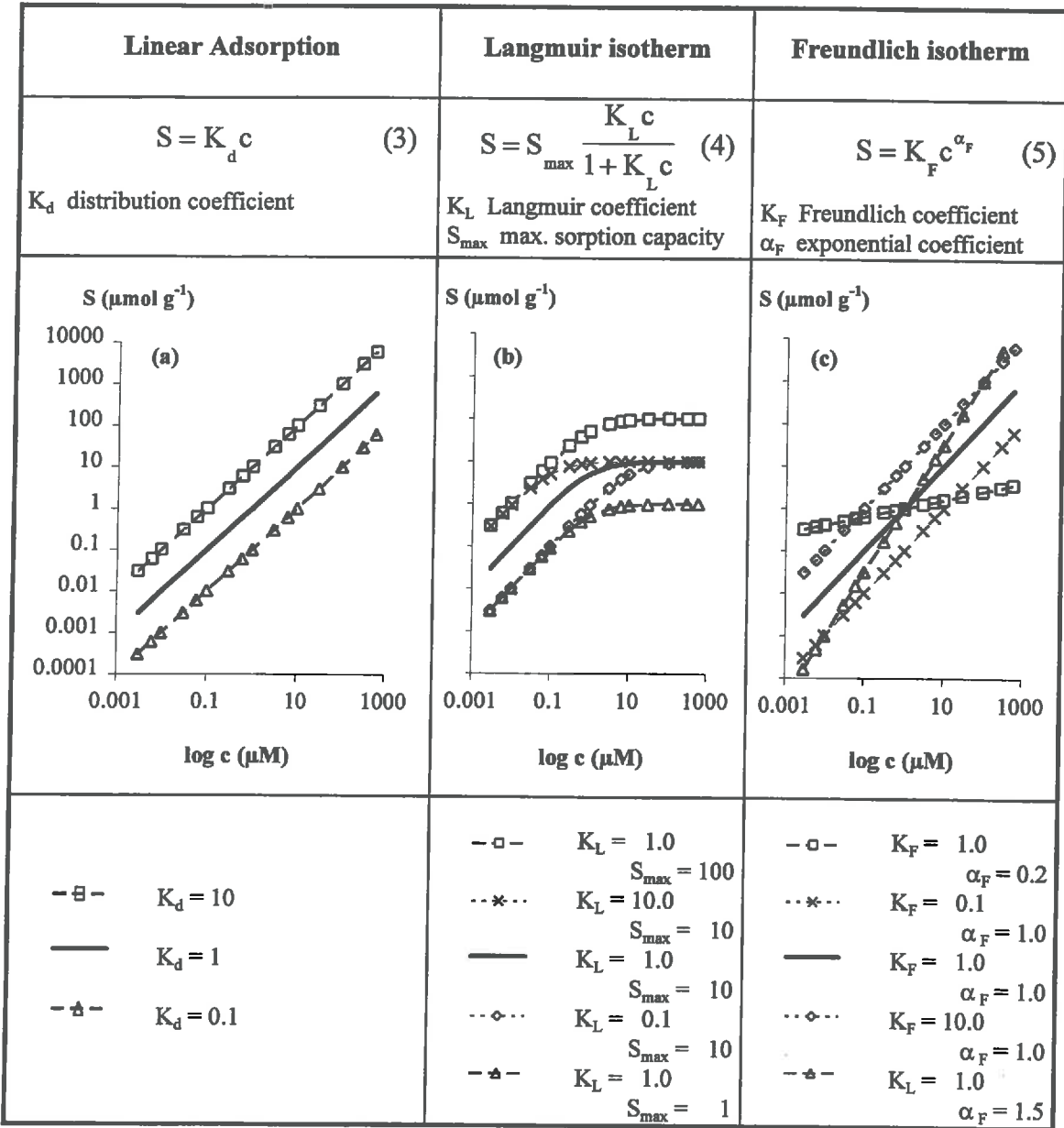


Figure 3 Adsorption isotherms (symbols added to facilitate reading, K_d in $l\ g^{-1}$, K_L in μM^{-1} , S_{\max} in $\mu mol\ g^{-1}$, K_F in $\mu mol^{1-\alpha_F} g^{-1}$)

The overall adsorption reaction can be described by combining two Langmuir isotherms:

$$S_1 = S_{\max 1} \frac{K_{\text{sorb1}} c}{1 + K_{\text{sorb1}} c} \quad \text{and} \quad S_2 = S_{\max 2} \frac{K_{\text{sorb2}} c}{1 + K_{\text{sorb2}} c} \quad (6a \text{ and } b)$$

where K_{sorb1} and K_{sorb2} are the two equilibrium coefficients in μM^{-1} , $S_{\max 1}$ and $S_{\max 2}$ are the two maximal adsorption capacities in $\mu\text{mol g}^{-1}$. The overall sorbed concentration S_{tot} is :

$$S_{\text{tot}} = S_1 + S_2 \quad (7)$$

When now different chemical environments are assumed to govern adsorption and desorption only the equilibrium coefficients could be supposed to change resulting in :

$$K_{\text{des1}} = K_{\text{sorb1}} \beta \quad \text{and} \quad K_{\text{des2}} = K_{\text{sorb2}} \beta \quad (8a \text{ and } b)$$

with K_{des1} and K_{des2} being the equilibrium coefficients controlling desorption. β is an empirical coefficients describing the isotherm shift. It is obtained in independent batch experiments. For this shift, the choice of the isotherm is critical, as in this experimentation type high solute concentration can be observed. Reactive transport is therefore very dependent from site saturation effects. It appears that the reduction of our multi-component system to a two-component one or a mono-component one with changing equilibrium constants allows its relative easy inclusion in continuous and discrete transport codes.

RESULTS

Hydrodynamic characterisation of the column (experiments H1 and H2)

In figure 4 the results at two different flow rates F (0.83 and $0.083 V_p h^{-1}$) are compared. A relative long uranyl pulse (about 3 pore volumes) was introduced. Both BTC's are nearly identical. This concerns as much the dispersivity λ (cm) as the exchange coefficient α (h^{-1}) between the mobile and the immobile water with their corresponding solute concentrations c_m and c_{im} . The dispersivity defined as quotient of the dispersion coefficient D ($cm^2 h^{-1}$) and the average pore velocity v ($cm h^{-1}$) was found to be 0.073 cm, corresponding to a Peclet number ($Pe = L v D^{-1}$) of about 200.

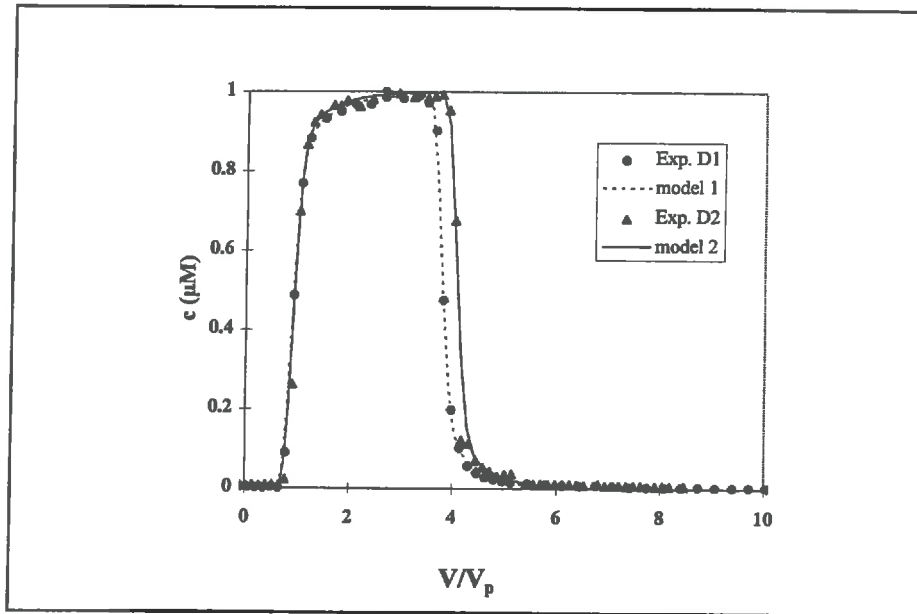


Figure 4 Experimental results and modelling of the hydrodynamic conditions in the column Model MIM with θ_m and θ_{im} as mobile/immobile water content and q as darcy velocity:

$$\frac{\partial c_m}{\partial t} + \frac{\theta_{im}}{\theta_m} \frac{\partial c_{im}}{\partial t} = D_m \frac{\partial^2 c_m}{\partial z^2} - \frac{q}{\theta_m} \frac{\partial c_m}{\partial z} \quad \text{and} \quad \frac{\partial c_{im}}{\partial t} = \frac{\alpha}{\theta_{im}} (c_m - c_{im})$$

$$L = 14.6 \text{ cm}, \theta = 0.467; \theta_m = 0.432; \theta_{im} = 0.035; \lambda = 0.073 \text{ cm}; \alpha = 1.7 \text{ h}^{-1}$$

$$\text{Exp. H1: } F = 0.83 V_p h^{-1}, T_0 = 2.88 V_p; \quad \text{Exp. H2: } F = 0.083 V_p h^{-1}, T_0 = 3.15 V_p$$

The curves could be simulated (model MIM, Gaudet et al., 1977) assuming 7.5 % of the pore water to be immobile (figure 4). This is a rather large value, given the small cavities and fissures of the cristobalite grains. The exchange between both water phases was assumed to follow a first order kinetics, the rate being $1.7 h^{-1}$. The sensitivity to this parameter decreases with the percentage of immobile pore water (Gaudet et al., 1977). Therefore nearly the same

values are found for the two flow rates. It is assumed that the entire effect is due to an immobile liquid phase. It is not possible to decide whether this slightly inclined plateau is exclusively due to the immobile water content or whether its caused by a weak rate-limited adsorption.

Experimental simulations of accidental uranyl desorption (Exp. D1 to D4)

When the desorbing conditions (pH 9) were imposed ($V/V_p = 0$) the system reacts rapidly. Thus one can assume that all desorption takes place at constant pH equal to 9 ± 0.2 (figure 5). The system is still relatively well buffered in experiments D3. On the contrary in experiment D4 the desorption and following complexation and/or re-adsorption liberates more protons than could be buffered by the carbonate system, resulting in a slightly decreasing pH at two pore volumes. The small difference in the tailing behaviour is due to the difficulty of defining 'equilibrium with the atmosphere'.

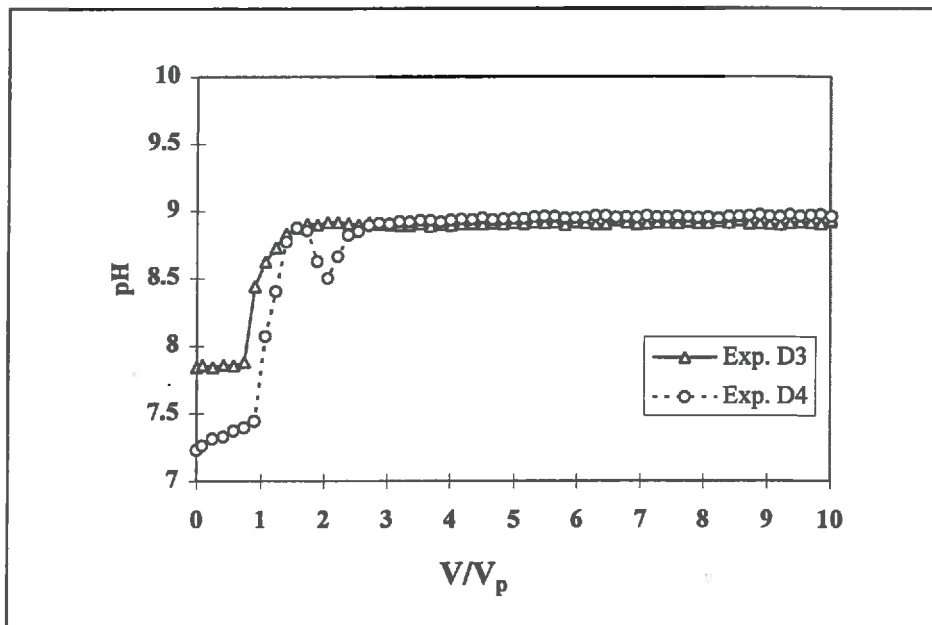


Figure 5 Development of the pH during experiments D3 and D4

Table 2 **Experimental results of the accidental desorption experiments**
 R_{app} apparent retardation factor obtained on the rising part of the BTC

	D1	D2	D3	D4
c_{max} (μM)	11.2	5.73	26	235
peak width (pore volumes)	3	5	2	0.6
R_{app} (pore volumes)	4.3	5.7	3	2

In experiments D1 to D4, the adsorption (accumulation period) was performed with the input concentration at trace level ($1\mu\text{M}$) whereas output maximum uranyl concentration ranged from 6 to $235\mu\text{M}$ (table 2). About 100 % of the introduced uranyl quantity was recovered at the column outlet for all column experiments (table 1).

Experimental uranyl BTC for experiments D1 to D4 are given in figures 6 and 7. Data are presented in three different ways to show the change in maximal concentration (a), the curve tailings in the small concentration range (b) and the comparison of the arrival of the break through and the form of the pulse (c).

Flow velocity effect (experiments D1 and D2)

It was shown previously (II, under constant chemical conditions) that smaller flow rates result in chemical reactions much nearer to equilibrium, and thus in steeper BTC's (smaller half widths), and in larger maximal concentrations, thus closer to the uranyl input concentrations. About the same tailing and the same retardation was found for both flow rates.

The comparison between the two experiments with different flow rates ($0.83 V_p h^{-1}$ in experiment D1 and $0.083 V_p h^{-1}$ in experiment D2; figure 6; tables 1 and 2) showed the following effects of decreasing flow rate:

- *Maximal concentration* decreased by half (figure 6a),
- No fundamental difference was observed in the *tailing behaviour* (figure 6b),
- *The peak half-width* nearly doubled and
- *The apparent retardation* on the rising part of the BTC's increased (figure 6a-c).

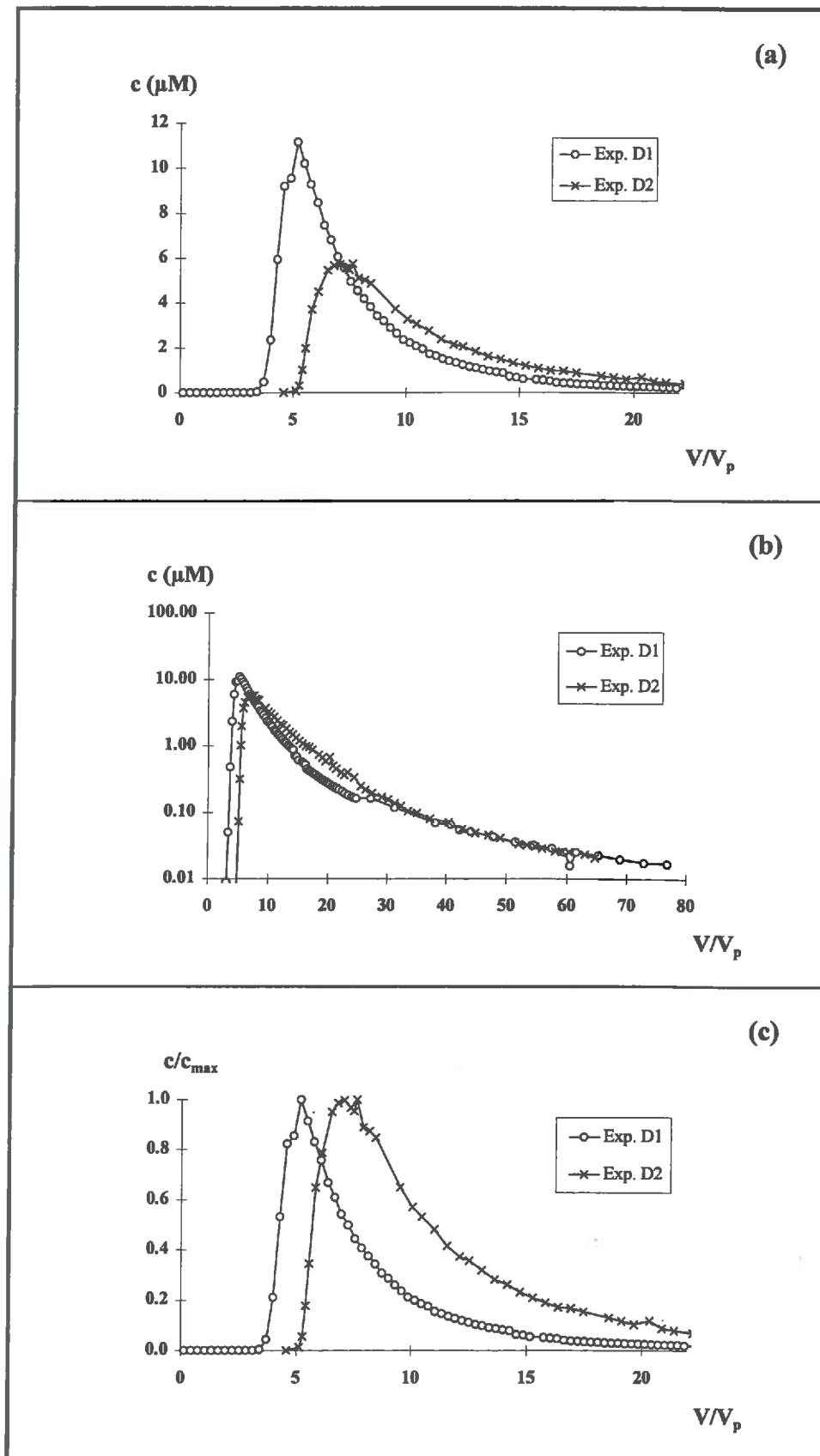


Figure 6 BTC's of exp. D1 and D2

The total uranyl quantity introduced in the system in experiment D2 was 96 % of the one of experiment D1. This difference is too small to explain the observed retardation factors, maximal concentrations and peak widths by the influence of a non-linear adsorption isotherm. They have to be related to reaction kinetics.

The different maximal concentrations, break-through times and peak widths lead to the assumption that in the presented experiments the uranyl adsorption is controlled by at least two reaction rates. The first adsorption reaction can be supposed to be at or near equilibrium in both experiments. The second much slower adsorption reaction seems to be negligible at exp. D1, but causes the later break through, the smaller maximal concentration and the broader peak in exp. D2. At this stage it is difficult to say, whether these kinetics are physical ones, related to diffusion within the microporosity or the immobile solution layer, and/or chemical ones, related to different adsorption mechanisms (different sites and/or different surface complexes).

Total uranyl load effect (Experiments D1, D3 and D4)

Longer adsorption periods resulted in larger total uranyl quantities in the system and thus in (tables 1 and 2, figure 7):

- an « exponential » increase in the maximal solution concentration at the outflow (figure 7a). A 2.5 and 7 fold increased total uranyl quantity in the system resulted in a 4.5 and 40 fold maximal concentration.
- a decreasing retardation (no quantification as results are obscured by reaction kinetics!) and
- a decreasing peak width (figure 7c).

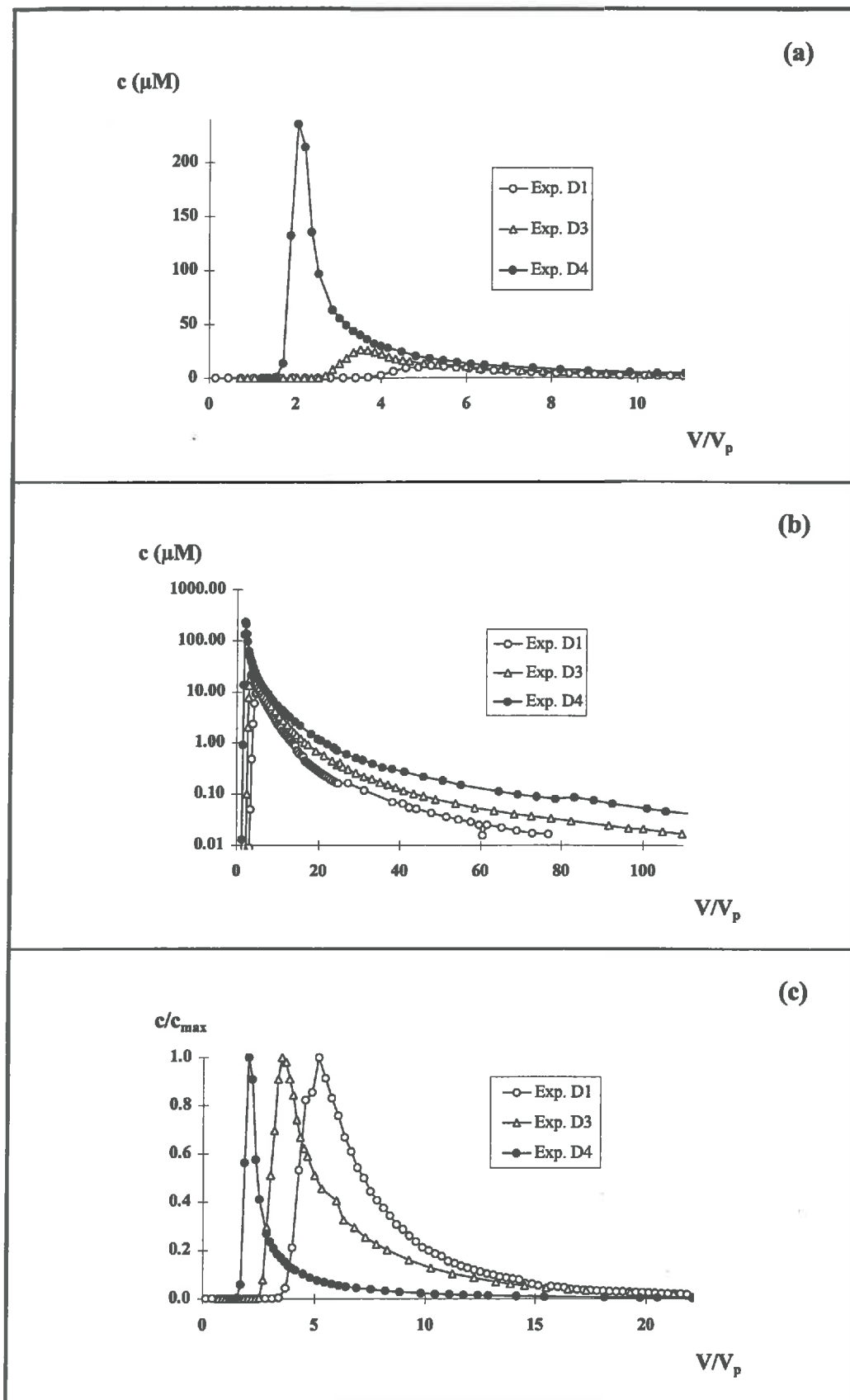


Figure 7 BTC's of experiments D1, D3 and D4

Therefore, the contamination front behaves practically like a very short concentration pulse. On its way through the contaminated porous medium, its concentration increases. In the case of *linear and instantaneous adsorption* the character of this increase depends directly on the value of the distribution coefficient K_d . Several particular cases can be thought of:

- $K_d \rightarrow 0$ results in a linear increase, limited only by the solute solubility under the given chemical conditions.
- $K_d = 1$ causes the solution concentration to approach the double volumic sorbed uranyl concentration (mol par ℓ pore volume) at infinity, the slope depends on the dispersion.
- At $K_d \rightarrow \infty$ no desorption takes place.

Once the desorption front has left the contaminated soil and is migrating in a non-contaminated, but sorbing porous medium, its further development is mainly controlled by the adsorption isotherm, reaction kinetics and physical transport including dispersion and diffusion. In the case of linear and instantaneous adsorption the distribution coefficient K_d controls the degree to which dispersion flattens the concentration peak in a cycle of repeated adsorption/desorption.

When a linear adsorption isotherm is coupled with reaction kinetics, rate limited desorption could be supposed to generally flatten the concentration peak (not observed in the presented experiments D1 and D2!). The interference of several rate laws could cause less re-adsorption in the cycle of repeated adsorption/desorption leading to an earlier break-through and a less flattened concentration peak (observed in experiments D1 and D2).

When the system is further complicated by non-linear (convex) adsorption the enrichment process in the contaminated porous material is intensified as in the same « background » chemical condition less uranyl is adsorbed. In the non-contaminated sorbing porous matrix non-linear adsorption will preserve the steep (*self-sharpening*) adsorption front, but will induce also a very long tailing of the desorption front.

Adsorption isotherm

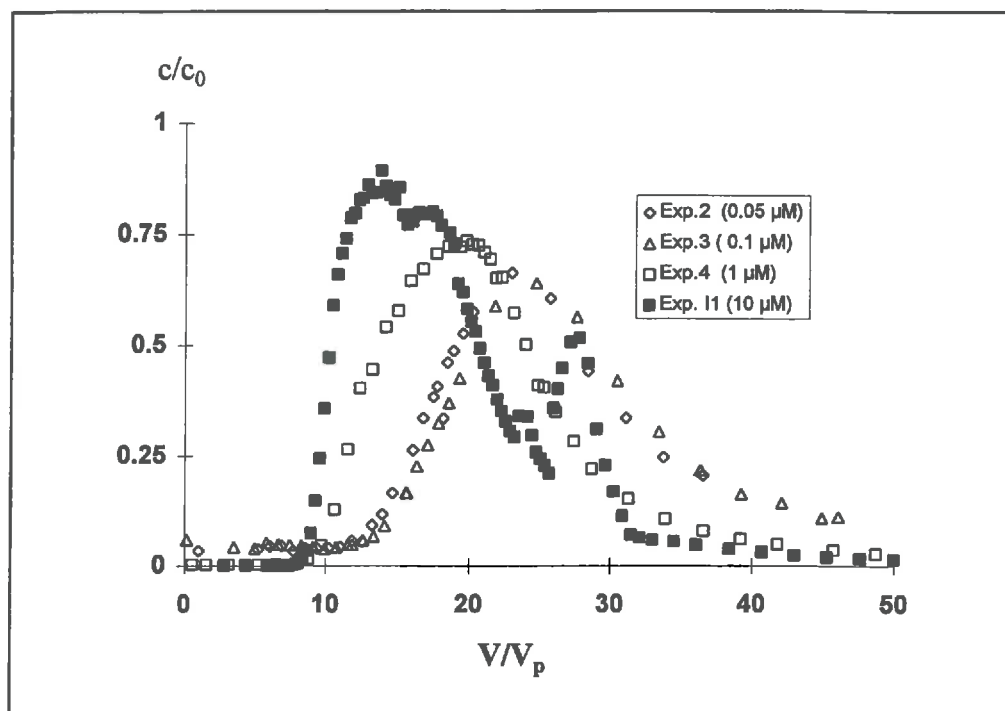


Figure 8 BTC's from experiment I1 and experiments 2, 3 and 4 from II ($F = 0.83 V_p h^{-1}$, $[NaHCO_3] = 10 \text{ mM}$, same column)

In a previous study (II) it was suggested that

- Linear adsorption resulted in nearly identical BTC's at 0.05 and 0.1 μM initial uranyl solution concentrations. The slightly asymmetric BTC's were accordingly explained by different kinetics for adsorption and desorption (experiments 2 and 3 in figure 8).
- For 1 μM a much smaller retardation was found leading to the assumption of a non-linearity in the adsorption isotherm in this concentration range. The corresponding BTC is significantly asymmetric, but as in the concentration range $< 0.1 \mu\text{M}$, linear adsorption is established the long tailing of the curve in this concentration range which has to be explained by reaction kinetics (experiment 4 in figure 8).
- The effect the reaction kinetics do have on the shape of the curve was shown by a repetition of the same experiment at a smaller flow velocity, where the BTC appeared to be much more asymmetric (experiment 4 in figure 8). The comparison of the two BTC's lead to the assumption that adsorption as well as desorption are controlled by just one reaction kinetics as the travel time of both curves caused the same retardation.

The results from experiment I1 confirm the nonlinearity (earlier break through) in the higher concentration range. Also the decreasing peak width, but increasing asymmetry is noted with increasing initial uranium concentration. The concentration oscillations in the desorption front are explained by small changes in the geochemical background conditions. « Accidental desorption » is repeated on a much smaller scale.

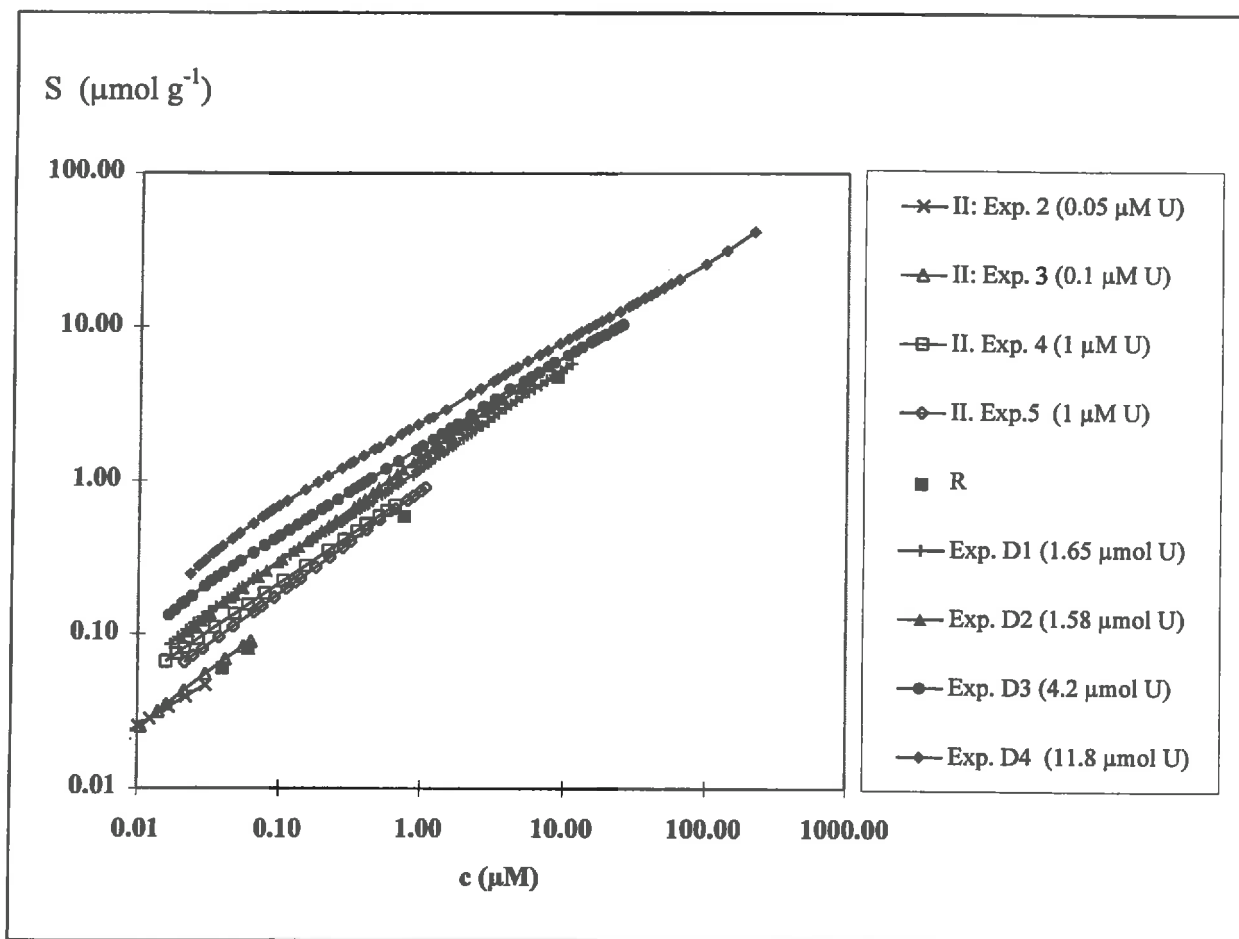


Figure 9 Adsorption isotherms obtained by numerical integration (eq. 1) of the experimental desorption fronts and deduced from the retardation R (eq. 2).

For the present work experiments total uranyl quantities are given as the retardation controlling maximal concentration within the column is unknown. For II. experiments 5 and experiments D2 $F = 0.083 V_p h^{-1}$, all others $F = 0.83 V_p h^{-1}$.)

The desorption fronts of the accidental desorption experiments (D1 to D4) show a similar, converging, behaviour and are therefore likely to be controlled by the same phenomenon. As the curves are also extremely asymmetric, a non-linear adsorption isotherm could be responsible for both, the similar asymmetry and their converging.

Sorption isotherms obtained by numerical integration of the desorption front are given in figure 9, both for experiments in stable geochemical background conditions and in experiments where these conditions were suddenly changed. Additionally the points of retardation factor deduced distribution coefficients (model CDR-cin in II) are shown. No unique *equilibrium* sorption isotherm is obtained. Thus desorption is assumed to be a kinetically limited reaction.

Table 3 Experimental results and conclusions concerning the URANYL-CARBONATE-GOETHITE-CRISTOBALITE system

c_0 initial uranyl solution concentration (μM)
 c uranyl solution concentration measured at the outlet (μM)
 n_0 total uranyl quantity in the system (μmol)

c_0 (μM)	n_0 (μmol)	experimental results	conclusion
constant chemical conditions (II)			
0.05 - 0.1	0.025 - 0.05	<ul style="list-style-type: none"> break through after 20 pore volumes rather symmetric flat BTC ($c = 0.6 c_0$) 	<ul style="list-style-type: none"> linear adsorption reaction kinetics
1 - 10	0.5 - 5	<ul style="list-style-type: none"> break through after 10-15 pore volumes asymmetric BTC different BTC for different flow rates $c = 0.75 c_0$ & $1.05 c_0$ 	<ul style="list-style-type: none"> non-linear adsorption reaction kinetics literature: several adsorption sites ¹⁾
changing chemical conditions (p.w.)			
(1)	1.58 - 11.8	<ul style="list-style-type: none"> enriching mechanism: no relation between c_0 and c \Rightarrow unknown c_{max} (actual retardation controlling concentration) \Rightarrow unknown isotherm form and kinetics (in the elevated concentration range) the column is only partly « contaminated » \Rightarrow unknown contaminated percentage 	<ul style="list-style-type: none"> too many unknowns for an « exact » numerical simulation \Rightarrow parameter identification under constant and varying chemical conditions

¹⁾ several adsorption sites on goethite: Benjamin and Leckie (1981), Venema et al. (1996) ; complete adsorption of 10 μM uranyl on 1 g goethite: Hsi and Langmuir (1985)

As the experiments with about the same total uranyl quantity in the system and different flow rates (experiments D1 and D2) did lead to different retardation's, the retardation factors of experiments D1-D4 could not be included in figure 9. Equally exp. I1 was not included as the desorption front was deformed by slightly changing chemical conditions during desorption.

The modelling of the BTC's under variable geochemical background conditions is based on the distribution coefficient as a function of pH. In II, the pH desorption edge was experimentally studied (figure 10). It appears that at a 1 mM sodium bicarbonate concentration (accumulating conditions) adsorption is 100 times stronger than at 10 mM (mobilisation).

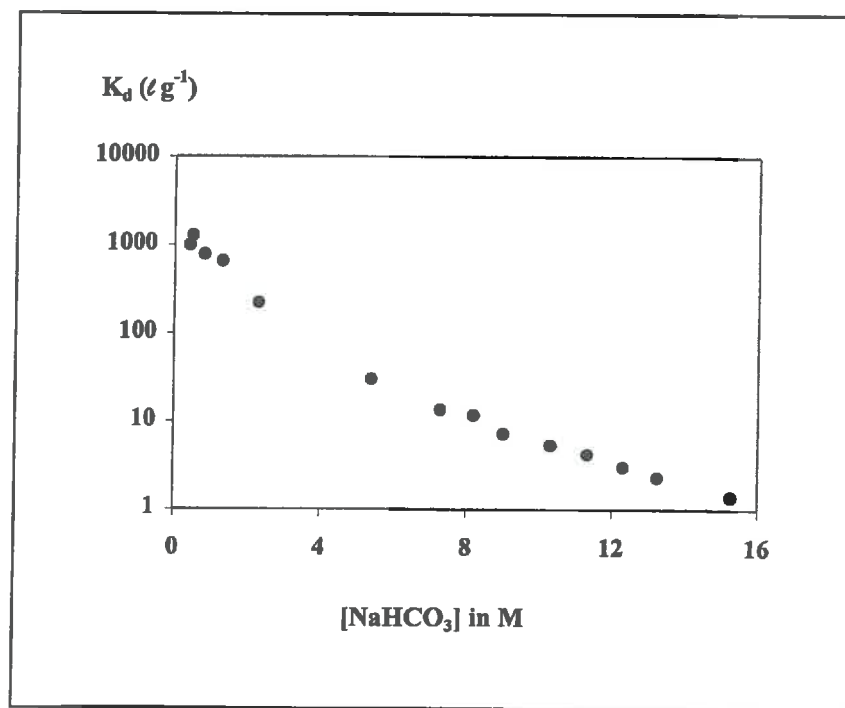


Figure 10 Distribution coefficients as a function of the sodium bicarbonate concentration (results from batch experiments in II, 0.82 g dm^{-3} goethite (coated on cristobalite), $1 \mu\text{M}$ total uranyl concentration)

PARAMETER IDENTIFICATION BY NUMERICAL TRANSPORT SIMULATIONS OR

In the present paper all transport simulations were accomplished using the code **IMPACT** (Jauzein, 1988; Jauzein et al., 1989). It is based on the mixing cell approach (discrete model). The great advantage of **IMPACT** is that it permits the inclusion of multiple solution species (multi-component model) and kinetics for all exchange reactions between the mobile and the stationary phase. With the code **IMPACT** the column is discretised in J mixing cells. Within one mixing cell concentrations are assumed to be constant. The dispersivity λ (cm) of the ECDE (II) based models is represented by the number of mixing cells J with $J = 2 Pe = L \lambda^{-1}$. The BTC's are numerically reproduced by taking samples of 5 cm^3 at the outlet of the last (J^{th}) mixing cell.

All calculations are presented in the normalised time unit of « displaced pore volumes » and using a sorbed concentration S' (M) which is related to the conventionally used sorbed concentration S (mol g^{-1}) by

$$S' = S \rho_d \theta \quad (9)$$

where ρ_d and θ are the bulk density in g cm^{-3} and the volumetric water content (analogue S_{max} and S'_{max}).

To understand how adsorption isotherms and reaction kinetics are shaping the BTC's under simplified flow conditions it is convenient to increase stepwise the number of involved parameters. In this part *invariant geochemical background conditions* are assumed. The pore volume $V_p = 36.2 \text{ cm}^3$, the number of mixing cells $J = 100$ and the flow rate $F = 30 \text{ cm}^3 \text{ h}^{-1}$ were chosen according to the experimental conditions. The isotherms used are hypothetical Langmuir ones. The initial concentration c_0 was assumed as $10 \text{ }\mu\text{M}$. The effects of *one and two site Langmuir isotherms* on the BTC's are tested under the local equilibrium assumption (LEA). Afterwards reaction kinetics are added. Afterwards it will be shown how accidental adsorption can be numerically approached by an « isotherm shift », combining the distribution coefficient which is changing due to *changing geochemical background conditions* to a non-linear adsorption isotherm.

Invariant geochemical background conditions

Langmuir isotherms and local equilibrium assumption (LEA, constant pulse length)

A Langmuir isotherm can be subdivided into three parts (figure 11):

- a linear part in the small concentration range where $S' \leq S'_{\max}/100$ with an apparent distribution coefficient K'_d

$$K'_d = \frac{S'}{c} = K_L \frac{S'}{S'_{\max}} \quad (10)$$

- the curved (« non-linear ») part where $S_{\max}/100 < S' < S'_{\max}$ and
- a second linear, but constant part in the high concentration range with $S' = S'_{\max}$.

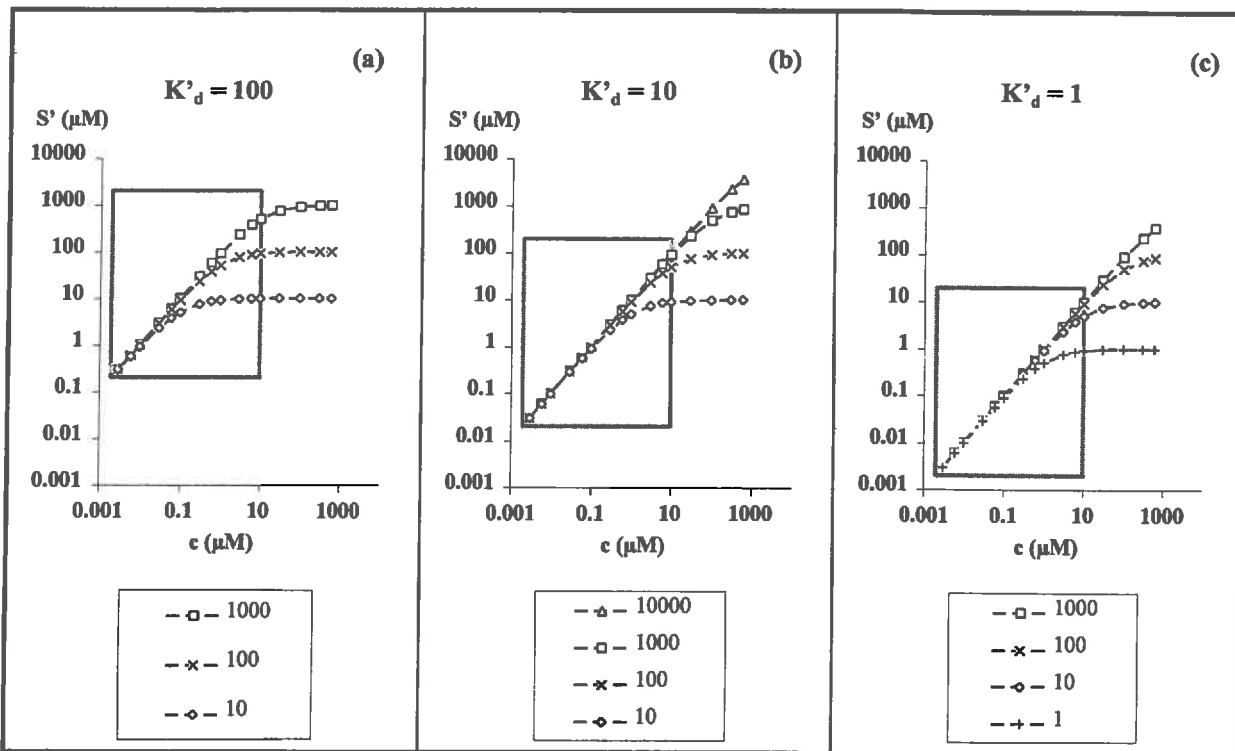


Figure 11 Langmuir isotherms with different apparent distribution coefficients for the transport simulations in figures 12 to 14 (numbers represent maximal adsorption capacities S'_{\max} , (in μM), the grey frame represents the chemical conditions within the transport simulations)

How the BTC is shaped by a Langmuir isotherm under the local equilibrium assumption depends on whether the initial uranyl solution concentration leads to site saturation. In figure

11 different sets of Langmuir isotherms are presented for K'_d equal to 100, 10 and 1. The chemical conditions of the transport simulations were indicated by frames.

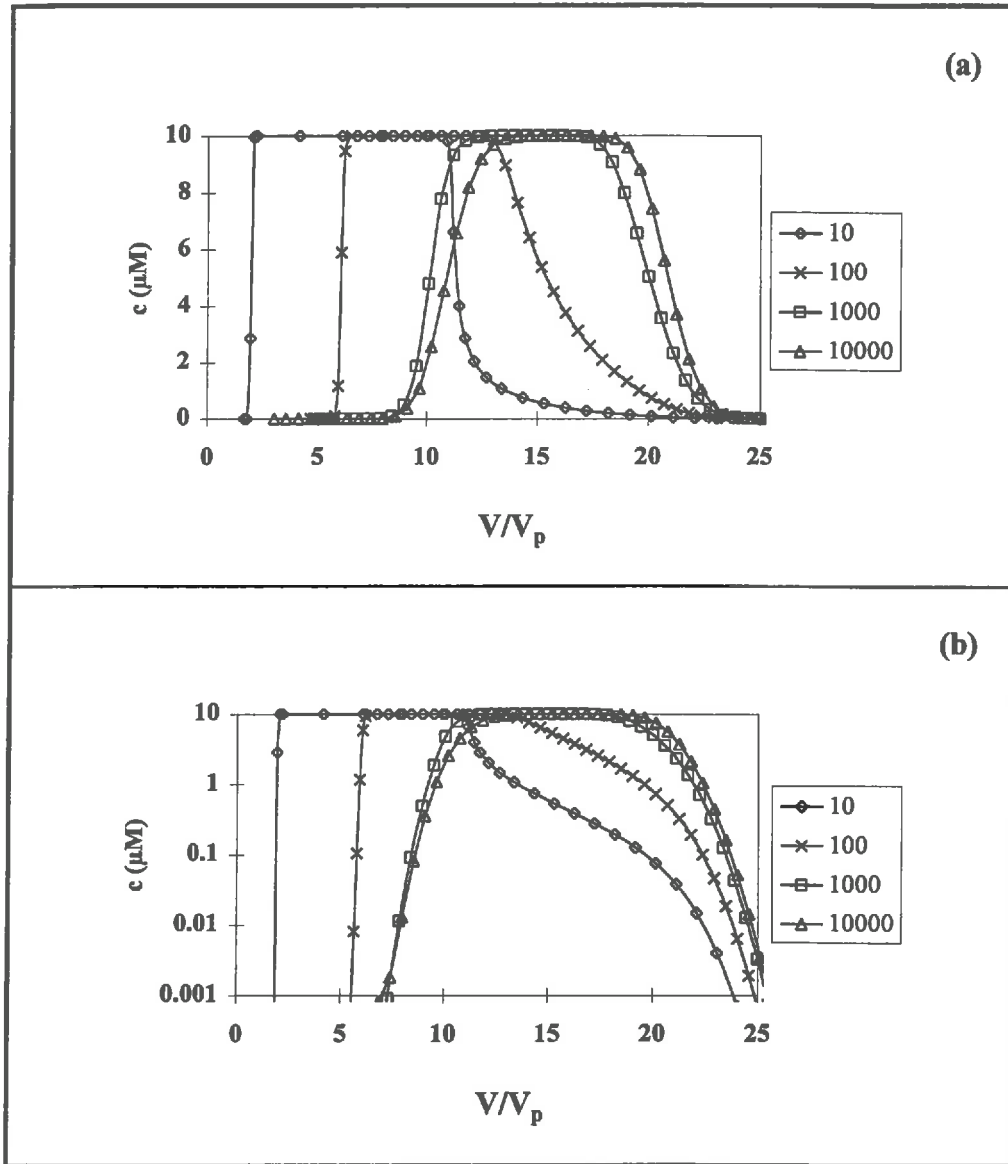


Figure 12 BTC's resulting from different Langmuir isotherms with $K'_d = 10$ (figure 11b) (numbers represent the maximum sorption capacity S'_{max} (μM); (a) and (b) show the same numerical results in a normal (a) and log (b) scale; modelling parameters: $F = 30 \text{ cm}^3 \text{ h}^{-1}$, $V_p = 36.2 \text{ cm}^3$, $J = 100$, $c_0 = 10 \text{ }\mu\text{M}$, $T_0 = 10 V_p$, samples = 5 cm^3)

In figure 12 the BTC's for Langmuir isotherms with $K'_d = 10$ (figure 11b) and different maximal sorption capacities are compared. The same numerical results were presented in a

normal (figure 12a) and a log scale (figure 12b) in order to show the influence on the high and the low concentration range.

For an input pulse concentration $c_0 = 10 \mu\text{M}$, the break through of the adsorption front is controlled by the maximal sorption capacity for S'_{max} equal to $10 \mu\text{M}$ and $100 \mu\text{M}$; the corresponding BTC's are strongly asymmetric. The adsorption fronts (*self-sharpening* after Buergisser et al., 1993) are much steeper than the desorption fronts. For $S'_{\text{max}} = 1000 \mu\text{M}$ and $10000 \mu\text{M}$ the BTC's are nearly symmetric (even in a logarithmic scale, figure 12b) and resemble the one caused by linear adsorption with a distribution coefficient $K'_d = 10$ (not shown). These results are consistent with linear adsorption at concentrations as compared to S_{max} .

A Langmuir isotherm can result in desorption fronts consisting of three parts corresponding to the above described parts of this isotherm and having a typical S-shape (observed mainly for $S'_{\text{max}} = 10 \mu\text{M}$ in figure 12):

- *high concentration range* ($c K'_d > S'_{\text{max}}$)

The adsorption reaction is only controlled by the limited site supply. The uranyl containing solution is replaced by convection without uranyl desorption. The solution concentration decreases rapidly, being mainly controlled by dispersion effects.

- « *non-linear* » *medium concentration range* ($S'_{\text{max}}/100 < c K'_d < S'_{\text{max}}$)

Control of the adsorption reaction shifts from the limited site supply to the apparent distribution coefficient K'_d (eq. 4). This range is the actual non-linearity of the isotherm. It results in a desorption front being much less steep (*diffusive* after Buergisser et al., 1993) than the first part. Its influence can comprise about one and a half concentration decade.

- *low concentration range* ($c K'_d \leq S'_{\text{max}}/100$), figure 12b

The adsorption reaction is completely controlled by the apparent distribution coefficient K'_d . The desorption front gets steeper, but not as steep as the first part. It appears that the dispersion effects get more important than in the concentration range of nearly complete adsorption.

The similarity among the non-linearity caused *diffusive* desorption front at $S'_{\max} = 10 \mu\text{M}$ and $100 \mu\text{M}$ is observed in the logarithmic representation (figure 12b). In this diagram it becomes obvious that a simple Langmuir isotherm can produce a *diffusive* desorption front only in a very limited concentration range (about one, maximal one and a half decades).

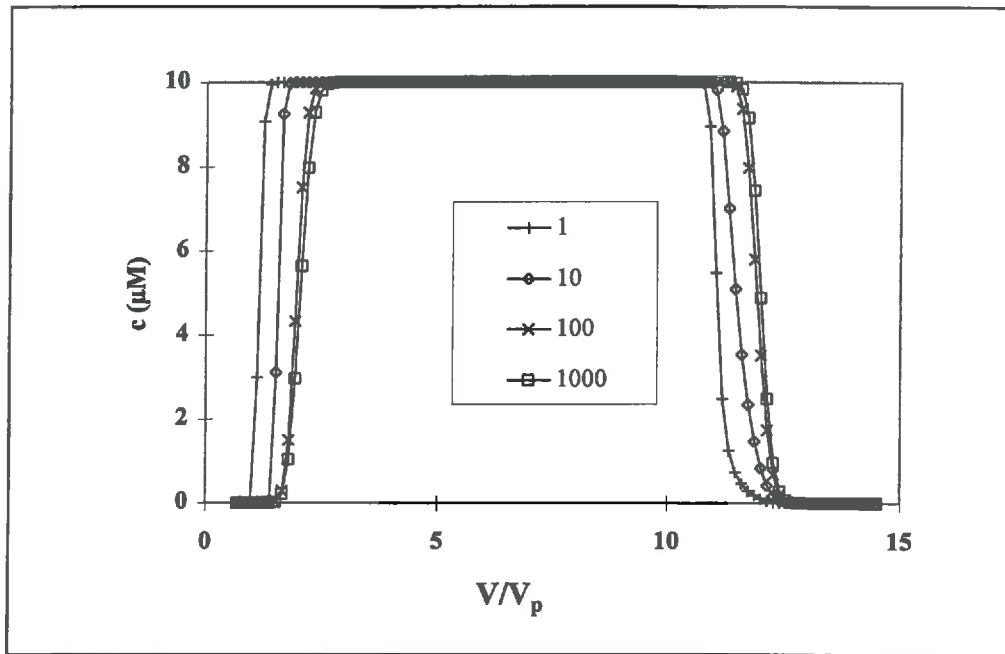


Figure 13 BTC's for different Langmuir isotherms with $K'_d = 1$ (isotherm in Figure 11c; numbers represent the maximal sorption capacities S'_{\max} (M); modelling parameters: $F = 30 \text{ cm}^3 \text{ h}^{-1}$, $V_p = 36.2 \text{ cm}^3$, $J = 100$, $c_0 = 10 \mu\text{M}$, $T_0 = 10 V_p$, samples = 5 cm^3)

The picture of the BTC's changes completely when the apparent distribution coefficient K'_d is very small (figure 13) or very large figure 14). In the case of $K'_d = 1$ (figure 13) it can be observed that the non-linearity is nearly invisible. For $K'_d = 100$ (figure 14) on the other hand we see that the non-linearity is much more important when seen in the scale of eluted pore volumes. When the diffusive desorption front is seen in the scale of the solution concentration the same behaviour is found as in figure 12b.

It can be observed in figure 12b for $S'_{\max} = 10$ and $100 \mu\text{M}$ and in figure 14 that the non-linearity caused *diffusive* desorption fronts are parallel for a given K'_d value. The corresponding adsorbed concentration represents a kind of a reservoir to create the diffusive desorption front.

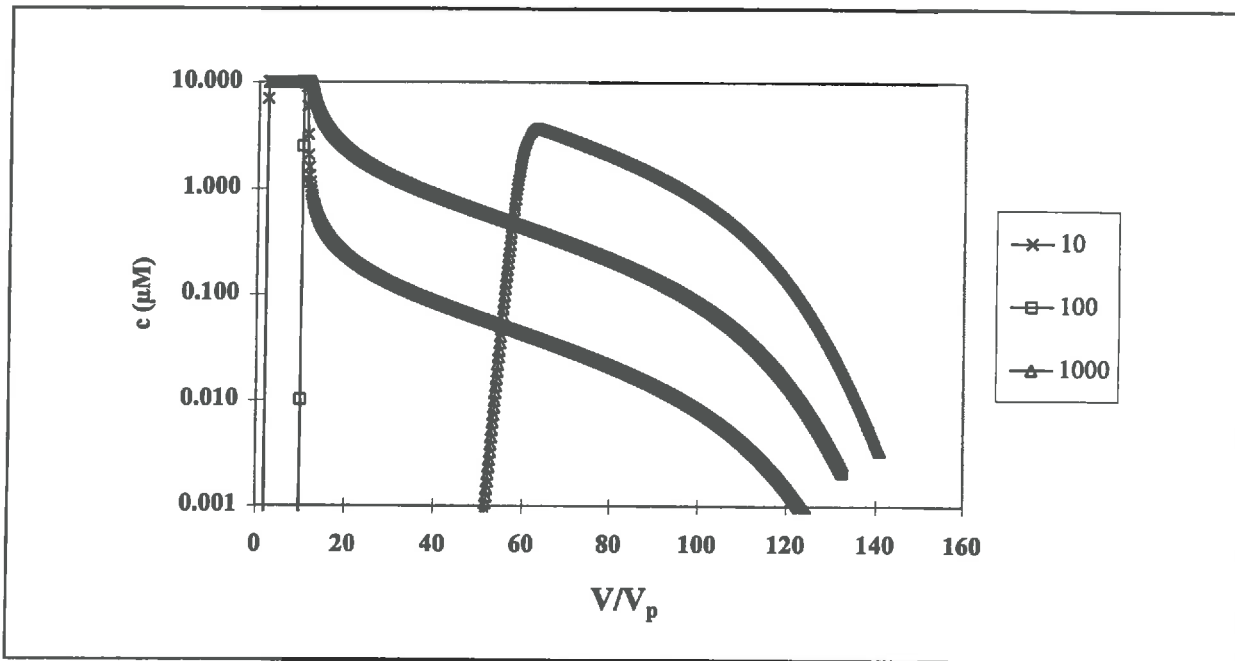


Figure 14 BTC for different Langmuir isotherms with $K'_d = 100$ (isotherm in figure 11a; numbers represent the maximal sorption capacities S'_{\max} (μM); modelling parameters: $F = 30 \text{ cm}^3 \text{ h}^{-1}$, $V_p = 36.2 \text{ cm}^3$, $J = 100$, $c_0 = 10 \mu\text{M}$, $T_0 = 10 V_p$, samples = 5 cm^3)

Langmuir isotherms (LEA) and different pulse lengths

Different pulse lengths are shifting the entire desorption front, as actually the sorbed concentration is not changed, once site saturation is reached (figure 15).

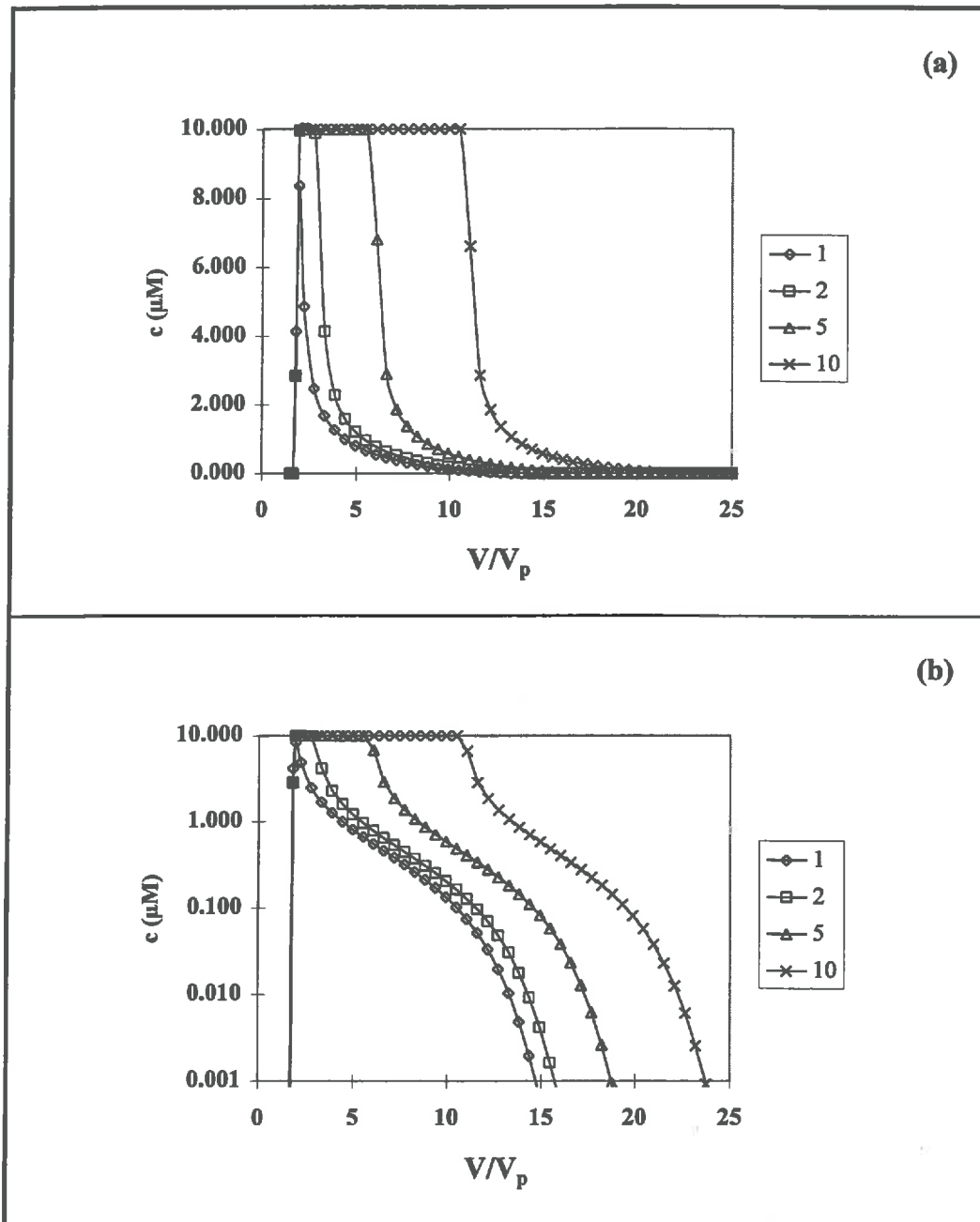


Figure 15 BTC's resulting from the Langmuir isotherm with $K'_d = 10$ and $S'_{\max} = 10 \mu\text{M}$ of figure 11b (numbers represent the pulse length T_0 in pore volume V_p ; (a) and (b) show the same numerical results in a normal (a) and log (b) scale; modelling parameters: $F = 30 \text{ cm}^3 \text{ h}^{-1}$, $V_p = 36.2 \text{ cm}^3$, $J = 100$, $c_0 = 10 \mu\text{M}$, samples = 5 cm^3)

Two site Langmuir isotherms at local equilibrium

The two site Langmuir isotherm is widely used to describe non-linear adsorption phenomena in composite solids such as soils (Sposito, 1982). Their application for iron (hydr)oxides seems equally justified as the existence of multiple adsorption sites has been described by several authors (Benjamin and Leckie, 1981; Spadini, 1993). The form of the resulting BTC depends mainly

- on the quotient between the two apparent distribution coefficients (different isotherms in figure 16a) and
- on the quotient between the two maximal sorption capacities (different isotherms in figure 16b).

When both parameters are sufficiently far from one another, a double S-shaped isotherm can be observed. In the following the overall adsorption is subdivided into two reactions onto two different « sites », which have to be considered as empirical model.

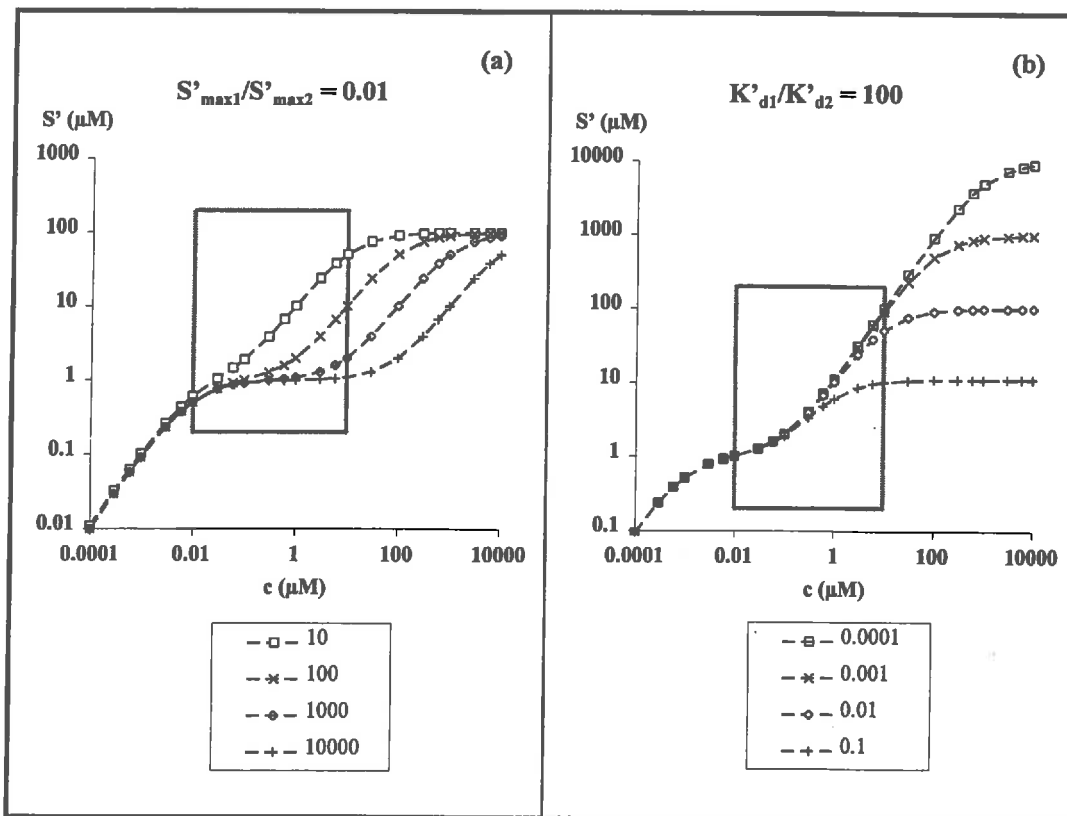


Figure 16 Two site Langmuir isotherms for simulations ($c_0 = 10 \mu\text{M}$) in figures 17 and 18
 (a) $K'_{d1} = 100$, $S'_{\max1} = 1 \mu\text{M}$, $S'_{\max2} = 100 \mu\text{M}$, numbers represent the K'_{d1}/K'_{d2}
 (b) $K'_{d1} = 1000$, $S'_{\max1} = 1 \mu\text{M}$, $K'_{d2} = 10$, numbers represent the $S'_{\max1}/S'_{\max2}$

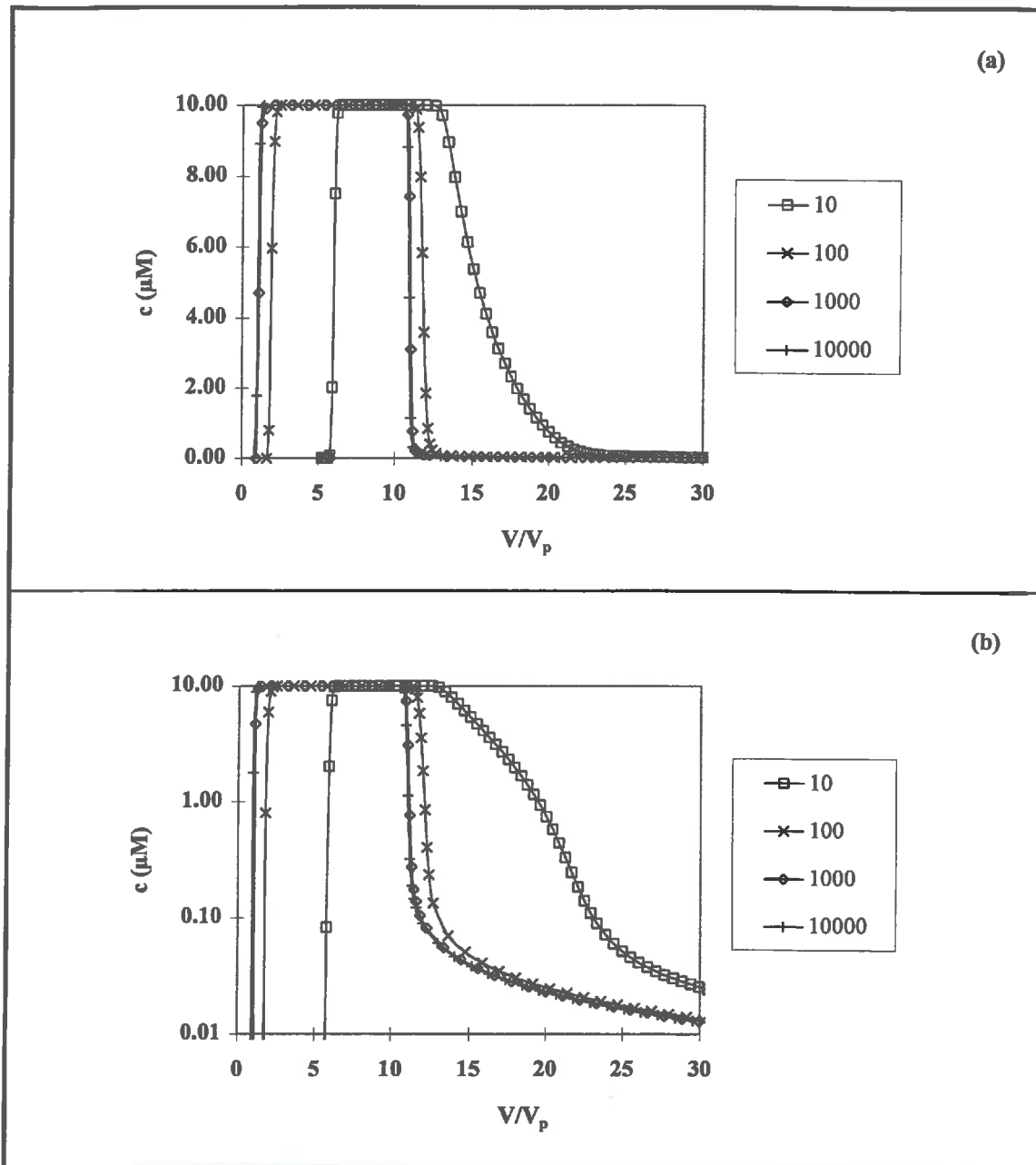


Figure 17 BTC's controlled by the two site Langmuir isotherms ($S'_{\max 1}/S'_{\max 2} = 0.01$) of figure 16a (numbers represent the maximum sorption capacity K'_{d1}/K'_{d2} ; (a) and (b) show the same numerical results in a normal (a) and log (b) scale; modelling parameters: $S'_{\max 1} = 1 \mu\text{M}$, $K'_{D1} = 100$, $S'_{\max 2} = 100 \mu\text{M}$, $F = 30 \text{ cm}^3 \text{ h}^{-1}$, $V_p = 36.2 \text{ cm}^3$, $J = 100$, $c_0 = 10 \mu\text{M}$, $T_0 = 10 V_p$, samples = 5 cm^3)

The resulting BTC's of isotherms being controlled by different quotients between the two apparent distribution coefficients and a constant maximal capacity ratio ($S'_{\max 1}/S'_{\max 2} = 0.01$) are shown in figure 17. It appears that for $K'_{d1}/K'_{d2} = 1000$ and 10000 the overall adsorption reaction is mainly controlled by adsorption on the first adsorption site, resulting in nearly no retardation as $c_0 K'_{d1} \gg S'_{\max 1}$. Actually we re-find the image from figure 13 for $K'_d = 1$.

For $K'_{d1}/K'_{d2} = 100$ a small retardation is observed but equally no *diffusive* desorption front can be recognised in the normal scale (figure 17a). Only for $K'_{d1}/K'_{d2} = 10$ the typical asymmetric BTC of a convex adsorption isotherm with its *self-sharpening* adsorption and the *diffusive* desorption front is observed.

When the desorption front of $K'_{d1}/K'_{d2} = 10$ is looked at in a log scale (figure 17b), the different parts of the isotherm can be distinguished:

- the flatter (*diffusive*) part due to the non-linearity caused by saturation of the high concentration sorption capacity,
- a steeper part due to linear adsorption on the high sorption capacity and
- a second *diffusive* part caused by saturation of the low concentration sorption capacity.

The second steep part is not represented (as in figure 12 for $S'_{\max} = 10 \mu\text{M}$).

The supplementary information given by the logarithmic presentations is obvious in figure 17b where the *diffusive* part of the desorption front can be observed even for the BTC's with negligible retardation ($K'_{d1}/K'_{d2} = 1000$ and 10000).

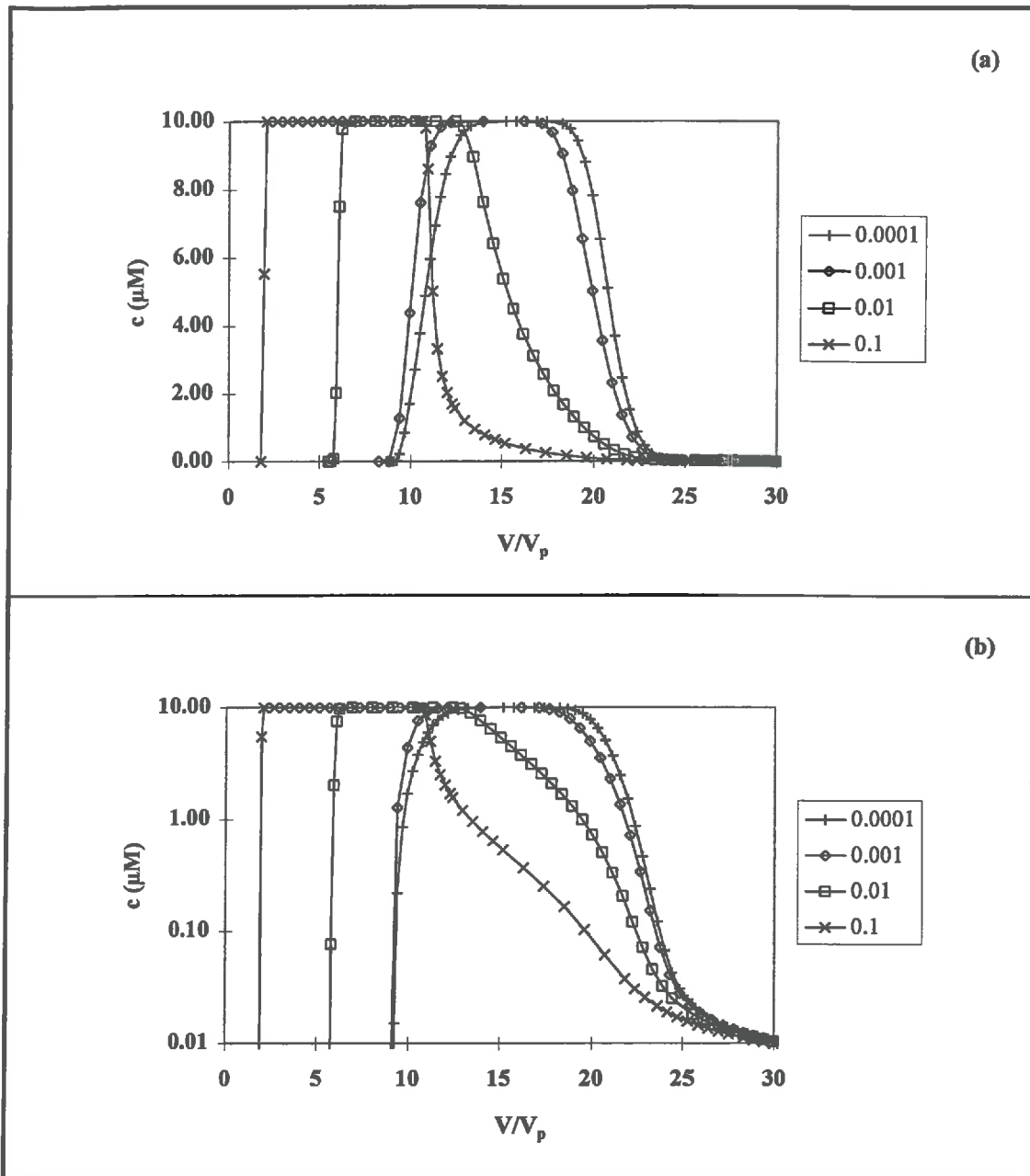


Figure 18 BTC's controlled by the two site Langmuir isotherms of figure 16b (numbers represent the ratio S'_{max1}/S'_{max2} ; (a) and (b) show the same numerical results in a normal (a) and log (b) scale; modelling parameters: $K'_{d1} = 1000$, $S'_{max1} = 1 \mu\text{M}$, $K'_{d2} = 10$, $F = 30 \text{ cm}^3 \text{ h}^{-1}$, $V_p = 36.2 \text{ cm}^3$, $J = 100$, $c_0 = 10 \mu\text{M}$, $T_0 = 10 V_p$, samples = 5 cm^3)

In figure 18 BTC's were compared for different ratios between the two sorption capacities, but at two constant apparent distribution coefficients. A completely different image is obtained the overall adsorption reaction changing from being dominated by linear adsorption to the second site for $S'_{max1}/S'_{max2} = 10^{-4}$ to being controlled by saturation of the second site

(figure 18a). The influence of the first (low concentration) adsorption reaction with its non-linear part can be observed in the logarithmic representation (figure 18b). All four BTC's converge within the *diffusive* part of the desorption front.

Langmuir isotherms and rate limited reaction (kinetics)

If now the chemical reactions are limited by reaction kinetics (figure 19) a completely different impact can be observed for the adsorption and the desorption front.

For the *self-sharpening adsorption front* one observes a general curve flattening when the adsorption is near local equilibrium. When the chemical reaction is very far from equilibrium the adsorption front approaches the rising part of a BTC without adsorption (having about the same shape as the adsorption front at local equilibrium) but has a declined plateau before reaching its initial solution concentration. Contrary to an immobile water content model, an earlier break-through is observed. This is due to the splitting of the overall water content in a mobile and an immobile phase, thereby reducing the flow accessible volume.

Within the *desorption front* the interaction between Langmuir-like adsorption and reaction kinetics is different (figure 19b):

- The *first steep part* (adsorption plateau with $c K'_d > S'_{max}$) gets even steeper.
- The *diffusive part* (being controlled by the non-linearity $S'_{max}/100 < c K'_d < S'_{max}$) is further flattened for adsorption near local equilibrium, but reduced for adsorption being far from local equilibrium.
- The *final steep part* (linear adsorption $c K'_d \leq S'_{max}/100$) seems to be controlled mainly by these kinetics resulting in a long exponentially decreasing concentration (*tailing*) over several solution concentration decades.

The presented experimental results proved an exponentially decaying behaviour over four decades and spanning 80 pore volumes, leading to the assumption that kinetics play a crucial role in designing the desorption front.

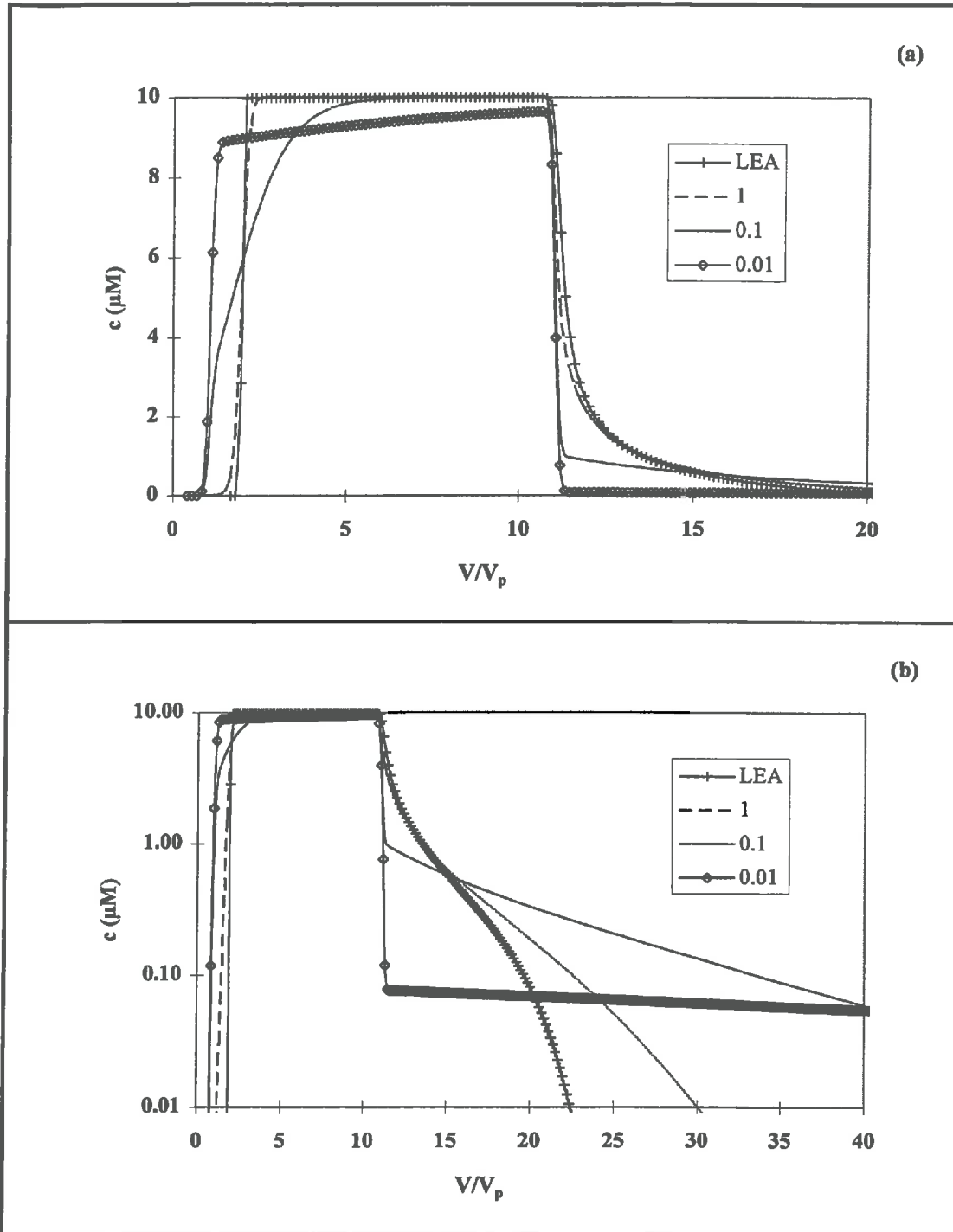


Figure 19 BTC's for a Langmuir isotherm with $K'_d = 10$ and $S'_{\max} = 10\mu\text{M}$ (figure 11b); (LEA local equilibrium assumption (LEA), numbers represent the reaction rate in h^{-1}); (a) and (b) show the same numerical results in a normal (a) and log (b) scale; modelling parameters: $F = 30 \text{ cm}^3 \text{ h}^{-1}$, $V_p = 36.2 \text{ cm}^3$, $J = 100$, $c_0 = 10 \mu\text{M}$, $T_0 = 10 V_p$, samples = 5 cm^3)

Rate limited Langmuir isotherms (kinetics) at different input concentrations

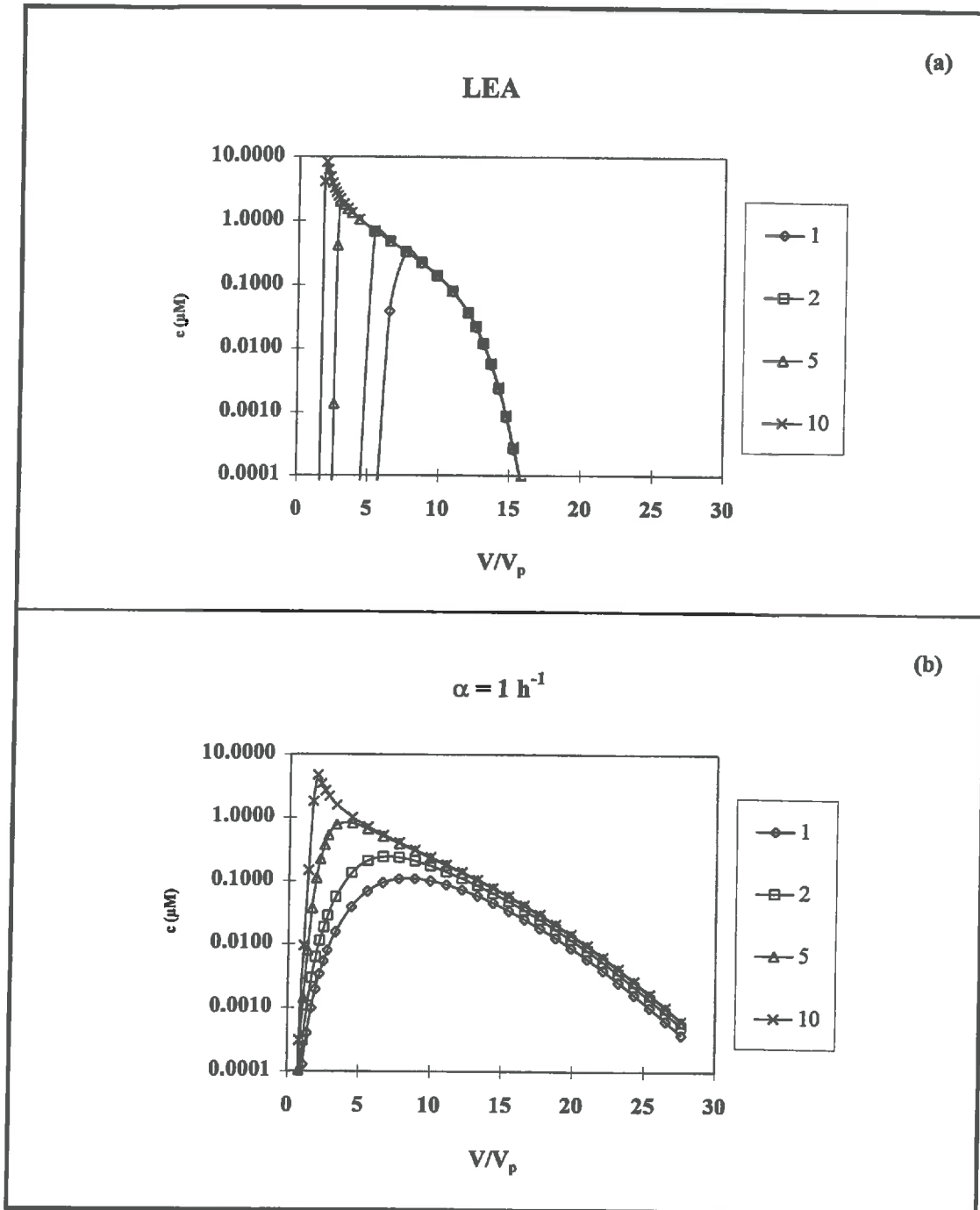


Figure 20 BTC's for a Langmuir isotherm at LEA (a) and with adsorption limited by a first order rate law (b); numbers represent the input solution concentration c_0 (μM); modelling parameters: $F = 30 \text{ cm}^3 \text{ h}^{-1}$, $V_p = 36.2 \text{ cm}^3$, $J = 100$, $T_0 = 10 V_p$, samples = 5 cm^3 , $K'_d = 10$, $S'_{\text{max}} = 10 \mu\text{M}$

When local equilibrium is assumed a Langmuir isotherm causes converging *diffusive* desorption fronts within its non-linear concentration range (figure 18a). This confirms the

converging behaviour already reported by numerous authors (e.g. Buergisser et al., 1993) for convex adsorption isotherms.

When a rate law limited adsorption is assumed the desorption fronts do not really converge.

Variant geochemical background conditions simulated by « isotherm shift »

The experimental results do not allow at this stage to draw conclusions on a unique reactive transport model, due to an excess of unknown variables: the exact isotherm and rate coefficients of the adsorption/desorption reaction, the percentage of the column being contaminated when passing from uranium accumulation to its mobilisation, and the maximum solution concentration within the column. Therefore the following simulations are only meant as giving an idea of the sensibility of the most important parameters: propagation rate of the peak expressed as arrival at the column outlet, its maximum concentration at the outlet and the long-term behaviour. The effects of *Freundlich* and *Langmuir* isotherms are compared. All modelling is done under the local equilibrium assumption, as a Freundlich isotherm and reaction kinetics have the same curve deforming effects and are not easily separated. The actual shift of a factor 100 is obtained from the experimental K_d values of figure 10.

Freundlich isotherms

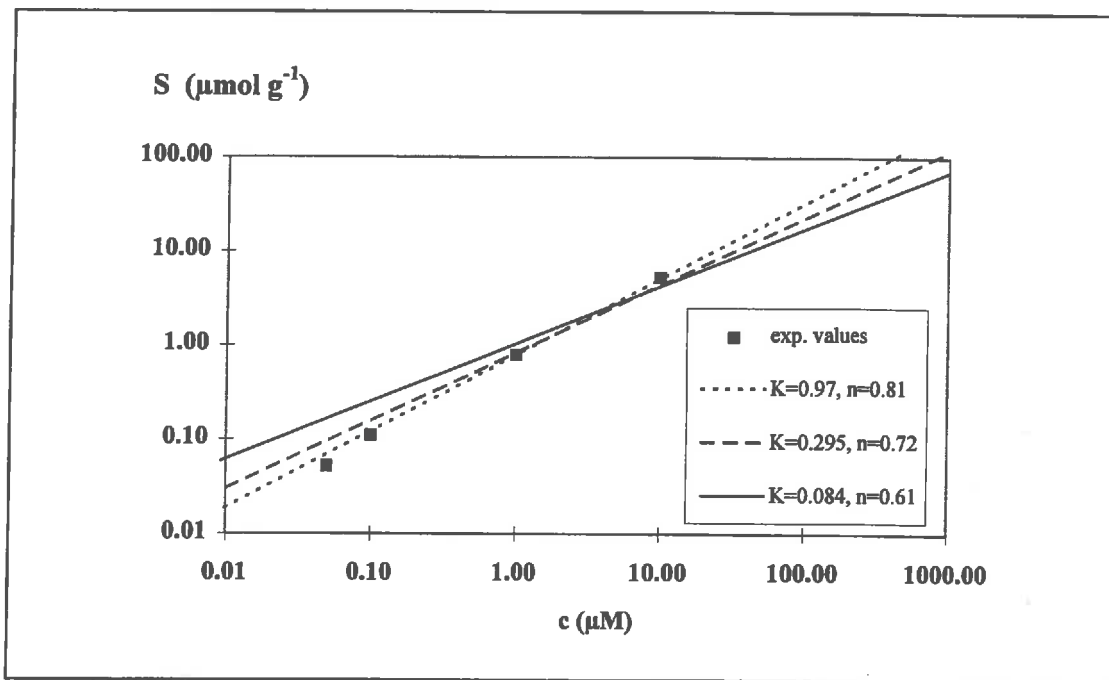


Figure 21 Freundlich isotherms for numerical simulations of an accidental desorption experiments under the local equilibrium assumption; experimental values from the retardation factor R (eq. 2)

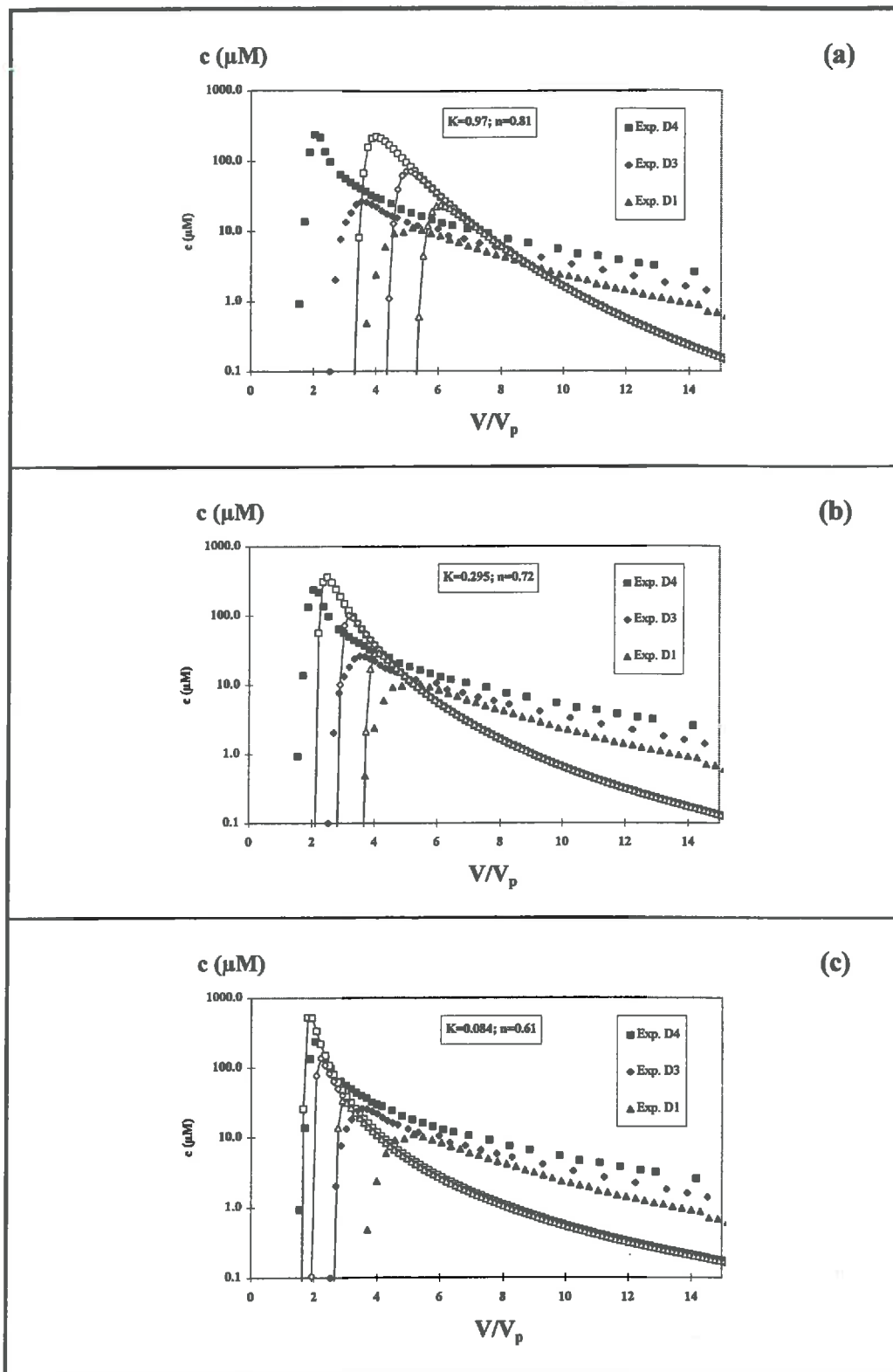


Figure 22 Experimental BTC's of experiments D1, D3 and D4 and simulations of an accidental desorption using the Freundlich isotherms from figure 21

In figure 21 three different isotherms are proposed to represent the experimental retardation factor related distribution coefficients. None of the resulting numerical BTC's (figure 22) reproduces really the experimental data. The isotherm which fits the adsorption data best ($K = 0.97$ and $n = 0.81$, figure 21) overestimates the retardation, the overall adsorption (figure 22a). Apparently, adsorption is no longer linear in the higher concentration range. Alternatively one attempted to decrease the exponent n while considering a similar apparent distribution coefficient K'_d .

$$K'_d = \frac{S}{c} = K_f c^{n-1} \quad (11)$$

It appears, that the difference between the retardation factors for the three curves is decreasing, and either exp. D1 and D3 (figure 22b) or exp. D4 (figure 22c) are at least partly well reproduced. The more the isotherm deviates from a line (i.e. the smaller exponent), the higher is the maximum outlet concentration and the tighter is the curve. It can therefore be noted, that the degree of nonlinearity of the curve intensifies the enrichment mechanism. Maximum concentrations get higher and the peak are tightened. The different tailing behaviour of the experimental and the numerical BTC's is certainly due to reaction kinetics (as qualitatively shown in figure 20 a and b).

Two site Langmuir isotherm

In a previous study it was suggested that a two site Langmuir isotherm is particularly appropriate to describe the adsorption of uranyl on goethite. The two maximum sorption capacities ($S_{\max 1} = 1.75 \mu\text{mol g}^{-1}$ and $S_{\max 2} = 350 \mu\text{mol g}^{-1}$) are estimated from comparison with literature data. In combination with adapted Langmuir coefficients to represent the apparent distribution coefficients K'_d they describe the retardation factor related sorption data perfectly (figure 23a). The numerical simulation of the accidental desorption under the local equilibrium assumption is however not satisfying (figure 23b). Adsorption is overestimated. It is interesting to note that the maximum concentration is overestimated for exp. D1 and underestimated for experience D4. Regarding the shape of the curves it appears that even under the (apparently wrong) local equilibrium assumption the long-term behaviour is well reproduced. The steeper part of the curve, which may be due to linear parts of the adsorption isotherm, is not in the same solution concentration interval for the numerical and experimental

curves. No justification for the site saturation in the numerical BTC's can be found in the experimental BTC's.

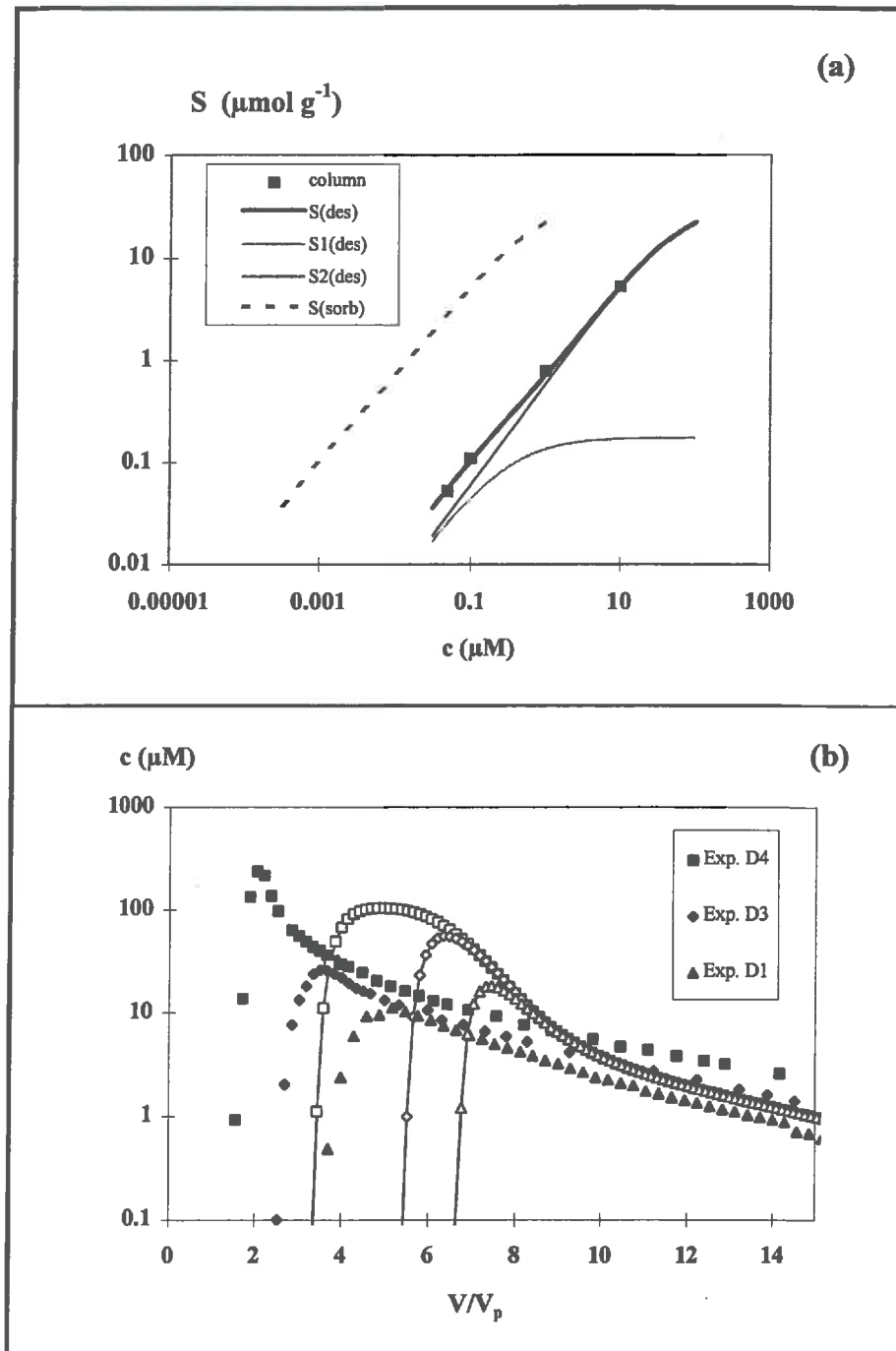


Figure 23 Langmuir isotherms for numerical simulations of accidental desorption experiments under the local equilibrium assumption (experimental values from the retardation factor R (eq. 2) shift = 100, $V_p = 36.2 \text{ cm}^3$, $F = 0.83 V_p \text{ h}^{-1}$, $S_{\text{max}1} = 1.75 \mu\text{mol g}^{-1}$, $S_{\text{max}2} = 350 \mu\text{mol g}^{-1}$, $K_{L1} = 5.37 \times 10^3 \text{ M}^{-1}$, $K_{L2} = 1050 \text{ M}^{-1}$)

Given the results of the experimental and numerical simulation of an accidental desorption, the approach to combine a background condition dependent distribution coefficient to a non-linear (convex, multi-sites) adsorption isotherm seems very promising to describe the mobilisation behaviour of uranyl and other sorbing cationic contaminants in the environment. With this approach an already complex (bi-dimensional) chemical system can be included in continuous ECDE related transport models.

DISCUSSION

A sharp increase of pore water pH and carbonate content can result from various reclamation actions such as sealing a carbonate rich mine waste (the change from open to closed system with regard to atmospheric CO₂ result in increasing pH), adding chalk to stabilise the waste, etc. Such a sudden pore water pH increase results (i) on the short term in a very intense breakthrough of concentrated uranium solution (concentration peak) and (ii) on the long term in a very long out-put of uranium rich waters (« tailing »).

The concentration peak would be predicted as most intense when:

- the adsorbed uranium concentration in the original medium (e.g. mine waste) is large, and
- uncontaminated underlying (sorbing) porous medium is small allowing no flattening of the concentration peaks by rate limited chemical reactions and dispersion.

This combination typically occurs in fine grained, clay rich mine waste lying on the top of large grain, high conductivity, alluvial material. This situation is typical to that encountered in SE Germany where on several sites uranium processing tailings have been stocked without much care about avoiding contamination of the underlying sediments.

The tailing, i.e. the presence of still large uranium concentration in the output solution after more than 50 pore volumes elution, may result:

- from various sites of adsorption, of decreasing concentration, but increasing affinity for uranium. In this case local equilibrium is assumed. Such a site distribution has been described for sorption on iron oxides and humic material, and is expected to be even broader for a complex material such as mine waste as in our simple model solid material (silica-goethite).
- from slow kinetics of the desorption reaction. This can be expected to have both physical and chemical origin. Physical diffusion in cracks and goethite canals can be rate limiting.

CONCLUSION

We simulated experimentally the accidental desorption of uranyl from a low contaminated artificial soil. We could show that the self-sharpening effects of the adsorption front due to the convex adsorption isotherm counteracts the flattening effect not only of dispersion but also of reaction kinetics. The diffuse desorption front on the other hand causes any clean up of contaminated solid porous material to be in effect a very long dilution process.

Practically the self-sharpening adsorption front results in a « sudden » break-through of a contamination front with a potentially high maximum concentration which is no longer related to the initial solution concentration during the adsorption phase, but to the total quantity of adsorbed uranyl in contact with the desorbing solution. The factor limiting the solution concentration of uranyl is the solubility of uranyl under the given chemical conditions.

Numerically we have shown how the different parameters such as the coefficient describing the isotherm shift, the isotherms themselves as well as the reaction kinetics influence the desorption front. For our experiments no exact modelling is done at this stage, as the model includes too many unknowns with the possibility of several solutions. In future studies equilibrium isotherm as well as kinetic studies have to be carried out to gain further information on the nonlinearity and rate-limitation of the adsorption reaction.

The approach to model accidental desorptions by shifting isotherms upon a change in geochemical conditions seems promising and more appropriate to describe natural processes than the classical linear K_d approach. The great advantage over comprehensive geochemical models is that this type of computation method can easily be included in complex continuous models. This isotherm shift describes very well the fact, that even small pH changes may have tremendous consequences such as a sudden release of large amounts of contaminant in surface or groundwaters, release which may be a threat for public health.

LITERATURE

- Benjamin, M. M. and Leckie, J. O. (1981):** Multiple site adsorption of Cd, Cu, Zn, and Pb on amorphous iron oxyhydroxide. *J. Coll. Interface Sci.*, 79, 209-221.
- Bernhard, G., Geipel, G., Brendler, V. and Nitsche, H. (1996):** Speciation of Uranium in Seepage Waters of a Mine tailing Pile Studied by Time-Resolved Laser-Induced Fluorescence Spectroscopy (TRLFS). *Radiochimica Acta*, 74, 87-91.
- Brachmann, A. (1997):** Zeitaufgelöste laser-induzierte Fluoreszenzspektroskopie zur Charakterisierung der Wechselwirkung des Uranylions mit Huminsäuren und Carboxylatliganden. Ph. D. thesis, TU Dresden.
- Brendler, V., Geipel, G., Bernhard, G. and Nitsche, H. (1996):** Complexation in the System $UO_2^{2+} / PO_4^{3-} / OH(aq)$: Potentiometric and Spectroscopic Investigations at very Low Ionic Strengths. *Radiochimica Acta*, 74, 75-80.
- Bruno, J., de Pablo, J., Duro, L. and Figuerola, E. (1995):** Experimental study and modelling of the U(VI)- $Fe(OH)_3$ surface precipitation/coprecipitation equilibria. *Geochim. Cosmochim. Acta*, 59(20), 4113-4123.
- Brusseau, M. L. (1995):** The effect of non-linear sorption on transformation of contaminants during transport in porous media. *J. Contam. Hydrology*, 17(4), 277-291.
- Buergisser, C. S., Cernik, M., Borkovec, M. and Sticher, H. (1993):** Determination of Non-linear Adsorption Isotherms from Column experiments: An Alternative to Batch Studies. *Environ. Sci. Technol.*, 27(5), 943-948.
- Catchpole, G. and Kirchner, G. (1995):** Restoration of Groundwater contaminated by alkaline in-situ leach uranium mining. Proceedings of the international Conference and Workshop on Uranium-Mining and Hydrology, Freiberg, Germany, Verlag Sven van Loga, Koeln.
- Chrisholm-Brause, C., Conradson, S. D., Buscher, C. T., Eller, P. G. and Morris, D. E. (1994):** Speciation of uranyl sorbed at multiple binding sites on montmorillonite. *Geochim. Cosmochim. Acta*, 58(17), 3625-3631.
- Dent, A. J., Ramsay, D. F. and Swanton, S. W. (1991):** An EXAFS Study of Uranyl Ion in Solution and Sorbed onto Silica and Montmorillonite Clay Colloids. *J. Colloid Interface Science*, 150(1), 45-60.
- Gaudet, J. P., Jegat, H., Vachaud, G. and Wierenga, P. (1977):** Solute transfer, with Exchange Between Mobile and Stagnant Water, through Unsaturated Sand. *Soil Sci. Soc. Am. J.*, 41(4), 665-671.
- Gaudet, J.-P. (1978):** Transfert d'eau et de soluté dans des sols non-saturés. Mesures et simulation. PhD thesis, Institut National Polytechnique de Grenoble, 230 p.
- Griffioen, J., Appelo, C. A. J. and van Veldhuizen, M. (1992):** Practice of Chromatography: Deriving Isotherms from Elution Curves. *Soil Sci. Soc. Am. J.*, 56(5), 1429-1437.
- Ho, C. H. and Miller, N. H. (1985):** Effect of Humic Acid on Uranium Uptake by Hematite Particles. *J. Colloid Interface Science*, 106(2), 281-288.
- Ho, C. H. and Miller, N. H. (1986):** Adsorption of uranyl species from Bicarbonate Solution onto Hematite Particles. *J. Colloid Interface Science*, 110(1), 165-171.
- Hsi, C.-K. and Langmuir, D. (1985):** Adsorption of uranyl onto ferric oxyhydroxides: Application of the surface complexation site-binding model. *Geochim. Cosmochim. Acta*, 49, 1931-1941.
- Jauzien, M. (1988):** Méthodologie d'étude du transport transitoire de solutés dans les milieux poreux: Outils théoriques et numériques, méthodes expérimentales, application à l'étude du transport transitoire du césium sous

- forme cationique (Cs^+) dans un aquifère alluvial. Ph. D. thesis, Institut National Polytechnique de Lorraine, Ecole Nationale Supérieure des Industries Chimiques, Nancy, 151 p.
- Jauzein, M., Andre, C., Margrita, R., Sardin, M. and Schweich, D. (1989):** A Flexible Computer Code for Modelling Transport in Porous Media: Impact. *Geoderma*, 44, 95-113.
- Kato, Y., Kimura, T., Yoshida, Z. and Nitani, N. (1996):** Solid-Liquid Phase Equilibria of Np(VI) and U(VI) under Controlled CO_2 Partial Pressures. *Radiochimica Acta*, 74, 21-25.
- Liger, M. (1996):** Rôle catalytique des oxyhydroxydes de Fe(III): Réduction de U(VI) par le Fe(II). Ph. D. thesis, Laboratoire de Géophysique Interne et Tectonophysique. Grenoble, Université Joseph Fourier, 173 p.
- Kohler, M., Curtis, G. P., Kent, D. B. and Davis, J. A. (1996):** Experimental investigations and modelling of Uranium(VI) transport under variable chemical conditions. *Water Resources Research*, 32(12), 3539-3551.
- McKinley, J. P., Zachara, J. M., Smith, S. C. and Turner, G. D. (1995):** The influence of uranyl hydrolysis and multiple site binding reactions on Adsorption of U(VI) to montmorillonite. *Clays and Clay Minerals*, 43(5), 586-598.
- Moll, H. (1997):** Zur Wechselwirkung von Uran mit Silikat in waessrigen Systemen. Ph. D. thesis, TU Dresden..
- Meinrath, G., Klenze, R. and Kim, J. I. (1996):** Direct Spectroscopic Speciation of Uranium(VI) in Carbonate Solutions. *Radiochimica Acta*, 74, 81-86.
- Morris, D. E., Chrisholm-Brause, C. J., Barr, M. E., Conradson, S. D. and Eller, P. G. (1994):** Optical spectroscopic studies of the sorption of UO_2^{2+} species on a reference smectite. *Geochim. Cosmochim. Acta*, 58(17), 3613-3623.
- Morrison, S. J., Spangler, R. R. and Tripathi, V. S. (1995a):** Adsorption of uranium(VI) on amorphous ferric oxyhydroxide at high concentrations of dissolved carbon(IV) and sulphur(VI). *J. Contam. Hydrology*, 17(4), 333-346.
- Morrison, S. J., Tripathi, V. S. and Spangler, R. R. (1995b):** Coupled reaction transport modelling of a chemical barrier for controlling uranium(VI) contamination in groundwater. *J. Contam. Hydrology*, 17(4), 347-363.
- Pompe, S. (1997):** Entwicklung huminsaeureaehnlicher Melanoidine als Funktionsmodelle fuer Huminsaeuren und ihr Vergleich mit Fluka-Huminsaeure hinsichtlich ihres Komplexierungsverhaltens gegenueber Uran(VI). Ph. D. thesis, TU Dresden.
- Reich, T., Moll, H., Denecke, M. A., Geipel, G., Bernhard, G., Nitsche, H., Allen, P. G., Bucher, J. J., Kaltsoyannis, N., Edelstein, N. M. and Shuh, D. K. (1996):** Characterisation of Hydrated Uranyl Silicate by EXAFS. *Radiochimica Acta*, 74, 219-223.
- Sandino, A. and Bruno, J. (1992):** The solubility of $(\text{UO}_2)_3(\text{PO}_4)_2 \cdot 4 \text{H}_2\text{O}(\text{s})$ and the formation of U(VI) phosphate complexes: Their influence in uranium speciation in natural waters. *Geochim. Cosmochim. Acta*, 56, 4135-4145.
- Spadini, L. (1993):** Struktur und Stabilitaet von Oberflaechenkomplexen im System Cd^{2+} - FeOOH . Institut fuer anorganische, analytische und physikalische Chemie. Ph. D. thesis, Universitaet Bern.
- Sposito, G. (1982):** On the Use of the Langmuir Equation in the Interpretation of "Adsorption" Phenomena: The "Two-Surface" Langmuir Equation. *Soil. Sci. Soc. Am. J.*, 46, 1147-1152.
- Torma, A. E., Pendleton, N. R. and Fleming, W. M. (1985):** Sodium carbonate-bicarbonate leaching of a New Mexico uranium ore and removal of long Half-life radionuclides from the leach residue. *Uranium*, 2, 17-36.

van Veldhuizen, M., Appelo, C. A. J. and Griffioen, J. (1995): The least squares quotient algorithm as a rapid tool for obtaining sorption isotherms from column elution curves. *Water Resources Res.*, 31(4), 849-857.

Waite, T. D., Davis, J. A., Payne, T. E., Waychunas, G. A. and Xu, N. (1994): Uranium(VI) adsorption to ferrihydrite: Application of a surface complexation model. *Geochim. Cosmochim. Acta*, 58(24), 5465-5478.

Wersin, P., Hochella, M. F., Persson, P. and Redden, G. (1994): Interaction between aqueous uranium(VI) and sulphide minerals: Spectroscopic evidence for sorption and reduction. *Geochim. Cosmochim. Acta*, 58(13), 2829-2843.

Yeh, G.-T. and Tripathi, V. S. (1991): A Model for simulating Transport of Reactive Multispecies Components: Model Development and Demonstration. *Water Resources Research*, 27(12), 3075-3094.

CONCLUSION

Dans ce travail, nous avons cherché à évaluer les risques de contamination induits par la présence des ions uranyle dans des déchets miniers ou dans d'autres terrains peu contaminés (terrains militaires par exemple). Ces risques résultent du relargage de l'uranium suite à un changement des conditions physico-chimiques du milieu. Pour le prédire, il faut décrire le couplage entre le transfert mécanique et les réactions chimiques de mobilisation. Pour la caractérisation de ce couplage nous nous sommes limités à des expériences de colonnes menées sur un sol artificiel.

Nous avons montré expérimentalement que les risques de contamination dépendent fortement de l'évolution des conditions géochimiques. Dans le cas où la stabilité de ces conditions est assurée, le risque de propagation des contaminants est relativement « faible » et « prévisible ». Si le système est dans la gamme de pH favorable à l'adsorption, l'uranium fixé reste plus ou moins immobile. C'est seulement après saturation des sites (rarement rencontrée dans les conditions du terrain!) que l'on risque d'observer l'apparition d'uranium dans des sources ou dans l'eau superficielle. Au contraire, dans des conditions moins favorables à l'adsorption (valeurs de pH extrêmes ou des concentrations élevées de ligands) une sortie de l'uranium du milieu poreux est un risque certain. En conditions géochimiques stables, le développement de la contamination est prévisible; on retrouve un front de contamination avec une concentration de l'uranium inférieure ou égale à la concentration de l'eau apportée (dans l'eau des mines ouvertes ou celle des terrils des déchets). En résumé, on peut constater qu'en conditions géochimiques invariantes, le système réagit « lentement » et que l'uranium reste normalement à l'état de traces. Si la continuité des conditions chimiques est au contraire interrompue, le système perd son inertie relative. Un tel changement brusque peut causer une désorption accidentelle avec propagation d'un front abrupt de contamination.

Pour comprendre les mécanismes contrôlant le transport réactif de l'uranyle, les réactions chimiques ont tout d'abord été traitées dans un système sans flux. La silice amorphe a été retenue comme modèle de surface réactive des déchets miniers. On peut avec cette dernière, observer la spéciation de l'uranyle par la spectroscopie « TRLIL ». Deux complexes de l'uranyle sur la surface ont été identifiés, et leur constante de formation quantifiée. Nous n'avons pas trouvé d'indications démontrant une polymérisation de l'uranyle à la surface de la silice. Ce résultat est cohérent avec la littérature, et de plus justifie l'utilisation de l'équation de Langmuir qui suppose une association de type 1 : 1 entre molécule adsorbée et site adsorbant.

Dans un deuxième temps, nous avons étudié le couplage entre transport mécanique et réactions chimiques dans des conditions géochimiques constantes. Nous avons étudié le système CRISTOBALITE-GOETHITE-URANYLE-CARBONATE. En comparant les expériences en réacteur fermé (sans flux) et en réacteur ouvert (colonne de laboratoire) nous avons montré que la fixation de l'uranium résulte d'un ensemble de plusieurs réactions chimiques dont nous avons déterminé les constantes thermodynamiques et les lois cinétiques. Cette fixation est nettement plus importante dans le réacteur ouvert qu'en réacteur fermé. Dans les colonnes, où le temps de contact est court, la dissolution de la cristobalite, et donc la libération de l'acide silicique, sont limitées. Or, l'acide silicique est un compétiteur potentiel de l'uranyle pour les sites d'adsorption de surface de la goethite. Dans la conception des expériences, il serait donc impératif de reproduire le temps de contact entre la phase mobile et la phase stationnaire observé sur le terrain. L'ensemble des réactions est encore plus complexe dans le cas d'un sol naturel ou d'une eau souterraine car on est en présence de nombreux composants.

Nous avons montré que le transport réactif de l'uranyle est en fait une interaction multiple et complexe composée :

- de réactions de fixation en équilibre thermodynamique. L'adsorption est décrite par une isotherme dont la forme linéaire ou non-linéaire est due à :
 - l'existence de plusieurs sites d'adsorption, avec effets de saturation,
 - la charge de la surface,

- la compétition entre complexants dissous et de surface pour l'uranyle ainsi que d'autres ions (principalement les ions silicates et carbonates/bicarbonates).
- de taux cinétiques
 - physiques liés à la microporosité et/ou à la couche d'eau immobile et
 - chimiques qui peuvent différer selon le sens de la réaction (adsorption ou désorption).
- du transfert convectif de la fraction mobile d'eau.

Dans une dernière étape, nous avons simulé expérimentalement les conditions d'une désorption accidentelle suite à une perturbation des conditions physico-chimiques du milieu. Nous avons mis en évidence que les concentrations dans l'eau à la sortie de la colonne dépassent largement celles apportées initialement. Si ces résultats sont qualitativement extrapolés au terrain, ils indiquent que l'évaluation d'un risque de contamination doit inclure l'étude de phénomènes « en cours » caractérisés par des équilibres dynamiques. En complément de l'étude classique de l'état apparent, y compris celle des conditions chimiques et des flux, il paraît donc indispensable de rechercher la géochimie antérieure pour estimer les risques qu'un front de contamination soit déjà « en route ». Dans la prévision de l'évolution des contaminations dans l'avenir, il est donc nécessaire d'inclure les effets à long terme.

La capacité d'adsorption de l'uranium réagit comme un système de tampon classique qui a pour un temps « neutralisé » des apports indésirables. Cependant si le système est soumis à d'autres conditions, même à une faible variation des conditions chimiques, il peut y avoir une mobilisation de l'uranium et une sortie d'eau à des concentrations très élevées parce que le réservoir pour la désorption est grand, particulièrement dans les terrils miniers.

Les expériences sous des conditions physico-chimiques variables ont ainsi permis de compléter les expériences menées en conditions stables.

L'avantage des expériences simplifiées est qu'elles mettent en jeu un nombre limité de paramètres à ajuster dans la modélisation. Mais ces systèmes représentent-ils les conditions complexes trouvées sur le terrain? Est-ce qu'une expérimentation adaptée à la situation réelle

ne serait pas d'avantage capable de donner des idées sur le développement potentiel du système dans l'avenir? La méthodologie de telles expériences a le grand inconvénient de ne pas permettre l'étude des phénomènes systématiquement (par exemple en ne changeant qu'un paramètre à la fois). Il en résulte un nombre de paramètres inconnus trop élevé pour une approche systématique, c'est à dire pour la recherche de la meilleure combinaison des paramètres qui conduisent au relargage, par un système faiblement pollué, d'une eau tellement chargée en contaminant qu'elle expose l'homme à un risque sanitaire réel.

PERSPECTIVES

Une évaluation des risques liés à un site pollué par l'uranium(VI) est basée sur un modèle qui prend en compte l'état actuel du milieu (conditions initiales) et des conditions aux limites. Généralement, les risques majeurs sont induits par des sollicitations du système qui correspondent à une brusque variation des conditions aux limites. Leur estimation se fait d'abord par la représentation avec des paramètres pertinents des conditions initiales dynamiques qui résultent du transport réactif (couplage entre le transfert d'eau et des réactions de fixation/mobilisation); puis par la simulation des réponses du système. Les études peuvent être découpées en plusieurs étapes:

Définir précisément l'état actuel de pollution du site à l'échelle du réacteur fermé et de la colonne de laboratoire et du point de vue du transfert couplé, sous des conditions dynamiques simplifiées (écoulement d'eau permanent dans un sol homogène et saturé en eau). Les mécanismes prépondérants pour la mobilité sont le mode de fixation avec les non-linéarités de l'isotherme d'adsorption entière (jusqu'à la limite de solubilité de l'uranium(VI) dans les conditions chimiques observées ou supposées) et les cinétiques des réactions chimiques. Les non-linéarités apparentes sont, entre autres, dues aux interactions des autres composants du système par des effets de compétition en solution et pour des sites et à la polymérisation du soluté en solution et à la surface.

La fluorescence induite par laser pulsé paraît un outil prometteur pour caractériser la spéciation de l'uranyle sur la surface, et à basse température, des mesures doivent être possibles pour des matières qui suppriment cette fluorescence aux températures ambiantes.

En prenant en compte la complexité des réactions de fixation avec leurs cinétiques, il paraît indispensable de tester sur colonnes de laboratoire la validité d'une modélisation avec des temps caractéristiques convectifs compatibles avec ceux du site concerné. Pour ces études, le choix de la taille des colonnes est critique : suffisamment longue pour vérifier les effets de conditions aux limites (identification des paramètres hydrodispersifs) et suffisamment courte pour avoir des temps de séjours compatibles avec la durée des études (paramètres chimiques).

En variant le débit de l'eau et la durée des créneaux de concentration de l'uranium à l'entrée de la colonne, les effets des cinétiques physiques et chimiques doivent être testés systématiquement.

Tester expérimentalement le modèle obtenu avec des conditions observées (géochimie constante) dans des conditions chimiques variables et probables.

Des observations directes (destructives ou non destructives) doivent être réalisées pour suivre la propagation d'un créneau d'une concentration élevée en uranyle dans une colonne. Le rayonnement de l'uranium permet une méthode non destructive qui fournit des données spatio-temporelles. Dans le cas où une méthode non destructive n'est pas possible, il sera conseillé de réaliser deux analyses destructives: la première pour déterminer la longueur de colonne contaminée, la deuxième à l'instant de l'arrivée du front de désorption dans la partie non-contaminée.

Combiner ce transfert couplé aux conditions dynamiques réelles du terrain.

Un écoulement d'eau transitoire et une teneur volumique en eau variable introduit des non-linéarités supplémentaires dans le système. Toute autre variation d'un facteur peut être étudiée (microbiologie, conditions redox).

Vérifier la pertinence de l'approche sur un terrain pilote.

Pour cela, il sera nécessaire de trouver un site qui soit contaminé par l'uranium(VI) depuis longtemps et qui ait connu un brusque changement des conditions chimiques.

Enfin une application de ces études pourra être de protéger les sites contaminés de tout changement géochimique.

REFERENCES BIBLIOGRAPHIQUES

- Aberg, M., Ferri, D., Glaser, J. et Grenthe, I. (1983):** Structure of the Hydrated Dioxouranium(VI) Ion in Aqueous solution. An X-ray Diffraction and ^1H NMR Study. *Inorg. Chem.*, 22, 3986-3989.
- Akratanakul, C. C., Boersma, L. et Klock, O. O. (1983):** Sorption processes in soils as influenced by pore water velocity. II. Experimental results. *Soil Sci.*, 135, 331-341.
- Atkinson, R. J., Posner, A. M. et Quirk, J. P. (1967):** Adsorption of potential-determining ions at the ferric oxide-aqueous electrolyte interface. *J. Phys. Chem.*, 71, 550-558.
- Barlett, J. R. et Conney, R. P. (1989):** On the determination of Uranium-Oxygen Bond Lengths in dioxouranium(VI) compounds by Raman spectroscopy. *Journal of Molecular Structure*, 193, 295-300.
- Bear, J. (1972):** Dynamics of Fluids in Porous media. American Elsevier, New York.
- Bell, J. T. et Biggers, R. E. (1968):** Absorption Spectrum of the Uranyl Ion in Perchlorate Media. III. Resolution of the Ultraviolet Band Structure, Some Conclusions Concerning the Excited State of UO_2^{2+} . *J. Mol. Spectroscopy*, 25, 312-329.
- Benjamin, M. M. et Leckie, J. O. (1981):** Multiple site adsorption of Cd, Cu, Zn, and Pb on amorphous iron oxyhydroxide. *J. Coll. Interface Sci.*, 79, 209-221.
- Bernhard, G., Geipel, G., Brendler, V. et Nitsche, H. (1996):** Speciation of Uranium in Seepage Waters of a Mine Tailing Pile Studied by Time-Resolved Laser-Induced Fluorescence Spectroscopy (TRLFS). *Radiochimica Acta*, 74, 87-91.
- Berthoud, T., Decambox, P., Kirsch, B., Maichien, P. et Moulin, C. (1988):** Direct Uranium Trace Analysis in Plutonium Solutions by Time-Resolved Laser-Induced Spectrofluorometry. *Anal. Chem.*, 60, 1296-1299.
- Bidoglio, G., Gibson, P. N., O'Gorman, M. et Roberts, K. J. (1993):** X-ray absorption spectroscopy investigation of surface redox transformations of thallium and chromium on colloidal mineral oxides. *Geochim. Cosmochim. Acta*, 57, 2389-2394.
- Brachmann, A. (1997):** Zeitaufgelöste laser-induzierte Fluoreszenzspektroskopie zur Charakterisierung der Wechselwirkung des Uranylions mit Huminsäuren und Carboxylatliganden. Ph. D. thesis, TU Dresden.
- Brendler, V., Geipel, G., Bernhard, G. et Nitsche, H. (1996):** Complexation in the System $\text{UO}_2^{2+}/\text{PO}_4^{3-}/\text{OH}^-(\text{aq})$: Potentiometric and Spectroscopic Investigations at very Low Ionic

Strengths. *Radiochimica Acta*, 74, 75-80.

Brese, N. E. et O'Keefe, M. (1991): Bond-valence parameters in solids. *Acta Cryst.*, B47, 192-197.

Brina, R. et Miller, A. G. (1992): Direct Determination of Trace Levels of Uranium by Laser-Induced Kinetic Phosphorimetry. *Anal. Chem.*, 64, 1413-1418.

Brown, I. D. et Altermatt, D. (1985): Bond valence parameters obtained from a systematic analysis of the inorganic crystal structure database. *Acta Cryst.*, B41, 244-247.

Bruno, J., de Pablo, J., Duro, L. et Figuerola, E. (1995): Experimental study and modelling of the U(VI)-Fe(OH)₃ surface precipitation/coprecipitation equilibria. *Geochim. Cosmochim. Acta*, 59(20), 4113-4123.

Brusseau, M. L. (1995): The effect of nonlinear sorption on transformation of contaminants during transport in porous media. *J. Contaminant Hydrology*, 17(4), 277-291.

Buergisser, C. S., Cernik, M., Borkovec, M. et Sticher, H. (1993): Determination of Nonlinear Adsorption Isotherms from Column experiments: An Alternative to Batch Studies. *Environ. Sci. Technol.*, 27(5), 943-948.

Catchpole, G. et Kirchner, G. (1995): Restoration of Groundwater contaminated by alkaline in-situ leach uranium mining. Proceedings of the international Conference and Workshop on Uranium-Mining and Hydrology, Freiberg, Germany, Verlag Sven van Loga, Koeln.

Charlet, L. et Manceau, A. (1992): X-Ray Absorption Spectroscopic Study of the Sorption of Cr(III) at the Oxide-Water Interface. II. Adsorption, Coprecipitation and Surface Precipitation on Hydrous Ferric Oxide. *J. Colloid Interface Sci.*, 148(443-458).

Charlet, L., Schindler, P. W., Spadini, L., Furrer, G. et Zysset, M. (1993): Cation adsorption on oxides and clays: The aluminium case. *Aquatic Science*, 55(4), 291-303.

Chaudhari, M. (1971): An improved Numerical Technique for Solving Multidimensional Miscible Displacement Equations. *Society of Petroleum Engineer Journal*, September, 277-284.

Chrisholm-Brause, C., Conradson, S. D., Buscher, C. T., Eller, P. G. et Morris, D. E. (1994): Speciation of uranyl sorbed at multiple binding sites on montmorillonite. *Geochim. Cosmochim. Acta*, 58(17), 3625-3631.

Davies, C. W. (1962): Ion Association. Washington, D.C., Butterworth.

Degoda, W. Ya. (1997): Personal communication.

Deissmann, G., Plueger, W. L. et Kistinger, S. (1995): Effects of Redox- and pH-changes on contaminants in acid mine waters from the Ronneburg Mine (Thuringia, Germany): A comparative laboratory study. *Uranium-Mining and Hydrology*, Freiberg, Germany, Verlag

Sven van Loga.

Dent, A. J., Ramsay, D. F. et Swanton, S. W. (1991): An EXAFS Study of Uranyl Ion in Solution and Sorbed onto Silica and Montmorillonite Clay Colloids. *J. Colloid Interface Science*, 150(1), 45-60.

Dzombak, D. A. et Morel, F. M. M. (1990): Surface Complexation Modelling: Hydrous Ferric Oxide. New York, John Wiley and Sons.

Eliet, V. (1996): Applications des techniques de fluorescence pour l'étude de l'Uranium dans des milieux homogènes et hétérogènes: réactions d'hydrolyse et photoréduction sur le bioxyde de Titane. Ph. D. Institut de l'Environnement du CCR d'Ispra, Université de Paris Sud, U.F.R. Scientifique d'Orsay, Paris, 206 p.

Eliet, V., Bidoglio, G., Omenetto, N., Parma, L. et Grenthe, I. (1995): Characterisation of Hydroxide Complexes of Uranium(VI) by Time-Resolved Fluorescence Spectroscopy. *J. Chem. Soc. Faraday Trans.*, 91(15), 2275-2285.

Farges, F., Ponader, C. W., Calas, G. et Brown, J., G. E. (1992): Structural environments of incompatible elements in silicate glass/melt systems. *Geochim. Cosmochim. Acta*, 56, 4205-4220.

Gampp, H., Maeder, M., Meyer, C. J. et Zuberbuehler, A. D. (1987): Evolving factor analysis. *Comments Inorg. Chem.*, 6(1), 41-60.

Gaudet, J.-P., Jegat, H., Vachaud, G. et Wierenga, P. (1977): Solute transfert, with Exchange Between Mobile and Stagnant Water, through Unsaturated Sand. *Soil Sci. Soc. Am. J.*, 41(4), 665-671.

Gaudet, J.-P. (1978): Transfert d'eau et de soluté dans des sols non-saturés. Mesures et simulation. Ph. D. thesis, Institut National Polytechnique de Grenoble, 230 p.

Geipel, G., Bernhard, G., Brendler, V. and Nitsche, H. (1996): Sorption of Uranium(VI) on Rock Material of a Mine Tailing Pile: Solution Speciation by Fluorescence Spectroscopy. *Radiochimica Acta*, 74, 235-238.

Geipel, G., Thime, M., Bernhard, G. et Nitsche, H. (1994): Distribution of Uranium and Radionuclides in an Uranium-Mining Rockpile in Schlema, Saxony. *Radiochimica Acta*, 66/67, 305-308.

Gellermann, R., Doerr, H. et Nindel, K. (1995): Determination of Migration parameters of decay series isotopes in groundwater of uranium mine Koenigstein. *Uranium-Mining and Hydrology*, Freiberg, Germany, Verlag Sven van Loga.

Glinka, Y. D. et Krak, T. B. (1995a): Luminescence spectra of uranyl ions adsorbed on disperse SiO₂ surfaces. *Physical review B*, 52(20), 14985-14995.

Glinka, Y., Krak, T. B. et Beljak, Y., N. (1995b): Investigations of adsorption properties of disperse SiO₂ surface by means of inorganic molecular probes using laser spectroscopy methods. *Journal of Molecular Structure*, 349, 215-218.

Glinka, Y., Krak, T. B., Beljak, Y., N., Degoda, V. Y. et Ogenko, V. M. (1995c): X-ray and photo-luminophors based on SiO₂-UO₂²⁺ adsorption systems. *Colloids and Surfaces. A, Physicochemical and Engineering Aspects*, 104, 17-27.

Grenthe, I., Fuger, J., Konings, R. J. M., Lemire, R. J., Mueller, A. B., Nguyen-Trung, C. et Wanner, H. (1992): *Chemical Thermodynamics of Uranium*, NEA-TDB, OECD, North-Holland, Amsterdam.

Griffioen, J., Appelo, C. A. J. et van Veldhuizen, M. (1992): Practice of Chromatography: Deriving Isotherms from Elution Curves. *Soil Sci. Soc. Am. J.*, 56(5), 1429-1437.

Ho, C. H. et Miller, N. H. (1985): Effect of Humic Acid on Uranium Uptake by Hematite Particles. *J. Colloid Interface Science*, 106(2), 281-288.

Ho, C. H. et Miller, N. H. (1986): Adsorption of uranyl species from Bicarbonate Solution onto Hematite Particles. *J. Colloid Interface Science*, 110(1), 165-171.

Hsi, C.-K. et Langmuir, D. (1985): Adsorption of uranyl onto ferric oxyhydroxides: Application of the surface complexation site-binding model. *Geochim. Cosmochim. Acta*, 49, 1931-1941.

Jauzein, M. (1988): Méthodologie d'étude du transport transitoire de solutés dans les milieux poreux: Outils théoriques et numériques, méthodes expérimentales, application à l'étude du transport transitoire du césium sous forme cationique (Cs⁺) dans un aquifère alluvial. Ph. D. thesis, Institut National Polytechnique de Lorraine, Ecole Nationale Supérieure des Industries Chimiques, Nancy, 151 p.

Jauzein, M., Andre, C., Margrita, R., Sardin, M. et Schweich, D. (1989): A Flexible Computer Code for Modelling Transport in Porous Media: Impact. *Geoderma*, 44, 95-113.

Jury, W. A. et Roth, K. (1990): *Transfer Functions and Solute Movement through Soil: Theory and Application*. Basel, Boston, Berlin, Birkhaeuser, 1990.

Kato, Y., Kimura, T., Yoshida, Z. et Nitani, N. (1996): Solid-Liquid Phase Equilibria of Np(VI) and U(VI) under Controlled CO₂ Partial Pressures. *Radiochimica Acta*, 74, 21-25.

Kato, Y., Meinrath, G., Kimura, T. et Yoshida, Z. (1994): A study of U(VI) Hydrolysis and Carbonate Complexation by Time-Resolved Laser-Induced Fluorescence Spectroscopy (TRLFS). *Radiochimica Acta*, 64, 107-111.

- Kohler, M., Curtis, G. P., Kent, D. B. and Davis, J. A. (1996):** Experimental investigations and modelling of Uranium(VI) transport under variable chemical conditions. *Water Resources Research*, 32(12), 3539-3551.
- Kohler, M., Wieland, E. et Leckie, J. O. (1992):** Metal-ligand-surface interactions during sorption of uranyl and neptunyl on oxides and silicates. *Water-Rock-Interaction*, Khrarka and Maest (eds.), Balkema, Rotterdam, 51-54.
- Kushnirenko, I. Y., Glinka, Y. D., Degoda, V. Y., Krak, T. B. et Ogenko, V. M. (1993):** Luminescent properties of uranyl ions adsorbed on the surface of disperse silicon dioxide. *J. of Applied Spectroscopy*, 59(3-4), 687-692.
- Landa, E. R. et Gray, J. R. (1995):** US Geological Survey research on the environmental fate of uranium mining and milling wastes. *Environmental Geology*, 26, 19-31.
- Liger, M. (1996):** Rôle catalytique des oxyhydroxydes de Fe(III): Réduction de U(VI) par le Fe(II). Ph. D. thesis, Laboratoire de Géophysique Interne et Tectonophysique, Université Joseph Fourier, Grenoble, 173 p.
- Ludwig, C. (1993):** Koordinationschemie an der Grenzschicht Oxid/Wasser, I. Ternaere Oberflaechenkomplex mit Cu(II) und organischen Liganden und TiO₂ (Anatas), II. Ein Modell zur Beschreibung der deprotonierung von Al₁₃O₄(OH)₂₄(H₂O)₁₂⁷⁺. Ph. D. thesis, Department of inorganic chemistry, University of Bern,.
- Lumsdon, D. G. et Evans, L. J., 1994.** Surface complexation Model Parameters for Goethite (α -FeOOH). *Journal of Colloid and Interface Sciences*, 164, 119-125.
- Manceau, A. et Charlet, L. (1994):** The mechanism of selenate Adsorption on Goethite and Hydrus Ferric Oxide. *Journal of Colloid and Interface Sciences*, 168, 87-93.
- Manceau, A., Charlet, L. Boisset, M. C., Didier, B. et Spadini, L. (1992):** Sorption and speciation of heavy metals on hydrus Fe and Mn oxides. From microscopic to macroscopic. *Applied Clay Science*, 7, 201-223.
- McKinley, J. P., Zachara, J. M., Smith, S. C. et Turner, G. D. (1995):** The influence of uranyl hydrolysis and multiple site binding reactions on Adsorption of U(VI) to montmorillonite. *Clays and Clay Minerals*, 43(5), 586-598.
- Meinrath, G., Klenze, R. et Kim, J. I. (1996):** Direct Spectroscopic Speciation of Uranium(VI) in Carbonate Solutions. *Radiochimica Acta*, 74, 81-86.
- Miller, D. M., Summer, M. E. et Miller, W. P. (1989):** A comparison of Batch and Flow Generated Anion Adsorption Isotherms. *Soil Sci. Soc. Am. J.*, 53, 373-380.
- Moll, H. (1997):** Zur Wechselwirkung von Uran mit Silikat in waessrigen Systemen. Ph. D. thesis, TU Dresden.

Moriyasu, M., Yokoyama, Y. et Ikeda, S. (1977): Quenching mechanisms of uranyl luminescence by metal ions. *J. Inorg. Nucl. Chem.*, 39, 2205-2209.

Morris, D. E., Chrisholm-Brause, C. J., Barr, M. E., Conradson, S. D. et Eller, P. G. (1994): Optical spectroscopic studies of the sorption of UO_2^{2+} species on a reference smectite. *Geochim. Cosmochim. Acta*, 58(17), 3613-3623.

Morrison, S. J., Spangler, R. R. et Tripathi, V. S. (1995a): Adsorption of uranium(VI) on amorphous ferric oxyhydroxide at high concentrations of dissolved carbon(IV) and sulfur(VI). *J. Contaminant. Hydrology*, 17(4), 333-346.

Morrison, S. J., Tripathi, V. S. et Spangler, R. R. (1995b): Coupled reaction transport modelling of a chemical barrier for controlling uranium(VI) contamination in groundwater. *J. Contaminant. Hydrology*, 17(4), 347-363.

Moulin, C., Decambox, P., Moulin, V. et Decaillon, J. G. (1995): Uranium Speciation in Solution by Time-Resolved Laser-Induced Fluorescence. *Analytical Chemistry*, 67(2), 348-353.

Oesthols, E. (1995): Thorium sorption on amorphous silica. *Geochim. Cosmochim. Acta*, 59(7), 1235-1249.

Pauling, L. (1929): The principles determining the structure of complex ionic crystals. *J. Amer. Chem. Soc.*, 51, 1010-1026.

Persaud, N., Davidson, J.M. et Rao, P.S.C. (1983): Miscible displacement of inorganic cations in a discrete homoionic exchange medium. *Soil Science*, 136(5), 269-278.

Pfannkuch H. F. (1963): Contribution à l'étude des déplacements de fluides miscibles dans un milieu poreux; Thèse de troisième cycle présentée à l'Université de Paris; *Revue de l'IFP*, vol. XVIII, n°2.

Pompe, S. (1997): Entwicklung huminsaeureaehnlicher Melanoidine als Funktionsmodelle fuer Huminsaeuren und ihr Vergleich mit Fluka-Huminsaeure hinsichtlich ihres Komplexierungsverhaltens gegenueber Uran(VI). Ph. D. thesis, TU Dresden.

Reich, T., Moll, H., Denecke, M. A., Geipel, G., Bernhard, G., Nitsche, H., Allen, P. G., Bucher, J. J., Kaltsoyannis, N., Edelstein, N. M. et Shuh, D. K. (1996): Characterisation of Hydrated Uranyl Silicate by EXAFS. *Radiochimica Acta*, 74, 219-223.

Sandino, A. et Bruno, J. (1992): The solubility of $(\text{UO}_2)_3(\text{PO}_4)_2 \cdot 4 \text{H}_2\text{O}_{(s)}$ and the formation of U(VI) phosphate complexes: Their influence in uranium speciation in natural waters. *Geochim. Cosmochim. Acta*, 56, 4135-4145.

Scheidegger, A. (1993): Die Adsorption von Protonen, Fluorid und Cadmium in einer Goethite-Saeule. Ph. D. thesis, ETH Zuerich, 149 p.

- Scheidegger, A., Buergisser, C. S., Borkovec, M., Sticher, H., Meeussen, H. et van Riemsdijk, W. (1994):** Convective transport of acids and bases in porous media. *Water Resources Research*, 30(11), 2937-2944.
- Schindler, P. W. et Gamsjaeger, H. (1972):** Acid-base reactions of the titanium dioxide (anatase)-water interface and the point of zero charge of titanium dioxide suspensions. *Colloid Z. Z. Polym.*, 250, 759.
- Schindler, P. W. et Stumm, W. (1987):** The surface chemistry of oxides, hydroxides and oxide minerals. *Aquatic Surface Chemistry*. Stumm. New York, John Wiley and Sons.
- Schindler, P. W., Fuerst, B., Dick, R. et Wolf, P. U. (1976):** Ligand properties of surface silanol groups. I. Surface complex formation with iron(3+), copper(2+), cadmium(2+) and lead(2+). *J. Colloid. Interface; Sci.*, 55(2), 469-475.
- Schindler, P. W. et Kamber, H. R. (1968):** Die Aciditaet von Silanolgruppen. *Helv. Chim. Acta*, 51, 1781-1786.
- Schweich, D. et Sardin, M. (1981):** Adsorption, partition, ion exchange and chemical reaction in batch reactors or in columns - A review. *Journal of Hydrology*, 50, 1-33.
- Sigg, L. M. (1979):** Die Wechselwirkung von Anionen und schwachen Saeuren mit α -FeOOH (Goethite) in waessriger Loesung. Ph. D. thesis ETH 6417, ETH Zuerich.
- Spadini, L. (1993):** Struktur und Stabilitaet von Oberflaechenkomplexen im System Cd^{2+} - FeOOH. Ph. D., Institut fuer anorganische, analytische und physikalische Chemie, Universitaet Bern.
- Sparks, D. L. et Jardine, P. M. (1982):** Comparison of batch and miscible displacement techniques to describe potassium adsorption kinetics in Delaware soils. *Soil Sci. Soc. Am. J.*, 46, 875-877.
- Sposito, G. (1982):** On the Use of the Langmuir Equation in the Interpretation of "Adsorption" Phenomena: The "Two-Surface" Langmuir Equation. *Soil. Sci. Soc. Am. J.*, 46, 1147-1152.
- Stanton, J. et Maatman, R. W. (1963):** The reaction between aqueous uranyl ion and the surface of silica gel. *J. Colloid Sci.*, 18, 132.
- Strickland, C. et Parsons, J. L. (1972):** Determination of reactive silicate. In: *Practical book of sea water analysis*. Ed. Fisheries Research Board of Canada. 65-70.
- Stumm, W. et Morgan, J. J. (1996):** *Aquatic chemistry: Chemical equilibria and rates in natural waters*. John Wiley and Sons, Inc., New York, Chichester, Brisbane, Toronto, Singapore.

- Swihart, G. H., Sen Gupta, P. K., Schlemper, E. O., Back, M. E. et Gaines, R. V. (1993):** The crystal structure moctezumite $[\text{PbUO}_2](\text{TeO}_3)_2$. *American Mineralogist*, 78, 835-839.
- Thompson, H. A., Brown Jr., G. E. et Parks, G. A. (1997):** EXAFS spectroscopic study of uranyl coordination in solids and aqueous solution. *American Mineralogist*, 82, 483-496.
- Toride, N., Leij, F. J. et van Genuchten, M. T. (1993):** A comprehensive Set of Analytical Solutions for Nonequilibrium Solute Transport With First-Order Decay and Zero-Order Production. *Water Resources Research*, 29(7), 2167-2182.
- Toride N. et Leij F. J. (1996):** Convective-Dispersive Stream Tube Model for Field-Scale Solute transport: Moment analysis. *Soil Sci. Soc. Am. J.*, 60, 342-352.
- Torma, A. E., Pendleton, N. R. et Fleming, W. M. (1985):** Sodium carbonate-bicarbonate leaching of a New Mexico uranium ore and removal of long Half-life radionuclides from the leach residue. *Uranium*, 2, 17-36.
- Turner, D. R. (1995):** A uniform approach to surface complexation modeling of radionuclide sorption. Report CNWRA 95-001 of the Nuclear Regulatory Commission Contract NRC-02-93-005, Center for Nuclear Waste Regulatory Analyses, San Antonio, Texas.
- van Geen, A., Robertson, A. P. et Leckie, J. O. (1994):** Complexation of carbonate species at the goethite surface: Implications for adsorption of metal ions in natural waters. *Geochim. Cosmochim. Acta*, 58(9), 2073-2080.
- van Genuchten, M. T. et Wierenga, P. J. (1976):** Mass Transfer Studies in Sorbing Porous Media I. Analytical solutions. *Soil Sci. Soc. Am. J.*, 40(4), 473-480.
- van Veldhuizen, M., Appelo, C. A. J. et Griffioen, J. (1995):** The least squares quotient algorithm as a rapid tool for obtaining sorption isotherms from column elution curves. *Water Resources Research*, 31(4), 849-857.
- Veal, B. W., Mundy, J. N. et Lam, D. J. (1987):** Actinides in silicate glasses. *Handbook on Physics and Chemistry of the Actinides*. A. J. Freeman and G. H. Lander, Elsevier, 271-309.
- Venema, P., Hiemstra, T. et van Riemsdijk, W.H. (1996):** Multisite Adsorption of Cadmium on Goethite. *J. Colloid Interface Sci.*, 183, 515-527.
- Vial, J.-C. (1997):** Personal communication.
- Waite, T. D., Davis, J. A., Payne, T. E., Waychunas, G. A. et Xu, N. (1994):** Uranium(VI) adsorption to ferrihydrite: Application of a surface complexation model. *Geochim. Cosmochim. Acta*, 58(24), 5465-5478.
- Wersin, P., Hochella, M. F., Persson, P. et Redden, G. (1994):** Interaction between aqueous uranium(VI) and sulfide minerals: Spectroscopic evidence for sorption and reduction. *Geochim. Cosmochim. Acta*, 58(13), 2829-2843.

Westall, J. C. (1982): A computer program for the determination of chemical equilibrium constants from experimental data. Version 1.2. Corvallis, Oregon, Oregon State University.

Westall, J. et Hohl, H. (1980): A comparison of Electrostatic Models for the Oxide/Solution Interface. *Advances Coll. Interface Sci.*, 12, 265-294.

Wheeler, J. et Thomas, J. K. (1984): Photochemistry of the Uranyl Ion in Colloidal Silica Solution. *J. Phys. Chem.*, 88, 750-754.

Yeh, G.-T. et Tripathi, V. S. (1991): A Model for simulating Transport of Reactive Multispecies Components: Model Development and Demonstration. *Water Resources Research*, 27(12), 3075-3094.

Yeh, G.-T. et Tripathi, V. S. (1990): HYDROGEOCHEM: A coupled model of hydrological and geochemical equilibrium of multi-component systems. Oak Ridge Natl. Lab., Oak Ridge, TN, ORNL-6371, 312 pp.

ANNEXE

Tableau 1 Constantes d'équilibre (logK) pour la spéciation en solution
(Grenthe et al., 1992; Stumm and Morgan, 1996)

Reaction	logK I = 0 M	logK I = 0.01 M
$\text{H}_2\text{CO}_3^\circ - \text{H}^+ \leftrightarrow \text{HCO}_3^-$	-6.35	-6.26
$\text{H}_2\text{CO}_3^\circ - 2 \text{H}^+ \leftrightarrow \text{CO}_3^{2-}$	-16.68	-16.42
$\text{H}_4\text{SiO}_4^\circ - \text{H}^+ \leftrightarrow \text{H}_3\text{SiO}_4^-$	-9.83	-9.74
$\text{H}_4\text{SiO}_4^\circ - 2 \text{H}^+ \leftrightarrow \text{H}_2\text{SiO}_4^{2-}$	-23	-22.73
$\text{UO}_2^{2+} - \text{H}^+ + \text{H}_2\text{O} \leftrightarrow \text{UO}_2\text{OH}^+$	-5.2	-5.29
$\text{UO}_2^{2+} - 2 \text{H}^+ + 2 \text{H}_2\text{O} \leftrightarrow \text{UO}_2(\text{OH})_2^\circ$	-10.3	-10.20
$\text{UO}_2^{2+} - 3 \text{H}^+ + 3 \text{H}_2\text{O} \leftrightarrow \text{UO}_2(\text{OH})_3^-$	-19.2	-19.2
$\text{UO}_2^{2+} - 4 \text{H}^+ + 4 \text{H}_2\text{O} \leftrightarrow \text{UO}_2(\text{OH})_4^{2-}$	-33.	-32.82
$2 \text{UO}_2^{2+} - \text{H}^+ + \text{H}_2\text{O} \leftrightarrow (\text{UO}_2)_2\text{OH}^{3+}$	-2.8	-2.71
$2 \text{UO}_2^{2+} - 2 \text{H}^+ + 2 \text{H}_2\text{O} \leftrightarrow (\text{UO}_2)_2(\text{OH})_2^{2+}$	-5.62	-5.71
$3 \text{UO}_2^{2+} - 4 \text{H}^+ + 4 \text{H}_2\text{O} \leftrightarrow (\text{UO}_2)_3(\text{OH})_4^{2+}$	-11.9	-12.08
$3 \text{UO}_2^{2+} - 5 \text{H}^+ + 5 \text{H}_2\text{O} \leftrightarrow (\text{UO}_2)_3(\text{OH})_5^+$	-15.55	-15.81
$3 \text{UO}_2^{2+} - 7 \text{H}^+ + 7 \text{H}_2\text{O} \leftrightarrow (\text{UO}_2)_3(\text{OH})_7^-$	-31.	-31.18
$4 \text{UO}_2^{2+} - 7 \text{H}^+ + 7 \text{H}_2\text{O} \leftrightarrow (\text{UO}_2)_4(\text{OH})_7^+$	-21.9	-22.25
$\text{UO}_2^{2+} + \text{H}_2\text{CO}_3^\circ - 2 \text{H}^+ \leftrightarrow \text{UO}_2\text{CO}_3^\circ$	-6.98	-7.07
$\text{UO}_2^{2+} + 2 \text{H}_2\text{CO}_3^\circ - 4 \text{H}^+ \leftrightarrow \text{UO}_2(\text{CO}_3)_2^{2-}$	-16.42	-16.24
$\text{UO}_2^{2+} + 3 \text{H}_2\text{CO}_3^\circ - 6 \text{H}^+ \leftrightarrow \text{UO}_2(\text{CO}_3)_3^{4-}$	-28.44	-27.65
$\text{UO}_2^{2+} + \text{H}_4\text{SiO}_4^\circ - \text{H}^+ \leftrightarrow \text{UO}_2\text{H}_3\text{SiO}_4^+$	-2.4	-2.49
$\text{H}_2\text{O} - \text{H}^+ \leftrightarrow \text{OH}^-$	-14	-13.91

Tableau 2 Constantes d'équilibre intrinsèques (logK) pour la spéciation sur la surface de la silice amorphe

(modèle de la couche compacte; $c_p = 1 \text{ g dm}^{-3}$; $A_s = 169 \text{ m}^2 \text{ g}^{-1}$; $\kappa = 7 \text{ F m}^{-2}$;
 $[\equiv\text{Si}(\text{OH})_2]_{\text{total}} = 0.51 \text{ mM}$; $[\text{H}_2\text{CO}_3^\circ]_{\text{libre}} = 16.4 \text{ }\mu\text{M}$; $[\text{H}_4\text{SiO}_4^\circ]_{\text{total}} = 0.9 \text{ mM}$; $[\text{UO}_2^{2+}]_{\text{total}} = 1 \text{ }\mu\text{M}$)

Reactions	logK	
	I = 0 M	I = 0.01 M
$\equiv\text{Si}(\text{OH})_2 - \text{H}^+ \leftrightarrow \equiv\text{SiO}_2\text{H}^-$	-6.98	-6.94
$\equiv\text{Si}(\text{OH})_2 + \text{UO}_2^{2+} - 2 \text{H}^+ \leftrightarrow \equiv\text{SiO}_2\text{UO}_2^\circ$	-4.81	-4.9
$\equiv\text{Si}(\text{OH})_2 + \text{UO}_2^{2+} - 3 \text{H}^+ + \text{H}_2\text{O} \leftrightarrow \equiv\text{SiO}_2\text{UO}_2\text{OH}^-$	-10.46	-10.5
$\equiv\text{Si}(\text{OH})_2 + \text{UO}_2^{2+} + \text{H}_2\text{CO}_3^\circ - 5 \text{H}^+ + \text{H}_2\text{O} \leftrightarrow \equiv\text{SiO}_2\text{UO}_2\text{OHCO}_3^{3-}$	-22.14	-22.1

Tableau 3 Constantes d'équilibre intrinsèques (logK) pour la spéciation sur la goethite

(modèle de la couche compacte; $c_p = 0.82 \text{ g dm}^{-2}$; $A_s = 80.5 \text{ m}^2 \text{ g}^{-1}$; $\kappa = 1.75 \text{ F m}^{-2}$;
 $[\equiv\text{Fe}^{\text{w}}\text{O}_2\text{H}]_{\text{total}} = 0.253 \text{ mM}$; $[\equiv\text{Fe}^{\text{s}}\text{O}_2\text{H}]_{\text{total}} = 1.25 \text{ }\mu\text{M}$; $[\text{H}_2\text{CO}_3^\circ]_{\text{free}} = 16.4 \text{ }\mu\text{M}$; $[\text{UO}_2^{2+}]_{\text{total}} = 1 \text{ }\mu\text{M}$
réacteur fermé: $[\text{H}_4\text{SiO}_4^\circ]_{\text{total}} = 0.76 \text{ mM}$; *colonne*: $[\text{H}_4\text{SiO}_4^\circ]_{\text{total}} = 21.4 \text{ }\mu\text{M}$)

Reactions	logK	
	I = 0 M	I = 0.01 M
$\equiv\text{Fe}^{\text{s/w}}\text{O}_2\text{H} + \text{H}^+ \leftrightarrow \equiv\text{Fe}^{\text{s/w}}\text{O}_2\text{H}_2^+$	7.33	7.37
$\equiv\text{Fe}^{\text{s/w}}\text{O}_2\text{H} - \text{H}^+ \leftrightarrow \equiv\text{Fe}^{\text{s/w}}\text{O}_2^-$	-9.88	-9.92
$\equiv\text{Fe}^{\text{s/w}}\text{O}_2\text{H} + \text{H}_2\text{CO}_3^\circ - \text{H}_2\text{O} \leftrightarrow \equiv\text{Fe}^{\text{s/w}}\text{OHCO}_3^\circ$	3.62	3.62
$\equiv\text{Fe}^{\text{s/w}}\text{O}_2\text{H} + \text{H}_2\text{CO}_3^\circ - \text{H}^+ - \text{H}_2\text{O} \leftrightarrow \equiv\text{Fe}^{\text{s/w}}\text{OCO}_3^-$	-3.40	3.35
$\equiv\text{Fe}^{\text{s/w}}\text{O}_2\text{H} + \text{H}_4\text{SiO}_4^\circ - \text{H}_2\text{O} \leftrightarrow \equiv\text{Fe}^{\text{s/w}}\text{OH}_3\text{SiO}_4^\circ$	3.5	3.5
$\equiv\text{Fe}^{\text{s/w}}\text{O}_2\text{H} + \text{H}_4\text{SiO}_4(\text{aq.}) - \text{H}^+ - \text{H}_2\text{O} \leftrightarrow \equiv\text{Fe}^{\text{s/w}}\text{OH}_2\text{SiO}_4^-$	-3.89	-3.85
modèle I: (Fe^w 1p, Fe^s 2p)		
$\equiv\text{Fe}^{\text{w}}\text{O}_2\text{H} + \text{UO}_2^{2+} - \text{H}^+ \leftrightarrow \equiv\text{Fe}^{\text{w}}\text{O}_2\text{UO}_2^+$	4.307	4.18
$\equiv\text{Fe}^{\text{s}}\text{O}_2\text{H} + \text{UO}_2^{2+} - 2 \text{H}^+ + \text{H}_2\text{O} \leftrightarrow \equiv\text{Fe}^{\text{s}}\text{O}_2\text{UO}_2\text{OH}^\circ$	-0.044	-0.13
modèle II (Fe^w 2p, Fe^s 2p)		
$\equiv\text{Fe}^{\text{w}}\text{O}_2\text{H} + \text{UO}_2^{2+} - 2 \text{H}^+ + \text{H}_2\text{O} \leftrightarrow \equiv\text{Fe}^{\text{w}}\text{O}_2\text{UO}_2\text{OH}^\circ$	-3.13	-3.22
$\equiv\text{Fe}^{\text{s}}\text{O}_2\text{H} + \text{UO}_2^{2+} - 2 \text{H}^+ + \text{H}_2\text{O} \leftrightarrow \equiv\text{Fe}^{\text{s}}\text{O}_2\text{UO}_2\text{OH}^\circ$	-0.044	-0.13

Fe^w = sites peu réactifs sur les surfaces dominantes des cristaux; Fe^s = sites très réactifs sur les petites surfaces (e.g. surfaces terminales ou défauts dans le réseau minéralogique). Pour l'adsorption des protons, des ions carbonates et des ions silicates, Fe^{s/w} représentent les deux.